Proteome-wide Identification and Characterization of Protein ADP-ribosylation in Mammalian Cells and Mouse Tissues

Dissertation

zur

Erlangung der naturwissenschaftlichen Doktorwürde

(Dr. sc. nat.)

vorgelegt der

Mathematisch-naturwissenschaftlichen Fakultät

der

Universität Zürich

von

Mario Peter Leutert

von

Schaffhausen, SH

Promotionskommission

Prof. Dr. Dr. Michael O. Hottiger

(Vorsitz und Leitung der Dissertation)

Prof. Dr. Alessandro A. Sartori

Prof. Dr. Bernd Wollscheid

Prof. Dr. Alexander Bürkle

Zürich, 2018

SUMMARY

In all organisms the functional and structural plasticity of proteins is defined by post-translational modifications (PTM). ADP-ribosylation is an ancient PTM that comes in a monomeric and polymeric form in mammalian cells and has been identified to be involved in important cellular processes and misregulated in disease. Inhibitors of ADP-ribosylation are now used in the clinic to treat cancer, however many aspects of the PTM remain enigmatic; especially which proteins are modified during which conditions, what are the amino acid acceptor sites and which sites are modified by which ADP-ribosyltransferase.

The aim of this thesis was to develop and apply mass spectrometry based methods to systematically and accurately map ADP-ribosylation sites in cells and tissues during physiological and pathological conditions and characterize their biological function.

First, we established a new enrichment protocol and optimized the mass spectrometry method, which let to the identification of the oxidative stress-induced ADP-ribosylome in HeLa cells and the finding that serine serves as the major nuclear ADP-ribose acceptor site. The modified proteins were mostly associated with functions in regulation of transcription, chromosome organization as well as DNA and RNA metabolic processes. We also found that a small number of tyrosines are ADP-ribosylated. Furthermore we identified high levels of arginine ADP-ribosylated proteins in mouse liver extracts on proteins having a role in metabolism.

Second, we found that ARTD1 is the main mediator of nuclear ADP-ribosylation during oxidative stress in cultured cells, having selectivity for serine and tyrosine modification. ARTD2 only modified a small number of detected targets. This suggested that ARTD1 catalyzes poly-ADP-ribosylation as well as *de novo* protein ADP-ribosylation.

Third we mapped the ADP-ribosylome of heart and skeletal muscle tissue and revealed a widespread role of ARTC1 arginine ADP-ribosylation of extracellular and plasma membrane proteins, as well as ARTC1 independent ADP-ribosylation in mitochondria.

Together, we could identify enzyme-substrate relationships for several hundred ADP-ribosylation sites catalyzed by ARTD1, ARTD2, ARTC1 and ARTC2.2 and we got mechanistic insight into the function of a few selected ADP-ribosylation sites. We are now able to accurately localize ADP-ribosylation sites and to map tissue and treatment specific ADP-ribosylation sites.

ZUSAMMENFASSUNG

Funktionelle und strukturelle Proteineigenschaften können in allen Organismen durch post-translationale Modifikationen (PTM) beeinflusst werden. ADP-Ribosylierung ist eine PTM, welche sowohl als Mono- als auch als Polymer vorkommt, in wichtige zelluläre Prozesse involviert ist und unter pathologischen Konditionen fehlreguliert sein kann. Obwohl Inhibitoren von ADP-Ribosylierung in der Krebsbehandlung eigesetzt werden, bleiben viele Aspekte unklar. Es ist ungenügend geklärt, welche Proteine unter welchen Bedingungen modifiziert sind, welche Aminosäuren als Akzeptoren fungieren und inwieweit die verschiedenen ADP-Ribosyltransferasen in die Etablierung der Modifikation involviert sind.

Das Ziel dieser Doktorarbeit war es, massenspektrometrische Methoden zu entwickeln, um systematisch und präzise ADP-Ribosylierungsstellen im Proteom von Zellen und Geweben zu kartieren und deren biologische Funktion zu analysieren.

In einem ersten Schritt haben wir ein neues Anreicherungsprotokoll für ADP-ribosylierte Peptide etabliert und die massenspektrometrische Methode dafür optimiert. Mithilfe dieses Protokolls, war es uns gelungen, das durch oxidativen Stress induzierte ADP-Ribosylom in HeLa Zellen zu identifizieren. Die modifizierten Proteine spielen eine Rolle in der transkriptionellen Regulation, Chromosomen Organisation sowie in DNA und RNA metabolischen Prozessen.

In einem zweiten Schritt konnten wir zeigen, dass ARTD1 der Hauptregulator der von oxidativem Stress induzierten, nukleären ADP-Ribosylierung war und Proteine selektiv an Serin oder Tyrosin modifizierte. ARTD2 war dagegen nur für die Modifikation einer kleinen Anzahl von unterschiedlichen identifizierten Proteinen verantwortlich.

In einem dritten Schritt haben wir das ADP-Ribosylom von Herz- und Skelettmuskeln der Maus charakterisiert. Wir konnten zeigen, dass ARTC1 eine weitreichende Rolle in der Arginin-spezifischen ADP-Ribosylierung von Membranproteinen, sowie extrazellulären Proteinen spielte. Im Gegensatz dazu, haben wir auch eine ARTC1 unabhängige, mitochondriale ADP-Ribosylierung beobachtet.

Diese Daten ermöglichten es uns, Substrat-Enzym-Beziehungen für mehrere hundert ARTD1-, ARTD2-, ARTC1- und ARTC2.2-abhängige ADP-Ribosylierungsstellen zu erstellen und die funktionelle Relevanz der Modifikation für einige Proteine zu studieren. Wir sind nun in der Lage ADP-ribosylierte Proteine und deren Modifikationsstellen präzise zu identifizieren und gewebe- und behandlungsspezifische ADP-Ribosylierungsstellen zu charakterisieren.

TABLE OF CONTENTS

SUMMARY **1**

ZUSAMMENFASSUNG **2**

TABLE OF CONTENTS **3**

INTRODUCTION **6**

1 PROTEOFORMS AND PROTEOME COMPLEXITY 6

2 PROTEIN ADP-RIBOSYLATION 8

3 ADP-RIBOSYLTRANSFERASES 8

3.1 Prokaryotic ADP-ribosylating toxins *8*

3.2 ARTD family of eukaryotic ADP-ribosyltransferases *10*

3.3 ARTC family of eukaryotic ADP-ribosyltransferases *11*

3.4 Sirtuins *12*

3.5 NAD+ metabolism and ADP-ribosyltransferases *12*

4 ADP-RIBOSYLHYDROLASES 13

5 ADP-RIBOSYLATION INTERACTORS 14

6 BIOLOGICAL ROLES OF INTRACELLULAR ADP-RIBOSYLATION 15

6.1 Biological functions of PARylation *15*

6.2 PARP inhibitors as therapeutics *17*

7 FUNCTIONAL ROLES OF EXTRACELLULAR ADP-RIBOSYLATION 18

8 LARGE-SCALE ANALYSIS OF POST-TRANSLATIONAL MODIFICATIONS BY MASS SPECTROMETRY 20

8.1 Identification of PTMs by mass spectrometry *20*

8.2 Enrichment of PTM carrying peptides *22*

8.3 Interpreting PTMs by proteomics exemplified by phosphoproteomics *23*

9 PROTEOME-WIDE IDENTIFICATION OF ADP-RIBOSYLATION BY MASS SPECTROMETRY 24

9.1 Challenges in identifying the ADP-ribosylome *24*

9.2 Affinity purification of ADP-ribosylated proteins *25*

9.3 Phosphoproteomic enrichment approaches *26*

9.4 Chemical-proteomic approaches based on boronate affinity chromatography *26*

9.5 Chemical proteomic enrichment based on NAD^+ or precursor labeling *27*

10 MASS SPECTROMETRIC IDENTIFICATION OF ADP-RIBOSE ACCEPTOR SITES 29

AIMS OF THE THESIS **31**

RESULTS **32**

1 OVERVIEW OF PUBLISHED MANUSCRIPTS 36

1.1 Proteome-wide identification of the endogenous ADP-ribosylome of mammalian cells and tissue *36*

1.2 Combining Higher-Energy Collision Dissociation and Electron-Transfer/Higher-Energy Collision Dissociation Fragmentation in a Product-Dependent Manner Confidently Assigns Proteomewide ADP-Ribose Acceptor Sites. *49*

1.3 Analysis of Chromatin ADP-Ribosylation at the Genome-wide Level and at Specific Loci by ADPr-ChAP *57*

1.4 Identification of ADP-Ribose Acceptor Sites on In Vitro Modified Proteins by Liquid Chromatography-Tandem Mass Spectrometry. *58*

1.5 Proteome-Wide Identification of In Vivo ADP-Ribose Acceptor Sites by Liquid Chromatography-Tandem Mass Spectrometry. *70*

1.6 Identification of PARP-Specific ADP-Ribosylation Targets Reveals a Regulatory Function for ADP-Ribosylation in Transcription Elongation *84*

2 OVERVIEW OF SUBMITTED MANUSCRIPTS 87

2.1 Comprehensive in vivo ADP-ribosylome analysis identifies tyrosine ADP-ribosylation of HPF1 and reveals that this modification modulates ARTD1 activity *87*

2.2 Proteomic analyses identify ARH3 as a serine mono ADP-ribosylhydrolase *124*

2.3 Ecto-ADP-ribosyltransferase ARTC2.1 functionally modulates FcγR1 and FcγR2B on microglia *125*

3 PREPARED BUT NOT YET SUBMITTED MANUSCRIPT 126

3.1 Proteomic characterization of the heart and skeletal muscle reveals widespread Arginine ADP-ribosylation by the ectopic ADP-ribosyltransferase ARTC1 ..... *126*

4 UNPUBLISHED RESULTS 170

4.1 ADP-ribosylation in NASH liver is sensitive to PARPi and NR treatment *170*

4.2 Widespread ARTC2.2 dependent ADP-ribosylation in the spleen *172*

4.3 Identification of the ARTC2.2 specific ADP-ribosylation of T Cells *173*

4.4 Determining ADP-ribosylation in thrombocytes *175*

4.5 Identifying ADP-ribosylation targets of bacterial toxins *177*

4.6 Targeted proteomic measurement of ADP-ribosylation sites on immunopurified proteins. *179*

4.7 SIRT6 is auto-ADP-ribosylated on Y12 ..... *180*

4.8 ADPRibase-Mn treatment of ADP-ribosylated peptides ... 181
4.9 Methods to unpublished results ... 184

DISCUSSION AND PERSPECTIVES ... 186

1 SUMMARY OF THE RESULTS ... 186
2 TOWARDS IDENTIFYING THE COMPLETE ADP-RIBOSYLOME AND LIMITATIONS OF CURRENT PROTEOMIC APPROACHES TO DO SO ... 187
3 TOWARDS AN ATLAS OF TISSUE SPECIFIC ADP-RIBOSYLATION ... 190
4 NUCLEAR SERINE ADP-RIBOSYLATION ... 192
5 EXTRACELLULAR ARGININE ADP-RIBOSYLATION AND ITS MEDICAL RELEVANCE ... 195
6 HOW TO PROCEED TO THE NEXT LEVEL – A SHORT PERSPECTIVE ... 196

ABBREVIATIONS ... 199

REFERENCES ... 201

ACKNOWLEDGMENTS ... 211

CURRICULUM VITAE ... 212

INTRODUCTION

The successful sequencing of the human genome in the last decade revealed that it consists of 20'000 to 25'000 genes, which is significantly lower than previously anticipated [1]. It is now clear that post-transcriptional and post-translational events are leading to a high number of functionally distinct proteins. Most of the proteome complexity is mediated by post-translational modification of proteins, such as phosphorylation, glycosylation or ADP-ribosylation [2]. In this introduction I will first provide an overview of the biological significance and diversity of PTMs in general and describe their mode of action on the example of phosphorylation, the most extensively studied PTM up to date. I will then focus on protein ADP-ribosylation, introduce transferases, hydrolases and interactors of protein ADP-ribosylation and discuss the diverse biological roles that have been assigned to this PTM. I will summarize the state of research of mass spectrometry based large-scale PTM analysis and then describe in detail existing mass spectrometric workflows for the study of ADP-ribosylated proteins.

1 Proteoforms and proteome complexity

Genes encode the information for the amino acid sequences of proteins, the foundation of the basic functional properties of a protein. Alternative mRNA splicing, allelic variations but mainly differential PTMs of proteins give rise to multiple different gene products, thereby vastly increasing the complexity of the proteome compared to the genome [2]. Specific molecular forms of proteins produced from a single gene are called proteoforms and can have functionally very different roles [3]. Proteoforms tremendously increase the functional and regulatory possibility of a cell far beyond the genetically encoded protein function. Hence, much of the complexity of the biological machinery is contributed by different proteoforms rather than by a high number of different genes.

In all kingdoms of life the dynamic functional and structural properties of proteins are defined and controlled by a variety of post-translational modifications [4]. PTMs are protein modifications that consist in the attachment of diverse chemical groups, the addition of peptides or polypeptides or the proteolytic

processing. Large-scale analysis revealed that at least 50% of the proteins in humans can carry site specific PTMs [2]. PTMs can also occur on multiple sites of the same protein, as for example in the histone code, however the combinatorial nature of multi-site PTMs is very complex and remains largely elusive up to date.

More than 300 chemically different PTMs are known [5]. Among the best-studied PTMs are covalent modification of amino acid side chains by phosphorylation, acetylation, ubiquitination and glycosylation. It is thought that the enzymes carrying out post-translational modification of proteins account for around 5% of the protein coding human genome [6]. Importantly, many PTMs are reversible; making PTM-controlled processes highly dynamic.

In the case of protein phosphorylation, 518 putative kinases and 189 protein phosphatases are expected to catalyze, respectively revert the modification in human [7, 8]. The complete phosphoproteome is not yet known for any species, but current estimates are that 40-45% of the eukaryotic proteome is a target for phosphorylation [9]. Phosphorylation is involved in many different biological processes ranging from signal transduction to regulation of enzyme activity, protein-protein as well as protein-ligand interaction, cellular localization and protein turnover, as shown in the overview in Figure 1 [4, 10]. It has become clear that inhibiting PTM-regulated processes has a high potential as a pharmaceutical intervention. That is exemplified by the 46 drugs targeting kinases, which were approved by the US Food and Drug Administration by 2016 [11].

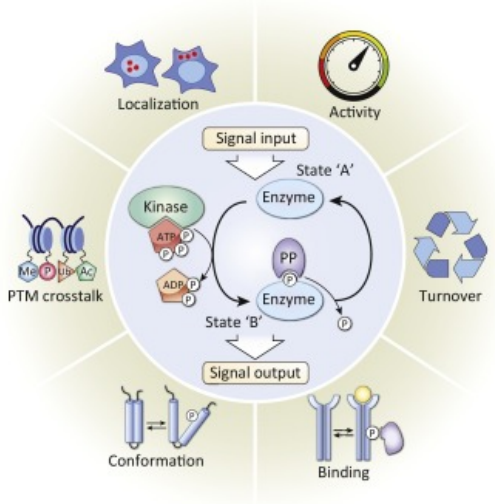

Figure 1 Diverse roles of reversible post-translational modification exemplified with protein phosphorylation. Protein kinases add a phosphate donated by ATP to a target protein; phosphatases are able to remove it again (center circle). Phosphorylation of an enzyme can act as a switch between different functional states of the protein, allowing cells to rapidly respond to certain stimuli. Examples how phosphorylation and other PTMs affect protein function are shown in the outer circle. Adapted from [10].

2 Protein ADP-ribosylation

Protein ADP-ribosylation is a covalent, post-translational modification that is catalyzed by ADP-ribosyltransferases (ARTs). These enzymes require nicotinamide adenine dinucleotide (NAD^+) as a substrate to transfer one ADP-ribose (ADPr) moiety onto specific amino acid residues (mono ADP-ribosylation or MARylation) or onto already protein bound ADP-ribose (poly-ADP-ribosylation or PARylation) [12]. In several bacterial pathogens toxins have been identified that have ADP-ribosylating activity toward host proteins in order to affect cell physiology [13]. 22 human ARTs are known, which are subdivided in ARTC (C for C2/C3 cholera toxin-like) and ARTD (D for diphtheria toxin like) according to the structural homology of their catalytic domain to bacterial toxins [14]. Additionally, two members of the Sirtuin family are considered to have ADP-ribosylating activity. Endogenous ADP-ribosylation is thought to be fully reversible and a set of ADP-ribosylhydrolases with different specificities has been identified. Furthermore, many proteins contain ADP-ribose interaction domain. A scheme of the ADP-ribosylation circle is shown in Figure 2.

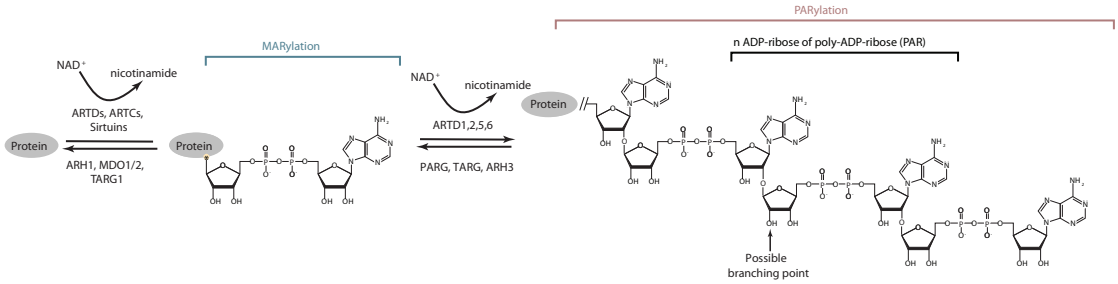

Figure 2 The ADP-ribosylation circle. ARTs and certain sirtuins can MARylate proteins on specific amino acid acceptor sites by consuming NAD^+. MARylation is reversible by ARH1, and MDO1/2. ARTD1, 2, 5 and 6 can extend MARylation to PARylation. PARylation can be reduced to MARylation by PARG, TARG and ARH3. Modified from [15].

3 ADP-ribosyltransferases

3.1 Prokaryotic ADP-ribosylating toxins

ADP-ribosyltransferases show a widespread distribution in biological systems. They are found in various prokaryotes. Bacterial ADP-ribosyltransferases often act as toxins by mono-ADP-ribosylating eukaryotic proteins to promote bacterial

pathogenesis in humans, insects or plants [16]. Toxin mediated ADP-ribosylation disrupts host cell activity by modulating the activity of host proteins [16] (as summarized in
Figure 3).

Toxin	Bacterium	Eukaryotic substrate
DT-like toxins		
DT	*Corynebacterium diphtheriae*	eEF2
PE	*Pseudomonas aeruginosa*	eEF2
ChxA	*Vibrio cholerae*	eEF2
CT-like toxins		
CT	*V. cholerae*	Gαs
Heat-labile enterotoxin	*Escherichia coli* (ETEC)	Gαs
PT	*Bordetella pertussis*	Gαi
C2-like binary toxins		
C2 toxin	*Clostridium botulinum*	G-actin
Iota toxin	*Clostridium perfringens*	G-actin
CDT	*Clostridium difficile*	G-actin
CST	*Clostridium spiroforme*	G-actin
VIP	*Bacillus cereus*	G-actin
SpvB	*Salmonella* spp.	G-actin
AexT	*Aeromonas hydrophila*	G-actin
Photox	*Photorhabdus luminescens*	G-actin
C3-like toxins		
C3bot	*C. botulinum*	RHOA, RHOB and RHOC
C3Stau/EDIN	*Staphylococcus aureus*	RHOA, RHOB, RHOC and RHOE
C3cer	*B. cereus*	RHOA, RHOB and RHOC
ExoS	*P. aeruginosa*	RAS, ERM proteins and vimentin
ExoT	*P. aeruginosa*	CrkI and CrkII
HopU1	*Pseudomonas syringae*	GRP7
SpyA	*Streptococcus pyogenes*	Vimentin and actin
Novel toxins		
TT	*Salmonella enterica*	Unknown
PTC3	*P. luminescens*	G-actin
PTC5	*P. luminescens*	RHOA, RHOB and RHOC

Figure 3 Overview of known ADP-ribosylating toxins, their bacterial origin and their eukaryotic substrate proteins. Adapted from [16].

Prominent examples are the ADP-ribosylation of the diphtamide in elongation factor 2, thereby inhibiting protein synthesis, and both ADP-ribosylation of the RHO GTPases, which are known to modulate the state of actin polymerization, and the direct ADP-ribosylation of actin lead to the destruction of the host actin cytoskeleton [16].

The catalytic domain of the ADP-ribosyltransferases from prokaryotes to eukaryotes show a high structural conservation, indeed it is suggested that diversification of the ARTs happened during the development of different bacterial

conflict system and that eukaryotes acquired the ART genes through subsequent horizontal gene transfer [17].

3.2 ARTD family of eukaryotic ADP-ribosyltransferases

The eukaryotic ARTD family, also known as poly(ADP-ribose)polymerases (PARP), consists of 17 proteins, all of which are intracellular and localized to various compartments (summarized in Figure 4) [12]. Four of them are known to catalyze PARylation (ARTD1, 2, 5 and 6), twelve catalyze MARylation (ARTD3, 4, 7, 8, 9, 10, 11, 12, 14, 15, 16 and 17) and at least one seems to be catalytically inactive (ARTD 13).

Name	Alternative names	Enzymatic activity	Domain architecture
ARTD1	PARP1	PAR - branched	
ARTD2	PARP2	PAR - branched	
ARTD3	PARP3	MAR	
ARTD4	PARP4, vPARP	MAR	
ARTD5	PARP5a, TNKS1	PAR - oligo	
ARTD6	PARP5b, TNKS2	PAR - oligo	
ARTD7	PARP15, BAL3	MAR	
ARTD8	PARP14, BAL2	MAR	
ARTD9	PARP9, BAL1	MAR	
ARTD10	PARP10	MAR	
ARTD11	PARP11	MAR	
ARTD12	PARP12	MAR	
ARTD13	PARP13, ZC3HAV1	Inactive	
ARTD14	PARP7, tiPARP	MAR	
ARTD15	PARP16	MAR	
ARTD16	PARP8	MAR	
ARTD17	PARP6	MAR	

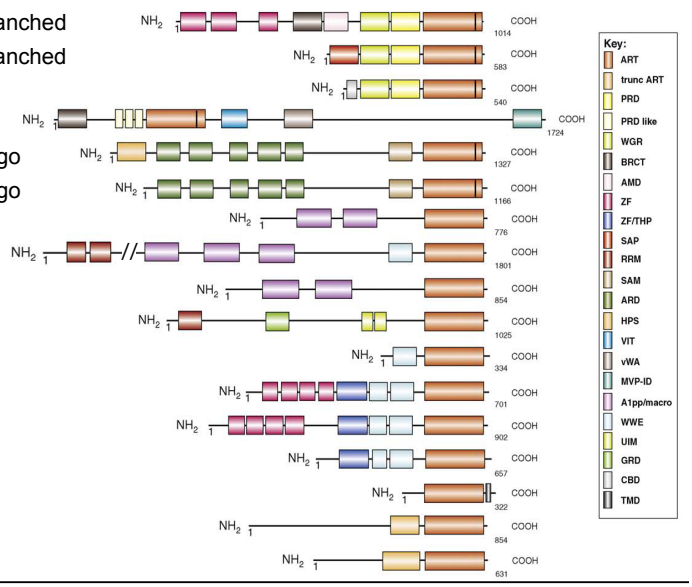

Figure 4 Overview of the ARTD family, enzymatic activity and domain architecture. Adapted from [14].

The ARTD nomenclature follows the structural homology and the implicated enzymatic features. ARTD1-6 are characterized by the conserved amino acid triade H-Y-E that has been identified in their active center [18]. These three residues have a key role in the catalytic transfer of ADP-ribose. The H and Y are important for binding NAD^+ and the E functions in catalysis and elongation of PAR [14]. All four ARTDs capable of PARylation (ARTD1, 2, 5 and 6) do contain this motif. ARTD3 and 4 also contain the H-Y-E motif, they are able to MARylate, however no direct evidence exists that they are also able to PARylate [19].

ARTD7, 8, 10-12, 14-17 contain a H-Y-I motif and they have been shown to be able to catalyze only MARylation [14]. Absence of the E in the motif is suspected to be the reason for their inability to catalyze PARylation. In order to still catalyze MARylation, it is proposed that these enzymes are using acidic residues of the substrate protein, in a substrate assisted catalysis process, to replace the missing E [20]. Indeed, mutating the catalytic E residue in ARTD1 leads to a shift from PARylation to MARylation [21]. ARTD9 and 13 are missing the H for NAD^+ binding and therefore have been considered to be catalytically inactive, however ARTD9 has recently been shown to have MARylation activity when in complex with the E3-ubiquitin ligase Dtx3L against the C-terminal carboxylate of ubiquitin [22].

3.3 ARTC family of eukaryotic ADP-ribosyltransferases

The ARTC family, also known as ecto-ARTs or GPI-linked $NAD(P)^+$-arginine ADP-ribosyltransferases, consists of four members in human (as summarized in Figure 5) and six members in mouse.

Name	Alternative name	Enzymatic activity	Domain architecture
ARTC1	ART1	MAR	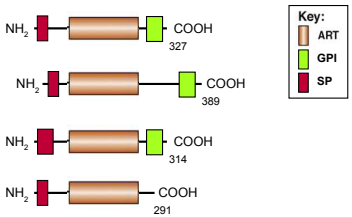
ARTC3	ART3	Inactive	
ARTC4	ART4	Inactive	
ARTC5	ART5	MAR	

Figure 5 Overview of the human ARTC family enzymatic activity and domain architecture. ARTC2.1 and 2.2 are not shown, since they are pseudo genes in human. As indicated in the key: glycosylphosphatidylinositol-anchor (GPI), signal peptide (SP), ADP-ribosyl transferase domain (ART). Adapted from [23] and Uniprot.

ARTC1, 2 and 5 contain the characteristic cholera toxin R-S-E catalytic motif in their active center. R and S are important for the NAD^+ binding and E functions again in the catalysis [14]. ARTC1-4 are facing the extracellular site of the cell and are bound with a glycosylphosphatidylinositol (GPI) anchor to the plasma membrane. Mainly based on mRNA expression data, human and mouse ARTC1 have been identified to be expressed in skeletal muscle, heart, epithelial cells and activated granulocytes [23]. ARTC2.1 and ARTC2.2 (also known as Art2a and Art2b respectively) are expressed in the mouse, but in human they contain a premature stop-codon and are

therefore not expressed [24]. In mouse ARTC2.2 seems to be constitutively active, however ARTC2.1 is only active in the presence of reducing agents, due to an inactivating disulfide bond, which is absent in all other ARTCs [23]. Mouse ARTC2.1 and ARTC2.2 are expressed on T cells [25]. ARTC3 and 4 lack the R-S-E motif, which prevents them from binding NAD^+ and renders them catalytically inactive. ARTC3 is expressed broadly and ARTC4 on erythrocytes. ARTC5 lacks the GPI-anchor and is therefore a secreted protein and is expressed in testis [25].

3.4 Sirtuins

The mammalian sirtuin family consists of 7 members (SIRT1-7) and is well known for their NAD^+ dependent deacetylation activity in the case of SIRT1-3, 5 and 6 [26]. Sirtuins deacetylate a variety of proteins, with histones being the most prominent targets. During protein deacetylation by sirtuins an NAD^+ molecule is cleaved to nicotinamide and ADP-ribose, whereas the acetyl group is transferred from an acetylated lysine to the ADP-ribose. This reaction generates nicotinamide, O-acetyl-ADP-ribose and a deacetylated lysine residue. The o-acetyl-ADP-ribose can be further processed by certain macrodomains and ARH (macroD2, C6orf130 and ARH3) enzymes, which also have a role in protein de-ADP-ribosylation as discussed below [27-29].

Protein MARylation has been proposed as an alternative reaction mechanism for some of the Sirtuins, however the reaction has been described as less efficient compared to the deacetylation activity. Still it is believed that the mitochondrial SIRT4 MARylates glutamate dehydrogenase (GDH), which has functional implications on the glutamine/glutamate turnover and on mitochondrial ATP-synthesis [30]. There are also some indications that SIRT6, which is localized to the nucleus, ADP-ribosylates certain targets including ARTD1 [31].

3.5 NAD+ metabolism and ADP-ribosyltransferases

Intracellular NAD^+ stems from two different sources; it is produced either by *de novo* synthesis or via a salvage pathway from precursor molecules. *De novo* synthesis starts from the amino acid tryptophan and the salvage pathway from the naturally occurring vitamins: nicotinamide (NA), nicotinic acid (NAM) and nicotinamide

riboside (NR) [32]. It is thought that distinct NAD^+ pools exist in the cytosolic/nuclear and mitochondrial compartment, however the pools are interconnected by a set of cellular processes. These pools individually regulate compartment specific metabolic pathways [33]. Three enzyme classes, the ARTs, the Sirtuins and the cADPr synthases require NAD^+ as a cofactor and compete for it. Activation of ARTD1, for example during excessive DNA damage, reduces NAD^+ levels to 20-30% of their normal levels, which dramatically reduces NAD^+ availability for nuclear Sirtuins, impairing their deacetylation function [33]. Also under steady-state conditions ARTD1 seems to consume high amounts of NAD^+, since NAD^+ is increased up to 2 fold in ARTD1-KO mouse tissue [34].

Apart from genetic interventions several strategies exist, which have the potential to boost NAD^+ levels, also in a compartment-specific manner. Among these are PARPi treatment or supplementation with NA, NAM, NR or NAM mononucleotide [32]. There are by now many examples of physiological and pathophysiological conditions where modulation of NAD^+ levels or NAD^+ metabolism has shown beneficial effects including aging, insulin resistance, fatty liver, dyslipidemia, hypertension, neurodegeneration, muscle function and heart function [32, 33].

The origin and role of extracellular NAD^+, the substrate of ARTCs, is still not very well understood. The NAD^+ concentration in plasma under normal conditions is estimated to be around 0.1 μM, however high amounts of NAD^+ can be released during lytic processes, such as tissue damage and necrosis [35, 36]. Furthermore, it is thought that NAD^+ as well as other nucleotides are released by controlled mechanisms during hypoxia and inflammation [35, 36]. Extracellular NAD^+ is rapidly degraded by ectoenzymes such as the NADase CD38 [23].

4 ADP-ribosylhydrolases

Several enzymes that remove ADP-ribose from mono- and poly-ADP-ribosylated substrates have been identified, most probably rendering ADP-ribosylation a fully reversible PTM [37]. Mammalian ADP-ribosylhydrolases characterized so far, include poly-ADP-ribose glycohydrolase (PARG) and ADP-ribosylhydrolase 3

(ARH3), both of which are able to hydrolyze poly-ADP-ribose and the mono-ADP-ribosyl arginine hydrolase 1 (ARH1) [38-40]. ARH2 is thought to be catalytically inactive [29]. In addition, the macrodomain-containing proteins MacroD1, MacroD2, and C6orf130 have also been shown to exhibit mono-ADP-ribosylhydrolase activity against ADP-ribosylated acidic amino acids [41-43].

5 ADP-ribosylation interactors

There are several protein domains known, which have binding affinity for specific parts of MAR or PAR (as indicated in Figure 6) [37].

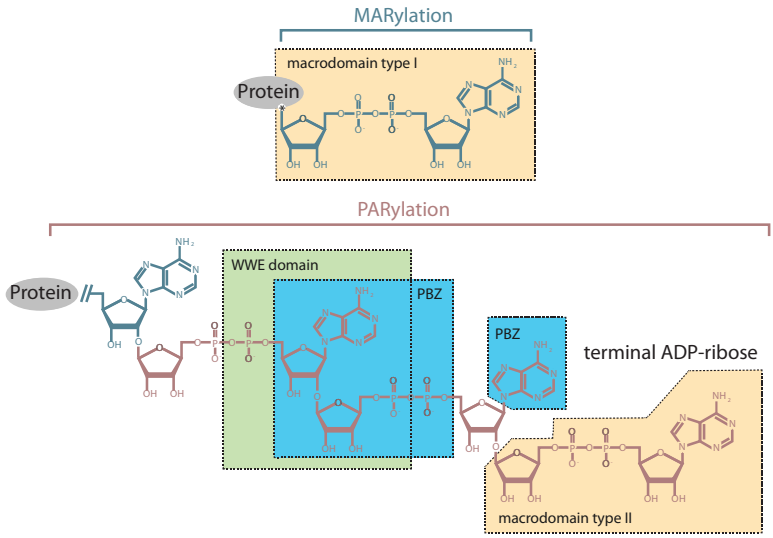

Figure 6 Overview of four distinct MAR and PAR binding domains and their specificity. Adapted from [37].

These domains include structurally well-characterized binding modules such as macrodomain, PAR-binding zinc finger (PBZ), WWE and PAR-binding motif (PBM) [37]. Forkhead-associated (FHA) and BRCA1 C-terminal (BRCT) domains, both previously associated with phospho-site binding, have also certain affinity towards ADP-ribosylation sites [44]. Furthermore, newly emerging PAR binders belong to previously described DNA or RNA binding domains such as the RNA recognition motif (RRM), oligonucleotide/oligosaccharide-binding fold (OB-fold), PIN domains as well as low complexity domains such as SR repeats, KR-rich motifs and RG/RGG repeats [44]. Proteins containing MAR or PAR binding domains include DNA repair factors, chromatin remodelers, cell cycle regulators, RNA-binding proteins,

transcription factors and E3-ubiquitin ligases. They are regulating multi-protein assemblies at sites of DNA damage, chromatin remodeling, phase separation of proteins through aggregation and PAR-dependent ubiquitination [44-46].

Interestingly, multiple ADP-ribose binding domains have been identified in bacteria, archea and viruses [29, 47-49]. Af1521 is a protein found in the thermophilic organism *Archaeoglobus fulgidus* which binds to MARylation and PARylation, with a relatively low dissociation constant of K_D=126± 21 nM for free ADP-ribose [47, 50]. Due to these properties Af1521 was broadly used as a tool to study ADP-ribosylation as discussed later [50].

6 Biological roles of intracellular ADP-ribosylation

6.1 Biological functions of PARylation

ARTD1, 2, 5 and 6 have been published to catalyze PARylation and several biological functions of these enzymes are discussed below. The first PARylation targets identified included the core histones and ARTD1 itself [51]. Based on the stability towards chemical treatments, it was initially proposed, that protein PARylation consists of ester and ketamine bonds formed by ADP-ribosylation of glutamic/aspartic acid residues and lysine/arginine residues respectively [52]. Specific glutamic acid residues in histones H1 and H2B, as well as the C-terminal lysine residue of H1, were reported as ADP-ribose acceptors [53, 54]. More recent studies however proposed, based on *in vitro* reactions in combination with site directed mutagenesis and MS measurement, that lysine residues are modified on ARTD1 and histones [55, 56]. However, the exact *in vivo* modification sites are still under debate [57-59].

ARTD1 activity has been shown to be regulated by post-translational modifications, such as phosphorylation, acetylation, SUMOylation and ADP-ribosylation, by direct protein-protein interactions or DNA damage-dependent activation [60]. Recently the protein C4orf27/HPF1 was found to act as a factor for ARTD1 PARylation, shifting ARTD1 activity from auto modification to histone PARylation and driving the specificity for serine ADP-ribosylation [61, 62].

ARTD1 is recruited to DNA double strand breaks and nicks through its DNA binding domain in response to DNA damage and was identified to play a role in DNA repair, re-initiation of stalled replication forks and regulation of telomere length [63, 64]. PARylation of ARTD1 itself and other proteins at the site of DNA damage serves as a scaffold for the recruitment of various DNA repair proteins and remodels the chromatin [65]. More specifically it was proposed that ARTD1 is involved in base excision repair and repair of single strand breaks, involving the binding of the single strand break intermediates [66]. These findings have been extended and it was appreciated more recently that ARTD1 also seems to have a role in double strand break repair [67]. Although ARTD1 is not required for viability in mice, these mice or isolated mouse embryonic fibroblasts exhibit some DNA repair defects and elevated chromosomal abnormalities [68, 69].

ARTD1 enzymatic activity is additionally involved in development, cell differentiation and pluripotency by means of chromatin ADP-ribosylation [70]. ARTD1 activity was also associated with regulation of metabolic functions, for example in the mouse liver, where the circadian entrainment of feeding behavior is regulated trough ADP-ribosylation of the CLOCK protein complex [71]. Furthermore, there is clear evidence that ADP-ribosylation by ARTD1, but also by other ARTD members, plays an important role in different aspects of the immune response and inflammation [72]. The high consumption of NAD^+ by ARTD1 to generate PAR has secondary effects on the energy metabolism, apoptotic pathways and on a number of NAD^+ dependent enzymes, such as the Sirtuins as discussed above (introduction chapter 3.5) [73].

ARTD2 is the closest paralog to ARTD1 and is able to bind DNA through its WGR domain, which can also interact with RNA [74, 75]. ARTD2 has been associated with DNA repair pathways, such as base excision repair, and chromosome stability, however ARTD1 contributes to more than 90% of PAR produced during DNA damage conditions [60, 75, 76]. ARTD2 KO mice are viable like ARTD1 KO, but interestingly ARTD1 and ARTD2 double KO mice die at the onset of gastrulation [77]. ARTD1 and 2 have been identified to work in concert for example at stalled replication forks [78]. ARTD2 is also associated with metabolic regulation and

ARTD2 KO mice show increased energy expenditure and mitochondrial biogenesis [34].

ARTD 5 and 6 (also known as Tankyrase 1 and 2) poly-ADP-ribosylate cellular targets, however their biological functions are very different from ARTD1 and ARTD2 and involve telomere homeostasis, Wnt/β-catenin signaling, glucose metabolism and cell cycle progression [79]. Interestingly, some of these functions are executed through a process that involves PARylation of a target proteins by ARTD5 or 6, which acts as a signal for ubiquitination of the same target by the ubiquitin E3-ligase RNF146 and subsequent proteasomal degradation [46].

6.2 PARP inhibitors as therapeutics

PARP inhibitors (PARPi) are small molecules that are designed to inhibit the ADP-ribosylation activity of different ARTDs. Most PARPi are thought to interact with the NAD^+ binding sites in the catalytic domains of ARTDs, but show very different selectivity, potency and cytotoxicity [80].

Initially, PARPi were evaluated for their ability to sensitize tumor cells to conventional DNA damage inducing treatments, due to the central role of ARTD1 and 2 in the DNA damage response [81]. Cells deficient for the homologous recombination DNA repair pathway, such as BRCA1/2 mutated cells, were found to be sensitive to PARPi. This finding laid the foundation for the broad use of PARPi in cancer research [82, 83]. It is thought that this sensitivity to PARPi is following a classical synthetic lethality set up, a genetic concept, which proposes that the simultaneous perturbation of two genes (or proteins) results in cellular death, whereas the single perturbation would not have an effect [81]. However, the exact mechanism how PARPi exhibit their cytotoxic effect is still not very well understood. Inhibition of ARTD1 is thought to lead to an accumulation of DNA damage through obstructed single-strand break repair and/or trapping of ARTD1 at damaged sites on the DNA, thereby impairing DNA replication [81]. Furthermore other ARTD associated roles might be involved in the response to PARPi, such as chromatin remodeling, transcription, normal DNA replication as well as inflammatory responses [84, 85].

The PARPi olaparib (KuDOS/AstraZeneca), rucaparib (Pfizer/Clovis) and niraparib (Merck/Tesaro), are now approved as a monotherapy of advanced ovarian cancer for patients with germ line mutated BRCA1/2, who relapsed from previous chemotherapeutic treatments [81]. More than 70 clinical trials are ongoing for testing PARPi in various cancers [84].

The anti-inflammatory effect of PARPi has been shown in a variety of local inflammation models, where PARPi have been used to prevent innate immune responses and the onset of inflammatory diseases. More specifically, PARPi have shown to ameliorate acute organ damage upon LPS treatment in animal models and they reduce ischemia reperfusion injury or attenuate inflammation in models of colitis [86-90].

7 Functional roles of extracellular ADP-ribosylation

Members of the ARTC family ADP-ribosylate membrane proteins and proteins present in extracellular body fluids [25]. It is thought that ARTC mediated ADP-ribosylation is highly arginine specific and it was shown that a N-glycosidic bond between arginine and ADP-ribose is generated [91]. Arginine is positively charged at a neutral pH and its ADP-ribosylation brings in two negative charges, which will affect the electrostatic surface potential of the protein and may thereby modulate protein-protein interactions [91].

ARTC1 ADP-ribosylates members of the integrin family of adhesion molecules on skeletal muscle cells and leukocytes. Integrins function as mechanical linker between the intracellular cytoskeleton and the extracellular matrix and as an out-side-in transmitter of information on location, local environment, adhesive state and surrounding matrix. The integrin family of proteins consists of alpha (e.g. ITGA7) and beta subtypes (e.g. ITGB1), which form transmembrane heterodimers. These complexes exist in several conformational states, which dictate their extracellular ligand binding affinity and their intracellular interaction with cytoplasmic proteins. In an inactive state the integrins are usually in a bent form, while when activated they show an extended form. However, several intermediate states exist. [92]. ADP-ribosylation of integrin α7 (ITGA7) by ARTC1 modulates the

binding of integrin α7β1 to laminin [93]. It is proposed that an arginine residue located in the central region of ITGA7 is involved in the interaction with a negative region of ITGB1 and at low NAD^+ concentration (10 μM), the arginine in ITGA7 is ADP-ribosylated, subsequently repels ITGB1 and induces the formation of a high affinity conformer. In contrast, increasing NAD^+ concentration (100 μM) lead to ADP-ribosylation of additional site(s) located in the headpiece of ITGA7, where the ligand-binding site is located, resulting in steric hindrance and direct inhibition of ligand binding [94].

Another identified ARTC1 ADP-ribosylation target is the defensin, human neutrophil peptide 1 (HNP1). HNPs are host defense peptides, which contribute to innate immunity by microbial killing and regulating the inflammatory response. ARTC1, found on airway epithelial cells, ADP-ribosylates HNP1 on R14 and R24, altering its biological activity. ADP-ribosylated HNP1 has decreased antimicrobial and cytotoxic activities but still stimulated T cell chemotaxis. ADP-ribosylated HNP1 was found in bronchoalveolar lavage fluid from smokers but not from nonsmokers [95, 96].

ARTC1, 2.1 and 2.2 are GPI-anchored membrane proteins and seem to be concentrated in lipid rafts on the cell surface. This could give them specificity to other membrane proteins associated with lipid rafts [25]. ARTC2.2 is expressed on T cells, and one of its major targets is the P2X7 ion channel. MARylation of P2X7 on R125 leads to its activation and thereby induces the influx of Ca^{2+} and Na^+ as well as the efflux of K^+ [97]. Downstream effects of P2X7 activation include inflammasome activation, processing and release of cytokines (IL-1β, IL-18, IL-1 receptor antagonist and IL-36α), and the release and activation of meatlloproteases (mainly ADAM10 and 17) resulting in the shedding of cell-surface molecules [98]. Prolonged activation of P2X7 stimulates apoptosis [98]. This is observed in a process called NAD^+-induced cell death, where ARTC2.2 mediated ADP-ribosylation keeps the P2X7 channel open, leading to T cell death, already at extracellular NAD^+ concentration as low as 1 μM [35]. Interestingly, a recent study has shown that the activation of T cells or the ADP-ribosylation of P2X7 by ARTC2.2 leads to membrane-proximal proteolysis of ARTC2.2 itself by ADAM17 [99]. The proteolytic

shedding of ARTC2.2 shifts its substrate specificity from membrane proteins to secretory proteins [99]. So far it is not clear what the targets of soluble ARTC2.2 are. Soluble ARTC2.2 may provide an unknown mode of regulation by the ADP-ribosylation of cytokines or other secretory proteins and might be directly involved in modulating inflammatory reactions. Interestingly, the presumed ADAM17 cleavage site within ARTC2.2 close to the GPI-anchor is conserved in the GPI-anchored ARTC1 as well as ARTC3, indicating that they might also be shed [99].

8 Large-scale analysis of post-translational modifications by mass spectrometry

8.1 Identification of PTMs by mass spectrometry

Mass spectrometry (MS) has emerged as a powerful tool to systematically identify and quantify the cellular proteome and is also very well suited for the study of PTMs. Mass spectrometry allows the measurement of whole protein entities, called top-down proteomics, or the study of peptides generated by proteolytic cleavage of proteins, called bottom up proteomics. The big advantage of top down proteomic is that it allows the measurement of multiple PTM on the same protein, thereby identifying the exact proteoform. Top-down proteomics is technically and computationally very demanding and up to date it is not possible to analyze complex mixture, therefore the preferred and most widely used approach for proteome and PTM discovery consists in a combination of bottom-up proteomics and data dependent acquisition (DDA) [100] (Figure 7). In bottom-up proteomics proteins are extracted from a specific sample and are enzymatically digested (most commonly by trypsin) into peptides. Based on their hydrophobicity the peptides are subsequently separated on a reverse-phase liquid chromatography column (LC), which is coupled online to an electrospray. Peptides are ionized and transferred to the mass spectrometer, where their mass is determined before they are selected for fragmentation in the gas phase to generate MS/MS spectra. In conventional DDA approaches the data is collected by selecting a fixed number of peptide precursors for fragmentation based on their relative intensity [101].

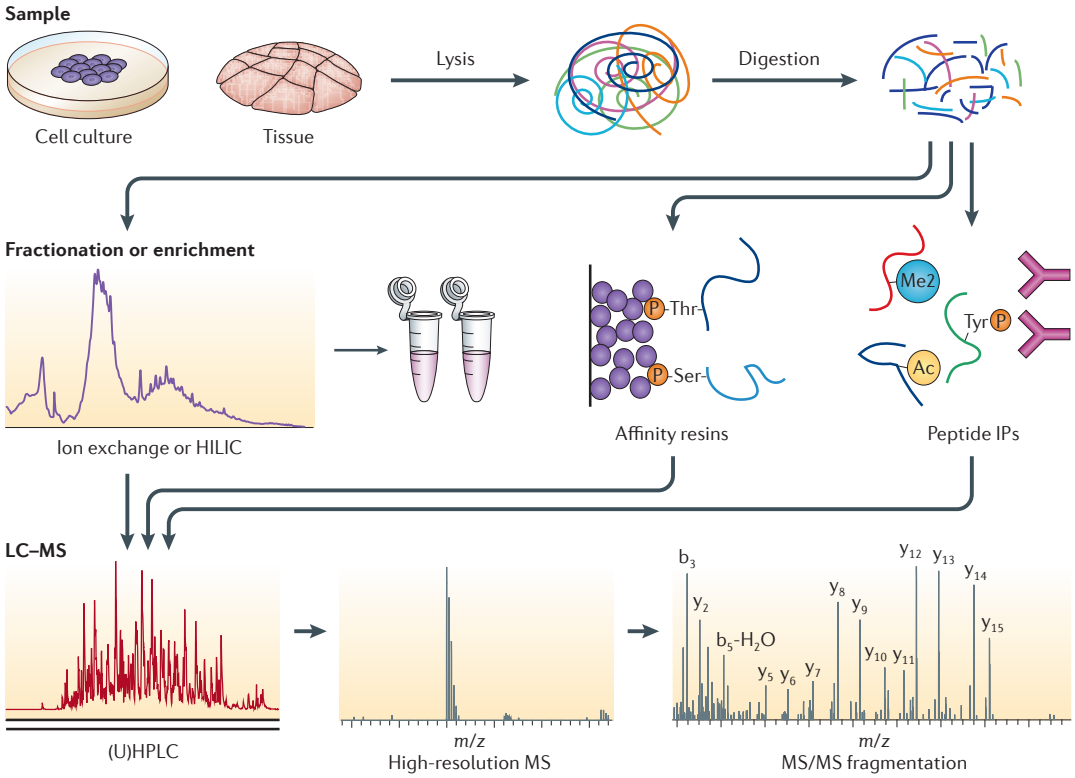

Figure 7 Proteomic workflow for the large scale identification of PTMs. Proteins are isolated from biological samples and are enzymatically digested into peptides. For large scale PTM analysis it is then necessary to reduce the complexity of the sample by enrichment of the modified peptides, using antibodies or affinity resins against the specific PTM (depicted here are phosphorylation, methylation and acetylation). Alternatively deep fractionation alone or in combination with enrichment also helps to reduce complexity. Samples are further resolved on a LC, eluted, ionized and introduced into the MS system. The MS records the peptide precursor ion mass-to-charge ratio (m/z) with high accuracy. In the common DAA mode single peptide precursors are then queried based on their intensity for fragmentation and a MS/MS measurement is performed to identify the peptide sequence and location of modifications. Adapted from [102].

Alternatively, other data collection methods, such as targeted proteomics or data independent acquisition (DIA) can be used and have been shown to increase the sensitivity and reproducibility of the measurement, also for peptides carrying PTMs. However, these latter approaches require advanced bioinformatics workflows and previous knowledge of the peptides one wants to look for [103].

To record peptide fragments in the MS/MS scan the selected peptide precursor needs to be fragmented. Usually collision-induced dissociation (CID) or higher-energy collisional dissociation (HCD) fragmentation is used, however other methods with different properties such as electron transfer dissociation (ETD) are available and are beneficial for the analysis of specific types of PTMs [100, 104, 105].

If the genome sequence of the analyzed organism is known, the MS/MS spectra can easily be analyzed by suitable software in order to identify the peptide sequence, map it to the respective protein, and relatively quantify the individual peptide types. PTMs on the peptides lead to characteristic mass shifts and can be computationally localized at single amino acid resolution on to the peptide sequence if the corresponding MS/MS spectrum has a high enough quality.

8.2 Enrichment of PTM carrying peptides

In order to reliably identify peptides carrying a specific type of PTM by MS in biological samples, it is often required to perform enrichments on the peptide or protein level, due to the low stoichiometry of PTM sites and the high sample complexity (Figure 7). In the case of serine/threonine phosphorylation the most efficient enrichment strategies consist of Immobilized Metal Affinity Chromatography (IMAC) or TiO_2 resins, which are however suboptimal for the less abundant tyrosine phosphorylation [106]. Tyrosine phosphorylation is more reliably identified using antibodies or engineered high affinity binding reagents [107]. Also for acetylation, ubiquitination and ubiquitination-like modifications antibody-based peptide enrichment techniques proved to be the most efficient methods for reliable identifications of many sites [106]. O- and N-glycosylation are successfully enriched using lectins which are carbohydrate binding proteins [106].

For individual PTM types, several factors need to be considered to perform proteomic experiments. This includes the absence of efficient enrichment reagents, the large amounts of starting material that is needed, the unfavorable physico-chemical properties of modified peptides and the PTM structure and stability. Certain modifications, such as glycosylation, with complex glycan structure, and nucleotide based PTMs may prove very difficult to be detected by MS due to ionization and fragmentation issues and might require enzymatic or chemical pre-treatment. Other modifications are very labile to sample preparation conditions such as pH, as for example histidine phosphorylation, undergo insource fragmentation upon ionization or are too extensively fragmented in the MS/MS to accurately localize them onto the peptide sequence [108, 109].

Stream-lined protocols for bottom-up proteomics are now widely available for a subset of PTMs such as phosphorylation, ubiquitination, ubiquitin-like modification, glycosylation, methylation, acetylation and other types of acylation [100]. Furthermore, many unique and innovative mass spectrometry based workflows have allowed the identification of exotic and previously unknown PTMs, such as different forms of lipidations [5].

8.3 Interpreting PTMs by proteomics exemplified by phosphoproteomics

At present, more than 260'000 PTM sites have been identified in the human proteome [110]. PTM proteomics studies have reached a remarkable depth and sophistication, with the main surprises being the high numbers of PTMs, their diversity and their involvement in all sorts of regulatory cellular processes, exemplified by several recent phospho-proteomic studies [100]. The deepest phospho-proteome ever measured for a single cell line identified 50'000 phospho-sites targeting 75% of the proteome [111]. Great improvements have also been made in the temporal resolution of PTM analysis. A recent study looking at the kinetics of phosphorylation based insulin signaling in mouse liver revealed that this is unexpectedly fast. *In vivo* insulin stimulation affected 10% of the liver phospho-proteome and maximal phosphorylation was already reached after 30s of insulin stimulation for many sites, such as functionally characterized phospho-sites on transcription factors [112].

To understand the principles of PTM signaling and function it is also important to study how PTMs and PTM sites evolved. The evolution of phospho-sites in the proteome was analyzed in closely related *Saccharomyces* fungi [113]. These species span a divergence time of around 18 million years, which is comparable with the time separating humans from their last common ancestor with the apes. 3000 to 5000 phospho-sites per species were detected and it was found that around 69% of phospho-sites were not present in the last common ancestor. Extending the analysis and comparing 18 different fungal species with a common ancestor 700 million years ago, the authors of that study found that only 2% of phosphorylation sites are conserved. This is in stark contrast to the conservation of

overall protein domains, where more than 73% are conserved since the last common ancestor. Lack of conservation appears to contradict the view that phosphorylation is a strictly controlled and regulated event. Indeed, it is likely that there exists a certain level of phosphorylation "noise", due to kinase promiscuity, however noise opens up the possibility for evolutionary adaptation and can be a phenotypic attribute [114]. It is proposed that the rapid evolution of phosphorylation or other PTMs can contribute to phenotypic diversity in various systems, for example in yeast adapting to a new environment, but also in cancer cells circumventing growth control [114].

9 Proteome-wide Identification of ADP-ribosylation by Mass Spectrometry

9.1 Challenges in identifying the ADP-ribosylome

To elucidate the functional role of protein ADP-ribosylation, systematical analysis of all ADP-ribosylated proteins and identification of their ADP-ribose acceptor sites are necessary. Mass spectrometry-based proteomics is probably the most powerful tool for the analysis of PTMs. However, the analysis of ADP-ribosylation has proven to be very challenging for several reasons, including the highly transient nature and the low abundance of ADP-ribosylated proteins, the special physicochemical properties of the PTM (bulky, highly charged, heterogeneous structure, labile), and the number of different amino acids that were reported to be modified (glutamic acid, aspartic acid, lysine, arginine, serine and cysteine) [14, 109]. Characterization of ADP-ribose acceptor sites by MS has significantly improved following the development of high-resolution mass spectrometers and novel fragmentation techniques. As discussed in the following sections, ADP-ribosylation sites can now be identified at a single amino acid resolution in many cases, since several enzymatic and chemical treatments have been established to reduce the complexity of ADP-ribosylation and since specialized MS methods combining multiple fragmentation types were integrated [109].

Comparable to many other PTMs, the fraction of ADP-ribosylated cellular proteins is very low. Thus, studying this group of modified proteins requires specific

ADP-ribosylated protein/peptide enrichment methodologies. Great successes have been made by applying affinity purifications, phosphoproteomic enrichment techniques or chemical proteomic approaches as discussed below. However, there is still no approach or reagent available that has a high efficiency for binding to ADP-ribose independent of the amino acid acceptor sites.

Sample preparation methods are critical since PARylation as well as MARylation are highly transient PTMs, which are reversed within minutes by hydrolases. Additionally, introduction of stress, DNA damage or release of NAD^+ during cell lysis may lead to sample preparation-induced ADP-ribosylation [50].

PARylation as a huge, heterogeneous and highly charged peptide modification is so far incompatible with current peptide MS methods and no established workflows are able to differentiate between MARylation and PARylation sites.

9.2 Affinity purification of ADP-ribosylated proteins

Several large scale proteomic studies have been performed in which specific ADPr affinity enrichment techniques were applied on the protein level in order to identify proteins that are associated with MAR or PAR [50, 115-117]. These studies could not identify which proteins are ADP-ribosylated, nor is the enrichment specific enough to determine ADP-ribosylation sites, however they represent an important early contribution to the identification of the ADP-ribosylome and several conclusions could be made. The experimental set up for these studies consisted of human cells that were exposed to genotoxic stress treatments to stimulate the PARylation activity of ARTD1 and 2. Cells were lysed and, subsequently, ADP-ribosylated proteins were enriched with the 10H anti-PAR antibody, or ADPr binding proteins, such as PARG-dead or Af1521. Proteins were digested into peptides and identified by MS. The enrichment is performed under non-denaturing conditions in these approaches, therefore the identified proteins consist not only of ADP-ribosylated proteins but also of ADP-ribose interactors and more importantly of the large non-covalent interaction network, summarized as the ADP-ribosylated interactome [50, 115-118]. These studies identified around 830 proteins, and could

link them to the canonical role of PARylation, the DNA damage response, but also to novel interesting biological functions, such as RNA processing, stress granules, the mitotic spindle and nucleoli [109]. The overlap of the identified proteins in the individual studies is very limited, less than 50%, most probably due to the very different enrichment approaches and different cell lysis procedures. To fully understand the functional contribution of ADP-ribosylation to biological processes and to make mechanistic predictions, it is important to resolve ADP-ribosylation at the level of the amino acid attachment site.

9.3 Phosphoproteomic enrichment approaches

Phosphopeptide enrichments were also found to co-enrich ADP-ribosylated peptides, and protocols have been optimized for the specific enrichment of ADP-ribosylated or phospho-ribosylated peptides [119-122]. Phosphodiesterases (such as snake venom phosphodiesterase) and NUDIX hydrolases were used to reduce MAR or PAR to a protein-bound phospho-ribose [122, 123]. The resulting phospho-ribosylated peptides are subsequently enriched using either Fe(III)-IMAC or TiO_2 microspheres, which have a high affinity for phospho groups. The conversion of protein-bound MAR or PAR to phospho-ribose leads to a detectable mass signature of 212.01 Da. Phosphoproteomic approaches have proven useful in the analysis of *in vitro* ADP-ribosylated proteins or purified protein fractions. In contrast, for cellular proteomic approaches these techniques lack sensitivity due to the co-enrichment of the much more abundant phosphorylated peptides and, thus, only few *in vivo* targets could be detected so far [124, 125].

9.4 Chemical-proteomic approaches based on boronate affinity chromatography

An enrichment protocol based on the isolation of ADP-ribosylated peptides by boronate affinity chromatography and subsequent modified peptide elution using hydroxylamine (NH_2OH) highlighted for the first time the widespread ADP-ribosylation of substrate proteins [58]. Boron covalently binds ADP-ribosylated proteins through esterification with the 1,2-*cis*-diol moieties within ADP-ribose. The ester bond between the first ADP-ribose unit of PAR and the side chain of the

carboxyl group of an ADP-ribosylated aspartic or glutamic acid is susceptible to NH_2OH attack. This reaction converts the ADP-ribosylated acidic amino acid into a hydroxamic acid derivative, adding 15.01 Da to the initial amino acid weight, which is detectable by MS and provides ADP-ribose acceptor site localization information (Figure 8A).

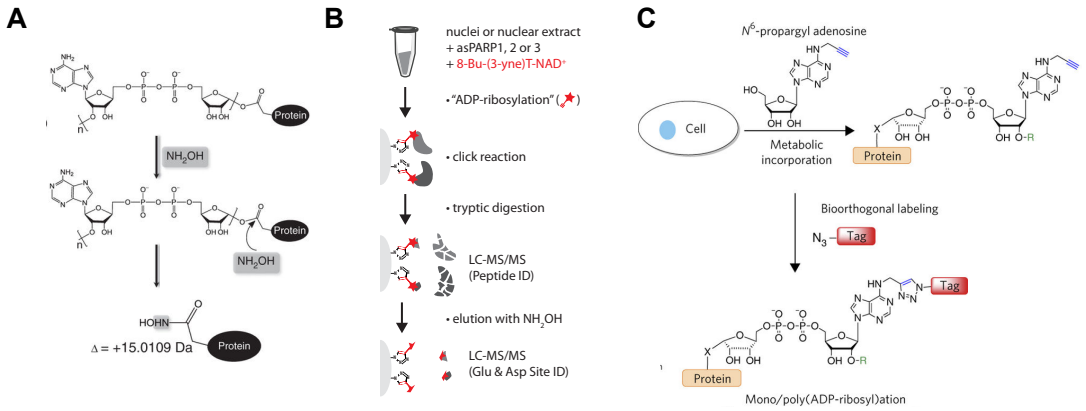

Figure 8 Overview of chemical proteomic strategies to identify ADP-ribosylation sites or ADP-ribosylated proteins. A) Principle of hydroxylamine elution, to identify ADP-ribosylation sites on acidic amino acids, as applied after boronate affinity chromatography. Adapted from [58]. B) Chemical-genetic enrichment approach using labeled NAD^+ and engineered ARTDs. Adapted from [126] C) Labeling of Adenosine, which is metabolically incorporated into cells, converted to labeled NAD^+ and used for ADP-ribosylation, can be employed to enrich modified proteins. Adapted from [127].

The major drawback of this protocol is that the chemical reaction employed here, limits the detection of ADP-ribosylated amino acids to glutamates and aspartates. Furthermore it is difficult to prove that the observed sites really stem from previously ADP-ribosylated residues. The study identified 1048 potential ADP-ribosylation sites on E and D on 340 proteins, involved in a wide array of nuclear functions. Most of the observed sites were sensitive to PARP inhibitor treatment. Additionally, hydroxylamine treatment has also been used as a stand-alone procedure without any enrichment, but this method only seems useful for strongly ADP-ribosylated targets [128].

9.5 Chemical proteomic enrichment based on NAD^+ or precursor labeling

Several chemical proteomic approaches exist in which NAD^+ or NAD^+ precursors are labeled with a functional chemical group, which can later be employed for ADP-ribosylated protein or peptide enrichment [59, 127, 129-131].

An *in vitro* chemical genetic methodology that allowed the identification of protein targets specific for ARTD1, ARTD2 and ARTD3 was recently published [59]. This approach is based on the combined use of a newly developed NAD^+ analog, 8-Bu(3-yne)T-NAD^+, and engineered analog-sensitive ARTD1, ARTD2, and ARTD3 mutant protein (asPARPs). Analog sensitivity was achieved by modifying the ART active site to accommodate the bulky 8-Bu(3-yne)T-NAD^+. Importantly, the modification of proteins using this NAD^+ analog allowed downstream azide-alkyne cycloaddition ("click" chemistry), which enabled ARTD target labeling and purification (Figure 8 B). In contrast to previous attempts [129, 130], screening of an NAD^+ analog library with systematically mutated ARTD1 isoforms identified functional combinations that are still able to promote PARylation [59]. Using this approach, HeLa cell nuclear extracts were co-incubated with purified salmon sperm DNA-activated asPARP1-3 and 8-Bu(3-yne)T-NAD^+. The asPARP-modified protein targets were purified by "click" chemistry-based azide-agarose crosslinking, trypsin digested, and identified by MS. Asp and Glu ADP-ribosylated peptides were eluted with hydroxylamine and the peptides as well as the hydroxamic acid signature measured by MS. The same workflow was also applied to nuclei isolated from *Parp1*$^{-/-}$ mouse embryonic fibroblasts (MEFs) overexpressing asPARP-1. A total of 467 *in vitro* ADP-ribosylated proteins were identified [59]. A handicap of this methodology is that 8-Bu(3-yne)T-NAD^+, like NAD^+, is not cell permeable, and can only be used in *in vitro* or in isolated nuclei-based ADP-ribosylation reactions. It is also unclear whether 8-Bu(3-yne)T-NAD^+-derived modifications are as reversible as authentic ADP-ribosyl modifications. Furthermore, exogenous addition of asPARPs and the NAD^+ analog may cause off-target modifications due to non-physiological concentrations. Potential modifications of other amino acids, e.g., Ser, Lys or Arg cannot be identified [126].

A Similar approach by another group was performed with the MARylating ARTD10 and 11, where several hundred targets were identified *in vitro* using HEK or HeLa cell lysates. The study showed that ARTD11 might have a role in nuclear pore biology [131].

In a novel innovative approach NAD^+ was not tagged itself, but an alkyne-adenosine analog, *N^6-propargyl* adenosine [127]. This analog is metabolically incorporated into mammalian cells, where it is converted to *N^6-propargyl* NAD^+ and eventually used by ARTDs for ADP-ribosylation. *N^6-propargyl* labeled ADP-ribosylated proteins were conjugated with azide–biotin, affinity purified with streptavidin beads and subjected to on-bead protease digestion that was followed by protein identification using MS (Figure 8 C). This approach has not been combined with ADPr site-specific mapping approaches yet, however the method is very promising, since it can be applied *in vivo*, unlike approaches where NAD^+ is labeled and engineered proteins need to be used.

10 Mass spectrometric identification of ADP-ribose acceptor sites

Great advances have been made in establishing techniques for the identification of the ADP-ribosylome. However, the most challenging part of this undertaking is to identify endogenous ADP-ribosylation sites on the protein sequences with a high probability. The functional role of ADP-ribosylation of a specific protein can only be addressed if the exact modification site is known. This knowledge is equally important for systems biology studies of the ADP-ribosylome as well as for mechanistic studies in which the modification site is mutated in recombinant proteins or directly in cells by targeted genome editing. For a long time, the identification of ADP-ribosylation sites has been hampered by low efficient and biased ADPr-peptide enrichment strategies (as discussed above), technical limitations of mass spectrometers or by insufficient bioinformatic solutions [58, 109, 132].

Major advancements have been made in the core technology of mass spectrometry over the last decade, thereby dramatically increasing the sensitivity and resolution, and it is expected that this fast development will continue [100]. Novel and customizable peptide fragmentation techniques are now widely available and facilitate PTM analysis. Early studies noticed that MS identification of ADP-ribosylation sites is highly dependent on the applied fragmentation technique. Initial studies of ADP-ribosylated peptides were dependent on collision-induced

dissociation (CID), the main fragmentation technique available at that time. The problem with CID was, that it either led to complete fragmentation of the ADP-ribose moiety or to incomplete fragmentation of the peptide backbone, preventing identification of ADP-ribosylation sites in most cases. It was noticed that fragmentation of the ADP-ribose moiety led to a set of indicative ADP-ribose marker ions (Figure 9) [133, 134].

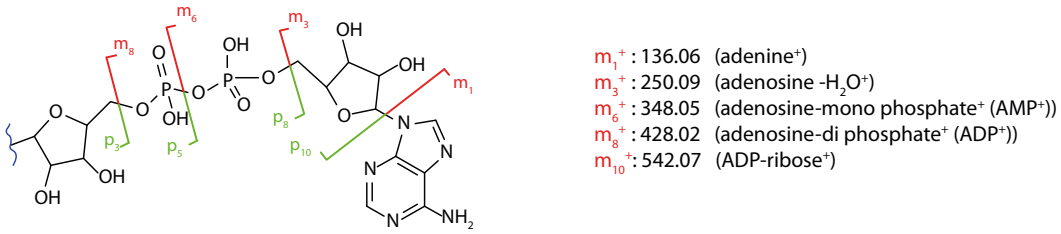

Figure 9 Marker ions produced by the fragmentation of the ADP-ribose moiety.

The introduction and wide availability of electron transfer dissociation (ETD) has been beneficial for the analysis of several PTMs since it leads to the stabilization of labile PTMs on the peptide and to a better fragment ion series, which allows better sequence and modification site assignments [135]. Indeed ETD has proven to be advantageous for the localization of ADP-ribosylation sites, since it usually leaves the ADP-ribose unit on the peptide fragment ions and leads to proper fragmentation of the peptide backbone [136, 137]. Systematic analysis of in vitro ADP-ribosylated ARTDs and histones revealed that also the now broadly available higher energy collisional dissociation (HCD) fragmentation led to the efficient identification of ADP-ribosylation sites [137]. HCD was a shown to be somewhat less accurate than ETD in localizing the ADP-ribosylation sites, however led to the identification of many more ADP-ribosylated peptides [134, 137]. Furthermore the indicative ADP-ribose fragmentation ions produced during HCD fragmentation were used in a product dependent manner to selectively fragment only potentially ADP-ribosylated peptides, increasing the number of identifications as well as the accuracy of the site assignments [137]. Still it is not clear if specific fragmentation methods have biases towards specific amino acid acceptor ADP-ribose linkages.

AIMS OF THE THESIS

ADP-ribosylation occurrence, dynamics and function on a system level remain elusive or only vaguely described. The aim of this PhD project was to map ADP-ribosylation sites across the proteome (i.e. the ADP-ribosylome), to identify their writers under basal and stressed conditions in cultured cells and in mouse tissues. Furthermore, we aimed to elucidate the functional consequences of particular identified sites. The thesis addressed the following specific aims:

(i) To develop proteomic methods for enrichment of endogenous ADP-ribosylated proteins or peptides and to analyze ADP-ribosylation sites by optimized mass spectrometric methods.

(ii) To define the contribution and site specificity of ARTD1 and ARTD2 to the cellular ADP-ribosylome under oxidative stress conditions in cultured cells.

(iii) To elucidate the mouse heart and skeletal muscle ADP-ribosylome under basal and inflammatory conditions with a focus on the role of ARTC1.

RESULTS

1 Overview of published manuscripts

1.1 Proteome-wide identification of the endogenous ADP-ribosylome of mammalian cells and tissue

Authors: Martello R.*, **Leutert M.***, Jungmichel S.*, Bilan V., Larsen S.C., Young C., Hottiger M.O., and Nielsen M.L.
*equal contribution

Journal: Nature Communications (2016), 10.1038/ncomms12917

Link: https://www.nature.com/articles/ncomms12917

Contribution: Prepared samples, performed MS measurement and analysis of mouse liver, HeLa and recombinant protein samples. Assisted in the development of certain aspects of the method. Performed *in vitro* ADP-ribosylation assays, (Figure 3c-e, Figure 4, Figure S3, Figure S4 c,f, Figure S5 c,d). Assisted in writing the paper.

1.2 Combining Higher-Energy Collision Dissociation and Electron-Transfer/Higher-Energy Collision Dissociation Fragmentation in a Product-Dependent Manner Confidently Assigns Proteomewide ADP-Ribose Acceptor Sites.

Authors: Bilan V.*, **Leutert M**.*, Nanni P.*, Panse C., and Hottiger M. O.
*equal contribution

Journal: Analytical chemistry (2016), 10.1021/acs.analchem.6b03365

Link: http://pubs.acs.org/doi/abs/10.1021/acs.analchem.6b03365

Contributions: Planned the experiments, prepared samples, optimized MS parameter and measurements, performed data analysis together with B.V and P.N. Assisted in writing the manuscript.

1.3 Analysis of Chromatin ADP-Ribosylation at the Genome-wide Level and at Specific Loci by ADPr-ChAP

Authors: Bartolomei G., **Leutert M**., Manzo M., Baubec T., Hottiger M.O.

Journal: Molecular Cell (2016), 10.1016/j.molcel.2015.12.025

Link: http://dx.doi.org/10.1016/j.molcel.2015.12.025

Contributions: Performed chromatin immuno purification and chromatin affinity purification experiments and biochemical assay (Figure 3 E, Figure S1 C,D, Figure S2 C,D, Figure S5 A-F).

1.4 Identification of ADP-Ribose Acceptor Sites on In Vitro Modified Proteins by Liquid Chromatography-Tandem Mass Spectrometry.

Authors: **Leutert M.***, Bilan V. *, Gehrig P., Hottiger M.O.
*equal contribution

Journal: Methods Molecular Biology (2017), 1608, 137-148.

Link: https://link.springer.com/protocol/10.1007%2F978-1-4939-6993-7_10

Contributions: Performed enrichment, MS measurement and data analysis together with P.G, wrote the chapter together with V.B and M.O.H.

1.5 Proteome-Wide Identification of In Vivo ADP-Ribose Acceptor Sites by Liquid Chromatography-Tandem Mass Spectrometry.

Authors: Larsen S.C.*, **Leutert M.***, Bilan, V., Martello, R., Jungmichel, S., Young, C., Hottiger, M.O., and Nielsen, M.L.
*equal contribution

Journal: Methods Molecular Biology (2017), 1608, 149-162.

Link: https://link.springer.com/protocol/10.1007%2F978-1-4939-6993-7_11

Contributions: Created figures and assisted in writing the chapter.

1.6 Identification of PARP-Specific ADP-Ribosylation Targets Reveals a Regulatory Function for ADP-Ribosylation in Transcription Elongation

Authors: **Leutert M.**, Pedrioli, D.M., and Hottiger, M.O.

Journal: Molecular Cell (2016), 10.1016/j.molcel.2016.07.006

Link: http://dx.doi.org/10.1016/j.molcel.2016.07.006

Contributions: Created figures and wrote the preview together with D.M.P. and M.O.H.

2 Overview of submitted manuscripts

2.1 Comprehensive in vivo ADP-ribosylome analysis identifies tyrosine ADP-ribosylation of HPF1 and reveals that this modification modulates ARTD1 activity

Authors: Leslie Pedrioli, D.M*, **Leutert M**.*, Bilan V., Nowak K., Gunasekera K., Ferrari E., Imhof R., Malmstöm L., Hottiger M.O.
*equal contribution

Contribution: Generated shARTD1 and shARTD2 HeLa cell lines, performed sample preparation, MS measurement and data analysis. Established label free quantification workflow and analysis of ADP-ribosylated peptides. Contributed in conceiving the project, participated in manual spectra validation and assisted in writing the paper.

2.2 Proteomic analyses identify ARH3 as a serine mono ADP-ribosylhydrolase

Authors: Abplanalp J., **Leutert M.**, Frugier E., Nowak K., Feurer R., Kato J., Kistemaker H. , Filippov D.V., Moss J., Caflisch J., Hottiger M.O.

Contribution: Performed sample preparation, MS measurements, label free quantification and data analysis. Established ADP-ribosylated peptide demodification and MS quantification assay. Assisted in writing the paper.

2.3 Ecto-ADP-ribosyltransferase ARTC2.1 functionally modulates FcγR1 and FcγR2B on microglia

Authors: Rissiek B., Menzel S., **Leutert M.**, Cordes M., Behr M., Ludewig P., Gelderblom M., Rissiek A., Adriouch S., Hottiger M.O., Koch-Nolte F., Magnus T.

Contribution: Performed sample preparation, MS measurements and data analysis and interpretation. Assisted in writing the paper.

3 Prepared but not yet submitted manuscript

3.1 Proteomic characterization of the heart and skeletal muscle reveals widespread Arginine ADP-ribosylation by the ectopic ADP-ribosyltransferase ARTC1

Authors: **Leutert M.**, Menzel S., Braren R., Rissiek B., Gehrig P., Zolkiewska A., Koch-Nolte F., Hottiger M.O.

Contribution: Conceived and planned the project, performed sample preparation, MS measurments, label free quantification and data analysis. Assisted in writing the paper.

nature COMMUNICATIONS

ARTICLE

Received 7 Apr 2016 | Accepted 15 Aug 2016 | Published 30 Sep 2016

DOI: 10.1038/ncomms12917 OPEN

Proteome-wide identification of the endogenous ADP-ribosylome of mammalian cells and tissue

Rita Martello[1,*], Mario Leutert[2,3,*], Stephanie Jungmichel[1,*], Vera Bilan[2,3], Sara C. Larsen[1], Clifford Young[1], Michael O. Hottiger[2] & Michael L. Nielsen[1]

Although protein ADP-ribosylation is involved in diverse biological processes, it has remained a challenge to identify ADP-ribose acceptor sites. Here, we present an experimental workflow for sensitive and unbiased analysis of endogenous ADP-ribosylation sites, capable of detecting more than 900 modification sites in mammalian cells and mouse liver. In cells, we demonstrate that Lys residues, besides Glu, Asp and Arg residues, are the dominant *in vivo* targets of ADP-ribosylation during oxidative stress. In normal liver tissue, we find Arg residues to be the predominant modification site. The cellular distribution and biological processes that involve ADP-ribosylated proteins are different in cultured cells and liver tissue, in the latter of which the majority of sites were found to be in cytosolic and mitochondrial protein networks primarily associated with metabolism. Collectively, we describe a robust methodology for the assessment of the role of ADP-ribosylation and ADP-ribosyltransferases in physiological and pathological states.

[1] Faculty of Health Sciences, Department of Proteomics, The Novo Nordisk Foundation Centre for Protein Research, University of Copenhagen, DK-2200 Copenhagen, Denmark. [2] Department of Molecular Mechanisms of Disease, University of Zurich, Zurich CH-8057, Switzerland. [3] Molecular Life Science Program of the Life Science Graduate School, University of Zurich, Zurich CH-8057, Switzerland. * These authors contributed equally to this work. Correspondence and requests for materials should be addressed to M.L.N. (email: michael.lund.nielsen@cpr.ku.dk).

Protein ADP-ribosylation refers to the process where an ADP-ribose moiety is transferred from NAD^+ to the amino acid side-chains of target proteins (as mono-ADP-ribose, MAR) or to an already protein bound ADP-ribose to form poly-ADP-ribose (PAR). These modifications are primarily catalysed by a class of enzymes known as ADP-ribosyltransferases (ARTs), with certain Sirtuin deacetylases also being able to catalyse ADP-ribosylation[1]. The ARTs can be divided further into two major subclasses: ARTCs (cholera toxin-like) and ARTDs (diphtheria toxin-like, formerly called poly(ADP-ribose) polymerases (PARPs)), depending on their conserved structural features[2].

While MARylation has been reported to modulate GSK3β kinase activity and NF-κB signalling[3], little is known about the biological functions of this type of modification. In contrast, PARylation has emerged as a crucial post-translational modification (PTM) in cancer development[4]. PARylation is a transient PTM[5], whose rapid cellular degradation is predominantly carried out by PAR glycohydrolase (PARG)[6]. While PARylation is a key component of the DNA damage response (DDR) via its central role in the base excision repair pathway, many of the molecular details and processes affected by ARTs remain poorly understood. As a result, a detailed understanding of the molecular mechanisms and functions affected by ADP-ribosylation remains elusive.

In particular, the inventory of the amino acid residues modified by ADP-ribosylation remains incomplete. Current experimental evidence suggests that ADP-ribosylation primarily occurs on four different amino acids; Lys[7], Arg[8], Asp and Glu residues[9]. In addition, Cys residues were reported to be MARylated by certain ARTDs or bacterial toxins[10]. High-resolution mass spectrometry (MS) has become a valuable tool for comprehensive identification of PTMs[11]. However, current MS-based approaches for mapping ADP-ribosylation sites are biased towards modifications of only Glu and Asp[9], or they lack sensitivity due to co-enrichment of other PTMs (that is, phosphorylated peptides)[12].

Moreover, protein ADP-ribosylation is a low-abundant PTM that is rapidly degraded. To overcome this challenge cellular PARG knockdowns (siPARG) or knockouts have been developed[9,12]. Unfortunately, cellular absence of PARG leads to physiological alterations in cells, hepatocellular carcinoma in mice[13], progressive neurodegeneration[14] and excessive accumulation of PAR chains that are not rapidly degraded and promote cell death via parthanatos[15]. Consequently, strategies requiring knockdown of PARG constitute an improper setting for analysing physiological ADP-ribosylation and its associated mechanisms, thus rendering these methods inapplicable for *in vivo* analysis of tissues without genetic interventions[16]. Moreover, while ADP-ribosylation has been known for more than 50 years, the cellular stoichiometry of the modification has remained elusive, primarily due to the lack of methodologies that can elucidate such information[17].

Recently a chemical genetic discovery method for ARTD targets was reported[18], where the NAD^+ analogue 8-Bu(3-yne)T-NAD^+ was incubated with cell lysates from cells overexpressing mutated ARTDs sensitive to the analogue or cell lysates spiked with recombinant mutated ARTDs. However, as NAD^+ is impermeable to the cell membrane, this method requires either the lysis of cells or the isolation of organelles (that is, nuclei) followed by the complementation of exogenous 8-Bu(3-yne)T-NAD^+, which renders the identification of ARTD-specific substrates under different cellular conditions, and at physiological NAD^+ levels unattainable. Moreover, the ADP-ribose acceptor sites identified using this methodology were limited to Glu and Asp modifications[9].

To address these limitations, we have developed a protocol for the unbiased mapping of endogenous ADP-ribosylation sites in proteins. Our method led to the identification of more than 500 endogenous ADP-ribosylation sites in a single analysis and, as a result, provides an unprecedented in-depth analysis of protein ADP-ribosylation. Importantly, as the described workflow is applied under genetically unperturbed physiological conditions, we have used our methodology to analyse ADP-ribosylation sites in both cultured mammalian cells and mouse liver. Collectively, the workflow presented here represents a major advance in the detection of ADP-ribose acceptor sites and the identification of cellular processes regulated by ADP-ribosylation. Thus, facilitating a better understanding of the complex physiological and pathological processes that involve ADP-ribosylation, and the treatment of such conditions with PARP (that is, ADP-ribosylation) inhibitors.

Results

Identification of endogenous ADP-ribosylation sites. We have developed a technology for sensitive analysis of endogenous ADP-ribosylation sites in both cells and tissues that overcomes several of the above-mentioned limitations of current approaches. Briefly, proteins are isolated from cells, digested into peptides first using LysC and then trypsin. We then treat the cellular peptide digest with PARG, thereby converting all PARylated amino acids to their MARylated counterparts[19]. While this prevents discriminating whether the modification was originally PARylation or MARylation, the conversion is crucial for feasible MS analysis. Furthermore, this has the advantage that MARylated peptides can be unbiasedly enriched with an ADP-ribose-specific domain[20]. In contrast to previously described methodologies[21], enrichment at the peptide level with Af1521 in combination with prior PARG treatment has not been performed before. Subsequently, the enriched ADP-ribosylated peptides and their acceptor sites are identified using a high-resolution Orbitrap mass spectrometer (Q Exactive HF). As no pre-fractionation steps are employed, the described workflow analyses ADP-ribosylated peptides from a single sample requiring only a few hours of sensitive LC-MS operation[22]. All peptides are fragmented using higher-energy collisional dissociation (HCD) ensuring high p.p.m. accuracy on both the precursor and fragment ions[23]. Furthermore, ADP-ribosylated peptide identification is aided by diagnostic ions originating from the fragmentation of the ADP-ribose group linked to the peptide[24,25] (Supplementary Fig. 1a). Superior advancements over current methodologies are as follows: First, sample preparation without ARTD, NAD^+ or PARG level perturbation[9,18] allows analysis of both cells and tissues under physiological conditions. This will allow us to broaden our understanding of the mammalian ADP-ribosylation complexity, and facilitating comparisons across any cellular condition, cell type and, even, species. To substantiate this, we have applied our established method to HeLa cells exposed to hydrogen peroxide (H_2O_2)-induced oxidative stress (Fig. 1a), and to normal mouse liver samples. Second, using the Af1521 macro domain to enrich ADP-ribosylated peptides, which has favourable binding preferences and relatively high ADP-ribose affinity with a Kd of ~0.13 μM (ref. 26), allowed unbiased modified amino acid analysis. Third, we have ensured prevention of lysis-induced ADP-ribosylation artefacts, as previously reported[20], thus facilitating assessment of the ADP-ribosylome during actual physiological conditions.

Identification of the H_2O_2-induced ADP-ribosylome. To benchmark our methodology, we treated HeLa cells with 500 μM H_2O_2, which induces PAR formation through oxidative stress

NATURE COMMUNICATIONS | DOI: 10.1038/ncomms12917

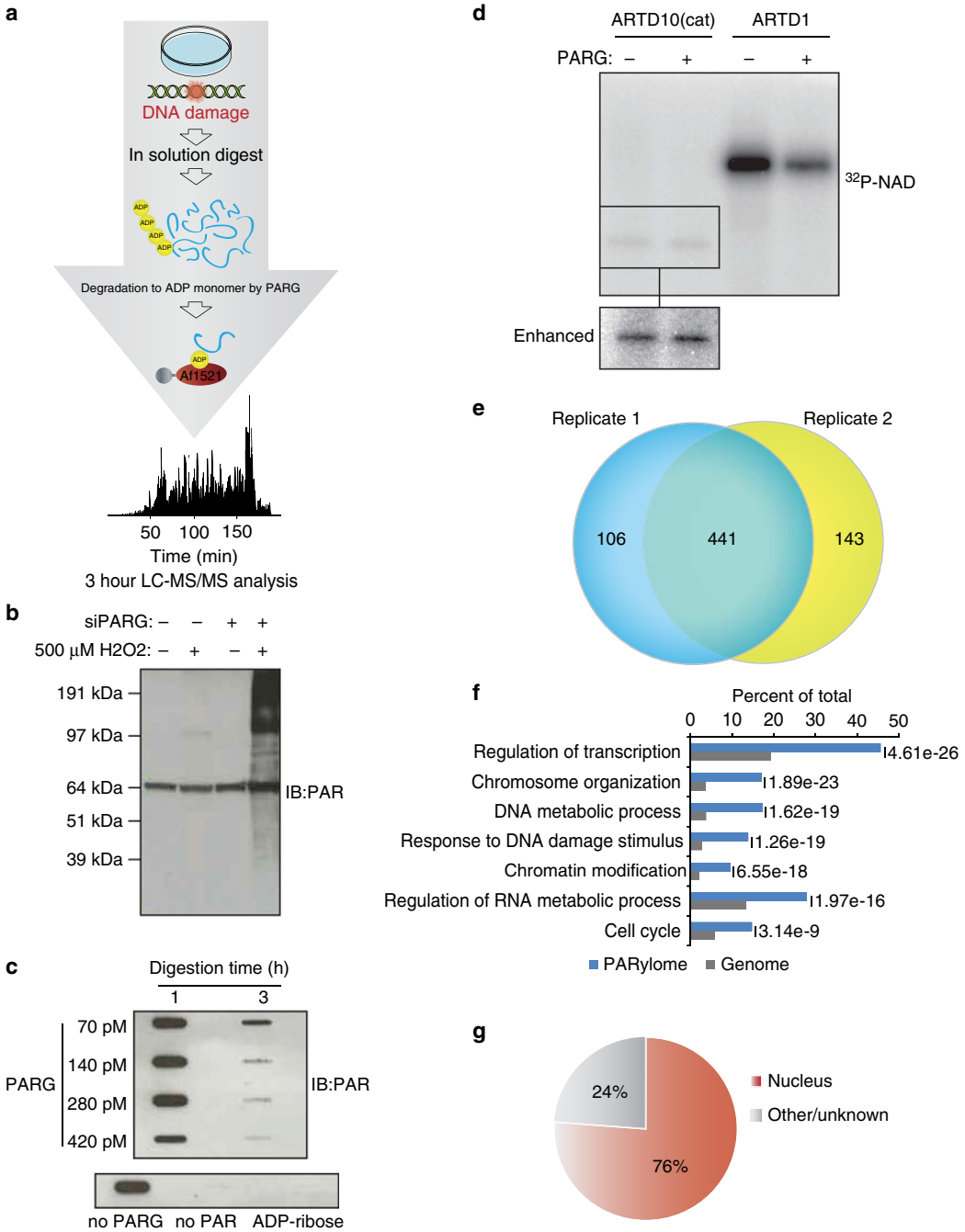

Figure 1 | Proteome-wide identification of endogenous ADP-ribosylation sites in human cell culture. (**a**) Schematic representation of the peptide-based enrichment strategy. HeLa cells were treated with genotoxic stress and digested into peptides. Tryptic digested peptides were treated with PARG enzyme to convert multimeric ADP-ribosylation into monomeric counterparts, and subsequently ADP-ribosylated peptides were enriched using GST-Af1521 macrodomain. Enriched peptides were analysed by high-resolution LC-MS/MS on an Orbitrap Q-Exactive HF instrument and the data was further processed by bioinformatic software tools. (**b**) Comparison of HeLa cells exposed with 500 µM H_2O_2. During cellular knock-down of PARG enzyme (siPARG) an abundant PAR signal is observed, while under physiological conditions the PAR signal is significantly weaker (compare second lane with fourth lane on gel). Previous methods for characterizing ADP-ribosylation solely worked under siPARG conditions while the methodology described here is applicable to physiological conditions. (**c**) Optimization of the incubation time and amount of PARG enzyme required for converting multimeric ADP-ribosylated peptides into monomeric counterparts. (**d**) Validation experiment that confirms PARG treatment does not remove MAR from investigated peptides. (**e**) Venn diagram of identified ADP-ribosylation sites identified in two biological replicate analyses. A strong overlap in identified sites signifies high reproducibility in the developed method. (**f**) GO functional annotation of significantly regulated proteins in the combined data set reveal strong enrichment of proteins involved in DNA repair processes compared with annotated GO genes across the entire human genome (indicated *P*-values < 0.005). (**g**) GO term annotation enrichment for cellular distribution of proteins harbouring ADP-ribosylation sites.

signalling. Under physiological conditions (non-siPARG conditions), H_2O_2 treatment induces PAR levels only faintly detectable by immunoblot (Fig. 1b), while cellular knock-down of PARG via small interfering RNA (siPARG) causes strong PAR formation (Fig. 1b). This demonstrates the requirement for improved sensitivity in studying ADP-ribosylation under unperturbed physiological conditions.

To ensure complete catalysis of PARylated into MARylated peptides we next assessed the amount of PARG required to catalyse a fixed amount of PAR. Previously, PAR levels in HeLa cells have been reported to range up to 0.1 amol per cell during H_2O_2 treatment[27]. Thus, we incubated 10 μM of purified PAR with increasing concentrations of PARG and assessed the temporal efficiency of the catalysis by immune-slot blot (Fig. 1c). Since the most efficient catalysis was observed when PAR was treated with PARG for 3 h, we concluded that this enzyme ratio allowed enzymatic catalysis of PARylated peptides into MARylated peptides during our enrichment procedure.

As some macrodomains can exhibit hydrolase activity on MAR moieties[28,29], we performed the Af1521 enrichment procedure at 4 °C and incubated samples for only two hours. Moreover, all subsequent sample handling steps were performed at 4 °C, which collectively prevents hydrolase activity of the Af1521 macro domain[20]. To confirm that PARG exerted no enzymatic hydrolase activity on MAR (ref. 19) in our workflow, we assessed whether PARG removes ADP-ribosylation from automodified ARTD1 (also PARP1) or ARTD10 (formerly PARP10; Fig. 1d), which are known PARylated and MARylated substrates[30], respectively.

Using autoradiography assays, hydrolysis of the attached radioactive [^{32}P]-PAR of the protein substrates was monitored (Fig. 1d), revealing that PARG was indeed able to convert PAR chains on ARTD1 into MAR, while no reaction was observed regarding the auto-MARylation of ARTD10 (Fig. 1d). These results confirmed that PARG hydrolase activity would not affect enrichment of MAR residues.

To evaluate the reproducibility of the methodology, we performed replicate enrichment experiments in HeLa cells. Following MS analysis, there was a 75% overlap of the high-confident ADP-ribose acceptor sites identified (localization scores >0.60) between replicates (Fig. 1e). Thus, this indicates high reproducibility in the established approach, which compares well with the reproducibility obtained in other proteomic experiments (Supplementary Note 1)[31]. From three replicates, we have identified 739 ADP-ribosylation sites (Localization score >0.60) on 480 proteins after H_2O_2 treatment (Supplementary Data 1), with the majority of identified proteins containing a single modification site (Supplementary Fig. 1b). To corroborate our identification analysis, we performed a separate MS analysis employing the complementary fragmentation technique electron transfer dissociation (ETD)[32], which confirmed the localization of several identified sites (Supplementary Fig. 1c,d; Supplementary Data 2).

Functional analysis using gene ontology (GO) confirmed that the identified proteins participate in biological processes known to involve ADP-ribosylation activity, including transcription, chromosome organization and response to DNA damage stimulus[33,34] (Fig. 1f). Reassuringly, we find that 76% of the ADP-ribosylated proteins localize to the nucleus (Fig. 1g), in line with the cellular localization of ARTD1 and ARTD2 (also PARP2). Moreover, the cellular abundance profile of identified ADP-ribosylation protein targets supports the notion that our methodology is not biased towards abundant proteins (Supplementary Fig. 1e). Collectively, these results confirm the feasibility and reproducibility of this novel proteomics approach for identifying the endogenous ADP-ribosylation sites in cultured HeLa cells.

Identification of Lys residues as endogenous acceptor sites. As the Af1521 macro domain binds to the ADP-ribose moiety[26] our methodology allows for unbiased detection of any ADP-ribose acceptor site. In support of this, no discernable difference was observed when the amino acid distribution of ADP-ribosylation sites was compared with the amino acid distribution of the same residues across the proteome (Fig. 2a). Among the identified ADP-ribosylation sites, we observed a significant portion of modifications residing on Lys residues, including the previously confirmed ARTD1 modification site K498 (ref. 7). ADP-ribosylation of Lys residues has been suggested as an artefact related to the release of ADP-ribose moieties during PARG cleavage of PAR chains[17]. This suggestion was made based on observations that ADP-ribose was found to non-enzymatically attach to Lys, Arg and Cys residues in a glycation process[35]. However, the incorporation rate (stoichiometry) achieved in this study, which utilized large amounts of histone proteins for *in vitro* reactions, were estimated to be below 2%, suggesting that this is an inefficient reaction[35]. To investigate whether PARG treatment of PAR chains causes glycation in our experimental setup, we performed a quantitative experiment using Stable Isotope Labelling by Amino acids in Cell culture (SILAC)[36]. Herein 'Heavy' SILAC cell lysates were treated with free PAR chains before PARG degradation, while 'Light' SILAC cell lysates were left untreated (Supplementary Fig. 2a). Since no PAR-inducing stress was exerted on these cells, identification of ADP-ribosylation sites exhibiting increased SILAC ratios would be indicative of chemical reactions caused by free ADP-ribose released by PARG. Here we identified 39 ADP-ribosylation sites equally distributed across Lys, Arg, Glu and Asp residues, and no increased SILAC ratios were observed for identified modification sites. These findings strongly suggest that PARG treatment does not lead to random glycation of Lys or Arg residues (Fig. 2b and Supplementary Data 3). To substantiate our findings, we performed a 'reverse' SILAC experiment where only light SILAC cells were treated with free PAR chains, which resulted in a similar outcome (Fig. 2b). These results confirm that ADP-ribose moieties released on PARG treatment are unlikely to cause relevant *in vitro* artefacts and, combined with the overall reproducibility of ADP-ribosylation site identification (Fig. 1e), suggest that the identified ADP-ribosylation sites were not derived from non-enzymatic glycation.

In addition, an *in vitro* experiment utilizing a synthesized histone H2B-like peptide (NH_2-PQPAKSAPAPKKG-OH) incubated with free ADP-ribose was performed analogous to previously reported experiments[35]. Briefly, the non-modified H2B peptide was incubated with 1 mM ADP-ribose at 37 °C at pH 9 or 7.5 for two time points (1 h or overnight incubation). Glycation levels were then determined using time-of-flight (TOF) MS (Supplementary Fig. 2b). On incubation with free ADP-ribose, only small levels of glycation were observed, dependent on pH and incubation time (Supplementary Fig. 2b). Tandem mass spectrometry (MS/MS) confirmed that glycation took place at Lys residues (Supplementary Fig. 2c), corroborating earlier observations that free ADP-ribose is able to modify Lys residues by non-enzymatic glycation. However, our data reveal that glycation occurs primarily at high pH and requires non-physiological concentrations of free ADP-ribose. In contrast, PARG-released ADP-ribose was not able to induce similar artefacts at detectable levels. Moreover, the non-enzymatic glycation of ADP-ribose occurred primarly on several Lys residues within the short H2B-peptide, which is in stark contrast to the different ADP-ribosylation sites observed in cell culture (Supplementary Fig. 1b). Collectively, these results strongly suggest that the ADP-ribosylation sites observed in our cell culture analysis were not caused by glycation.

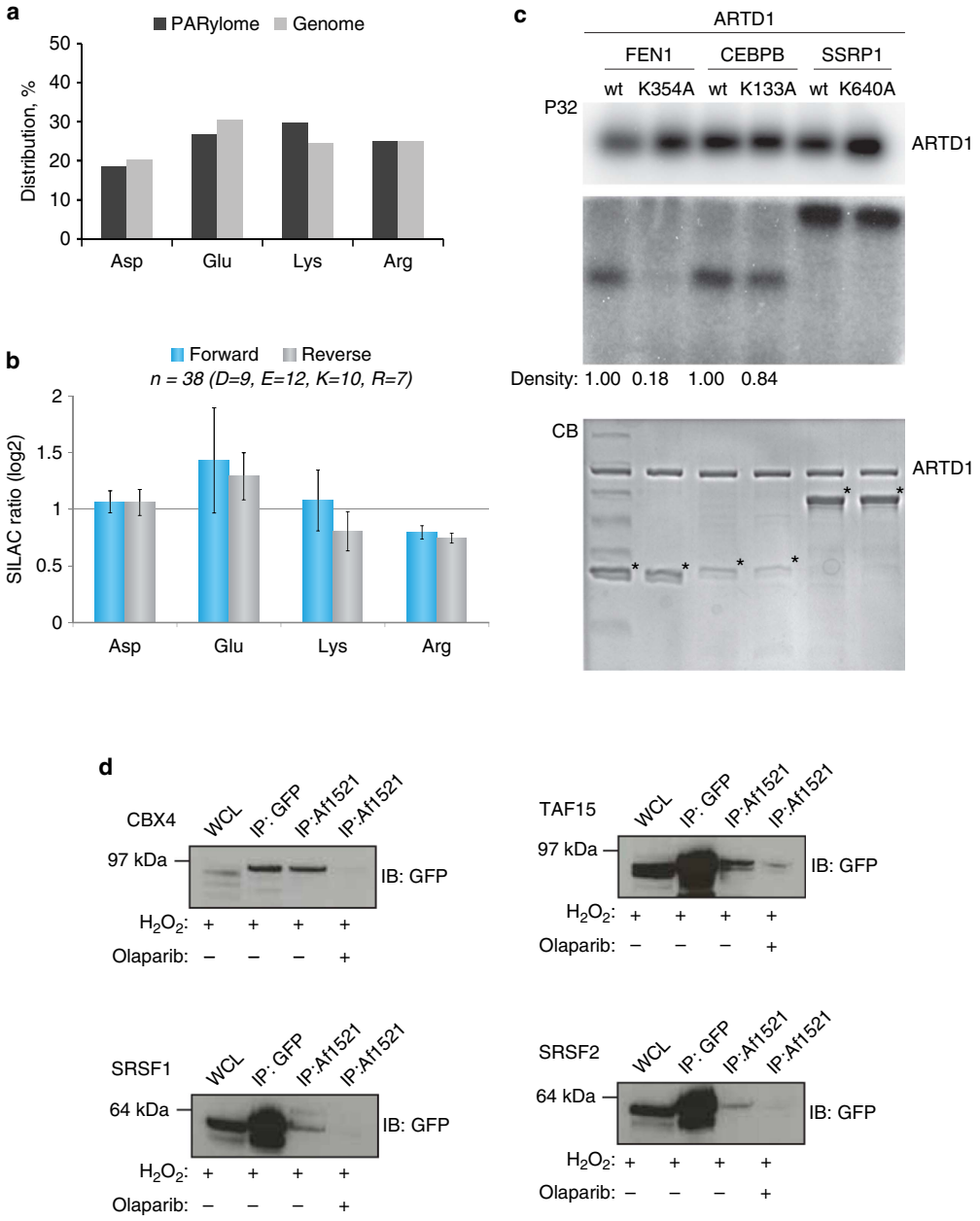

Figure 2 | Lysine residues are *in vivo* targets of ADP-ribosylation in human cells. (**a**) Distribution of ADP-ribosylation acceptor sites compared with their distribution in the genome. (**b**) Assessment of peptide glycation by free ADP-ribose. Distribution of log2 transformed SILAC ratios, and ADP-ribosylation acceptor sites, from forward and reverse SILAC experiments as outlined in Supplementary Fig. 2a. No increased SILAC ratios were observed for the different acceptor sites when cells were treated with PAR, supporting the notion, that the observed modifications are not derived from glycation. (**c**) *In vitro* PARylation of identified protein targets. Purified full-length human ARTD1 was incubated with recombinantly expressed proteins in the presence of ^{32}P-NAD$^+$ and double-stranded DNA oligomer. Samples were resolved by SDS–PAGE, stained with Coomassie (CB; lower panel) and ^{32}P-incorporation was detected by autoradiography (P32; upper panel). (**d**) HeLa cells stably expressing SRSF1, SRSF2 CBX4 or TAF15 as GFP-fusion proteins were treated with H_2O_2 and PARP (that is, ADP-ribosylation) inhibitor olaparib as control experiment. Lysates were subjected to Af1521 WT pull-down or GFP-immunoprecipitation and subsequently analysed by immunoblotting with GFP antibody. Error bars are 95% confidence intervals with $n = 4$.

To further validate Lys residue ADP-ribosylation *in vivo*, we biochemically confirmed the Lys modification sites identified on FEN1, CEBPB and SSRP1 in cells using an *in vitro* PARylation assay. To this end, recombinant proteins for these target substrates were purified as wild type (WT) and potentially modification-deficient mutant variants, with the latter harbouring K-to-A mutations at Lys residues that we found to be modified (K354A for FEN1, K133A for CEBPB and K640A for SSRP1) (Supplementary Data 1). All proteins were incubated with purified ARTD1 in the presence of [^{32}P]-NAD$^+$ and a DNA fragment to measure the incorporation of NAD$^+$ radioactivity by autoradiography[37]. Activation of ARTD1 was confirmed by a

strong automodification (Fig. 2c, upper panel). Using ARTD1 we detected strong ADP-ribosylation signals for all three WT protein candidates, confirming that these are ADP-ribosylation substrates. When Fen1, CEBPB or SSRP1 were trans-modified with either ARTD1, ARTD1 + PJ34, ARTD1 Y907A/C908R (catalytically dead) or ARTD1 E988K (1.25% of wild-type activity; only monomers are added), modification of the substrates was not observed (Supplementary Fig. 3), confirming that glycation is not a problem in our *in vitro* assays.

However, in our data set we observed several other ADP-ribosylation sites in this protein, although these had lower localization scores. These findings suggest that the K640 modification may only contribute a low percentage of the total ADP-ribosylation levels for SSRP1. Conversely, for the K133A mutant of CEBPB9, we observed a 16% decrease in the ADP-ribosylation signal. Analogously, when K354 was mutated to Ala in FEN1, a reduction in total PAR signal was also observed, thus confirming that this residue constitutes an ADP-ribosylation site. Altogether, these findings demonstrate that Lys residues are indeed specific targets of ADP-ribosylation. In addition, we confirmed SRSF1, SRSF2, TAF15 and CBX4 as *in vivo* ADP-ribosylated protein substrates using western blot (WB) analysis (Fig. 2d). These targets were selected for three reasons: TAF15 is a known ADP-ribosylated substrate during oxidative stress[9,20] and serves to demonstrate the ability of the methodology to confirm known targets. For SRSF1, the identified modification sites were observed with localization scores of 0.5, and therefore do not constitute *bona fide* high-confident sites (Supplementary Data 1). Importantly, we demonstrate that the data obtained could still be used to infer that SRSF1 is an ADP-ribosylation target substrate as WB confirmed the MS results. Finally, both SRSF2 and CBX4 are novel ADP-ribosylation targets harbouring high-confident modifications sites.

ADP-ribosylation and PAR formation dynamics correlate. Since the established enrichment approach requires PARG enzymatic conversion of ADP-ribosylated acceptor sites into their MARylated counterparts, we examined the dynamics of the H_2O_2-induced ADP-ribosylation sites identified using SILAC. For this, Light SILAC cells were stimulated for only a few seconds with 500 μM H_2O_2 (~0 min), while heavy SILAC cells were treated with the same concentration of H_2O_2 for various durations (0, 5, 10, 30, 60 and 120 min) (Supplementary Fig. 4a). Using this approach, we investigated the effect oxidative stress (H_2O_2 treatment) has on the abundance of ADP-ribosylation sites determined by quantitative MS: if the identified ADP-ribosylation site is induced on oxidative stress, then the relative SILAC peptide intensity ratio between light and heavy peaks will be higher in the heavy isotope encoded sample, thereby exhibiting an increased SILAC ratio. Following MS analysis of H_2O_2-treated SILAC samples, we extracted and compared the temporal SILAC ratios of identified ADP-ribosylation sites, and observed the highest SILAC ratios at early time points (5 and 10 min H_2O_2 treatment) (Fig. 3a). To examine whether changes in SILAC ratios correlate with the dynamics of cellular PAR formation, we compared the SILAC readout signal (Fig. 3a) to the PAR signals analysed by immunofluorescence in the same cells. Although the employed antibody primarily recognizes only longer PAR chains, the employed approach constitutes a widely used methodology to evaluate relative differences (that is, dynamic changes) in cellular PAR formation[38–40] (Fig. 3b; Supplementary Fig. 4b). From triplicate IF experiments a good temporal and kinetic correlation between the measured SILAC ratios (Fig. 3a) and PAR IF signals was observed (Fig. 3b), with both analyses exhibiting the highest increase at 5–10 min of H_2O_2 treatment. Moreover, the dynamic changes observed are similar to results obtained from immuno-slot-blot analysis of PAR formation (Supplementary Fig. 4c), and to those reported in mouse embryonic fibroblasts treated with 100 μM H_2O_2. Also in these experiments a peak of PAR formation was observed after 5 min, with subsequent turnover after 15–20 min (ref. 39). Collectively, these data show that the upregulation of ADP-ribosylation sites determined by SILAC ratios correlates with the increase in PAR formation using IF analysis.

Determination of endogenous ADP-ribosylation stoichiometry. Today, large-scale proteomics experiments have been very successful in determining the relative abundance of PTMs between different cellular states[11]. However, an inherent challenge in PTM analyses is the estimation of stoichiometry, referred to as the fraction of a given protein modified with a particular PTM at a given amino acid. To obtain stoichiometry information, we used the information gathered in our H_2O_2-treated SILAC experiments (Fig. 3a and Supplementary Data 1), and combined it with data characterizing general protein regulation during H_2O_2 treatment[41]. Briefly, ADP-ribosylated peptides have opposite ratios of their unmodified counterparts, which can be used to calculate the absolute stoichiometry of modified sites from any two SILAC states. This calculation is made under the assumption that the sum of modified and unmodified peptides remains constant between SILAC states[41]. From a single experiment, we obtained stoichiometry values for 55 ADP-ribosylation sites, revealing that half of the ADP-ribosylation sites have less than 11% stoichiometry on H_2O_2 treatment (that is, the fraction of a given modification site occupied by ADP-ribosylation; Supplementary Fig. 4d). In line with the overall transient nature of the modification, these findings suggest a tight enzymatic regulation of ADP-ribosylation stoichiometry. Moreover, several of the arginine residue ADP-ribosylation sites were measured with high stoichiometry (Supplementary Fig. 4e, Supplementary Data 4). Whether these represent protein targets modified by ARTs other than ARTD1 and 2, or represent MARylation rather than PARylation remains to be determined.

Comparing this ADP-ribosylome to Asp/Glu ADP-ribosylomes. With the wide range of ADP-ribosylated proteins identified, we sought to compare our list of modified proteins with the previously reported proteins ADP-ribosylated at Asp/Glu (ref. 9). Although these analyses were conducted in different cell lines and under different physiological conditions, we found that 36 per cent of the reported Asp/Glu ADP-ribosylated proteins were also modified in our data set (Fig. 3c). Similarly, 38% of the targets identified in our previous report using the Af1521 domain for identification of ADP-ribosylated proteins[20] were also identified with the current methodology (Supplementary Fig. 4f). This overlap increased to 52 percent when only H_2O_2-induced ADP-ribosylation substrates were compared, supporting the notion that differences in the substrates identified do not stem from the methodologies but from differences in cellular conditions (Supplementary Fig. 4f). Similarly, when comparing our data set with an *in vitro* analysis where 8-Bu(3-yne)T-NAD^+ was incubated with cell lysates and mutated analogue-sensitive ARTDs[42] an overlap of only 30% was observed (Fig. 3d). These findings suggest that *in vivo* and *in vitro* strategies target different ARTD substrates.

To further investigate the comparability of the different enrichment strategies, we performed SILAC experiments in which the PARP inhibitor olaparib was introduced before

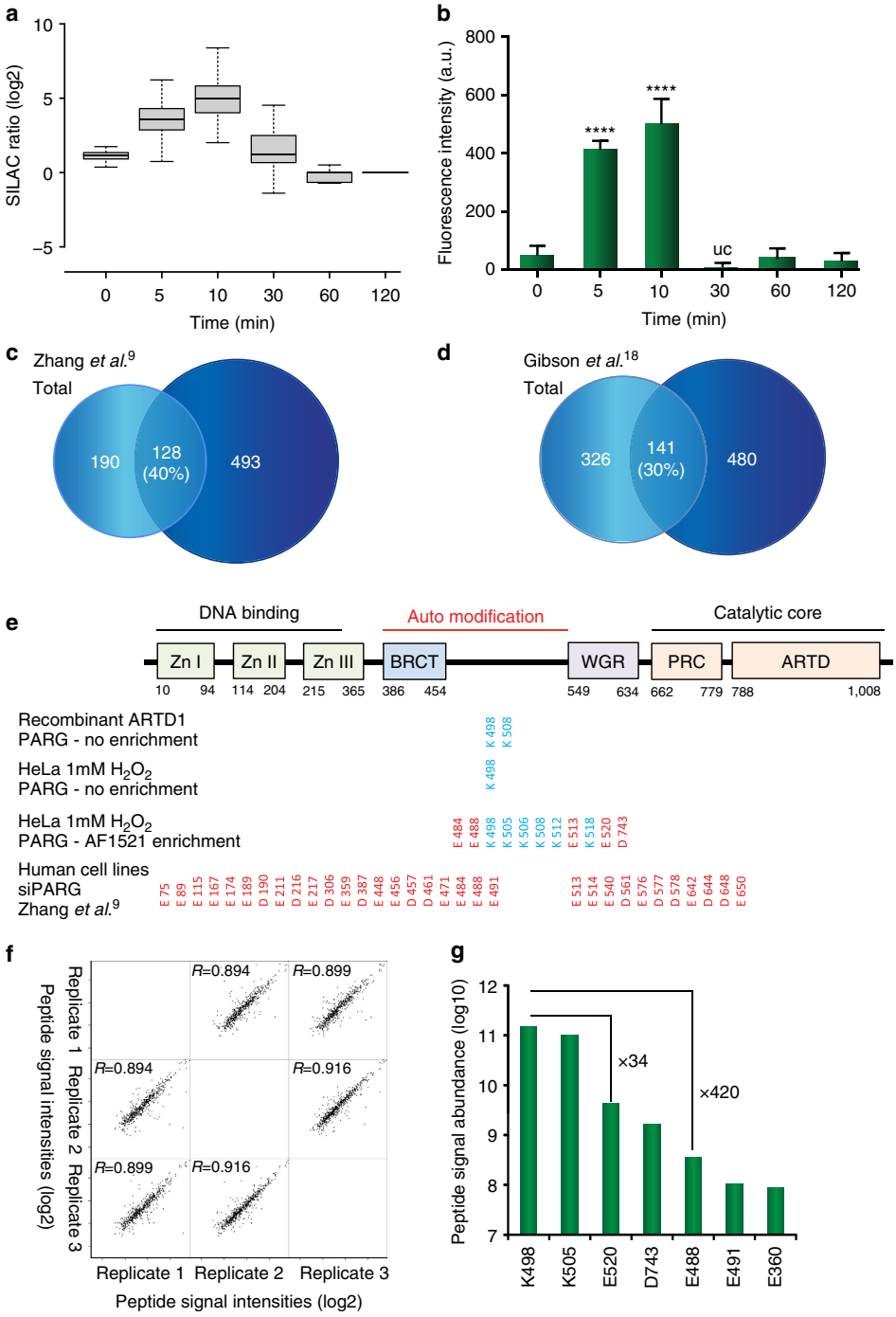

Figure 3 | SILAC ratios of ADP-ribosylation sites. (**a**) Boxplot analysis of logarithmized H/L SILAC ratios from six SILAC experiments representing HeLa cells treated with H_2O_2 in a temporal manner (see Supplementary Fig. 2a). Strongest regulation of ADP-ribosylation sites is observed when cells are treated for 5–10 min of genotoxic stress. (**b**) Densiometric evaluation of IF analysis of HeLa cells treated with H_2O_2 for different time points. The strongest abundance in PAR signal is observed after 5–10 min treatment of H_2O_2, in good correlation with observed increase in SILAC ratios on MS analysis (Fig. 2a). Experiments were performed in triplicates. (**c**) Venn diagram depicts overlap between identified ADP-ribosylated proteins compared with previously reported Asp and Glu ADP-ribosylated proteins. (**d**) Venn diagram depicts overlap between identified ADP-ribosylated proteins compared with previously reported Asp and Glu ADP-ribosylated proteins using an *in vitro* strategy. (**e**) Comparison of identified ARTD1 ADP-ribosylation sites across different experiments as indicated. (**f**) Multi-scatter plot of measured peptide signal intensities from triplicate ADP-ribosylation experiments. A strong Pearson correlation signifies high reproducibility in the measured abundance of ADP-ribosylated peptide species. (**g**) Abundance measurement for seven ADP-ribosylation sites, demonstrating that lysine residue K498 is abundantly modified in ARTD1. Error bars are 95% confidence intervals with $n=3$.

oxidative stress and compared the outcome with the analogous ADP-ribosylome experiment[9]. In two SILAC experiments, both light and heavy SILAC cells were treated with H_2O_2, while only light SILAC cells were treated with olaparib (1 μM or 10 μM)[43]. A strong Pearson correlation in SILAC ratios between the experiments ($R = 0.69$) signifies that the ADP-ribosylation sites identified were similarly affected by the employed olaparib concentrations (Supplementary Fig. 4g). Using the STRING database of physical and functional interactions[44], we found that the proteins harbouring ADP-ribosylation sites regulated by olaparib were strongly connected with ARTD1 and ARTD2 (Supplementary Fig. 5a). Moreover, the regulated proteins were also strongly associated with biological processes known to involve ARTDs (Supplementary Fig. 5b) and therefore most probably constitute ADP-ribosylated candidates.

Next, we compared the protein distribution of identified modification sites between this data set and the above-mentioned methodology. In the Asp/Glu ADP-ribosylome[9], a total of 1,048 ADP-ribosylation sites residing on 320 proteins were identified, which corresponds to 3.3 modifications per identified substrate. In contrast, our combined data set includes 958 ADP-ribosylation sites on 565 proteins, or 1.7 modifications per identified substrate. Considering that only half of the identified sites in our data set reside on Glu or Asp residues (Fig. 2a), the boronic acid approach, which employs non-physiological siPARG conditions, identifies more ADP-ribosylation sites per identified substrate. Notably, this increase is analogous to the observed increase in overall PAR signal on siPARG treatment (Fig. 1b).

We then compared the ADP-ribosylation sites only identified on ARTD1. In the Asp/Glu ADP-ribosylome analysis by Zhang *et al.*[9], a total of 37 ADP-ribosylation sites were reported for ARTD1 (Fig. 3e), of which 23 resided on Glu residues, which corresponds to 31% of the total number of Glu within human ARTD1. In contrast, the Af1521 analysis only identified ADP-ribosylation in a total of 11 amino acid acceptor sites across all experiments (Fig. 3e). To investigate whether the differences in the number of identified ADP-ribosylation sites might be abundance-driven, we performed an analysis of HeLa lysates without Af1521 enrichment. In addition, we performed a similar analysis with recombinant ARTD1, where automodified ARTD1 was treated with PARG but not enriched by Af1521. From these experiments, we solely found K498 to be modified in the non-enriched HeLa sample, whereas both K498 and K505 were identified on recombinant ARTD1 (Fig. 3e). These data suggest that certain Lys residues within the auto-modification domain of ARTD1 are most abundantly present in the analysed samples, which is similar to previous mutational observations for ARTD1 (ref. 7). We observed a strong reduction in the *in vitro* PAR signal when the three lysine residues within the automodification domain of ARTD1 (K498R, K521R and K524R)[7] were mutated. Thus, indicating that these sites are indeed relevant for automodification of ARTD1 and supporting our observations that K498 is a major PAR acceptor site of ARTD1.

To quantify ARTD1 modification sites in more detail, we next compared the peptide signal abundance between replicate Af1521 analyses (Fig. 1e). To this end, the intensity values for all identified peptide sequences were compared across replicate samples. A strong Pearson correlation between replicates ($R > 0.89$) demonstrates that the measured peptide signal intensities can be used as a reliable measure for modification site abundance (Fig. 3f). To further investigate quantification of ADP-ribosylation sites, we performed abundance assessment for seven modification sites on ARTD1 that were reliably identified in two out of the three replicate experiments (Fig. 3g). The analysis revealed that ADP-ribosylation located on lysine K498 yielded the strongest signal abundance. Although peptides from the same protein might exhibit different 'flyability'[45], an observed 34-fold and 420-fold difference in signal intensity compared with nearby modification sites residing on glutamic acids E520 and E488, respectively, suggests that K498 is an abundant auto-modification site on ARTD1. Besides, ADP-ribosylation on K498, both E488 and E491 reside on comparable tryptic peptide sequences within ARTD1, so that the observed differences in abundance cannot be attributed to different peptide ionization propensities. We observed that quantified ADP-ribosylation sites preferentially reside within the auto-modification domain of ARTD1 under physiological conditions (Fig. 3g,e).

Analysing endogenous ADP-ribosylation sites in mouse liver. Tissues can contain many different cell types that display a wide range of protein concentrations, which poses challenges to proteomic identification and the analysis of PTMs. Moreover, many tissues contain a broad range of different mono-ARTs, including members of the ARTD family, SIRTs and ARTCs (ref. 46). To further explore the general applicability of the new method, we characterized the endogenous ADP-ribosylome of mouse liver, a tissue that has already been described to regulate cellular processes in an ADP-ribosylation-dependent manner[47]. Three C57BL/6 mice were killed before their livers were collected and frozen in liquid nitrogen. The tissue was then ground up and processed as described for the HeLa cells (Fig. 4a). In triplicate analyses, we identified 901 modified peptides with unique ADP-ribosylation acceptor sites, of which 414 were identified in at least two different liver samples (Fig. 4b, Supplementary Data 5). The distribution of ADP-ribosylation sites was similar to the cell culture analysis, with 70% of identified proteins harbouring only one modification site (Fig. 4c). Strikingly, the majority (86%) of identified ADP-ribosylation acceptor sites in the mouse liver were Arg, while Lys, Asp and Glu were detected only at very low levels compared with HeLa cells (Fig. 4d). Notably, several Lys residues modified with ADP-ribosylation were also found on cytoplasmic proteins in this analysis (Supplementary Data 5), providing evidence that lysine residues being *in vivo* targets of ADP-ribosylation under physiological conditions.

GO analysis of the modified proteins revealed a high enrichment in mitochondrial, cytoplasmic, nuclear and membrane proteins (Fig. 4e). Among the identified ADP-ribosylated proteins, we found several previously reported ADP-ribosylated proteins. These included ARTD12 (formerly PARP12), which has been described to have MAR and auto-ADP-ribosylation activity; ARTC2, which is a GPI-anchored arginine-specific MARylating enzyme that can be shed and circulated in the blood; and glutamate dehydrogenase 1, which is known to be regulated through ADP-ribosylation by SIRT4 (refs 48,49). In agreement with experiments done in HeLa cells, we also found that histone H2B and several RNA helicases were modified. These results indicate that the established enrichment protocol can readily be employed to investigate the non-induced ADP-ribosylomes of tissues, which include both intra- and extra-cellular ADP-ribosylated proteins.

Discussion

Here, we describe the establishment of a robust and highly reproducible technology for the first unbiased proteome-wide view of a mammalian ADP-ribosylome, which includes the exact identification of endogenous ADP-ribose acceptor sites under different physiological conditions in cells and for the first time also in organ tissue. We show that PARG treatment of peptides before enrichment with Af1521, allows specific identification of ADP-ribosylated amino acids and highly sensitive identification

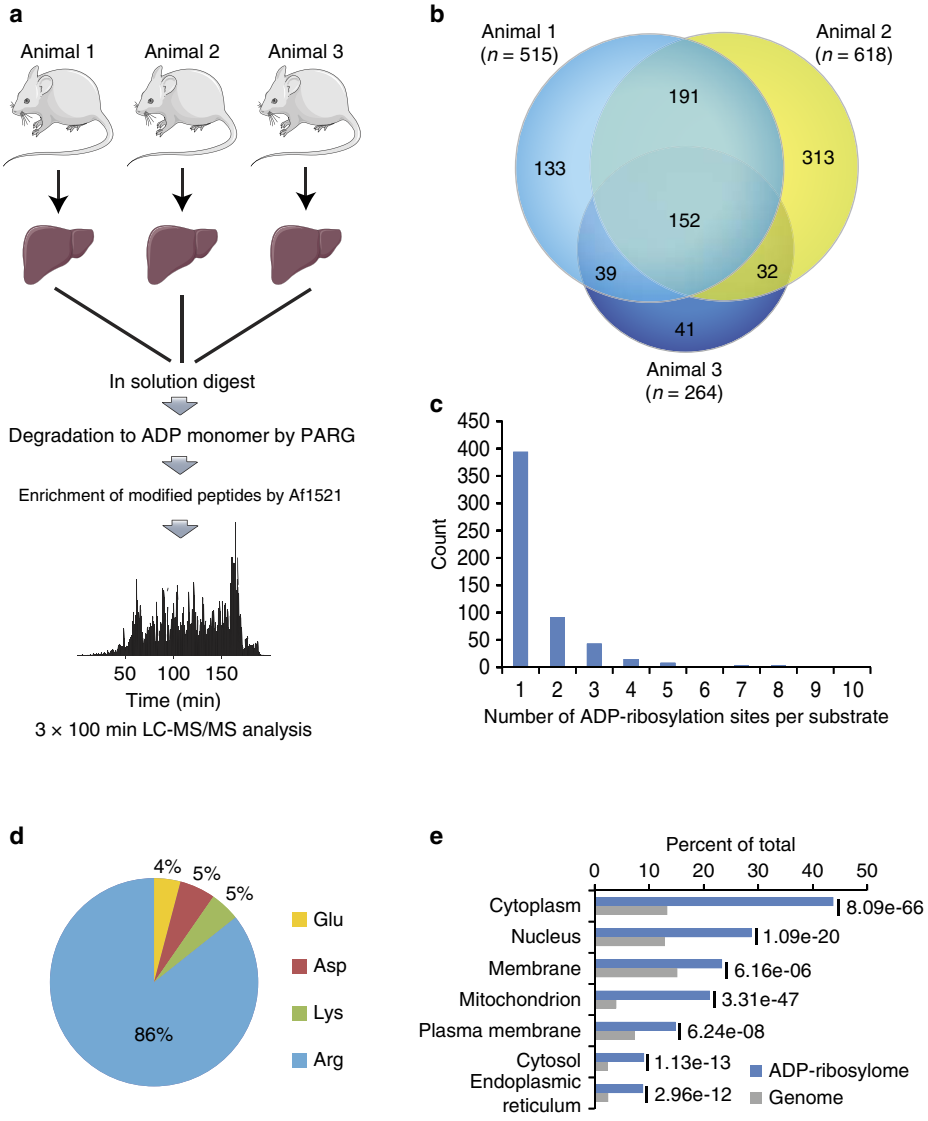

Figure 4 | Proteome-wide identification of endogenous ADP-ribosylation sites in mammalian tissue. (**a**) Experimental setup for mammalian liver tissue analysis. In total, liver samples derived from three mice were investigated and prepared as indicated. Mouse images were adapted from the Servier Image Bank under the Creative Commons licences CC-BY. (**b**) Venn diagram of identified ADP-ribosylation sites from three liver samples. A strong overlap between analysed sampled signifies good reproducibility in the identified ADP-ribosylation sites across investigated tissue samples. (**c**) Distribution of ADP-ribosylation sites across proteins. (**d**) Distribution of ADP-ribosylated amino acids. The majority (86%) of identified sites reside on arginine residues indicative of differential ART activity compared with cell culture analysis (Fig. 1g). (**e**) GO term annotation enrichment for cellular distribution of proteins identified in liver samples harbouring ADP-ribosylation sites.

of the corresponding proteins. And we demonstrate that the detected modifications are not derived from non-enzymatic glycation and, contrary to previous claims[50], Af1521 does not hydrolyse the modification under the applied conditions. Besides, this method supports the identification of ADP-ribosylated proteins without complementing cell lysates or organelles with NAD^+ analogues and mutated ARTDs (ref. 18) and is, consequently, able to analyse the ADP-ribosylome under different cellular conditions derived from endogenous ARTD protein and NAD^+ levels in both cells and tissue.

The streamlined methodology led to the identification of more than 900 endogenous ADP-ribosylation sites belonging to more than 500 proteins in both culture and tissue cells. Our results suggest that this methodology could be used in combination with high-throughput screening techniques to identify endogenous proteins affected by ADP-ribosylation and/or those modulated by ADP-ribosylation inhibitors (also called PARP inhibitors). ARTD1 is a key regulator within the DDR (ref. 33), which has recently become a highly attractive target for cancer therapy[51,52]. Although not specific for ARTD1, several ADP-ribosylation inhibitors have been approved or are currently being evaluated in clinical trials as mono-therapeutic or combination therapy agents. Our ability to now analyse the endogenous ADP-ribosylome from different cancer cells or tissues constitutes a promising approach that should advance of our understanding of ADP-ribosylation in a clinical setting.

FEN1 is a structure-specific nuclease with 5′-flap endonuclease and 5′–3′ exonuclease activities involved in DNA replication and repair, and ARTD1 recruits FEN1 to DNA damage intermediates[53]. The K354 reside of FEN1 becomes acetylated through the acetyltransferase p300, which reduces the DNA-binding activity of FEN1 (ref. 54), while ubiquitylation of the same lysine mediates the proteosomal degradation of FEN1 during G2/M phase[55]. These PTM-based regulatory mechanisms support the notion that ADP-ribosylation at K354 might relate to a currently uncharacterized regulatory function of FEN1. The observed ADP-ribosylation of the SUMO-protein ligase CBX4 suggests nuclear cross-talk between PARylation and SUMOylation, which might be more widely occurring than previously anticipated. Such cross-talk could be analogous to previously reported ADP-ribosylation-dependent ubiquitylation (PARdu)[56]. In fact, CBX4 is known to mediate SUMO conjugation in the DDR, and the recruitment of CBX4 to sites of DNA lesions is dependent on ADP-ribosylation[57]. Thus, our observation that CBX4 becomes ADP-ribosylated during oxidative stress strongly suggests that we have identified a previously uncharacterized DDR regulatory mechanism controlled by PARylation-dependent SUMOylation (PARsu).

The presented methodology is suitable for the identification of key endogenous ADP-ribosylation events in biological processes. We find that ADP-ribosylated proteins are on average less modified under physiological conditions than reported under siPARG treatment[9], which suggests that deregulation of PARG alters physiological ADP-ribosylation homoeostasis (Fig. 1b)[13,39]. Moreover, our MS analysis supports that Lys residues K498 and K505 are major acceptor sites in ARTD1, which follows previous mutational analysis of ADP-ribosylation sites on ARTD1 (ref. 7). Our analysis indicates that under physiological conditions ARTD1 is activated *in cis*[58], contradicting the observed *in trans* activation of ARTD1 under siPARG treatment[9].

Comparison of the SILAC and IF data obtained from HeLa cells revealed that the dynamic changes induced by H_2O_2 for these two data sets correlate well with each other. The relative increase in peptide abundance may thus suggest that the ADP-ribosylation sites detected reflect PARylation, at least partially. However, since the methodology described here cannot discriminate between MAR and PAR, each regulated ADP-ribosylation site will require follow-up experiments to determine whether they are indeed PARylated or MARylated.

The importance of tissue-specific protein ADP-ribosylation mapping is underscored by the substantial differences in ADP-ribosylation observed between cell culture and tissue (that is, liver). In mouse liver tissue the majority of ADP-ribosylated proteins localize to compartments containing enzymes with MAR activity, such as ARTD10, ARTD8, ARTC and SIRT4, suggesting that these proteins are primarily MARylated rather than PARylated (Fig. 4e). These observations are further supported by the increased levels of modified Arg residues, and membrane and extracellular proteins, which might stem from ARTC activity. Moreover, our data substantiates initial studies where ADP-ribosylation was observed on Arg residues within rat liver proteins[59]. From the analysed liver extracts, ARTD1 was not found to be auto-ADP-ribosylated, highlighting the fact that the enzyme is mainly inactive under normal, non-stressed conditions.

Our organ analysis of ADP-ribosylation provides evidence that the modification is involved in multiple physiological functions. For example, KEGG pathway analysis reveals that proteins involved in actin cytoskeleton and endoplasmic reticulum regulation are enriched in ADP-ribosylation (Supplementary Fig. 5c). These pathways have previously been associated with ADP-ribosylation[60,61], but the mechanism by which the modifications are catalysed (that is, ARTDs or ARTCs (ref. 62)) remains to be investigated. NAD^+ can be released on necrosis or mechanic stress in tissue, which in turn likely activates ARTCs during organ collecting[63]. Considering that ARTCs have higher affinity for NAD^+ compared with ARTD1, this renders ARTCs more prone to activation following NAD^+ release during tissue collecting. Moreover, we find that proteins involved in metabolic processes, oxidative-reduction processes and mitochondrial content are distinctly enriched in ADP-ribosylation targets (Fig. 4e and Supplementary Fig. 5f), which suggests these processes may be influenced by the modification. While the exact mechanisms are not well understood, inhibition of ARTDs is known to enhance these processes[64]. With ARTD1 activation known to affect cellular metabolism *via* direct PARylation events, transcriptional reprogramming, or alterations in cellular NAD^+ levels[64], our tissue analysis supports the hypothesis that metabolic consequences on ADP-ribosylation inhibition might occur via alterations in NAD^+ levels[65]. This is based on ARTD1 being an avid NAD^+ consumer, and that ADP-ribosylation inhibition increases the cellular levels of NAD^+ available for other ARTDs (ref. 65), in a manner reminiscent of the reported interplay between ARTD1 activity and deacetylase SIRT1 (ref. 66). Furthermore, with immortalized cell lines exhibiting mitochondria and metabolic processes deficiencies[67], hereby rendering them impractical for ADP-ribosylation inhibition/activation and cellular metabolism investigations, highlights that methodologies allowing proteomics-based whole tissue analyses are required to investigate this antagonistic interplay in more detail.

In conclusion, our novel methodology allows for the unbiased and sensitive characterization of ADP-ribosylation sites under physiological conditions, while the data presented here extends current ADP-ribosylation knowledge and highlights the widespread occurrence of the modification. Although the methodology presented cannot currently distinguish between MARylated and PARylated peptide species, adjustment of the binding reaction stringency and combining the enrichment with specific MAR-binding domains, will most likely facilitate dissecting peptide MAR- versus PARylation in a more specific manner[68]. Importantly, the approach presented supports comprehensive and quantitative evaluation of the mammalian ADP-ribosylome of cell lines and tissue samples. Thus, allowing downstream interrogation of disease pathways in which ARTs are implicated.

Methods

Cell culture and transfection. HeLa cells were grown in Dulbecco's modified Eagle's medium (D-MEM; Invitrogen) supplemented with 10% foetal bovine serum and penicillin/streptomycin (100 U ml^{-1}) (Gibco). Stable HeLa-Kyoto cells expressing CBX4, SRSF2, SRSF1 and FUS tagged with C-terminal GFP under the control of an endogenous promoter were generated by transfecting BAC transgenes and were kindly provided by Prof Anthony Hyman (Max Planck Institute, Dresden). Selection was maintained by adding 400 μg ml^{-1} G418 (Sigma Aldrich) to the culture medium. SILAC HeLa cells were grown in SILAC D-MEM (Invitrogen) supplemented with 10% dialyzed foetal bovine serum, L-glutamine, penicillin/streptomycin, and either L-lysine and L-arginine, L-lysine 4,4,5,5-D4 and L-arginine-U-13C6, or L-lysine-U-13C6-15N2 and L-arginine-U-13C6-15N4 (Cambridge Isotope Laboratories)[36]. The siRNA oligonucleotides against endogenous PARG (ID: 4390826) was purchased from Ambion as well as Negative Control siRNA#1. SiRNA transfections were performed using Lipofectamine RNAiMAX (Invitrogen) according to the manufacturer's protocol and lysed 48 h after transfection. All HeLa cells used for experiments were tested negative for mycoplasma.

Sample preparation. Cells were stimulated with H_2O_2 (Sigma Aldrich) for 10 min in PBS at 37 °C, collected by washing with ice-cold PBS and lysed in modified RIPA buffer (50 mM Tris pH 7.5, 400 mM NaCl, 1 mM EDTA, 1% Nonidet P-40, 0.1% Na-deoxycholate), protease inhibitor mixture (Roche) supplemented with 2 mM Na-orthovanadate, 5 mM NaF, 5 mM Glycero-2-phosphate, 1 μM ADP-HPD (Millipore) and 40 μM PJ-34 (Enzo Life Sciences) and cleared by high-speed centrifugation. Proteins were precipitated by adding fourfold excess volumes of

ice-cold acetone and stored at −20 °C overnight. Subsequently, proteins were solubilized in a urea solution (6 M urea/2 M thiourea/10 mM HEPES pH 8.0). Protein concentrations in lysates were measured using Bradford assay (Bio-Rad). Next, proteins were reduced by adding dithiothreitol to a final concentration of 1 mM, and alkylated with chloroacetamide at 5.5 mM. Proteins were digested using endoproteinase Lys-C (1:100 w/w) and modified sequencing grade trypsin (1:100 w/w) after a fourfold dilution in 50 mM ammonium bicarbonate solution. Protease digestion was terminated by slow addition of trifluoroacetic acid to pH 2. Precipitates were removed by centrifugation for 10 min at 3,000*g*. Peptides were purified using reversed-phase Sep-Pak C18 cartridges (Waters). Peptides were eluted off the Sep-Pak with 50 and 80% acetonitrile.

GST-protein expression and purification of Af1521. BL21 was used for long transformation. Briefly, 1 µl of cooled plasmid was added to BL21 and left on ice for 15 min. Bacteria were heat shocked at 42 °C for 45 sec, incubated for 1 min on ice and then mixed with SOC for 40 min at 37 °C. Bacteria were streaked onto Amp-plates and left overnight at 37 °C. The following day a single colony was inoculated in LB media and grown overnight at 37 °C. The starter culture was diluted and grown to an OD600 of 0.55–0.65. Protein expression was induced by adding IPTG to final concentration of 0.5 mM and incubated for 5–6 h. Bacteria were spun down and pellet frozen at −80 °C.

The bacterial pellet was thawn and incubated for 20 min in lysis buffer (50 mM Tris–HCl, pH 7.5, 150 mM NaCl, 1 mM MgCl2, 1 mM dithiothreitol, 1 × Bug Buster (Novagen), 1 µl ml^{-1} Benzonase (Sigma Aldrich), 200 µg ml^{-1} lysozyme (Sigma Aldrich), protease inhibitor mixture (Roche)). After breaking cells by vortexing with glass beads, cell debris was pelleted by centrifugation. The cleared lysate was incubated for 4 h at 4 °C rolling with equilibrated glutathione sepharose 4B (Sigma Aldrich). Beads were washed four times in wash buffer (50 mM Tris–HCl, pH 7.5, 150 mM NaCl and 1 mM dithiothreitol), resuspended in wash buffer and kept at 4 °C for up to 3 weeks.

Enrichment of ADP-ribosylated peptides. After eluting off Sep-Pak, appropriate amounts of IP buffer (50 mM Tris–HCl, pH 8, 10 mM MgCl2, 250 µM dithiothreitol and 50 mM NaCl) was added before the acetonitrile and the volume was reduced by vacuum centrifugation. PAR complexity was reduced by incubation with PARG (4.2 µg per sample) for 3 h at 37 °C. The peptide mixture was cooled down before it was incubated rotating for 2 h at 4 °C with the purified Af1521 macro domain. The peptides were washed three times in ice-cold IP buffer followed by one wash in water, and modified peptides were eluted with 2 × 100 µl 0.15% TFA in Milli-Q water. Peptide eluates were desalted on reverse phase C18 StageTips[69].

Mass spectrometric analysis. All MS experiments were performed on a nanoscale EASY-nLC 1000 UHPLC system (Thermo Fisher Scientific) connected to an Orbitrap Q-Exactive Exactive equipped with a nanoelectrospray source (Thermo Fisher Scientific). Each sample was eluted off the StageTip, auto-sampled and separated on a 15 cm analytical column (75 µm inner diameter) in-house packed with 1.9-µm C18 beads (Reprosil Pur-AQ, Dr Maisch) using a 3 h gradient ranging from 5 to 64% acetonitrile in 0.5% formic acid at a flow rate of 200 nl min^{-1}. The effluent from the high-performance liquid chromatography was directly electrosprayed into the mass spectrometer. The Q Exactive Plus mass spectrometer was operated using data-dependent acquisition, with all samples being analysed using a 'sensitive' acquisition method[22] and a normalized collision energy of 28. Back-bone fragmentation of eluting peptide species were obtained using HCD which ensured high-mass accuracy on both precursor and fragment ions.

Mass spectrometry analysis of ADP-ribosylation sites by ETD. ETD spectra of ADP-ribosylated peptides were acquired on an Orbitrap Fusion Lumos mass spectrometer (Thermo Scientific) operating in positive ion mode. Full MS scans (*m/z* 300–1,500) were performed at 120,000 resolution (*m/z* 200) in the Orbitrap, with the AGC target set at 4e5. Precursor selection was prioritized on the basis of highest charge state followed by highest intensity. Peptides (charge states from 3 + to 6 +) were selected by the quadrupole (1.3 *m/z* isolation window) before reaction with fluoranthene radical anions (ETD reagent target 4e5). ETD reaction times were set at 1.7τ for each charge state. MS/MS spectra were acquired using a normal ion trap scan rate with a maximum injection time of 50 ms (AGC target 2e5). A Venn diagram comparing identified protein targets derived from the ETD with HCD analysis is shown in Supplementary Fig. 6a.

***In vitro* TOF-MS analysis of H2B peptide sequence.** 1 µg of HK326 peptide (PQPAKSAPAPKKG) was incubated with 1 mM ADP-ribose in 50 mM sodium phosphate buffer (pH 7.5 and pH 9.5) for 1 h or overnight at 37 °C. Samples were desalted using Reversed-phase m-C18 ZipTips (for MALDI-MS) and eluted with MALDI matrix solution (a-cyano-4-hydroxycinnamicacid in 0.3 mM di-ammonium hydrogen citrate (Fluka), 60% acetonitrile in H_2O) directly on the target plate. MALDI analyses were performed on a 4800 MALDI TOF/TOF system in linear mode.

Identification of peptides and proteins. All raw data analysis was performed with MaxQuant software suite version 1.3.0.5 supported by the Andromeda search engine[70]. Data were searched against a concatenated target/decoy (forward and reversed) version of the UniProt Human fasta database encompassing 71,434 protein entries (downloaded from www.uniprot.org on 2013-07-03). Mass tolerance for searches was set to maximum 7 p.p.m. for peptide masses and 20 p.p.m. for HCD fragment ion masses. Data were searched with carbamidomethylation as a fixed modification and protein *N*-terminal acetylation, methionine oxidation and mono-ADP-ribosylation (*m/z* 541,06110: C10H13N5O9P2) on lysine, arginine, glutamic and aspartic acids as variable modifications. A maximum of three mis-cleavages was allowed while requiring strict trypsin specificity, and only peptides with a minimum sequence length of seven were considered for further data analysis. Peptide assignments were statistically evaluated in a Bayesian model on the basis of sequence length and Andromeda score. Only peptides and proteins with a false discovery rate of <1% were accepted, estimated on the basis of the number of accepted reverse hits, and false discovery rate values were finally estimated separately for modified and unmodified peptides. Protein sequences of common contaminants such as human keratins and proteases used were added to the database. For SILAC quantification a minimum of two ratio-counts was required.

Enrichment of GFP-tagged and ADP-ribosylated proteins. Cells expressing the tagged versions of the proteins of interest were collected by washing with PBS and lysed in modified RIPA buffer (50 mM Tris pH 7.5, 400 mM NaCl, 1 mM EDTA, 1% Nonidet P-40, 0.1% Na-deoxycholate), protease inhibitor mixture (Roche) supplemented with 2 mM Na-orthovanadate, 5 mM NaF, 5 mM Glycero-2-phosphate, 1 µM ADP-HPD (Millipore) and 40 µM PJ-34 (Enzo Life Sciences). Lysates were diluted in modified RIPA without salt and then cleared by high-speed centrifugation.

GFP-immunoprecipitaion was performed with 20 µl GFP-Trap_A agarose beads (Chromotek). 1 mg of protein mixtures were incubated for 2 h rotating at 4 °C before washing and subsequent elution with 2 × Laemmli sample buffer (Thermo Fisher Scientific) at 90 °C. Pull down of ADP-ribosylated proteins was performed similarly but using 200 µl crosslinked Af1521 macro domain and 2 mg of protein mixtures.

Western blotting. The following antibodies were used in this study: rabbit polyclonal PAR 1:1,000 (ALX-210–890A, Enzo Life Science) and mouse monoclonal GFP 1:1,000 (11814460001, Roche).

Total cell lysates together with the eluates were resolved on 4–12% gradient SDS–PAGE gels (Thermo Fisher Scientific) and proteins were transferred onto nitrocellulose membranes (Sigma Aldrich). Membranes were blocked using 5% BSA solution in PBS supplemented with Tween-20 (0.1%). Secondary antibodies coupled to horseradish peroxidase (Jackson ImmunoResearch Laboratories) were used for immunodetection. The detection was performed with Novex ECL Chemiluminescent Substrate Reagent Kit (Invitrogen). For slot blot analysis, PAR polymer (Trevigen) was incubated with different concentrations of PARG and spottet directly onto PVDF membranes (Millipore) using the slot blot chamber (Fisher Scientific) according to manufacturer's protocol. Cropped WBs presented in Fig. 2d have been included as uncropped scans in Supplementary Fig. 6b.

Immunofluorescence microscopy. HeLa cells were seeded on coverslips and the following day stimulated for indicated time points with H_2O_2. After washing with PBS, cells were fixed in methanol/acetic acid solution and incubated for 5 min at 37 °C. Coverslips were blocked in 5% milk powder, transferred to a humid chamber and incubated with rabbit polyclonal PAR (Enzo Life Science) for 1 h at 37 °C and with secondary antibody Alexa Fluor 488 (Invitrogen) for 1 h at 37 °C, stained with DAPI for 2 min, washed in PBS and mounted. Images were acquired on a DFC345 FX microscope (Leica) and analysed using ImageJ.

Immuno-slot-blot. For the immuno-slot-blot analysis, HeLa cells were treated and lysed as described in sample preparation, and proteins were vacuum aspirated onto a Hybond P 0.2 PVDF (Amersham Biosciences) using a slot-blot manifold (Amersham Biosciences). The membrane was blocked with 5% milk powder in 10 mM Tris–HCL (pH 8.0), 150 mM NaCl and 0.05% (v/v) Tween 20 (TBST buffer) and incubated with polyclonal PAR antibody (Enzo Life Science) diluted 1:1,000 in 5% milk powder in TBST for 1 h at RT and with secondary antibody IRDye 800CW goat anti-rabbit IgG (LI-COR) 1:15,000 in TBST for 1 h at RT. Signals were detected by the Odyssey infrared imaging system (LI-COR) and the immunoblot signal was quantified using GelEval (FrogDance Software).

***In vitro* radiography assay.** 10 pmol of ARTD1 and ARTD10 were automodified with 100 nM NAD$^+$ for 10 min at 37 °C, respectively, hereby inducing short PAR chains on ARTD1 and MAR on ARTD10 through auto-catalysis[29]. Samples were filtered through G50 columns to remove excess amount of unincorporated NAD$^+$, and subsequently treated with 10 pmol PARG for additional 1 h at 37 °C. Using autoradiography assays the hydrolysis of attached radioactive 32 P-NAD$^+$ of the protein substrates were subsequently monitored. For transmodification reactions,

50 pmol of target protein was incubated with 10 pmol ARTD1 for 10 min at 37 °C. The reaction was stopped by adding Laemmli buffer and boiling for 5 min at 95 °C. After separation of samples by SDS–PAGE, the radiolabelled ADP-ribosylation signal was determined by GelEval (FrogDance Software).

Preparation of mouse liver extracts. Male 9-week-old C57BL/6 mice were maintained on a 12-h light–dark cycle with regular unrestricted diet. Mice were killed in a CO_2 chamber. Excised livers were washed in PBS and shock frozen in liquid nitrogen. Ice-cold modified RIPA buffer (supplemented with PARP-, PARG- and protease inhibitors as described before) was added to the shock frozen livers and they were lysed operating the Tissue Lyser II (Qiagen) device at 30 HZ for 4×30 s. The lysate was further sonicated until it became fluid and all liver pieces were dissolved. The lysate was cleared by high-speed centrifugation and processed similar as described for the cell culture samples. 20 mg of liver protein was used as starting material for the digest.

Bioinformatic analyses. Statistical analysis and hierarchical clustering was performed using the Perseus software suite (Max Planck Institute of Biochemistry, Department of Proteomics and Signal Transduction, Munich). Significantly enriched Gene Ontology terms were determined using the Functional Annotation Tool of the DAVID Bioinformatics database. Protein interaction networks were analysed using the interaction data from the STRING database (v. 9.05) and visualized using Cytoscape (v. 2.8.3). Protein abundance assessment was performed using a deep proteome reference data set for HeLa cells. All Venn diagrams were generated using the online Venny program (http://bioinfogp.cnb.csic.es/tools/venny/).

Comments related to animal study. C57BL/6J mice were bread at the animal facility of the University of Zurich. No randomization or blinding were used for these studies, and no animals had to be excluded. All animal experiments were carried out in accordance with the Swiss and EU ethical guidelines and have been approved by the local animal experimentation committee of the Canton of Zurich under licence #2012207 and following the 3R guidelines.

Data availability. The mass spectrometry proteomics data have been deposited to the ProteomeXchange Consortium via the PRIDE partner repository[71] with the data set identifier PXD004245. The additional data that support the findings of this study are available from the corresponding author on request.

References

1. Rack, J. G. *et al.* Identification of a class of protein ADP-ribosylating sirtuins in microbial pathogens. *Mol. Cell* **59,** 309–320 (2015).
2. Hottiger, M. O., Hassa, P. O., Luscher, B., Schuler, H. & Koch-Nolte, F. Toward a unified nomenclature for mammalian ADP-ribosyltransferases. *Trends Biochem. Sci.* **35,** 208–219 (2010).
3. Feijs, K. L. *et al.* ARTD10 substrate identification on protein microarrays: regulation of GSK3beta by mono-ADP-ribosylation. *Cell Commun. Signal.* **11,** 5 (2013).
4. Rouleau, M., Patel, A., Hendzel, M. J., Kaufmann, S. H. & Poirier, G. G. PARP inhibition: PARP1 and beyond. *Nat. Rev. Cancer* **10,** 293–301 (2010).
5. Polo, S. E. & Jackson, S. P. Dynamics of DNA damage response proteins at DNA breaks: a focus on protein modifications. *Genes Dev.* **25,** 409–433 (2011).
6. Meyer-Ficca, M. L., Meyer, R. G., Coyle, D. L., Jacobson, E. L. & Jacobson, M. K. Human poly(ADP-ribose) glycohydrolase is expressed in alternative splice variants yielding isoforms that localize to different cell compartments. *Exp. Cell Res.* **297,** 521–532 (2004).
7. Altmeyer, M., Messner, S., Hassa, P. O., Fey, M. & Hottiger, M. O. Molecular mechanism of poly(ADP-ribosyl)ation by PARP1 and identification of lysine residues as ADP-ribose acceptor sites. *Nucleic Acids Res.* **37,** 3723–3738 (2009).
8. Vandekerckhove, J., Schering, B., Barmann, M. & Aktories, K. Clostridium perfringens iota toxin ADP-ribosylates skeletal muscle actin in Arg-177. *FEBS Lett.* **225,** 48–52 (1987).
9. Zhang, Y., Wang, J., Ding, M. & Yu, Y. Site-specific characterization of the Asp- and Glu-ADP-ribosylated proteome. *Nat. Meth.* **10,** 981–984 (2013).
10. McDonald, L. J. & Moss, J. Enzymatic and nonenzymatic ADP-ribosylation of cysteine. *Mol. Cell. Biochem.* **138,** 221–226 (1994).
11. Olsen, J. V. & Mann, M. Status of large-scale analysis of post-translational modifications by mass spectrometry. *Mol. Cell. Proteomics.* **12,** 3444–3452 (2013).
12. Daniels, C. M., Ong, S. E. & Leung, A. K. Phosphoproteomic approach to characterize protein mono- and poly(ADP-ribosyl)ation sites from cells. *J. Proteome. Res.* **13,** 3510–3522 (2014).
13. Min, W., Cortes, U., Herceg, Z., Tong, W. M. & Wang, Z. Q. Deletion of the nuclear isoform of poly(ADP-ribose) glycohydrolase (PARG) reveals its function in DNA repair, genomic stability and tumorigenesis. *Carcinogenesis* **31,** 2058–2065 (2010).
14. Hanai, S. *et al.* Loss of poly(ADP-ribose) glycohydrolase causes progressive neurodegeneration in Drosophila melanogaster. *Proc. Natl Acad. Sci. USA* **101,** 82–86 (2004).
15. Yu, S. W. *et al.* Apoptosis-inducing factor mediates poly(ADP-ribose) (PAR) polymer-induced cell death. *Proc. Natl Acad. Sci. USA* **103,** 18314–18319 (2006).
16. Cuzzocrea, S. *et al.* Role of poly(ADP-ribose) glycohydrolase in the development of inflammatory bowel disease in mice. *Free Radic. Biol. Med.* **42,** 90–105 (2007).
17. Daniels, C. M., Ong, S.-E. & Leung, A. K. L. The promise of proteomics for the study of ADP-Ribosylation. *Mol. Cell* **58,** 911–924 (2015).
18. Gibson, B. A. *et al.* Chemical genetic discovery of PARP targets reveals a role for PARP-1 in transcription elongation. *Science* **353,** 45–50 (2016).
19. Slade, D. *et al.* The structure and catalytic mechanism of a poly(ADP-ribose) glycohydrolase. *Nature* **477,** 616–620 (2011).
20. Jungmichel, S. *et al.* Proteome-wide identification of poly(ADP-Ribosyl)ation targets in different genotoxic stress responses. *Mol. Cell* **52,** 272–285 (2013).
21. Sylvestersen, K. B., Young, C. & Nielsen, M. L. Advances in characterizing ubiquitylation sites by mass spectrometry. *Curr. Opin. Chem. Biol.* **17,** 49–58 (2013).
22. Kelstrup, C. D., Young, C., Lavallee, R., Nielsen, M. L. & Olsen, J. V. Optimized fast and sensitive acquisition methods for shotgun proteomics on a quadrupole orbitrap mass spectrometer. *J. Proteome. Res.* **11,** 3487–3497 (2012).
23. Rosenthal, F., Nanni, P., Barkow-Oesterreicher, S. & Hottiger, M. O. Optimization of LTQ-orbitrap mass spectrometer parameters for the identification of ADP-Ribosylation Sites. *J. Proteome. Res.* **14,** 4072–4079 (2015).
24. Hengel, S. M. & Goodlett, D. R. A review of tandem mass spectrometry characterization of adenosine diphosphate-ribosylated peptides. *Int. J. Mass. Spectrom.* **312,** 114–121 (2012).
25. Tao, Z., Gao, P. & Liu, H. W. Identification of the ADP-ribosylation sites in the PARP-1 automodification domain: analysis and implications. *J. Am. Chem. Soc.* **131,** 14258–14260 (2009).
26. Karras, G. I. *et al.* The macro domain is an ADP-ribose binding module. *Embo J.* **24,** 1911–1920 (2005).
27. Martello, R., Mangerich, A., Sass, S., Dedon, P. C. & Burkle, A. Quantification of cellular poly(ADP-ribosyl)ation by stable isotope dilution mass spectrometry reveals tissue- and drug-dependent stress response dynamics. *ACS Chem. Biol.* **8,** 1567–1575 (2013).
28. Jankevicius, G. *et al.* A family of macrodomain proteins reverses cellular mono-ADP-ribosylation. *Nat. Struct. Mol. Biol.* **20,** 508–514 (2013).
29. Rosenthal, F. *et al.* Macrodomain-containing proteins are new mono-ADP-ribosylhydrolases. *Nat. Struct. Mol. Biol.* **20,** 502–507 (2013).
30. Kleine, H. *et al.* Substrate-assisted catalysis by PARP10 limits its activity to mono-ADP-ribosylation. *Mol. Cell* **32,** 57–69 (2008).
31. Tabb, D. L. *et al.* Repeatability and reproducibility in proteomic identifications by liquid chromatography-tandem mass spectrometry. *J. Proteome. Res.* **9,** 761–776 (2010).
32. Coon, J. J., Shabanowitz, J., Hunt, D. F. & Syka, J. E. Electron transfer dissociation of peptide anions. *J. Am. Soc. Mass Spectrom.* **16,** 880–882 (2005).
33. Bryant, H. E. *et al.* PARP is activated at stalled forks to mediate Mre11-dependent replication restart and recombination. *Embo J.* **28,** 2601–2615 (2009).
34. Kraus, W. L. & Lis, J. T. PARP goes transcription. *Cell* **113,** 677–683 (2003).
35. Cervantes-Laurean, D., Jacobson, E. L. & Jacobson, M. K. Glycation and glycoxidation of histones by ADP-ribose. *J. Biol. Chem.* **271,** 10461–10469 (1996).
36. Ong, S. E. *et al.* Stable isotope labeling by amino acids in cell culture, SILAC, as a simple and accurate approach to expression proteomics. *Mol. Cell. Proteomics.* **1,** 376–386 (2002).
37. Messner, S. *et al.* PARP1 ADP-ribosylates lysine residues of the core histone tails. *Nucleic Acids Res.* **38,** 6350–6362 (2010).
38. Shah, G. M. *et al.* Approaches to detect PARP-1 activation *in vivo*, *in situ*, and *in vitro*. *Methods Mol. Biol.* **780,** 3–34 (2011).
39. Cortes, U. *et al.* Depletion of the 110-kilodalton isoform of poly(ADP-ribose) glycohydrolase increases sensitivity to genotoxic and endotoxic stress in mice. *Mol. Cell. Biol.* **24,** 7163–7178 (2004).
40. Andersson, A. *et al.* PKCalpha and HMGB1 antagonistically control hydrogen peroxide-induced poly-ADP-ribose formation. *Nucleic Acids Res.* http://dx.doi.org/10.1093/nar/gkw442 (2016).
41. Olsen, J. V. *et al.* Quantitative phosphoproteomics reveals widespread full phosphorylation site occupancy during mitosis. *Sci. Signal.* **3,** ra3 (2010).
42. Gibson, B. A. & Kraus, W. L. Small molecules, big effects: a role for chromatin-localized metabolite biosynthesis in gene regulation. *Mol. Cell.* **41,** 497–499 (2011).
43. Garnett, M. J. *et al.* Systematic identification of genomic markers of drug sensitivity in cancer cells. *Nature* **483,** 570–575 (2012).
44. Szklarczyk, D. *et al.* STRING v10: protein-protein interaction networks, integrated over the tree of life. *Nucleic Acids Res.* **43,** D447–D452 (2015).

45. Steen, H., Jebanathirajah, J. A., Springer, M. & Kirschner, M. W. Stable isotope-free relative and absolute quantitation of protein phosphorylation stoichiometry by MS. *Proc. Natl Acad. Sci. USA* **102,** 3948–3953 (2005).
46. Butepage, M., Eckei, L., Verheugd, P. & Luscher, B. Intracellular mono-ADP-Ribosylation in signaling and disease. *Cells* **4,** 569–595 (2015).
47. Asher, G. *et al.* Poly(ADP-ribose) polymerase 1 participates in the phase entrainment of circadian clocks to feeding. *Cell* **142,** 943–953 (2010).
48. Vyas, S. *et al.* Family-wide analysis of poly(ADP-ribose) polymerase activity. *Nat. Commun.* **5,** 4426 (2014).
49. Menzel, S. *et al.* Nucleotide-induced membrane-proximal proteolysis controls the substrate specificity of T Cell Ecto-ADP-Ribosyltransferase ARTC2.2. *J. Immunol.* **195,** 2057–2066 (2015).
50. Daniels, C. M., Ong, S.-E. & Leung, A. K. L. Phosphoproteomic approach to characterize protein mono- and poly(ADP-ribosyl)ation sites from Cells. *J. Proteome. Res.* **13,** 3510–3522 (2014).
51. Garber, K. PARP inhibitors bounce back. *Nat. Rev. Drug. Discov.* **12,** 725–727 (2013).
52. Vyas, S. & Chang, P. New PARP targets for cancer therapy. *Nat. Rev. Cancer.* **14,** 502–509 (2014).
53. Kleppa, L. *et al.* Kinetics of endogenous mouse FEN1 in base excision repair. *Nucleic Acids Res.* **40,** 9044–9059 (2012).
54. Hasan, S. *et al.* Regulation of human flap endonuclease-1 activity by acetylation through the transcriptional coactivator p300. *Mol. Cell.* **7,** 1221–1231 (2001).
55. Guo, Z. *et al.* Sequential posttranslational modifications program FEN1 degradation during cell-cycle progression. *Mol. Cell* **47,** 444–456 (2012).
56. Zhang, Y. *et al.* RNF146 is a poly(ADP-ribose)-directed E3 ligase that regulates axin degradation and Wnt signalling. *Nat. Cell Biol.* **13,** 623–629 (2011).
57. Chou, D. M. *et al.* A chromatin localization screen reveals poly (ADP ribose)-regulated recruitment of the repressive polycomb and NuRD complexes to sites of DNA damage. *Proc. Natl Acad. Sci. USA* **107,** 18475–18480 (2010).
58. Langelier, M. F., Planck, J. L., Roy, S. & Pascal, J. M. Structural basis for DNA damage-dependent poly(ADP-ribosyl)ation by human PARP-1. *Science* **336,** 728–732 (2012).
59. Moss, J. & Stanley, S. J. Amino acid-specific ADP-ribosylation. Identification of an arginine-dependent ADP-ribosyltransferase in rat liver. *J. Biol. Chem.* **256,** 7830–7833 (1981).
60. Aktories, K. *et al.* Botulinum C2 toxin ADP-ribosylates actin. *Nature* **322,** 390–392 (1986).
61. Jwa, M. & Chang, P. PARP16 is a tail-anchored endoplasmic reticulum protein required for the PERK- and IRE1alpha-mediated unfolded protein response. *Nat. Cell Biol.* **14,** 1223–1230 (2012).
62. Aktories, K. & Barbieri, J. T. Bacterial cytotoxins: targeting eukaryotic switches. *Nat. Rev. Micro.* **3,** 397–410 (2005).
63. Koch-Nolte, F., Fischer, S., Haag, F. & Ziegler, M. Compartmentation of NAD^+-dependent signalling. *FEBS Lett.* **585,** 1651–1656 (2011).
64. Bai, P. & Canto, C. The role of PARP-1 and PARP-2 enzymes in metabolic regulation and disease. *Cell Metab.* **16,** 290–295 (2012).
65. Houtkooper, R. H., Canto, C., Wanders, R. J. & Auwerx, J. The secret life of NAD^+: an old metabolite controlling new metabolic signaling pathways. *Endocr. Rev.* **31,** 194–223 (2010).
66. Bai, P. *et al.* PARP-1 inhibition increases mitochondrial metabolism through SIRT1 activation. *Cell Metab.* **13,** 461–468 (2011).
67. Pan, C., Kumar, C., Bohl, S., Klingmueller, U. & Mann, M. Comparative proteomic phenotyping of cell lines and primary cells to assess preservation of cell type-specific functions. *Mol. Cell. Proteomics.* **8,** 443–450 (2009).
68. Bartolomei, G., Leutert, M., Manzo, M., Baubec, T. & Hottiger, M. O. Analysis of chromatin ADP-Ribosylation at the genome-wide level and at specific loci by ADPr-ChAP. *Mol. Cell* **61,** 474–485 (2016).
69. Rappsilber, J., Ishihama, Y. & Mann, M. Stop and go extraction tips for matrix-assisted laser desorption/ionization, nanoelectrospray, and LC/MS sample pretreatment in proteomics. *Anal. Chem.* **75,** 663–670 (2003).
70. Cox, J. & Mann, M. MaxQuant enables high peptide identification rates, individualized p.p.b.-range mass accuracies and proteome-wide protein quantification. *Nat. Biotechnol.* **26,** 1367–1372 (2008).
71. Vizcaino, J. A. *et al.* The PRoteomics IDEntifications (PRIDE) database and associated tools: status in 2013. *Nucleic Acids Res.* **41,** D1063–D1069 (2013).

Acknowledgements

We thank members of the NNF-CPR for fruitful discussions and careful reading of the manuscript. Ms Monika Fey is acknowledged for the expression and purification of recombinant human PARG (University of Zurich) and Paolo Nanni for technical support for the MS measurements (FGCZ, University of Zurich). Stephan Christen and Deena Leslie Pedrioli provided editorial assistance and critical input during the writing (University of Zurich). The work carried out in the laboratory of MLN was in part supported by the Novo Nordisk Foundation Center for Protein Research; the Novo Nordisk Foundation (grant number NNF14CC0001 and NNF13OC0006477); the Lundbeck Foundation (Grant number R171-2014-1496); The Danish Council of Independent Research, grant number DFF 4002-00051 (Sapere Aude) and grant agreement number DFF 4183-00322A. ADP-ribosylation research in the laboratory of MOH is funded by the Kanton of Zurich, the University Research Priority Program (URPP) in Translational Cancer Biology at the University of Zurich, and the Swiss National Science Foundation (grant 310030B_138667).

Author contributions

R.M., S.J. and M.L.N. developed the method and M.L., V.B. and M.O.H. provided critical inputs. R.M., S.J., M.L., V.B. and S.C.L. performed HeLa MS experiments. M.L. and V.B. performed *in vitro* ADP-ribosylation assays, R.M. and V.B. performed the *in vitro* glycation analysis, and M.L. performed the liver tissue analysis. R.M. performed IF experiments and S.C.L performed validation by WBs. S.C.L. and C.Y. performed ETD measurements. M.O.H. and M.L.N. wrote the paper.

Additional information

Supplementary Information accompanies this paper at http://www.nature.com/naturecommunications

Competing financial interests: The authors declare no competing financial interests.

Reprints and permission information is available online at http://npg.nature.com/reprintsandpermissions/

How to cite this article: Martello, R. *et al.* Proteome-wide identification of the endogenous ADP-ribosylome of mammalian cells and tissue. *Nat. Commun.* **7,** 12917 doi: 10.1038/ncomms12917 (2016).

analytical chemistry

Article

pubs.acs.org/ac

Combining Higher-Energy Collision Dissociation and Electron-Transfer/Higher-Energy Collision Dissociation Fragmentation in a Product-Dependent Manner Confidently Assigns Proteomewide ADP-Ribose Acceptor Sites

Vera Bilan,[†,‡,∥] Mario Leutert,[†,‡,∥] Paolo Nanni,[§,∥] Christian Panse,[§] and Michael O. Hottiger*[,†]

[†]Department of Molecular Mechanisms of Disease, University of Zurich, 8057 Zurich, Switzerland

[‡]Ph.D. Program in Molecular Life Sciences, University of Zurich/ETH Zurich, 8057 Zurich, Switzerland

[§]Functional Genomics Center Zurich, University of Zurich/ETH Zurich, 8057 Zurich, Switzerland

Supporting Information

ABSTRACT: Protein adenosine diphosphate (ADP)-ribosylation is a physiologically and pathologically important post-translational modification. Recent technological advances have improved analysis of this complex modification and have led to the discovery of hundreds of ADP-ribosylated proteins in both cultured cells and mouse tissues. Nevertheless, accurate assignment of the ADP-ribose acceptor site(s) within the modified proteins identified has remained a challenging task. This is mainly due to poor fragmentation of modified peptides. Here, using an Orbitrap Fusion Tribrid mass spectrometer, we present an optimized methodology that not only drastically improves the overall localization scores for ADP-ribosylation acceptor sites but also boosts ADP-ribosylated peptide identifications. First, we systematically compared the efficacy of higher-energy collision dissociation (HCD), electron-transfer dissociation with supplemental collisional activation (ETcaD), and electron-transfer/higher-energy collision dissociation (EThcD) fragmentation methods when determining ADP-ribose acceptor sites within complex cellular samples. We then tested the combination of HCD and EThcD fragmentation, which were employed in a product-dependent manner, and the unique fragmentation properties of the ADP-ribose moiety were used to trigger targeted fragmentation of only the modified peptides. The best results were obtained with a workflow that included initial fast, high-energy HCD (Orbitrap, FT) scans, which produced intense ADP-ribose fragmentation ions. These potentially ADP-ribosylated precursors were then selected and analyzed via subsequent high-resolution HCD and EThcD fragmentation. Using these resulting high-quality spectra, we identified a xxxxxxKSxxxxx modification motif where lysine can serve as an ADP-ribose acceptor site. Due to the appearance of serine within this motif and its close presence to the lysine, further analysis revealed that serine serves as a new ADP-ribose acceptor site across the proteome.

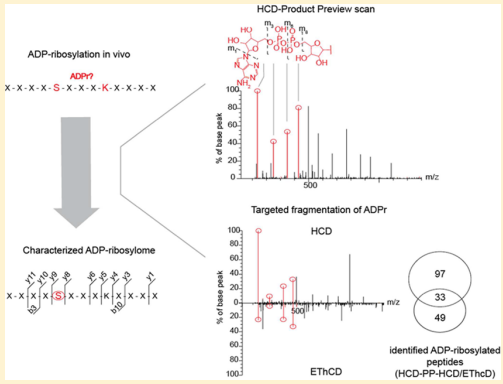

Protein adenosine diphosphate (ADP)-ribosylation is a reversible post-translational modification (PTM) that results from hydrolysis of nicotinamide adenine dinucleotide (NAD^+) and, subsequently, covalent conjugation of a mono-ADP-ribose unit (MAR) to the acceptor protein (MARylation reaction) or to an ADP-ribose moiety already attached to the protein, forming poly-ADP-ribose (PAR; PARylation reaction).[1] The enzyme diphtheria toxin-like ADP-ribosyltransferase 1 (ARTD1) and other ARTD family members [also known as poly ADP-ribosyltransferases (PARPs)] are the major enzymes responsible for catalyzing this reaction in cells.[2,3] Lysine (K), arginine (R), and aspartic (D) and glutamic (E) acids are the main acceptors of ADP-ribosylation.[2] Additionally, cysteine, diphthamide, phosphoserine, and asparagine serve as possible ADP-ribosylation acceptor sites.[4] ADP-ribosylation regulates several important cellular functions, including stress responses,[5] epigenetic transcriptional regulation,[6,7] RNA splicing and transport,[8] and cell fate determination.[7,9]

The introduction of mass spectrometry (MS)-based techniques drastically improved the ability to detect ADP-ribosylated proteins and their modification site(s). Several MS-based approaches have been described;[10−12] unfortunately, despite these advances, accurate mass spectrometric ADP-ribose acceptor site localization remains challenging. This may be due to the poor ionization capacity and hampered fragmentation properties of the modified peptides, especially PARylated peptides. To tackle this, several strategies have been

Received: August 26, 2016
Accepted: December 28, 2016
Published: December 28, 2016

DOI: 10.1021/acs.analchem.6b03365
Anal. Chem. 2017, 89, 1523−1530

developed to reduce PAR complexity and to improve identification accuracy. Zhang et al.[11] applied boronic acid enrichment with a chemical elution approach in which the ADP-ribosylated peptides are exposed to hydroxylamine. Unfortunately, this method is limited to ADP-ribosylated glutamic (E) and aspartic (D) acids. Several acceptor-site-independent enzymatic conversion approaches, including the use of phosphodiesterases [i.e., snake venom phosphodiesterase (SVP)[13]] or ADP-ribosylhydrolases [i.e., poly-ADP-ribose glycohydrolase (PARG)[14]], have also been recently developed. Phosphodiesterase treatment converts PAR and MAR into phosphoribose (212.01 Da), while PARG treatment converts PAR into MAR (541.06 Da). Indeed, these MAR and PAR modification size reductions improve the ionization capacities of all modified peptides. However, the ADP-ribosyl group and its fragmentation pattern provide interesting features that can be used during MS measurement and downstream bioinformatic analysis. Upon higher-energy collision dissociation (HCD), the ADP-ribose moiety fragments into characteristic marker ions that are mainly represented by adenine$^+$ (136.06), adenosine$-H_2O^+$ (250.09), AMP$^+$ (348.07), and ADP$^+$ (428.03) (Figure S1A).[15] The presence of these ADP-ribosylation marker ions can be exploited during the measurement process to trigger product-dependent MS events. Moreover, the presence of marker ions in MS/MS spectra validates the presence of ADP-ribosylation on the precursor ion and allows for accurate scoring of its assignment with a search engine. Unfortunately, in some cases, these ions dominate the spectra and obstruct proper precursor fragmentation. Thus, optimization of the applied normalized collision energy (NCE) should be performed to balance precursor fragmentation and marker ions' intensity.

Hengel et al.[16] suggested that electron-transfer dissociation with supplemental collisional activation (ETcaD) fragmentation could enhance precise ADP-ribose acceptor site localization. When comparing ETcaD to HCD fragmentation, we found that the HCD method identified ADP-ribosylation sites with the same localization probability as ETcaD.[15] Nevertheless, when HCD and ETcaD fragmentation were combined in one run (so-called "product-dependent method") on an LTQ Orbitrap Velos mass spectrometer, the identification of ADP-ribosylation sites in in vitro ADP-ribosylated samples increased.

New-generation Orbitrap Fusion and Orbitrap Lumos Tribrid mass spectrometers (Thermo Scientific) introduced an electron-transfer/higher-energy collision dissociation (EThcD) peptide fragmentation methodology that combines HCD and ETcaD into one fragmentation event. This has the advantage that peptide backbone fragmentation is improved and that dual fragmentation generates data-rich MS/MS spectra containing both b/y and c/z ions, which ultimately improves peptide sequence coverage and PTM localization confidence.[17] EThcD fragmentation has already proven beneficial for unambiguous phosphorylation site localization, even on peptides with several possible amino acid acceptors.[18]

In this study, we strove to exploit these features of the Orbitrap Fusion Tribrid mass spectrometer for analysis of ADP-ribosylated peptides. As a model system, we used HeLa cells challenged with oxidative stress in combination with Af1521 peptide enrichment.[14] First, individual HCD, ETcaD, and EThcD fragmentation performances were evaluated by comparing the quality and quantity of identified ADP-ribosylated peptides and ADP-ribosylation site assignment accuracy. Overall, we found that HCD and EThcD fragmentation methods identified complementary ADP-ribosylated peptide sets and outperformed ETcaD. In a second step, we exploited the ADP-ribose marker ion properties and evaluated how combining HCD and EThcD into one product-dependent method performed relative to the individual fragmentation methods. This led to the development of a specialized ADP-ribosylation analysis workflow on the Orbitrap Fusion, which significantly augmented our ability to globally characterize the cellular ADP-ribosylome and confidently assign ADP-ribosylation sites.

EXPERIMENTAL SECTION

ADP-Ribosylated Peptide Enrichment. HeLa cells (Kyoto) were cultured in Dulbecco's modified Eagle's medium [DMEM, supplemented with 10% fetal calf serum (FCS) and 1% penicillin/streptavidin] at 37 °C with 5% CO_2. Cells were treated for 10 min with 1 mM H_2O_2 to induce PAR formation and then further processed and enriched with Af1521 macrodomain protein as previously described.[14]

Liquid Chromatographic/Mass Spectrometric Analysis. Mass spectrometric analysis was performed on an Orbitrap Fusion mass spectrometer, which combines three mass analyzers (Orbitrap, quadrupole, and ion trap), coupled to a nano EasyLC 1000 liquid chromatograph (Thermo Fisher Scientific). Solvent compositions in channels A and B were 0.1% formic acid in H_2O and 0.1% formic acid in acetonitrile, respectively. Self-made 75 μm × 150 mm columns, packed with reverse-phase C18 material (ReproSil-Pur 120 C18-AQ, 1.9 μm, Dr. Maisch GmbH), were used, and aliquots (4 μL) of peptide solution were loaded onto the columns and eluted over 80 min at a flow rate of 300 nL/min. An elution gradient protocol from 2% to 25% B, followed by two steps, 35% B for 5 min and 95% B for 5 min, was used. The mass spectrometer (Tune page v2.0) was set to acquire full-scan MS spectra (300−1500 m/z) at 120 000 resolution at 200 m/z; precursor automated gain control (AGC) target was set to 200 000. Charge-state screening was enabled, and precursors with +2 to +5 charge states and intensities >50 000 were selected for tandem mass spectrometry (MS/MS). Ions were isolated by use of the quadrupole mass filter with a 2 m/z isolation window. Wide quadrupole isolation was used, and injection time was set to 50 ms. The cycle time was set to 3 s (top speed mode). In total, five different MS/MS acquisition methods were performed in randomized order and their performances were compared. These included (a) Orbitrap HCD MS/MS (HCD only); (b) Orbitrap ETcaD MS/MS (ETcaD only); (c) Orbitrap EThcD MS/MS (EThcD only); (d) data-dependent HCD followed by EThcD MS/MS when more than one ADP-ribose fragment peak (136.0623, 250.0940, 348.07091, and 428.0372) was observed in the HCD scan (HCD-PD-EThcD; where PD = product-dependent); (e) low-resolution and high-energy data-dependent HCD (named preview HCD), followed by high-quality HCD and EThcD MS/MS when more than two ADP-ribose fragment peaks (136.0623, 250.0940, 348.07091, and 428.0372) were observed in the HCD scan (HCD-PP-HCD-EThcD, where PP = product preview). The parameters for MS/MS fragmentations changed according to the method applied. The AGC values for MS/MS analysis were set to 500 000 and the maximum injection time was 240 ms for all experiments. For the HCD preview scan (method e) only, AGC target was set to 50 000 and injection time was set to 60 ms. With the exception of the HCD preview scan, whose

DOI: 10.1021/acs.analchem.6b03365
Anal. Chem. 2017, 89, 1523−1530

normalized collision energy (NCE) was set to 38% in order to obtain higher marker ion intensities, all other HCD fragmentations were performed at an NCE of 35%. For ETcaD and EThcD fragmentations, the "use-calibrated charge-dependent parameter" option was selected. In all cases, precursor masses previously selected for MS/MS measurement were excluded from further selection for 30 s, and the exclusion window was set at 10 ppm. All measurements were acquired using internal lock mass calibration on m/z 371.1010 and 445.1200. A complete description of all tandem MS experiments employed in this study can be found in Table S1.

Data Analysis. MS and MS/MS spectra were converted to Mascot generic format (MGF) by use of Proteome Discoverer, v2.1 (Thermo Fisher Scientific, Bremen, Germany). When multiple fragmentation techniques (HCD, ETcaD, or EThcD) were utilized, separate MGF files were created from the raw file for each type of fragmentation. All MS/MS spectra were deconvoluted by use of the MS Spectrum Processor (http://ms.imp.ac.at/?goto=ms2spectrumprocessor). In the ETcaD and EThcD spectra, the precursor, charge-reduced precursor(s), and neutral loss peaks were removed within a 0.5 Da window. The MGFs were searched against the UniProtKB human database (taxonomy 9606, version 20140422), which included 35 787 Swiss-Prot entries, 37 802 TrEMBL entries, 73 589 decoy hits, and 260 common contaminants. Mascot 2.5.1.3 (Matrix Science) was used for peptide sequence identification with previously described search settings.[15] Briefly, a peptide tolerance of 10 ppm and MS/MS tolerance of 0.05 Da were used. For the HCD runs, singly charged b and y ion series, immonium ions, water loss, and ammonia loss ion series were searched. For ETcaD, singly charged c, y, z, (z + 1), and (z + 2) series were considered. For EThcD, singly charged b, c, y, z, (z + 1), and (z + 2) ion series, immonium ions, and water and ammonia loss ion series were used. Enzyme specificity was set to trypsin, and up to four missed cleavages were allowed. Decoy hits were used to control false discovery rates (FDR) on the peptide and protein levels. The ADP-ribose variable modification was set differently for HCD, EThcD, and ETcaD spectra searches. For HCD and ETcaD MGFs, the modification was set as previously described.[15] For EThcD MGFs, the modification was set to a mass shift of 541.0611 and marker ions at m/z 428.0372, 348.0709, 250.0940, and 136.0623 were ignored for scoring. An ADP-ribosylated peptide was considered to be correctly identified when the Mascot score was >20 and the expectation value was <0.05. To define ADP-ribosylation site localizations, Mascot site localization analysis[19] was used, and sites with a Mascot-derived site localization confidence of ≥95% were considered as correctly assigned. To obtain site localization information, the searches were subjected to analysis via B-fabric.[20]

To screen the spectra for the presence of ADP-ribose marker ions (m/z = 136.0623, 250.0940, 348.0709, and 428.0372), all of the Mascot output.dat files were further analyzed by use of PTM MarkerFinder contained in the The Comprehensive R Archive Network (CRAN) package protViz (available through https://cran.rproject.org/package=protViz).[21] Spectra containing >2 marker ions and marker ion intensity sum ≥3% (for HCD > 10%) of the total ion intensities were considered as putative ADP-ribosylated modified peptide spectra.

Finally, peptide coverage information was obtained by use of an in-house R script using the CRAN protViz package. The ".dat" files were screened for the presence of the in silico-computed m/z peak of fragment ions. Ion intensity was set to 5% of total spectrum intensity with a mass tolerance of 10 ppm.

Motif Discovery by Use of Scaffold PTM. Identification of ADP-ribosylation motifs was carried out by use of Scaffold PTM software, v.2.1.3 (Proteome Software). All files were imported into Scaffold software, v.4.2.0 (Proteome Software), and filtered according to a 0.1% FDR peptide threshold and a 3% FDR protein threshold.

RESULTS AND DISCUSSION

EThcD Complements HCD Identification of ADP-Ribosylated Peptides. In this study, we analyzed the ADP-ribosylome of HeLa cells during oxidative stress, which was triggered by treating the cells with 1 mM H_2O_2 for 10 min. Oxidative stress is a well-known and very potent inducer of protein ADP-ribosylation. This is thought to be catalyzed by nuclear ADP-ribosyltransferase (ARTD1, ARTD2, and/or ARTD3) activation.[5,22,23] Following H_2O_2 treatment, cells were lysed in the presence of PARP and PARG inhibitors. The recovered proteins were digested with trypsin, PAR modifications were reduced to MARs via PARG treatment, and ADP-ribosylated peptides were affinity-purified by use of the Af1521 macrodomain.[14] Initial parameter optimizations on the Orbitrap Fusion Tribrid mass spectrometer, with HCD fragmentation, revealed that an NCE of 35 was ideal for the fragmentation of ADP-ribosylated peptides. In addition, spectral quality increased when higher numbers of ions (AGC 5 × 10^5) were accumulated over longer periods of time (240 ms) (Figure S1B). These optimized acquisition settings were implemented in all further HCD-based MS applications. Due to the presence of phosphate groups in the MAR, we tried to include the fragmentation of +1 charge state precursors, but overall identification were decreased due to the fragmentation of chemical contamination precursors. The performance of HCD to identify ADP-ribosylated peptides, compared to ETcaD or EThcD fragmentation, was evaluated on these HeLa cell-derived samples (n = 4/MS method). Each fragmentation method was evaluated on the basis of the ADP-ribose fragmentation pattern and the number and properties of the identified ADP-ribosylated peptides. As previously reported,[15] initial spectra analyses revealed that primary HCD spectra signals for ADP-ribosylated peptides were generated from ADP-ribose fragmentation (Figure 1).

Applying the PTM Markerfinder tool[21] to the spectra generated by HCD fragmentation, we identified 5313 spectra with ≥2 ADP-ribose marker ions with total intensities >10% (Figure S1C). The adenine$^+$ (136.0618) marker ion was the most intense ion identified, while all other marker ions were

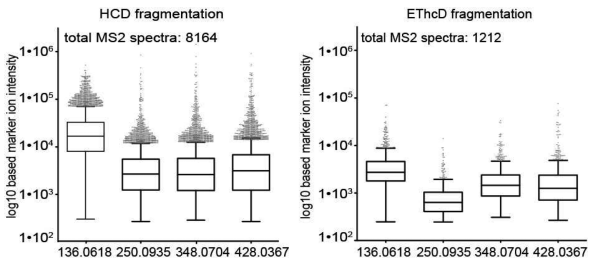

Figure 1. Intensity distribution of marker ions in HCD and EThcD fragmentation. Spectra where the marker ions represented at least 3% of total intensity and with ≥2 marker ions were analyzed.

DOI: 10.1021/acs.analchem.6b03365
Anal. Chem. 2017, 89, 1523−1530

produced with about 10 times lower intensities (Figure 1 and Figure S1D). In contrast, ETcaD fragmentation failed to generate any ADP-ribose marker ion-containing spectra, even when the total ion intensity threshold was decreased to 3%. The absence of marker ions in ETcaD spectra was expected on the basis of the mild nature of this fragmentation method, as well as the fact that modifications are kept intact during this fragmentation.[24] ADP-ribose marker ions were, however, observed in the EThcD analysis, but they represented only 3−5% of total ion intensities. Decreasing the marker ion intensity threshold to 3% for HCD- and EThcD-produced spectra significantly increased the number of spectra containing marker ions for EThcD: 1212 total MS/MS spectra versus 8164 spectra for HCD (Figure 1). However, out of the total marker ion-containing spectra, around 70% were multiple spectra from the same precursors (i.e., duplicate spectra). After these duplicates had been removed, 380 and 2291 MS/MS spectra belonging to unique precursors were identified by EThcD and HCD, respectively. The adenosine$-H_2O^+$ (250.0935) ion had the lowest marker ion intensity in EThcD, while HCD fragmentation-generated marker ions (except 136.06 ion) all had similar intensities (Figure 1). Overall, the relative average abundance of ADP-ribose fragments following EThcD fragmentation was about 5-fold lower than in HCD spectra. Thus, the EThcD- and HCD-produced marker ion profiles could be used to validate ADP-ribosylated identification. We were not able define amino-acid-specific marker ion intensity patterns that could be used to characterize modification acceptor sites; instead, the marker ions enabled ADP-ribose-containing peptide-spectrum match (PSM) spectral identification. Next, we compared the fragmentations by the number of unique identified peptides. A unique peptide was defined as a peptide with a unique modification site. In this case, two peptides with identical amino acid sequence but with different site localization were considered as two unique peptides. In agreement with our previous findings, ETcaD fragmentation failed to identify large numbers of ADP-ribosylated peptides[15] (Table 1, Figure 2A).

Table 1. Analysis of ADP-Ribosylated Peptides Identified by HCD, ETcaD, and EThcD Fragmentations

	ADP-ribosylated PSMs[a]	ADP-ribosylated peptides	ADP-ribosylated sites	
method	total	total	total	loc probability >95% (% total identifications)
HCD	276	105	92	60 (63.8)
ETcaD	113	52	40	20 (51.9)
EThcD	195	70	56	30 (60.5)

[a]PSM, peptide-spectrum match.

In contrast, HCD identified twice as many unique ADP-ribosylated peptides (52 for ETcaCD vs 105 for HCD) and ETcaD fragmentation required longer acquisition times than HCD, which decreased the overall number of MS/MS spectra generated (total number of MS/MS spectra 45 532 vs 65 795).

The overall decrease in identified spectra may partially explain why fewer ADP-ribosylated peptides were identified by the ETcaD fragmentation method. EThcD fragmentation, which generated 47 112 spectra, identified 70 unique ADP-ribosylated peptides. This finding highlights the superior performance of this fragmentation method when compared to ETcaD. Comparative analysis of peptides identified by the different fragmentation methods revealed that EThcD identified 42 unique ADP-ribosylated peptides (gain of 26% total) that were not detected with HCD fragmentation (Figure 2B). Seventeen of these EThcD-unique ADP-ribosylated peptides were also assigned in the ETcaD run. Moreover, ETcaD identified 13 unique ADP-ribosylated peptides (19% gain) that were not present in either the EThcD or HCD runs. Further investigation into the physical properties of the identified ADP-ribosylated peptides (charge, length, and chemical composition) revealed that ETcaD demonstrated a clear preference for higher charge-state precursors (3+ and 4+). We did not, however, observe any differences in average ADP-ribosylated peptide length or chemical composition for the tested fragmentation methods (Figure S2). In conclusion, as judged by the number of PSMs and unique identified ADP-ribosylated peptides, HCD fragmentation performed best. EThcD fragmentation performed less favorably but identified additional modified peptides. These findings suggested that a combination of HCD and EThcD could be beneficial for in-depth ADP-ribosylome characterization. For HCD, around 40% of unique ADP-ribose marker ion-containing spectra were assigned by the Mascot search. The unassigned spectra might be partially explained by the poor fragmentation of ADP-ribosylated peptides, peptides that are shorter or longer than the set threshold, peptides that fall under the applied scoring threshold in Mascot, and/or a not fully optimized search algorithm. This suggests the possibility for further improvements in the bioinformatics analysis pipeline, including the development of algorithms that score the presence of marker ions.

HCD and EThcD Localize ADP-Ribose Acceptor Sites with High Confidence. Previous studies reported the benefit of EThcD to accurately localize serine and threonine phosphorylation sites.[18] Therefore, we compared how the different fragmentation methods performed when attempting to confidently assign four described ADP-ribosylation acceptor sites: lysine (K), arginine (R), glutamic acid (E), and aspartic acid (D) HCD, ETcaD, and EThcD localized all four acceptor amino acids with high confidence. For HCD fragmentation measurements, the modification acceptor sites were assigned with confidence >95% for 63.8% of the identified unique ADP-ribosylated sites. ETcaD assigned 51.9% of the unique ADP-ribosylated sites with similar confidence (Table 1). EThcD performed comparably to HCD, assigning 60.5% of the unique ADP-ribosylated sites with >95% confidence. Moreover, acceptor sites identified with a localization probability of less than 60% represented only 4% of all ADP-ribose acceptor sites identified with EThcD, whereas they comprised 18% of the ADP-ribosylated sites identified with HCD (Figure 2C). This fact points to better peptide fragmentation with EThcD in comparison to HCD.

To understand the localization probabilities in more detail, we compared the peptide coverage information obtained from all fragmentation methods and looked for the presence of characteristic ions, which were defined as the first fragment ions carrying the modification. To evaluate peptide sequence coverage, the number of ions used by Mascot for scoring was normalized to the length of the peptide (the presence of a full ion series corresponds to a coverage ratio of 1). In agreement with the localization probability assignments, HCD and EThcD performed comparably, with slightly better fragmentation than ETcaD (Figure S1E). Furthermore, each fragmentation method was compared on the basis of the presence of acceptor-site-

DOI: 10.1021/acs.analchem.6b03365
Anal. Chem. 2017, 89, 1523−1530

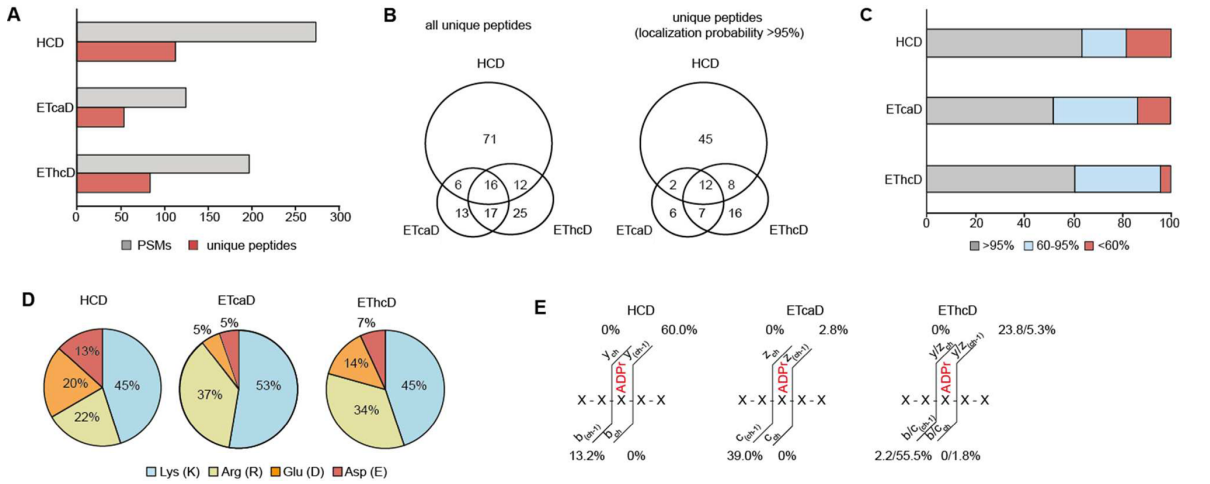

Figure 2. Evaluation of HCD, ETcaD, and EThcD fragmentation performance for ADP-ribosylated peptide identification. (A) Number of ADP-ribosylated peptide spectrum matches (PSMs) and unique peptides identified by each fragmentation. (B) Venn diagram showing overlap in the unique peptide identified by each fragmentation method. (C) Distribution of ADP-ribosylated localization probability of unique ADP-ribosylated peptides identified with each fragmentation method. Values were normalized to total numbers of unique ADP-ribosylated peptides. (D) Distribution of amino acid acceptor sites from unique ADP-ribosylated peptides. Only peptides with localization probability >95% were considered. (E) Presence of modification-characteristic ions in the spectra of ADP-ribosylated peptides. Characteristic ions were defined as the first fragment ions carrying the modification. The number close to the ion shows the frequency at the ion was observed with the specified fragmentation method.

characterizing ions (Figure 2E). For each fragmentation, characteristic y/b or z/c ions were not observed (only in 1.8% c-ion series generated by EThcD but not with other fragmentations). However, HCD and EThcD often produced ions before the modification site, whereas ETcaD did not generate ions close to the assigned modification site.

Overall, ETcaD performed significantly worse than HCD and EThcD for ADP-ribosylation site identification and localization. For this reason, ETcaD was excluded from further analysis. In agreement with previous phosphoproteomics studies,[18,25] we found that the localization probabilities for ADP-ribosylation showed a general improvement when EThcD fragmentation methods were used. Together, ADP-ribosylated peptides with localization probabilities >95% represented ~60% of all HCD- and EThcD-identified acceptor sites. EThcD did, however, provide slightly better-quality spectra. In a previous study, performed on an Orbitrap Velos, only 10% of the identified acceptor sites had localization probabilities >95%.[15] Thus, this study showed a significant improvement in unambiguous site assignment, which was largely due to technological improvements and the development of new fragmentation techniques. Together, these findings suggest that both HCD and EThcD could be used to confidently localize ADP-ribosylated acceptor sites.

ADP-Ribose Marker-Ion-Dependent Combination of HCD and EThcD Improves ADP-Ribosylated Peptide Identification. Our previous study,[15] together with the findings presented above, suggest that combining different fragmentation methods in an ADP-ribose marker ion product-dependent manner could increase the number of ADP-ribosylated peptides identified by use of the Orbitrap Fusion. The observation that the EThcD fragmentation-identified sites were complementary to those identified via HCD, combined with excellent localization scores generated from both fragmentation methods, prompted us to develop a method that would combine HCD and EThcD into a single measurement. Furthermore, to optimize measurement efficiency and focus specifically on ADP-ribosylated peptides, we integrated a precursor selection criterion that is based on the detection of ADP-ribose marker ions, whose presence triggers subsequent product-dependent EThcD and/or HCD. For this product-dependent method (HCD-PD-EThcD), HCD MS/MS spectra were generated as described for the single HCD method. When at least one ADP-ribose marker ion was observed during the HCD MS/MS scan, the same precursor was selected again and fragmented by EThcD. The HCD-PD-EThcD methodology significantly increased ADP-ribosylated PSMs (429 vs 276 for HCD alone; Figure 3A and Table 2). Despite this increase, only a 20% increase in unique ADP-ribosylated peptides identifications was observed (126 unique ADP-ribosylated peptides vs 105 for HCD alone). This could,

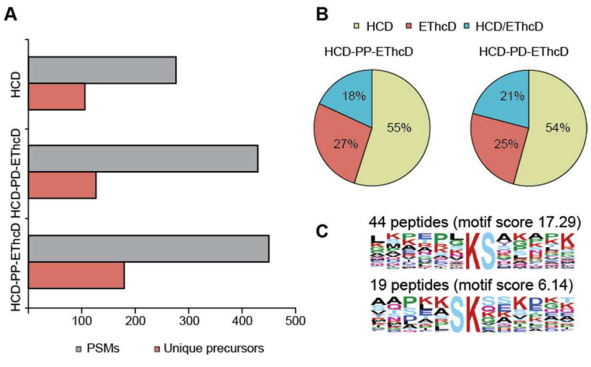

Figure 3. Evaluation of HCD-PD-EThcD and HCD(FT)-PP-EThcD performance for ADP-ribosylated peptide identification. (A) Number of PSMs and unique peptides (score >20, expectation <0.05) identified by each product-dependent method. (B) Contribution of HCD and EThcD fragmentations in product-dependent methods for identification of ADP-ribosylated peptides. (C) Putative ADP-ribosylation motif for lysine as ADP-ribose acceptor site. ADP-ribosylated modification motif for K sites was identified with Scaffold PTM.

DOI: 10.1021/acs.analchem.6b03365
Anal. Chem. 2017, 89, 1523−1530

Table 2. Identification of ADP-Ribosylated Peptides via Product-Dependent Methods Including Contribution of HCD and EThcD to Total Assignment

	ADP-ribosylated PSMs[a]	ADP-ribosylated peptides		ADP-ribosylated sites	
method	total	total	%	total	%
HCD-PD-EThcD	429	126		99	
including HCD	265	69	55	58	59
EThcD	164	30	24	22	22
overlap		27	21	19	19
HCD-PP-EThcD	450	179		141	
including HCD	349	97	54	86	61
EThcD	196	49	27	31	22
overlap		33	19	24	17

[a]PSM, peptide-spectrum match.

potentially, result from mass spectrometer speed capacity saturation.

To fully exploit the advantages of this dual fragmentation method, we aimed to optimize the instrument's cycle time and implement a new method called HCD-PP-HCD/EThcD. In this workflow, every MS1 spectrum acquisition was followed by a product preview (PP) HCD MS/MS scan, performed in the Orbitrap (FT acquisition) at low resolution (30K) with high NCE (38). These settings resulted in fast MS/MS lower-quality spectra acquisitions that gave very intense ADP-ribose marker ion signals. Given that PP FT-HCD injection times are 4 times shorter than FT-HCD injection times, these alterations generated 4 times more scans per duty cycle. After initial PP-FT-HCD scans, the instrument was then programmed to select precursors with >2 ADP-ribose marker ions to record additional MS/MS spectra via high-quality HCD and EThcD fragmentation. When compared to the HCD-PD-EThcD method described above, this new HCD-PP-HCD/EThcD strategy identified an additional 42% unique ADP-ribosylated peptides (Figure 3A), and it identified 70% more when compared to HCD alone. The contribution of EThcD fragmentation to the identification of ADP-ribosylated peptides in these product-dependent methods was similar to the performance of EThcD alone and contributed to at least 22% of all identifications (Figure 3B and Table 2).

Given these positive results, we also attempted to implement an HCD (IT)-PP-HCD/EThcD method. Unfortunately, we found that the preview scan in the ion trap (IT) led to a high proportion of false positives and the overall performance of this method was worse than other product-dependent methods (data not shown). Product-dependent methods, which combine HCD and ETcaD fragmentations, have been previously reported for analysis of complex post-translational modifications, as in glycoproteins.[26,27] Therefore, we optimize machine duty time and tested whether use of ADP-ribose marker-ion-triggered product-dependent MS/MS measurements would promote efficient ADP-ribosylation acceptor site identification. To this end, we found that the fast, high-energy, low-resolution preview HCD MS/MS scans, which triggered subsequent MS/MS (>2 ADP-ribose fragmentation ions), optimized machine capacity and efficiently selected the appropriate ADP-ribosylated precursors. Moreover, when combined with subsequent HCD and EThcD, this strategy significantly enhanced ADP ribosylated peptide identifications compared to HCD or EThcD alone.

Improved ADP-Ribosylation Site Assignments Identified a Lysine ADP-Ribosylation Motif. Next, we assessed the distribution of known ADP-ribose acceptor sites (K, R, D, E) that were identified with high localization confidence (localization probability >95%) by the different fragmentation methods. Interestingly, K was the most abundant acceptor amino acid identified in this analysis, representing 45% of total unique sites for both HCD and EThcD and 52% for ETcaD. We also found that R was more often observed as acceptor site in ETcaD or EThcD fragmentation methods and that the identification of E and D acceptor sites was underrepresented in the ETcaD fragmentation data sets (Figure 2D and Figure

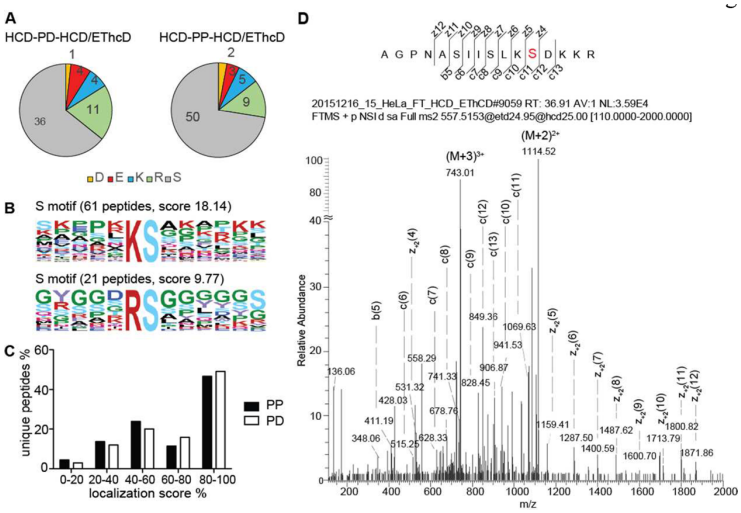

Figure 4. (A) Distribution of amino acid acceptor sites of unique ADP-ribosylated peptides. Only peptides with localization probability >95% were considered. The number of unique peptides is indicated. (B) ADP-ribosylation motif for S sites. (C) Distribution of ADP-ribosylated localization probability of unique ADP-ribosylated peptides identified with each fragmentation method. (D) EThcD fragmentation of an ADP-ribosylated peptide modified on S.

DOI: 10.1021/acs.analchem.6b03365
Anal. Chem. 2017, 89, 1523−1530

S3A). These high-quality ADP-ribosylated peptide spectra and their corresponding acceptor site identifications prompted us to further analyze the peptide sequences for potential ADP-ribosylation motifs. When the lysine acceptor sites were studied, 48% of the modification sites (44 out of 90) contained a xxxxxxKSxxxxx motif and 20% had a xxxxxxSKxxxxx motif (19 out of 90) (Figure 3C and Figure S3B and Table S2). We were not able to detect any consensus modification sequences for D, E, or R acceptor sites in our data set.

Proteomewide Identification of Serine ADP-Ribosylation Sites. The appearance of serine adjacent to the lysine acceptor site at the xxxxxxKSxxxxx motif prompted us to re-evaluate our data and determine whether serine could also be a potential ADP-ribose acceptor site. Indeed, including serine as a fifth potential ADP-ribose acceptor site increased ADP-ribosylated PSM detection (additional 524 PSMs for HCD-PP-HCD/EThcD method; Figure S3C) and led to the identification of 137 additional unique ADP-ribosylated precursors. Analysis of confidently identified ADP-ribose acceptor sites suggests that serine is a major target for ADP-ribosylation (Figure 4A). These findings are in agreement with a recent study that reported that histones were predominantly ADP-ribosylated at serine residues.[28] Further analyses of the ADP-ribosylated serine spectra confirmed the existence of a xxxxxxKSxxxxx motif (Figures 3C and 4B). Additionally, a novel xxxxxxRSxxxxx motif was also identified in 21 unique serine-ADP-ribosylated peptides (Figure 4B and Table S3). Of the assigned modified serines, 24% were without an adjacent K or R.

Importantly, the quality of the spectra remained high, but inclusion of serine within our analysis pipeline increased the number of peptides with localization probabilities around 50% (Figure 4C). This could be associated with the presence of the xxxxxxKSxxxxx or xxxxxxRSxxxxx motifs in the identified peptides, which makes it difficult to confidently assign the ADP-ribosylation site, as only two fragment ions (HCD) or four fragment ions (EThcD) discriminated these sites. In support of this, we found that, within the HCD-PP-HCD/EThcD data, ~75% of the unique peptides with localization probabilities <60% also had at least one additional possible ADP-ribose acceptor site adjacent to the assigned modification site, while 58% of the unique peptides with localization probabilities >60% had no adjacent possible acceptor site. We obtained highly confident assignments for serine ADP-ribose acceptor sites located adjacent to lysine residues (Figure 4D). In fact, when serine was included as a potential ADP-ribose acceptor site in our searches, significantly lower numbers of ADP-ribosylated lysines were assigned and those identified were mainly supported by HCD spectra (Figure S3D). Overall we observed proteomewide occurrence of serine ADP-ribosylation, due to novel assigned ADP-ribosylated precursors as well as a partial shift of previously assigned lysine-ADP-ribosylation to a proximal serine (Figure 4A). Interestingly, the use of EThcD fragmentation allowed us to identify a new peptide species that carries two ADP-ribose moieties (Figure S4). Another ARTD1 dual-modified precursor had been previously identified following MS analysis of in vitro-modified ARTD1.[13] Initially the two sites were assigned to K508 and E520 as acceptor sites (Figure S4A), and after inclusion of S as a potential acceptor site in the Mascot search parameters, the modifications were then assigned to S507 and either S519 or E520 (only S507 was confidently assigned) (Figure S4B).

CONCLUSIONS

Several techniques to enrich, process, and analyze ADP-ribosylated peptides from complex samples have been published. These techniques, however, usually employ standard mass spectrometric methods. The analysis of complex PTMs like ADP-ribosylation, however, requires an optimized methodology that tackles the specific features of the PTM and resulting modified peptides. Here, we harnessed the full MS potential of the Orbitrap Fusion Tribrid and exploited the unique properties of ADP-ribose fragmentation to establish an ADP-ribosylome customized MS workflow. Parameter optimization and systematic performance comparisons of HCD, ETcaD, and EThcD fragmentation of endogenous ADP-ribosylated peptides revealed that HCD alone identified the most modified peptides. Importantly, we also discovered that EThcD fragmentation identified 42 unique ADP-ribosylated peptides that were not present in the HCD data set. These findings suggested that a combination of HCD and EThcD fragmentation would allow in-depth characterization of the cellular ADP-ribosylome. To this end, we established a HCD-PP-HCD/EThcD method that supported robust ADP-ribosylome discovery studies. The method consists of several important implementations: (1) initial fast, high-energy HCD scans that promote generation of ADP-ribose marker ions and allows preselection of potential ADP-ribosylated peptide precursors and (2) two high-resolution HCD and EThcD measurements of the preselected precursors. This method significantly improved the efficient identification of ADP-ribosylated peptides, and high quality MS/MS spectra were acquired that allowed the accurate localisation of ADP-ribose acceptor sites within the peptide. To our knowledge, this HCD-PP-HCD/EThcD workflow is the most optimized and efficient method for ADP-ribosylation site identification in complex samples. Importantly, the improvements described here generated a unique and highly accurate data set that allowed us to define the first modification motif for K and S as ADP-ribose acceptor sites.

Identification of ADP-ribosylation motifs would greatly benefit the effort to identify potential ADP-ribosylation targets, as was seen in the phosphorylation field. It remains to be clarified if and what the biological relevance of the identified motif is, since this might help to determine the target specificity of the ARTD enzymes. Furthermore, the techniques for proteomewide ADP-ribosylation site mapping are only started to develop.

Applying different fragmentation techniques to ADP-ribosylated peptides led to the recognition of serine as ADP-ribose acceptor across the proteome. This discovery suggests that additional amino acid ADP-ribose acceptor sites could be present in vivo. Importantly, this novel methodology produces high-quality spectra for ADP-ribosylated peptides. This is critical to the identification of all possible ADP-ribose acceptor amino acids via thorough bioinformatic analysis and subsequent biochemical validation.

ASSOCIATED CONTENT

Supporting Information

The Supporting Information is available free of charge on the ACS Publications website at DOI: 10.1021/acs.analchem.6b03365.

Three tables listing overview of evaluated MS/MS methods and identified ADP-ribosylated peptides with K and S motifs and corresponding protein IDs; four

DOI: 10.1021/acs.analchem.6b03365
Anal. Chem. 2017, 89, 1523−1530

figures showing MS/MS fragmentation of ADP-ribosylated peptides, physicochemical characteristics of ADP-ribosylated peptides identified with HCD, ETcaD, and EThcD fragmentations, search results with K, R, D, E, and S modification sites, and EThcD fragmentation of dual-modified peptide (PDF)

AUTHOR INFORMATION

Corresponding Author

*E-mail michael.hottiger@dmmd.uzh.ch; phone +41 44 635 54 74; fax +41 44 635 54 68.

ORCID

Paolo Nanni: 0000-0001-8429-3557

Michael O. Hottiger: 0000-0002-7323-2270

Author Contributions

[||]V.B., M.L., and P.N. contributed equally.

Notes

The authors declare no competing financial interest.

The raw file, peak list files (MGFs), and result files (mzIdent) from the present study were uploaded into Proteome Xchange and can be accessed within PXD004676 data set number.

ACKNOWLEDGMENTS

We thank Monika Fey for the expression and purification of recombinant human PARG. Stephan Christen and Deena Leslie Pedrioli (University of Zurich) provided editorial assistance and critical input during the writing. ADP-ribosylation research in the laboratory of M.O.H. is funded by the Swiss National Science Foundation (SNF 310030B_138667), Krebsliga (KFS-3740-08-2015-R), and SystemX IPhD Project SXPHIO_141998/1.

REFERENCES

(1) Sung, V. M. *Biochimie* **2015**, *113*, 35−46.

(2) Hottiger, M. O.; Hassa, P. O.; Luscher, B.; Schuler, H.; Koch-Nolte, F. *Trends Biochem. Sci.* **2010**, *35*, 208−219.

(3) Barkauskaite, E.; Jankevicius, G.; Ahel, I. *Mol. Cell* **2015**, *58*, 935−946.

(4) Rosenthal, F.; Hottiger, M. O. *Front. Biosci., Landmark Ed.* **2014**, *19*, 1041−1056.

(5) Luo, X.; Kraus, W. L. *Genes Dev.* **2012**, *26*, 417−432.

(6) Guetg, C.; Santoro, R. *Epigenetics* **2012**, *7*, 811−814.

(7) Hottiger, M. O. *Annu. Rev. Biochem.* **2015**, *84*, 227−263.

(8) Bock, F. J.; Todorova, T. T.; Chang, P. *Mol. Cell* **2015**, *58*, 959−969.

(9) Erener, S.; Hesse, M.; Kostadinova, R.; Hottiger, M. O. *Mol. Endocrinol.* **2012**, *26*, 79−86.

(10) Jungmichel, S.; Rosenthal, F.; Altmeyer, M.; Lukas, J.; Hottiger, M. O.; Nielsen, M. L. *Mol. Cell* **2013**, *52*, 272−285.

(11) Zhang, Y.; Wang, J.; Ding, M.; Yu, Y. *Nat. Methods* **2013**, *10*, 981−984.

(12) Gibson, B. A.; Zhang, Y.; Jiang, H.; Hussey, K. M.; Shrimp, J. H.; Lin, H.; Schwede, F.; Yu, Y.; Kraus, W. L. *Science* **2016**, *353*, 45−50.

(13) Daniels, C. M.; Ong, S. E.; Leung, A. K. *J. Proteome Res.* **2014**, *13*, 3510−3522.

(14) Martello, R.; Leutert, M.; Jungmichel, S.; Bilan, V.; Larsen, S. C.; Young, C.; Hottiger, M. O.; Nielsen, M. L. *Nat. Commun.* **2016**, *7*, No. 12917.

(15) Rosenthal, F.; Nanni, P.; Barkow-Oesterreicher, S.; Hottiger, M. O. *J. Proteome Res.* **2015**, *14*, 4072−4079.

(16) Hengel, S. M.; Shaffer, S. A.; Nunn, B. L.; Goodlett, D. R. *J. Am. Soc. Mass Spectrom.* **2009**, *20*, 477−483.

(17) Senko, M. W.; Remes, P. M.; Canterbury, J. D.; Mathur, R.; Song, Q.; Eliuk, S. M.; Mullen, C.; Earley, L.; Hardman, M.; Blethrow, J. D.; Bui, H.; Specht, A.; Lange, O.; Denisov, E.; Makarov, A.; Horning, S.; Zabrouskov, V. *Anal. Chem.* **2013**, *85*, 11710−11714.

(18) Frese, C. K.; Zhou, H.; Taus, T.; Altelaar, A. F.; Mechtler, K.; Heck, A. J.; Mohammed, S. J. *Proteome Res.* **2013**, *12*, 1520−1525.

(19) Savitski, M. M.; Lemeer, S.; Boesche, M.; Lang, M.; Mathieson, T.; Bantscheff, M.; Kuster, B. *Mol. Cell. Proteomics* **2011**, *10*, No. M110.003830.

(20) Turker, C.; Akal, F.; Joho, D.; Panse, C.; Barkow-Oesterreicher, S.; Rehrauer, H.; Schlabach, P. In *EDBT '10: Proceedings of the 13th International Conference on Extending Database Technology*, 2010; pp 717−720; DOI: 10.1145/1739041.1739135.

(21) Nanni, P.; Panse, C.; Gehrig, P.; Mueller, S.; Grossmann, J.; Schlapbach, R. *Proteomics* **2013**, *13*, 2251−2255.

(22) Boehler, C.; Gauthier, L. R.; Mortusewicz, O.; Biard, D. S.; Saliou, J. M.; Bresson, A.; Sanglier-Cianferani, S.; Smith, S.; Schreiber, V.; Boussin, F.; Dantzer, F. *Proc. Natl. Acad. Sci. U. S. A.* **2011**, *108*, 2783−2788.

(23) Andersson, A.; Bluwstein, A.; Kumar, N.; Teloni, F.; Traenkle, J.; Baudis, M.; Altmeyer, M.; Hottiger, M. O. *Nucleic Acids Res.* **2016**, *44*, 7630−7645.

(24) Mikesh, L. M.; Ueberheide, B.; Chi, A.; Coon, J. J.; Syka, J. E.; Shabanowitz, J.; Hunt, D. F. *Biochim. Biophys. Acta, Proteins Proteomics* **2006**, *1764*, 1811−1822.

(25) Frese, C. K.; Altelaar, A. F.; van den Toorn, H.; Nolting, D.; Griep-Raming, J.; Heck, A. J.; Mohammed, S. *Anal. Chem.* **2012**, *84*, 9668−9673.

(26) Wu, S. W.; Pu, T. H.; Viner, R.; Khoo, K. H. *Anal. Chem.* **2014**, *86*, 5478−5486.

(27) Saba, J.; Dutta, S.; Hemenway, E.; Viner, R. *Int. J. Proteomics* **2012**, *2012*, No. 560391.

(28) Leidecker, O.; Bonfiglio, J. J.; Colby, T.; Zhang, Q.; Atanassov, I.; Zaja, R.; Palazzo, L.; Stockum, A.; Ahel, I.; Matic, I. *Nat. Chem. Biol.* **2016**, *12*, 998−1000.

DOI: 10.1021/acs.analchem.6b03365
Anal. Chem. 2017, 89, 1523−1530

CellPress

Molecular Cell
Technology

Analysis of Chromatin ADP-Ribosylation at the Genome-wide Level and at Specific Loci by ADPr-ChAP

Giody Bartolomei,[1,2] Mario Leutert,[1,2] Massimiliano Manzo,[1,2] Tuncay Baubec,[1] and Michael O. Hottiger[1,*]
[1]Department of Molecular Mechanisms of Disease, University of Zurich, Winterthurerstrasse 190, 8057 Zurich, Switzerland
[2]Molecular Life Science PhD Program of the Life Science Zurich Graduate School, University of Zurich, 8057 Zurich, Switzerland
*Correspondence: michael.hottiger@dmmd.uzh.ch
http://dx.doi.org/10.1016/j.molcel.2015.12.025

SUMMARY

Chromatin ADP-ribosylation regulates important cellular processes. However, the exact location and magnitude of chromatin ADP-ribosylation are largely unknown. A robust and versatile method for assessing chromatin ADP-ribosylation is therefore crucial for further understanding its function. Here, we present a chromatin affinity precipitation method based on the high specificity and avidity of two well-characterized ADP-ribose binding domains to map chromatin ADP-ribosylation at the genome-wide scale and at specific loci. Our ADPr-ChAP method revealed that in cells exposed to oxidative stress, ADP-ribosylation of chromatin scales with histone density, with highest levels at heterochromatic sites and depletion at active promoters. Furthermore, in growth factor-induced adipocyte differentiation, increased chromatin ADP-ribosylation was observed at PPARγ target genes, whose expression is ADP-ribosylation dependent. In combination with deep-sequencing and conventional chromatin immunoprecipitation, the established ADPr-ChAP provides a valuable resource for the bioinformatic comparison of ADP-ribosylation with other chromatin modifications and for addressing its role in other biologically important processes.

INTRODUCTION

Protein ADP-ribosylation is an ancient post-translational protein modification with high biochemical complexity (i.e., different length and branching of ADP-ribose polymers) that consists of the transfer of the ADP-ribose moiety from NAD^+ to specific amino acid residues on substrate proteins and to ADP-ribose itself (Hottiger, 2015). The reaction is catalyzed by various ADP-ribosyltransferases (ARTs) and a subgroup of NAD^+-dependent sirtuins (Aravind et al., 2014; Hottiger et al., 2010; Houtkooper et al., 2012). From the existing 18 intracellular diphtheria toxin-like ADP-ribosyltransferases (ARTDs, formerly known as poly (ADP-ribose) polymerases [PARPs]), ARTD1 (PARP1) and ARTD2 (PARP2) are found in the nucleus, whereas the other ARTDs are found in the nuclear and cytoplasmic, or only in the cytoplasmic compartment (Hottiger, 2015). Currently, little is known about the substrate specificity of ARTDs and the mechanisms directing this specificity. Protein ADP-ribosylation can be divided into two subtypes: mono-ADP-ribosylation (MARylation), which defines a reaction where only mono-ADP-ribose (MAR) is transferred to the amino acid of a target protein, and poly-ADP-ribosylation (PARylation), which involves the transfer and elongation of the initial ADP-ribose moiety to generate poly-ADP-ribose chains (Alvarez-Gonzalez and Mendoza-Alvarez, 1995).

Protein ADP-ribosylation is recognized by different protein domains (readers) and reversed by ADP-ribosylhydrolases (erasers). Among the recently identified readers, some recognize both mono-ADP-ribosylated (MARylated) and poly-ADP-ribosylated (PARylated) proteins (e.g., Af1521 macrodomain), whereas others only bind to PARylated proteins (e.g., WWE domain) (Hottiger, 2015). The WWE domain is a globular domain that contains two conserved tryptophans (W) and a glutamate (E) residue and is usually found as a single or double domain. Crystal and solution NMR structures of individual WWE-domains have been described for the E3 ubiquitin-protein ligase RNF146 (Wang et al., 2012), as well as for ARTD11 and ARTD8 (He et al., 2012). WWE domains have a strong affinity for *iso*-ADP-ribose within the PAR chain and have been proposed to be involved in ADP-ribosylation signaling (Aravind, 2001; He et al., 2012; Wang et al., 2012).

At the molecular level, ADP-ribosylation affects the function of the modified proteins or provides a scaffold for the recruitment of regulatory proteins (Gibson and Kraus, 2012; Izhar et al., 2015). A large body of studies has been performed to elucidate the cellular functions of the nuclear ARTD family members. In higher organisms, ADP-ribosylation regulates important cellular processes such as DNA replication and repair, telomere maintenance, gene transcription, chromatin architecture, proteasomal functions, cell morphology, cell viability, cell cycle, and cell death (reviewed in Gibson and Kraus, 2012; Hassa et al., 2006; Kraus and Hottiger, 2013; Leung, 2014; Schreiber et al., 2006; Virág et al., 2013).

ADP-ribosylation has gained much attention in recent years, because its pharmacological inhibition by PARP inhibitors has been shown to induce synthetic lethality in certain cancer cells and to be therapeutically beneficial against certain forms of ovarian cancer (Benafif and Hall, 2015; Rouleau et al., 2010;

Chapter 10

Identification of ADP-Ribose Acceptor Sites on In Vitro Modified Proteins by Liquid Chromatography–Tandem Mass Spectrometry

Mario Leutert*, Vera Bilan*, Peter Gehrig, and Michael O. Hottiger

Abstract

Protein ADP-ribosylation is a covalent, reversible posttranslational modification (PTM) catalyzed by ADP-ribosyltransferases (ARTs). Proteins can be either mono- or poly-ADP-ribosylated under a variety of physiological and pathological conditions. To understand the functional contribution of protein ADP-ribosylation to normal and disease/stress states, modified protein and corresponding ADP-ribose acceptor site identification is crucial. Since ADP-ribosylation is a transient and relatively low abundant PTM, systematic and accurate identification of ADP-ribose acceptor sites has only recently become feasible. This is due to the development of specific ADP-ribosylated protein/peptide enrichment methodologies, as well as technical advances in high-accuracy liquid chromatography–tandem mass spectrometry (LC-MS/MS). The standardized protocol described here allows the identification of ADP-ribose acceptor sites in in vitro ADP-ribosylated proteins and will, thus, contribute to the functional characterization of this important PTM.

Key words ADP-ribosylation, ADP-ribosylome, ARTD, PARP, PARG, Mass spectrometry, Ti^{4+}-IMAC enrichment, Phosphoenrichment

1 Introduction

Protein ADP-ribosylation is a covalent posttranslational modification (PTM) catalyzed by different ADP-ribosyltransferases (ARTs). These enzymes use nicotinamide adenine dinucleotide (NAD^+) as a substrate to transfer the ADP-ribose (ADPr) moiety onto specific amino acid side chains, a process termed protein mono-ADP-ribosylation (MARylation). ARTs can also mediate poly-ADP-ribosylation (PARylation) by transferring the ADPr moiety onto an existing protein-bound ADP-ribose unit. Currently, 22 cellular human ARTs are known. They are subdivided into ARTCs (C for C2/C3 toxin like) and ARTDs (D for diphtheria toxin like, also

*These authors contributed equally to this chapter.

Alexei V. Tulin (ed.), *Poly(ADP-Ribose) Polymerase: Methods and Protocols*, Methods in Molecular Biology, vol. 1608,
DOI 10.1007/978-1-4939-6993-7_10,

called PARPs). While ARTCs are membrane-associated or secreted ARTs, human ARTDs form a family of 18 intracellular enzymes with confirmed or putative mono- or poly-ADP-ribosyltransferase activity [1–3].

Several enzymes that remove ADP-ribose from mono- and poly-ADP-ribosylated substrates have also been identified, rendering ADP-ribosylation a fully reversible PTM. Several mammalian ADP-ribosylhydrolases have been characterized so far, including poly-ADP-ribose glycohydrolase (PARG), ADP-ribosylhydrolase 3 (ARH3), both of which are able to hydrolyze poly-ADP-ribose, and the mono-ADP-ribosylarginine hydrolase 1 (ARH1). In addition, the macrodomain-containing proteins MacroD1, MacroD2, and C6orf130 have recently also been shown to exhibit mono-ADP-ribosylhydrolase activity [4–6].

To elucidate the functional role of protein ADP-ribosylation, systematical analysis of all ADP-ribosylated proteins and identification of their ADP-ribose acceptor sites are necessary. Comparable to many other PTMs, the fraction of ADP-ribosylated cellular proteins is very low. Thus, studying this group of modified proteins requires specific ADP-ribosylated protein/peptide enrichment methodologies. Mass spectrometry (MS)-based proteomics is probably the most powerful tool for the analysis of PTMs. However, the analysis of this PTM has proven to be very challenging for several reasons, including the highly transient nature and the low abundance of ADP-ribosylated proteins, the special physicochemical properties of the PTM (bulky, highly charged, heterogeneous structure, labile), and the number of different amino acids that were reported to be modified (acidic and basic amino acids with a primary amino group on the side chain) [7]. Characterization of ADP-ribose acceptor sites by MS has significantly improved following the development of high-resolution mass spectrometers and novel fragmentation techniques.

In the past few years, several methods for the identification of ADP-ribose acceptor sites on in vitro and in vivo ADP-ribosylated proteins have been published. Zhang et al. [8] established an enrichment protocol based on the isolation of ADP-ribosylated peptides by boronate affinity chromatography and subsequent modified peptide elution using hydroxylamine (NH_2OH). This methodology leaves a characteristic mass signature of 15.01 Da at the ADP-ribose acceptor site [8]. A major drawback of this protocol is that the chemical reaction employed here limits the detection of ADP-ribosylated amino acids to glutamates and aspartates only. Other groups have also used boronate affinity enrichment, but in combination with acidic elution, which leaves the ADP-ribose moiety intact and leads to a release of all bound peptides. This, unfortunately, resulted in high background of unmodified peptides. Additionally, hydroxylamine treatment has also been used as a stand-alone procedure without any enrichment, but this method only seems useful for strongly ADP-ribosylated targets [9, 10].

Phosphoproteomic approaches were also found to co-enrich ADP-ribosylated peptides, and protocols have been optimized for the specific enrichment of ADP-ribosylated or phosphoribosylated peptides [11–14]. Chapman et al. [13] and Daniels et al. [14] used phosphodiesterases to reduce the mono- and poly-ADP-ribosylation modification (MAR or PAR, respectively) to a protein-bound phosphoribose. The resulting phosphoribosylated peptides are subsequently enriched using either Fe(III)-immobilized metal ion affinity chromatography (IMAC) or TiO_2 microspheres. The conversion of protein-bound MAR or PAR to phosphoribose leads to a detectable mass signature of 212.01 Da.

The most recent enrichment approach published by Martello et al. [15] makes use of PARG enzymatic treatment to convert in vivo PARylated peptides into MARylated peptides, which are subsequently enriched by the ADP-ribose binding protein Af1521 and described in the Chap. 11 of this book. This technique allows the accurate and reproducible identification of ADP-ribose acceptor sites in vivo. However, this enrichment strategy has so far not been tested or optimized for in vitro modified proteins.

Here, we thus describe an updated protocol using a Ti^{4+}-IMAC enrichment based on the work done by Chapman et al. [13] and Daniels et al. [14] to map ADP-ribose acceptor sites on in vitro ADP-ribosylated proteins. This protocol is more readily applicable to a variety of different samples than the boronate affinity chromatography-based protocol described by our group in the previous edition of this book for in vitro modified proteins [9]. More importantly, this new methodology is not biased against specific ADP-ribose acceptor sites. The problem that phosphorylated peptides might co-enrich with phosphoribosylated/ADP-ribosylated peptides and interfere with the sensitivity of the detection is not an obstacle due to the low complexity of in vitro modified samples.

2 Materials

All solutions prepared with type 1 analytical grade water.

2.1 ADP-Ribosylation Assay and PARG Treatment

1. hARTD1 is expressed and purified from insect cells as carboxyl-terminal His-tagged protein and stored in liquid nitrogen.
2. hPARG is expressed and purified from insect cells as carboxyl-terminal His-tagged protein and stored in liquid nitrogen (*see* **Note 1**).
3. 10 mM β-Nicotinamide adenine dinucleotide (NAD^+) (>99% Sigma–Aldrich as hydrate) stored at −80 °C.
4. 10 mM PJ-34 (≥98% Sigma-Aldrich as hydrochloride hydrate) stored at −20 °C.

5. ADP-ribosylation buffer (always prepare freshly): 50 mM Tris–HCl pH 8.0, 4 mM $MgCl_2$, 250 μM DTT, and cOmplete™ EDTA-free Protease Inhibitor Cocktail.

2.2 FASP Trypsin Digestion

1. 5× disulfide bond reduction buffer: 250 mM DTT, 250 mM Tris–HCl pH 8.2, and 5 M urea.
2. 0.5 ml Microcon 30 kDa centrifugal filter units with Ultracel-30 membranes (Millipore, MRCF0R030).
3. Urea buffer: 8 M urea in 50 mM Tris–HCl pH 8.2.
4. Iodoacetamide solution: 0.05 M iodoacetamide in urea buffer (kept protected from light).
5. 0.5 M NaCl.
6. 0.05 M ammonium bicarbonate (prepare freshly).
7. Sequencing grade modified trypsin (Promega).

2.3 ADP-Ribosylated Peptide Enrichment

1. MagReSyn® $Ti4^+$-IMAC from ReSyn Biosciences.
2. 70% ethanol.
3. Loading Buffer: 1 M glycolic acid in 80% acetonitrile.
4. Wash buffer: 80% acetonitrile and 0.1% acetic acid in H_2O.
5. Elution buffer: 50 mM Tris–HCl pH 8, 10 mM diammonium hydrogen phosphate, and 5% acetonitrile.

2.4 Stage Tip Desalting

1. C18 Empore high-performance extraction disks (3 M).
2. 100% methanol.
3. Stage Tip Solution A: 0.5% acetic acid in H_2O.
4. Stage Tip Solution B: 80% acetonitrile and 0.5% acetic acid in H_2O.
5. Stage Tip Elution Solution: 60% acetonitrile and 0.5% acetic acid in H_2O.

2.5 Mass Spectrometry

1. HPLC solvent A: H_2O containing 0.1% formic acid.
2. HPLC solvent B: Acetonitrile containing 0.1% formic acid.
3. Frit column (inner diameter 75 μm, length 15 cm) packed with reversed phase material (C18-AQ, particle size 1.9 μm, pore size 120 Å, Dr. Maisch GmbH, Germany).
4. Instrumentation: Orbitrap Fusion Tribrid mass spectrometer (Thermo Scientific, San Jose, CA), connected to an Easy-nLC 1000 HPLC system (Thermo Scientific) (*see* **Note 2**).

3 Methods

3.1 Overview of the Protocol

In vitro auto- and especially trans-ADP-ribosylation reactions are often not efficient and lead to a low abundance of ADP-ribosylated proteins. We, therefore, recommend ADP-ribosylated peptide

enrichment following a previously described phosphoenrichment technique that is based on immobilized titanium ion affinity chromatography [16]. This protocol facilitates modified peptide enrichment and increases the possibilities of a successful analysis, including ADP-ribosylation site determination. In vitro reactions should be carried out according to the optimized protocols for the different ADP-ribosyltransferases. The original protocol used phosphodiesterases to reduce mono- and poly-ADP-ribosylation modifications (MAR or PAR, respectively) to a protein-bound phosphoribose and to enrich subsequently phosphoribosylated peptides. We have, however, found that treatment of ADP-ribosylated proteins with poly(ADP-ribose) glycohydrolase (PARG), which reduces the complexity of PAR to protein-bound mono-ADP-ribose, works very reliable and allows efficient ADP-ribose enrichment as well. PARG-treated proteins are further digested with trypsin using filter-aided sample preparation (FASP) protocol [17]. The ADP-ribosylated peptides are finally enriched with magnetic microspheres with chelated Ti^{4+} ions. This protocol is optimized to use only very mild buffers for the binding, washing, and peptide elution steps in order to preserve the ADP-ribose and its linkage to the modified amino acid residue. Samples are desalted using a C18 Stage Tip protocol [18] and analyzed on an Orbitrap Fusion Tribrid mass spectrometer. HCD fragmentation has previously been shown to lead to reproducible identification of ADP-ribosylated peptides, and this method allows the accurate identification of the modified amino acid [19]. Mascot searches are performed to identify ADP-ribose acceptor sites by setting ADP-ribosylation as a variable modification for lysine, arginine, glutamate, and aspartate. A representative, annotated spectrum of an identified ADP-ribosylated ARTD1 peptide after the Ti^{4+} IMAC enrichment and the HCD ADP-ribose fragmentation pattern are shown in Fig. 1.

3.2 ADP-Ribosylation Assay and PARG Treatment

1. For in vitro auto-ADP-ribosylation of ARTD1, incubate 20 pmol hARTD1 in the presence of 10 pmol annealed double-stranded oligomer (5-GGAATTCC-3) and 100 nM NAD^+ in ADP-ribosylation buffer (*see* **Note 3**). Reaction volume: 50 µl, reaction conditions: 15 min, 30 °C. Terminate the reactions by adding PJ-34 (ADP-ribosylation inhibitor) to a final concentration of 10 µM. To generate larger amounts of modified target protein, several reactions can be run in parallel (*see* **Note 4**).
2. To reduce the complexity of PAR and generate MARylated proteins, samples are incubated with 5 pmol hPARG. Adjust the $MgCl_2$ and NaCl buffer concentrations to 10 mM and 50 mM, respectively, and incubate for 1 h at 37 °C.
3. For the identification of ADP-ribose acceptor sites in peptides, proceed immediately with the FASP trypsin digestion, or, alternatively, freeze the proteins at −20 °C.

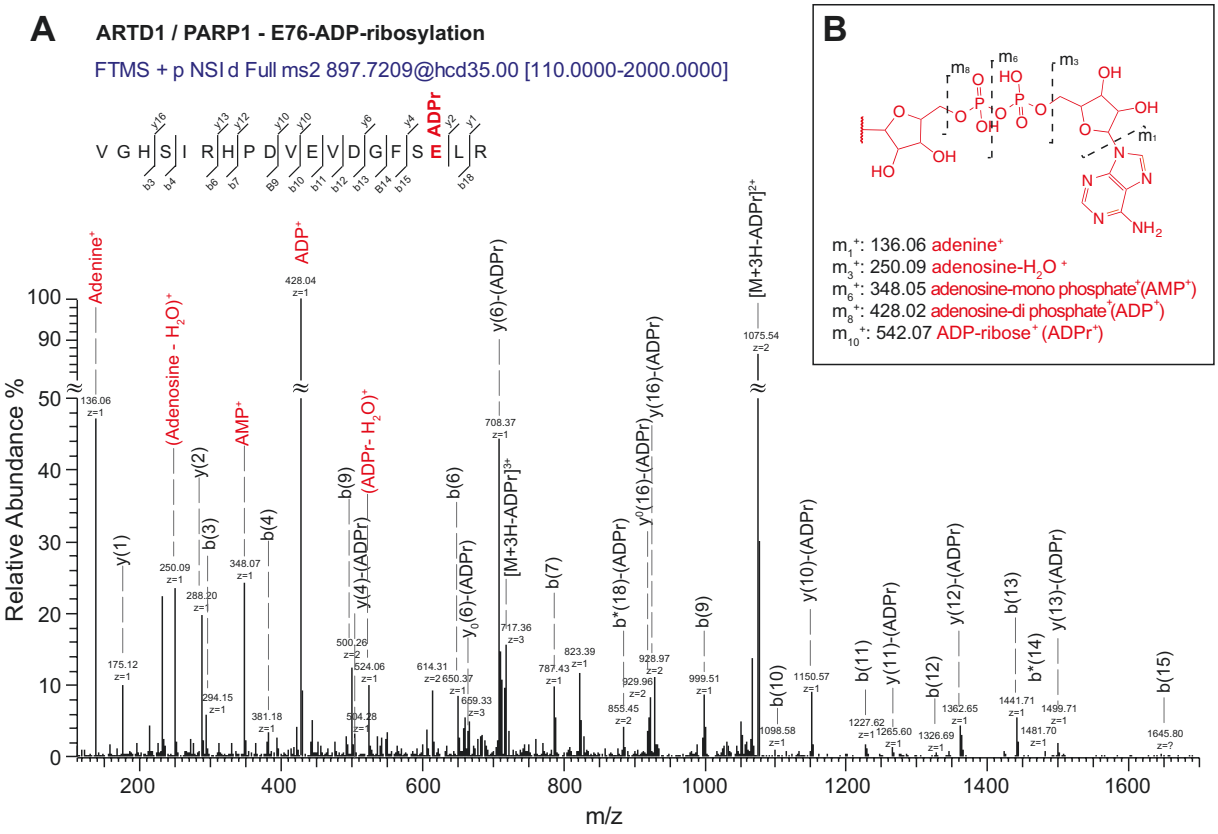

Fig. 1 HCD Fragmentation of an ADP-ribosylated peptide. (**a**) Representative annotated spectrum for the ARTD1 peptide VGHSIRHPDVEVDGFSELR that was found to be ADP-ribosylated on E76. ADP-ribose fragmentation ions are shown in *red*. (**b**) Nomenclature of ADP-ribose fragments as described by Hengel et al. [20]. The ADP-ribose fragment ions with strong signals in the HCD MS/MS spectra are shown

3.3 FASP Trypsin Digestion

1. Add 5× reduction buffer to the protein sample to achieve 1×, and incubate at 37 °C for 30 min to reduce the disulfide bonds.
2. Load up to 250 µl of reduced sample onto the Microcon-30 kDa centrifugal filter unit. Centrifuge at 14,000 × *g* for ~15–20 min at room temperature (RT). Repeat until the sample is completely loaded onto the filter.
3. Add 200 µl of urea buffer to the filter unit. Centrifuge at 14,000 × *g* for ~20 min at RT.
4. Add 100 µl iodoacetamide solution to the filter unit. Gently shake for 5 min and centrifuge at 14,000 × *g* for ~15–20 min at RT.
5. Add 100 µl of urea buffer to the filter unit. Centrifuge at 14,000 × *g* for ~ 15 min at RT. Repeat step twice.
6. Add 100 µl of 0.5 M NaCl to the filter unit. Centrifuge at 14,000 × *g* for ~15–20 min at RT. Repeat step once.
7. Add 100 µl of ammonium bicarbonate solution to the filter unit. Centrifuge at 14,000 × *g* for ~15–20 min at RT. Repeat step twice.

8. Transfer the filter units to new collection tubes.
9. Add 120 µl of trypsin (1:25 trypsin to protein), dissolved in ammonium bicarbonate solution, to the filter unit, and gently shake for 1 min.
10. Incubate the filter units at RT overnight in a humidity chamber.
11. The next day, centrifuge the filter units at 14,000 × *g* for ~15–20 min. The flow-through contains the digested proteins.
12. Re-elute the column with 80 µl of ammonium bicarbonate solution.
13. Dry the eluted peptides in a vacuum concentrator (*see* **Note 5**).

3.4 Enrichment of ADP-ribosylated Peptides

1. Thoroughly resuspend MagReSyn® Ti^{4+}-IMAC microspheres to ensure homogeneous suspension.
2. Transfer 25 µl (0.5 mg) MagReSyn® Ti^{4+}-IMAC to a 2 ml microcentrifuge tube.
3. Place the tube on a magnetic separator, allow 10 s for the microspheres to clear, and discard the storage solution.
4. Wash the microspheres, with gentle agitation, in 200 µl of 70% ethanol for 5 min.
5. Place the tube on the magnetic separator, and allow the microspheres to clear. Discard the ethanol solution.
6. Repeat **steps 4** and **5**.
7. Add 50 µl loading buffer to microspheres, and let stand for 60 s to equilibrate.
8. Place the tube on the magnetic separator and allow the microspheres to clear. Remove the loading buffer. Important: The microspheres equilibration step should be performed immediately before sample loading.
9. Repeat the equilibration process two additional times.
10. Mix dried protein digests with 100 µl of loading buffer, incubate for 5min at RT and add mixture to the equilibrated microsphere pellet (*see* **Note 6**).
11. Incubate at room temperature for 30 min with continuously shaking to ensure adequate sample and microsphere interaction.
12. Place the tube on the magnetic separator and allow the microspheres to clear. Discard the coupling supernatant.
13. Remove unbound sample by washing microspheres with 100 µl loading buffer for 30 s with gentle agitation.
14. Place the tube on a magnetic separator, and allow 10 s for the microspheres to clear. Remove the supernatant.
15. Remove nonspecifically bound peptides by resuspending the microspheres in 100 µl wash buffer for 2 min with gentle agitation.

16. Place the tube on a magnetic separator, and allow 10 s for the microspheres to clear and remove the supernatant.
17. Repeat **steps 15** and **16** twice for a total of three washes.
18. Elute the bound peptides from the microspheres by adding 60 µl elution buffer and letting stand for 15 min. Ensure that the microspheres remain in suspension by gently agitating the tube.
19. Place the tube on the magnetic separator and allow the microspheres to clear. Remove the eluate and transfer it to a new tube.
20. Repeat the elution **steps 18** and **19** twice for a final elution volume of 180 µl.

3.5 Stage Tip Desalting

1. Prepare Stage Tips by plugging two C18 disks in a 200 µl pipette tip (*see* **Note 7**).
2. Make a hole in the lid of a 1.5 ml Eppendorf tube and fit stage tip in. The tip should be tightly attached to the lid, and the tip should not touch the bottom of the tube.
3. Activate the Stage Tip by adding 200 µl 100% methanol to the stage tip, and centrifuge at 1000 × *g* for approx. 3 min.
4. Add 200 µl Stage Tip Solution B to the stage tip, and centrifuge at 1000 × *g* for approx. 3 min.
5. Add 200 µl Stage Tip Solution A to the stage tip, and centrifuge at 1000 × *g* for approx. 3 min.
6. Add 200 µl of your peptide sample, and centrifuge at 1000 × *g* for approx. 3 min. Repeat step until the whole sample is loaded.
7. Wash Stage Tip by adding 50 µl of Stage Tip Solution A, and centrifuge at 1000 × *g* for approx. 3 min until Stage Tip is completely dry.
8. Elute Stage Tip by adding 20 µl of Stage Tip Elution solution, and centrifuge at 1000 × *g* for approx. 1 min. Repeat elution step once more and combine elutions.
9. Partially dry the eluted samples in a vacuum concentrator (*see* **Note 5**). The samples can be stored at −20 °C or directly proceed by LC-MS/MS.

3.6 LC-MS/MS

All data are acquired on an Orbitrap Fusion Tribrid mass spectrometer connected to an Easy-nLC 1000 HPLC system (*see* **Note 2**). 4 µl of peptide sample in 0.1% formic acid are loaded and separated at a flow rate of 300 nl per min. The following LC gradient was applied: 0 min: 2% HPLC solvent B, 60 min: 30% B, 70 min: 97% B, and 80 min: 97% B.

Survey scans were recorded in the Orbitrap mass analyzer in the range of *m/z* 350–1800, with a resolution of 120,000 and a maximum injection time of 50 ms. Higher-energy collisional

dissociation (HCD) spectra were acquired in the Orbitrap mass analyzer. A maximum injection time of 240 ms, an AGC target value of 5e5, and a resolution of 120,000 were used. The precursor ion isolation width was set to m/z 2.0, and the normalized collision energy was 35%. Charge state screening was enabled, and charge states 2–5 were included. The threshold for signal intensities was 5e4, and precursor masses already selected for MS/MS acquisition were excluded for further selection during 30 s.

3.7 Database Analysis and Configuration of Mascot Modifications

MS data are analyzed as previously described [19]. MS and MS/MS spectra are converted into Mascot generic format (mgf) using Proteome Discoverer, v2.1 (Thermo Fisher Scientific, Bremen, Germany). All high-resolution HCD MS/MS spectra are deconvoluted using MS Spectrum Processor, v0.9 [21]. Searches were performed against the UniProtKB human database (taxonomy 9606, version 20140422), which includes 35′787 Swiss-Prot, 37′02 TrEMBL entries, 73′589 reversed sequences, and 260 common contaminants. Mascot 2.5.1 (Matrix Science) is used for peptide identification using the following search settings: singly charged b and y ion series, immonium ions, and water and ammonia loss ion series are searched. Enzyme specificity is set to trypsin, allowing up to four missed cleavages. The ADP-ribose variable modification is set to a mass shift of 541.0611, with scoring of the neutral losses equal to 347.0631 and 249.0862. The marker ions at *m/z* 428.0372, 348.0709, 250.0940, 136.0623 are ignored for scoring. Lysine, arginine, and glutamic and aspartic acid are set as variable ADP-ribose acceptor sites. Peptides are considered correctly identified when a Mascot score >20, and an expectation value <0.05 are obtained. To assess the location of the ADP-ribose acceptor sites, we use the site localization analysis provided by Mascot, which is based on the work by Savitski et al. [21] and was developed especially for phosphorylation. Due to the lack of a better estimate, we define correctness as having a confidence of ≧95% in the Mascot site localization analysis (*see* **Note 8**).

4 Notes

1. As an alternative to PARG treatment, enzymes converting ADP-ribose to phosphoribose (e.g., nudix hydrolases, snake venom phosphodiesterase I) can be used, but these require individually optimized reaction conditions and are expensive in the case of snake venom phosphodiesterase I [14, 22]. None of the available methods to date are capable of distinguishing between mono- and poly-ADP-ribose acceptor sites. We envision that a specific set of binding proteins with affinities for

either PAR or MAR or conversion of PAR in to a specific moiety could solve this problem in the near future.

2. We measured all our samples on an Orbitrap Fusion Tribrid mass spectrometer, but it is also possible to conduct a similar analysis on other mass spectrometers with optimized machine settings.
3. Higher NAD^+ concentrations can trigger the generation of very long ADP-ribose polymers that might interfere with trans-ADP-ribosylation or subsequent analysis.
4. We started our analysis with 50 μg ARTD1 and ended up with enough material for nine mass spectrometry injections. The amount of initial starting protein and the peptide solution that is injected into the mass spectrometer need to be optimized depending on the efficiency of the ADP-ribosylation reaction, the HPLC, and the mass spectrometer used for the analysis.
5. Partial drying of the peptides (leave 1–2 μl) increases the overall yield.
6. To control for the enrichment and MS analysis, standard phosphopeptides can be added into the sample prior to sample preparation.
7. Video tutorial describing how to build and use the stage tips [18]: https://www.biochem.mpg.de/226863/Tutorials.
8. This method is not optimized for ADP-ribosyl modifications due to the lack of standard peptides with known modification sites. For this reason, even if Mascot states a correctness of 95% for the site localization, this value is arbitrary and cannot be validated experimentally. If required, other amino acid acceptor sites can be included as variable modification sites.

Acknowledgments

The authors would like to thank Paolo Nanni (member of the Functional Genomics Center Zurich, University of Zurich/ETH Zurich, Zurich, Switzerland) for advice and technical assistance. We also thank Felix R. Althaus (Institute of Pharmacology and Toxicology, University of Zurich-Vetsuisse) for providing hPARG-expressing baculovirus. Stephan Christen and Deena Leslie Pedrioli (both University of Zurich) provided editorial assistance and critical input during the writing. Work on ADP-ribosyltransferases in the laboratory of M.O.H is supported by Kanton of Zurich and the Swiss National Science Foundation (310030_157019).

Mario Leutert and Vera Bilan contributed equally to this chapter.

References

1. Hassa PO, Haenni SS, Elser M, Hottiger MO (2006) Nuclear ADP-ribosylation reactions in mammalian cells: where are we today and where are we going? Microbiol Mol Biol Rev: MMBR 70(3):789–829. doi:10.1128/MMBR.00040-05
2. Hottiger MO, Hassa PO, Luscher B, Schuler H, Koch-Nolte F (2010) Toward a unified nomenclature for mammalian ADP-ribosyltransferases. Trends Biochem Sci 35(4):208–219. doi: 10.1016/j.tibs.2009.12.003
3. Vyas S, Matic I, Uchima L, Rood J, Zaja R, Hay RT, Ahel I, Chang P (2014) Family-wide analysis of poly(ADP-ribose) polymerase activity. Nat Commun 5:4426. doi:10.1038/ncomms5426
4. Slade D, Dunstan MS, Barkauskaite E, Weston R, Lafite P, Dixon N, Ahel M, Leys D, Ahel I (2011) The structure and catalytic mechanism of a poly(ADP-ribose) glycohydrolase. Nature 477(7366):616–620. doi:10.1038/nature10404
5. Rosenthal F, Feijs KL, Frugier E, Bonalli M, Forst AH, Imhof R, Winkler HC, Fischer D, Caflisch A, Hassa PO, Luscher B, Hottiger MO (2013) Macrodomain-containing proteins are new mono-ADP-ribosylhydrolases. Nat Struct Mol Biol 20(4):502–507. doi:10.1038/nsmb.2521
6. Jankevicius G, Hassler M, Golia B, Rybin V, Zacharias M, Timinszky G, Ladurner AG (2013) A family of macrodomain proteins reverses cellular mono-ADP-ribosylation. Nat Struct Mol Biol 20(4):508–514. doi:10.1038/nsmb.2523
7. Daniels CM, Ong SE, Leung AK (2015) The promise of proteomics for the study of ADP-ribosylation. Mol Cell 58(6):911–924. doi:10.1016/j.molcel.2015.06.012
8. Zhang Y, Wang J, Ding M, Yu Y (2013) Site-specific characterization of the Asp- and Glu-ADP-ribosylated proteome. Nat Methods 10(10):981–984. doi:10.1038/nmeth.2603
9. Rosenthal F, Messner S, Roschitzki B, Gehrig P, Nanni P, Hottiger MO (2011) Identification of distinct amino acids as ADP-ribose acceptor sites by mass spectrometry. Methods Mol Biol 780:57–66. doi:10.1007/978-1-61779-270-0_4
10. Gagne JP, Ethier C, Defoy D, Bourassa S, Langelier MF, Riccio AA, Pascal JM, Moon KM, Foster LJ, Ning Z, Figeys D, Droit A, Poirier GG (2015) Quantitative site-specific ADP-ribosylation profiling of DNA-dependent PARPs. DNA Repair 30:68–79. doi:10.1016/j.dnarep.2015.02.004
11. Matic I, Ahel I, Hay RT (2012) Reanalysis of phosphoproteomics data uncovers ADP-ribosylation sites. Nat Methods 9(8):771–772. doi:10.1038/nmeth.2106
12. Lang AE, Schmidt G, Schlosser A, Hey TD, Larrinua IM, Sheets JJ, Mannherz HG, Aktories K (2010) Photorhabdus luminescens toxins ADP-ribosylate actin and RhoA to force actin clustering. Science 327(5969):1139–1142. doi:10.1126/science.1184557
13. Chapman JD, Gagne JP, Poirier GG, Goodlett DR (2013) Mapping PARP-1 auto-ADP-ribosylation sites by liquid chromatography-tandem mass spectrometry. J Proteome Res 12(4):1868–1880. doi:10.1021/pr301219h
14. Daniels CM, Ong SE, Leung AK (2014) Phosphoproteomic approach to characterize protein mono- and poly(ADP-ribosyl)ation sites from cells. J Proteome Res 13(8):3510–3522. doi:10.1021/pr401032q
15. Martello R, Leutert M, Jungmichel S, Bilan V, Larsen SC, Young C, Hottiger MO, Nielsen ML (2016) Proteome-wide identification of the endogenous ADP-ribosylome of mammalian cells and tissue. Nat Commun 7:12917. in press
16. Zhou H, Ye M, Dong J, Han G, Jiang X, Wu R, Zou H (2008) Specific phosphopeptide enrichment with immobilized titanium ion affinity chromatography adsorbent for phosphoproteome analysis. J Proteome Res 7(9):3957–3967. doi:10.1021/pr800223m
17. Wisniewski JR, Zougman A, Nagaraj N, Mann M (2009) Universal sample preparation method for proteome analysis. Nat Methods 6(5):359–362. doi:10.1038/nmeth.1322
18. Rappsilber J, Mann M, Ishihama Y (2007) Protocol for micro-purification, enrichment, pre-fractionation and storage of peptides for proteomics using StageTips. Nat Protoc 2(8):1896–1906. doi:10.1038/nprot.2007.261
19. Rosenthal F, Nanni P, Barkow-Oesterreicher S, Hottiger MO (2015) Optimization of LTQ-orbitrap mass spectrometer parameters for the identification of ADP-ribosylation sites. J Proteome Res 14(9):4072–4079. doi:10.1021/acs.jproteome.5b00432
20. Hengel SM, Shaffer SA, Nunn BL, Goodlett DR (2009) Tandem mass spectrometry investigation of ADP-ribosylated kemptide. J Am Soc Mass Spectrom 20(3):477–483. doi:10.1016/j.jasms.2008.10.025

21. Savitski MM, Mathieson T, Becher I, Bantscheff M (2010) H-score, a mass accuracy driven rescoring approach for improved peptide identification in modification rich samples. J Proteome Res 9(11):5511–5516. doi:10.1021/pr1006813

22. Daniels CM, Thirawatananond P, Ong SE, Gabelli SB, Leung AK (2015) Nudix hydrolases degrade protein-conjugated ADP-ribose. Sci Rep 5:18271. doi:10.1038/srep18271

Chapter 11

Proteome-Wide Identification of In Vivo ADP-Ribose Acceptor Sites by Liquid Chromatography–Tandem Mass Spectrometry

Sara C. Larsen*, Mario Leutert*, Vera Bilan, Rita Martello, Stephanie Jungmichel, Clifford Young, Michael O. Hottiger, and Michael L. Nielsen

Abstract

ADP-ribosylation is a posttranslational modification (PTM) that affects a variety of cellular processes. In recent years, mass spectrometry (MS)-based proteomics has become a valuable tool for studying ADP-ribosylation. However, studying this PTM in vivo in an unbiased and sensitive manner has remained a difficult challenge. Here, we describe a detailed protocol for unbiased analysis of ADP-ribosylated proteins and their ADP-ribose acceptor sites under physiological conditions. The method relies on the enrichment of mono-ADP-ribosylated peptides using the macrodomain Af1521 in combination with liquid chromatography–high-resolution tandem MS (LC-MS/MS). The 5-day protocol explains the step-by-step enrichment and identification of ADP-ribosylated peptides from cell culture stage all the way through to data processing using the MaxQuant software suite.

Key words ADP-ribosylation, ADP-ribosylome, Mass spectrometry, Proteomics, Af1521 macrodomain enrichment, Affinity purification, PARG

1 Introduction

Protein ADP-ribosylation is a posttranslational modification (PTM) where an ADP-ribose moiety is transferred from NAD^+ to the amino acid side-chains of target proteins (mono-ADP-ribosylation, MARylation), which subsequently can serve as an attachment point for additional ADP-ribose moieties (poly-ADP-ribosylation, PARylation). ADP-ribosylation is primarily catalyzed

*These authors equally contributed to this work.

Alexei V. Tulin (ed.), *Poly(ADP-Ribose) Polymerase: Methods and Protocols*, Methods in Molecular Biology, vol. 1608,
DOI 10.1007/978-1-4939-6993-7_11,

by ADP-ribosyltransferases (ARTs) and certain Sirtuin deacetylases [1, 2]. A detailed understanding of the molecular mechanisms and functions regulated by ADP-ribosylation remains elusive. This is partially due to the fact that the amino acid residues modified in vivo by ADP-ribosylation remains unclear. Current experimental evidence suggests that ADP-ribosylation in eukaryotes occurs primarily on the side chains of the following four amino acids; Lys [3], Arg [4], Asp and Glu residues [5]. In addition, Cys residues were reported to be MARylated not only by bacterial toxins, but also by certain ARTDs [6, 7].

Protein ADP-ribosylation is a low abundant and rapidly degraded PTM. To overcome the challenge posed by rapid ADP-ribosylation turnover, cellular poly(ADP-ribosyl) glycohydrolase (PARG) have been knocked down by siRNA or abolished by genetic deletion (i.e., using PARG knockout cells) [5, 8]. Unfortunately, these conditions establish a non-physiological cellular setting that induces physiological alterations in the investigated cells and tissues [9–11]. Thus, it is more than questionable whether studying ADP-ribosylation and its associated mechanisms of action under these conditions is biologically relevant.

High-resolution mass spectrometry (MS) has become a valuable tool for comprehensive identification of PTMs [12]. Two MS-based approaches for mapping ADP-ribose acceptor sites in vivo were recently published. Unfortunately, these techniques are limited as they can only identify Glu and Asp modifications [5] or lack sensitivity due to co-enrichment of phosphorylated peptides [8]. In addition, a chemical genetic discovery-based method for ARTD target identification was recently reported [13]. However, this approach does not support the identification of ARTD-specific substrates under different cellular conditions or physiological NAD^+ levels. To address the limitations of these approaches, we have developed a novel and straight forward methodology that allows unbiased mapping of endogenous ADP-ribose acceptor sites in proteins under physiological cellular conditions [14]. Importantly, this new methodology represents a major advancement in the detection of in vivo ADP-ribose acceptor sites and the identification of cellular processes regulated by ADP-ribosylation.

2 Materials

We recommend preparing all buffers using sequencing grade chemicals and Milli-Q water.

2.1 Cell Culture and Lysis

1. Cells of interest. The protocol described here has been successfully applied to HeLa cells.
2. Dulbeccos Modified Eagle's Medium (D-MEM) supplemented with 10% fetal bovine serum (FBS) and penicillin/streptomycin (100 U/mL).

3. Phosphate-buffered saline (PBS).
4. Hydrogen peroxide or alternative ADP-ribosylation-inducing agent of interest.
5. Modified RIPA buffer (high salt): 50 mM Tris–HCl, pH 7.5, 400 mM NaCl, 1 mM EDTA, 1% NP-40, 0.1% Na-deoxycholate, 40 μM PJ-34, 1 μM ADP-HPD (*see* **Note 1**), protease inhibitor cocktail.
6. Modified RIPA buffer (no salt): 50 mM Tris–HCl, pH 7.5, 1 mM EDTA, 1% NP-40, Protease inhibitor cocktail.
7. 100% Acetone.
8. Equipment: Cell lifters.
9. Equipment: Centrifuge (with cooling) including a swinging bucket rotor.

2.2 In-Solution Digestion

1. Denaturation buffer: 6 M urea, 2 M thiourea, 10 mM HEPES, pH 8.0.
2. Bradford reagent or alternative assay for measuring protein concentration.
3. Reduction buffer: 1 M dithiothreitol (DTT).
4. Alkylation buffer: 550 mM chloracetamide (CAA).
5. Lys-C protease.
6. Digestion buffer: 25 mM ammonium bicarbonate (ABC).
7. Sequencing grade modified trypsin.
8. 10% trifluoroacetic acid (TFA)
9. Equipment: Centrifuge (with cooling) including a swinging bucket rotor.
10. Equipment: Thermomixer.

2.3 Concentration of Peptides on Sep-Pak

1. 100% acetonitrile.
2. 0.1% TFA.
3. Equipment: Centrifuge including a swinging bucket rotor.
4. Equipment: Sep-Pak C18 Classic Cartridges.

2.4 GST-Protein Expression and Purification of Af1521

1. Bacterial expression plasmid containing N-terminal GST-fused macrodomain Af1521 [15].
2. BL21 chemically competent *E. coli* cells.
3. Super Optimal broth with Catabolite repression (SOC).
4. LB-Agar plates containing ampicillin (Amp-plates).
5. Lysogeny broth (LB) medium.
6. Terrific Broth (TB) medium.
7. Isopropyl-beta-D-thiogalactopyranoside (IPTG).

8. Lysis buffer: 50 mM Tris–HCl, pH 7.5, 150 mM NaCl, 1 mM $MgCl_2$, 1 mM DTT, 1× BugBuster, 1 μL/mL benzonase, 200 μg/mL lysozyme, protease inhibitor cocktail.
9. Glass beads.
10. Glutathione Sepharose 4B.
11. Wash buffer: 50 mM Tris–HCl, pH 7.5, 150 mM NaCl, 1 mM DTT.
12. Equipment: Centrifuge (with cooling) including a fixed angle rotor for eppendorf tubes.
13. Equipment: Centrifuge (with cooling) including a swinging bucket rotor.

2.5 Enrichment of ADP-Ribosylated Peptides

1. 50% acetonitrile.
2. 80% acetonitrile.
3. 5× affinity precipitation (AP) buffer: 250 mM Tris–HCl, pH 8.0, 50 mM $MgCl_2$, 1.25 mM DTT, 250 mM NaCl. (For 1× AP buffer dilute 5× AP buffer in Milli-Q).
4. hPARG is expressed and purified from insect cells as carboxyl-terminal His-tagged protein and stored in liquid nitrogen.
5. Purified Af1521.
6. 0.15% TFA.
7. Equipment: Vacuum concentrator (SpeedVac).
8. Equipment: NanoDrop or alternative assay for measurement of peptide concentration.
9. Equipment: Centrifuge (with cooling) including a fixed angle rotor for eppendorf tubes.
10. Tabletop centrifuge.

2.6 Purification and Desalting of Peptides for Mass Spectrometric Analysis

1. C18 material.
2. Methanol.
3. Buffer B: 80% acetonitrile, 0.5% acetic acid.
4. Buffer A: 0.5% acetic acid.
5. Equipment: StageTip adapters for microcentrifuge tubes.
6. Equipment: Centrifuge including a fixed angle rotor for eppendorf tubes.

2.7 LC-MS/MSAnalysis of ADP-Ribosylated Peptides

1. StageTip elution buffer 1: 40% acetonitrile, 0.5% acetic acid.
2. StageTip elution buffer 2: 60% acetonitrile, 0.5% acetic acid.
3. Buffer A*: 5% acetonitrile, 0.1% TFA.
4. C18-packed nanospray column. We use 15 cm analytical columns (75 μm inner diameter) pulled and packed in-house with 1.9 μm C18 beads (Reprosil Pur-AQ, Dr. Maisch, Germany).

5. Equipment: Liquid chromatography (LC) system, e.g., nanoscale UHPLC system EASY-nLC1200.
6. Equipment: Nanospray column heater (Sonation GmbH).
7. Equipment: Mass spectrometer, e.g., a Q Exactive HF (Thermo Fisher Scientific).
8. Data analysis software such as the freely available MaxQuant software suite (www.maxquant.org).

3 Methods

Here, we describe a sensitive and unbiased method for the identification of in vivo ADP-ribosylated peptides and amino acid acceptor sites using high-resolution LC-MS/MS. This methodology facilitates the study of basal ADP-ribosylation levels as well as their changes upon stimulation. In principle, the protocol is applicable to any cell line, as long as enough material can be collected. Basal in vivo ADP-ribosylation levels are low, but can be enhanced via genotoxic stress-mediated activation of ARTDs [16]. Thus, despite fast and gentle sample handling, DNA shearing during cell lysis was shown to cause artifactual PAR formation [17]. Therefore, it is crucial to complement the lysis buffer with PARP and PARG inhibitors to preserve the physiological ADP-ribosylome and avoid lysis-induced artifacts. To enhance identification of ADP-ribosylation sites, the isolated proteins are first digested to peptides and then treated with PARG, which converts all PARylated amino acids to their MARylated counterparts. While PARG treatment does not allow distinguishing between PARylation and MARylation, the conversion allows for feasible MS analysis. The resulting MARylated peptides are then unbiasedly enriched using ADP-ribose-specific binder, such as the Af1521 macrodomain, which has a Kd of ~0.13 μM to ADP-ribose [15, 17, 18]. Finally, the enriched modified peptides and their ADP-ribose acceptor sites are identified by high-resolution LC-MS/MS.

The protocol described here can be divided into the following parts: (1) culture and lysis of cells, (2) digestion of proteins, (3) concentration of peptide solution, (4) expression and purification of the Af1521 macrodomain, (5) enrichment of ADP-ribosylated peptides, (6) purification of samples for MS analysis, and (7) analysis of the peptide mixture using LC-MS/MS. A scheme of the workflow is depicted in Fig. 1.

The protocol described below has been optimized for ADP-ribose acceptor site identification of in vivo modified proteins from cultured cells. However, this method is with optimization of the extraction conditions also suitable for whole tissue ADP-ribosylome characterization.

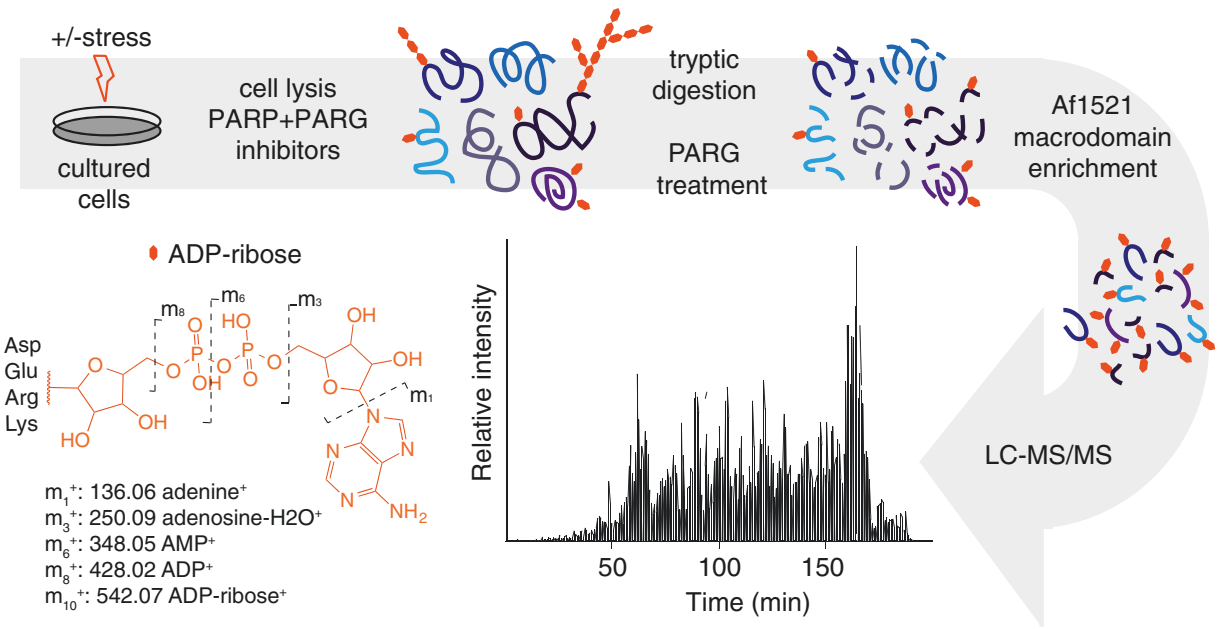

Fig. 1 Schematic overview of the peptide-based purification strategy. Cell culture is treated with genotoxic stress (or other stimuli) and cells are subsequently lysed with PARP and PARG inhibitors present in the lysis buffer. Proteins are digested into peptide species using trypsin, and treated with PARG enzyme to convert multimeric ADP-ribosylation into monomeric counterparts. The ADP-ribosylated peptides are then enriched using the GST-AF1521 macrodomain, and enriched peptides are subsequently analyzed and the acceptor sites identified using high resolution LC-MS/MS. For improved identification of ADP-ribosylated peptides diagnostic ions related to the specific fragmentation pattern of the ADP-ribose moiety are used. Following this, the acquired data is further processed by bioinformaticssoftware tools

3.1 Cell Culture and Lysis

1. Seed cells into eight 150 mm cell culture dishes per condition and grow to ~80% confluency. This will yield approximately 30–40 mg of total protein.
2. Wash cells once with warm PBS. Add H_2O_2 (0.5–1 mM) in PBS and incubate for 5–10 min at 37 °C (*see* **Note 2**).
3. Carefully wash the cells briefly with ice-cold PBS. Make sure to remove all PBS.
4. Place the washed 150 mm cell culture dishes on ice. Add 0.2 mL ice-cold modified RIPA (high salt) to each plate and incubate on ice for 5 min. Scrape the cells off the bottom of the plate and transfer the entire content of the plate into a 15 mL Falcon tube placed on ice.
5. Centrifuge at 5000 × *g* for 20 min at 4 °C to clear the lysate. Transfer supernatant to a 50 mL Falcon tube for acetone precipitation.
6. Dilute sample with salt-free RIPA to obtain a final NaCl concentration of 133 mM (this makes the pellet easier to dissolve in urea) (*see* **Note 3**).
7. Precipitate the proteins by adding a fivefold volume of ice-cold acetone (80% acetone final concentration) and incubate

overnight at −20 °C. Samples in acetone can be stored at −20 °C for several weeks.

3.2 In-Solution Digestion

1. Centrifuge acetone-precipitated proteins at 1000 × *g* for 5 min at 4 °C and carefully discard all of the acetone.
2. At room temperature, add denaturation buffer (urea) to the 50 mL Falcon tube containing the protein pellet and resuspend. The added volume depends on the pellet size; ideally the protein concentration should be ~5 mg/mL (*see* **Note 4**).
3. Determine protein concentration for example by Bradford assay.
4. Reduce disulfide bridges and unwind proteins by adding 1/1000 volume of reduction buffer, mix well and shake at 500 rpm for 60 min at room temperature.
5. Alkylate the free –SH groups by adding 1/100 volume of alkylation buffer and shake at 500 rpm in the dark for 60 min at room temperature.
6. Digest the precipitated proteins to peptides by adding Lys-C (1 μg per 100 μg protein) to the sample and shake for 3–4 h at room temperature. Lys-C will cleave at the carboxyl side of lysine.
7. Dilute the sample 1:4 with 25 mM ABC to reduce urea concentration to <2 M. Make sure the pH is 8.0–8.5; if the pH is too high, add water.
8. Add trypsin (1 μg per 100 μg protein) and shake overnight at room temperature. Trypsin will cleave at the carboxyl side of lysine and arginine.
9. Terminate trypsin digestion by dropwise (carefully!) adding 10% TFA until peptide solution reaches pH 2.

3.3 Concentration of Peptides on Sep-Pak

1. Clarify the peptide mixture by centrifugation at 1800 × *g* for 5 min at room temperature. Transfer supernatant to fresh tube.
2. Insert the Sep-Pak C18 column into a 10 mL syringe. The capacity of the Sep-Pak is approximately 5% (wt/wt) of packing material.
3. Add 5 mL of 100% acetonitrile to pre-wet the Sep-Pak cartridge.
4. Wash column two-times with 4 mL 0.1% TFA. Use a P-200 pipette to remove bubbles at the top of the Sep-Pak; this will ensure even flow through the Sep-Pak material.
5. Load ~5 mL of the peptide mixture onto the Sep-Pak column (the column might turn yellow), remove any bubbles that form at the top of the Sep-Pak and allow gravity flow of the sample

through the column. Repeat until the entire sample has entered the Sep-Pak C18 column.

6. Wash the column three-times with 5 mL water. Measure the pH of the flow-through. It must be >6, otherwise more washes with water are required. Store the Sep-Pak at 4 °C (for up to several months) until further use.

3.4 GST-Protein Expression and Purification of Af1521

1. Add 1 μg of cooled Af1521 WT plasmid to freshly thawed chemically competent BL21 cells, stir carefully, and leave on ice for 15 min.
2. Heat shock for 45 s at 42 °C.
3. Incubate for 1 min on ice.
4. Add 900 μL SOC and shake vigorously for 40 min at 37 °C.
5. Centrifuge at 2000 × *g* for 2 min at room temperature and discard approximately 600 μL of the supernatant.
6. Resuspend the cells in the remaining media, spread the suspension to LB + Amp plates, and incubate overnight at 37 °C.
7. Inoculate 5 mL of LB media containing ampicillin (100 μg/mL) with a single colony of Amp^RBL21 cells and incubate overnight at 37 °C, 230 rpm.
8. Dilute overnight culture 1:500 into 100 mL of pre-warmed TB media containing ampicillin (100 μg/mL) in a 0.5 mL flask (*see* **Note 5**).
9. Incubate at 37 °C, 230 rpm and measure OD_{600} every 30 min.
10. When the culture has reached an OD_{600} of 0.55–0.65, induce protein expression by adding freshly thawed IPTG (0.5 mM).
11. Express proteins by incubating for 5–6 h at 30 °C, 230 rpm.
12. Pour 50 mL of the bacteria suspension into a 50 mL Falcon tube and centrifuge at 3000 × *g* for 15 min at room temperature.
13. Discard the supernatant and repeat **step 12** with another 50 mL of the bacteria.
14. Freeze pellet at −80 °C. Pellets can be stored at −80 °C for several months.
15. Thaw pellet at room temperature and resuspend in 4 mL fresh lysis buffer. Incubate rotating at room temperature for 20 min.
16. Break cells by adding glass beads and vortex for approximately 30 s.
17. Transfer lysate to microcentrifuge tubes and pellet cell debris by centrifugation at 14,500 × *g* for 5 min at 4 °C.
18. Transfer 2 mL of Glutathione Sepharose 4B slurry to a 15 mL Falcon tube.

19. Add 8 mL of wash buffer and centrifuge at 2000 × *g* for 2 min at 4 °C.
20. Discard supernatant, add 9 mL of wash buffer, and centrifuge at 2000 × *g* for 2 min at 4 °C.
21. Discard supernatant, transfer the cleared GST-Af1521 lysate to the 15 mL Falcon tube containing the equilibrated beads, and incubate at 4 °C for 4 h with head-over-tail rotation.
22. Centrifuge the slurry at 2000 × *g* for 2 min at 4 °C and discard the supernatant.
23. Wash beads four-times with wash buffer. Mix by inverting the tube five-times. Centrifuge at 2000 × *g* for 2 min at 4 °C between each wash step.
24. Discard final supernatant and resuspend beads in wash buffer to give a final volume of 10 mL. Bead-coupled proteins can be stored at 4 °C for several weeks (*see* **Note 6**).

3.5 Enrichment of ADP-Ribosylated Peptides

1. Elute the peptides off the Sep-Pak (from Subheading 3.3, **step 6**) with 3 mL 50% acetonitrile, followed by 1.5 mL 80% acetonitrile. Pool peptide eluates.
2. Aliquot the 4.5 mL pooled peptide elution into four 1.5 mL microcentrifuge tubes. Add 40 µL of 5× AP buffer to each tube, mix by pipetting up and down.
3. Reduce the volume of each aliquot to 200 µL via vacuum centrifugation at 45 °C. This will take ~60 min.
4. Pool the four concentrated aliquots into a single tube (~800 µL final volume).
5. Clear concentrated peptide solution via centrifugation at 1800 × *g* for 5 min at 4 °C. Store supernatant on ice.
6. Determine peptide concentration by for example using a NanoDrop at 280 nm. Use ~10 mg of peptides for enrichment of ADP-ribosylated peptides. Keep 100 µg of unenriched peptides for proteome analysis.
7. To degrade PAR to MAR, add 4.2 µg PARG per 10 mg of peptides and incubate for 3 h at 37 °C, 300 rpm.
8. Cool peptide mixture on ice.
9. Add 500 µL of the bead-coupled GST-Af1521 macrodomain slurry (Subheading 3.4, **step 24**) and incubate for 2 h at 4 °C with head-over-tail rotation.
10. Centrifuge at 1000 × *g* for 1 min at 4 °C and remove supernatant.
11. Wash beads three-times with 1 mL of ice-cold 1× AP buffer. Mix by inverting tubes three-times and immediately centrifuge at 1000 × *g* for 1 min at 4 °C and remove supernatant.

12. Wash beads three-times with 1 mL of ice-cold water. Mix by inverting tubes five-times and immediately centrifuge at 1000 × *g* for 1 min at 4 °C and remove supernatant.
13. Elute the enriched ADP-ribosylated peptides by adding 100 µL 0.15% TFA to the beads. Tap the bottom of the tube several times (do not vortex) and let stand at room temperature for 10 min.
14. Tap the bottom of the tube again, pellet beads via quick (a few seconds) centrifugation, remove the supernatant using a gel-loading tip and transfer to a new, labeled microcentrifuge tube.
15. Repeat elution step with an additional 100 µL of 0.15% TFA for 10 min, combine the eluates and load onto an activated and equilibrated C18 stage tip (see below for preparation).

3.6 Purification and Desalting of Peptides for Mass Spectrometric Analysis

1. Prepare one C18 StageTip per sample. The making of StageTips is described in Rappsilber et al. [19]. We recommend stacking two C18 discs on top of each other for each StageTip.
2. Activate the discs by adding 100 µL 100% methanol to the StageTips and passing through the C18 material via centrifugation at 600 × *g* for approximately 2 min at room temperature. Do not let the material dry.
3. Condition the discs by adding 100 µL Buffer B and centrifugation at 600 × *g* for approximately 2 min at room temperature.
4. Equilibrate the discs by adding 100 µL Buffer A and centrifugation at 600 × *g* for approximately 2 min at room temperature.
5. Load the eluted peptides (Subheading 3.5, **step 15**) onto the activated StageTip and centrifuge at 600 × *g* at room temperature untilthe entire sample has entered the StageTip (~4 min).
6. Wash the StageTips by adding 50 µL Buffer A and centrifuge at 600 × *g* at room temperature until the StageTip is dry (~3 min). Dried StageTips can be stored at 4 °C for several months.

3.7 LC-MS/MS Analysis of ADP-Ribosylated Peptides

1. Elute enriched ADP-ribosylated peptides from the StageTip by adding 20 µL of StageTip elution buffer 1, followed by 20 µL of StageTip elution buffer 2 into a 96-well plate suitable for the LC autosampler.
2. Remove acetonitrile from the eluates via vacuum centrifugation until volume is approximately 7 µL. This will take approximately 25 min at 30 °C. If less than 7 µL are left, top up to 7 µL with Buffer A.
3. Add 1 µL of Buffer A* to all wells.
4. For peptide separation, we typically use an in-house packed analytical LC column made from 15 cm long fused silica (75 µm inner diameter) and packed with 1.9 µm C18 beads (Dr. Maisch, Germany).

5. Program an LC method with nLC gradient of 60 min or more. We recommend analyzing each sample using a 180 min reverse-phase gradient ranging from 5% to 64% acetonitrile in 0.5% formic acid at a flow rate of 250 nL/min (*see* **Note 7**).
6. Injection volume should be kept to ≦5 μL for each sample (*see* **Note 8**).
7. To facilitate the identification of the ADP-ribosylated peptides, we recommend analyzing the samples on a Q-Exactive mass spectrometer using the "sensitive settings" as described in [20] (*see* **Note 8**). Briefly, the sensitive settings use a "top 10 method" on the Q Exactive with 60,000 MS resolution and 60,000 MS/MS resolution.
8. Set the scan range of the MS to 400–1600 m/z, and the MS/MS fixed first mass to 100 m/z.
9. Set the automatic gain control (AGC) target of the MS should to 1e6 or higher and to 1e5 (10× lower) for MS/MS.
10. Keep maximum injection time at 45 ms for MS and 110 ms for MS/MS.
11. Normalized collisional energy should be set to a value between 25 and 30, we recommend 28 as safe median.
12. Set the dynamic exclusion to 30 s.
13. Process raw files using the MaxQuant software suite supported by the Andromeda search engine. We recommend the following settings:

Fixed modifications: Carbamidomethyl (C)

Variable modifications: Oxidation (M), Acetyl (Protein N-term), mono-ADP-ribosylation ($C_{10}H_{13}N_5O_9P_2$) on lysine, arginine, glutamic acid, and aspartic acid.

To increase the confidence of ADP-ribosylated peptide identifications, we typically add neutral losses and diagnostic ion masses in the MaxQuant search parameters (*see* **Note 9**).

Max. missed cleavages: 3

Min. peptide length: 7

Protein FDR: 0.01; Peptide FDR: 0.01; Site FDR: 0.01.

4 Notes

1. The stability of ADP-HPD in solution is critical. Following reconstitution of the powder, aliquots are only stable for up to 1 week at −20 °C.
2. We recommend inducing ADP-ribosylation by treating the cells for example with H_2O_2 for 5–10 min, because this significantly increases the number of ADP-ribosylated targets that

can be detected. However, several other stimuli/DNA damage-inducing agents can be used.

3. Protein concentration can be determined after lysis (e.g., by Bradford) and an aliquot of the protein lysate can be kept for western blotting. If stable isotope labeling by amino acids in cell culture (SILAC) is applied, we recommend mixing the heavy and light SILAC samples prior to acetone precipitation (Subheading 3.1, **step 7**). Alternatively, samples can be mixed following resuspension in urea (Subheading 3.2, **step 2**).
4. It is important to perform the urea protein pellet resuspension step at room temperature (Subheading 3.2, **step 2**). At low temperatures, urea will crystalize and at high temperatures urea can induce artifacts [21].
5. We recommend making several starting cultures for preparation of a large batch of Af1521.
6. For western blotanalysis, we recommend cross-linking the GST-Af1521 macrodomain to the GST-sepharose beads. In brief, wash resin three-times with 10 mL 0.2 M borate-NaOH, pH 9.0, centrifuge at 2000 × *g* for 2 min at room temperature between each wash. Add 10 mL fresh DMP solution (20 mM) and incubate for 60 min at room temperature with head-over-tail rotation. Centrifuge at 2000 × *g* for 2 min at room temperature. Stop the cross-linking reaction by adding 10 mL 0.2 M ethanolamine. Wash resin three-times with 0.1 M glycine-HCl, pH 2.5 to remove any remaining non-covalently linked molecules. Cross-linking can be verified by SDS-PAGE. GST-protein should only elute from the resin prior to addition of DMP.
7. The described LC settings are applied for the analysis of enriched ADP-ribosylated peptides from treated cells. The LC gradient needs to be adjusted depending on the complexity of the sample and instrument used.
8. An injection volume of 5 μL will take approximately 20 min to load onto the column at a constant pressure of 500 bars. An injection volume of more than 5 μL will result in longer loading times. By using a nanoscale UHPLC system, e.g., EASY-nLC1200 (Thermo Fisher Scientific) the loading pressure can be increased and the loading time thereby shortened.
9. To help assign ADP-ribosylated peptides in MaxQuant, the following parameters can be added to the Andromeda search engine:

   Monoisotopic mass: 541.0611088074.

   Composition: H(21)C(15)N(5)O(13)P(2).

   Position: notCterm.

NeutralLoss: H(21)C(15)N(5)O(13)P(2) for lysine, arginine, aspartic acid and glutamic acid.

Diagnostic peak: H(5)C(5)N(5), H(11)C(10)N(5)O(3), H(14)C(10)N(5)O(7)P, H(15)C(10)N(5)O(10)P(2), H(21)C(15)N(5)O(13)P(2) for lysine, arginine, aspartic acid and glutamic acid.

Acknowledgments

Ms. Monika Fey is acknowledged for the expression and purification of recombinant human PARG (University of Zurich) and Paolo Nanni for technical support for the MS measurements (FGCZ, University of Zurich). We also thank Felix R. Althaus (Institute of Pharmacology and Toxicology, University of Zurich-Vetsuisse) for providing hPARG expressing baculo virus. Stephan Christen and Deena Leslie Petrioli provided editorial assistance and critical input during the writing (University of Zurich). The work carried out in the laboratory of MLN was in part supported by the Novo Nordisk Foundation Center for Protein Research; the Novo Nordisk Foundation (grant number NNF14CC0001 and NNF13OC0006477); the Lundbeck Foundation (Grant number R171-2014-1496); The Danish Council of Independent Research, grant agreement number DFF 4002-00051 (Sapere Aude) and grant agreement number DFF 4183-00322A. ADP-ribosylation research in the laboratory of MOH is funded by the Kanton of Zurich, the University Research Priority Program (URPP) in Translational Cancer Biology at the University of Zurich, and the Swiss National Science Foundation (grant 310030B_138667).

References

1. Haigis MC, Mostoslavsky R, Haigis KM, Fahie K, Christodoulou DC, Murphy AJ, Valenzuela DM, Yancopoulos GD, Karow M, Blander G, Wolberger C, Prolla TA, Weindruch R, Alt FW, Guarente L (2006) SIRT4 inhibits glutamate dehydrogenase and opposes the effects of calorie restriction in pancreatic beta cells. Cell 126(5):941–954. doi:10.1016/j.cell.2006.06.057
2. Rack JG, Morra R, Barkauskaite E, Kraehenbuehl R, Ariza A, Qu Y, Ortmayer M, Leidecker O, Cameron DR, Matic I, Peleg AY, Leys D, Traven A, Ahel I (2015) Identification of a class of protein ADP-ribosylating sirtuins in microbial pathogens. Mol Cell 59(2):309–320. doi:10.1016/j.molcel.2015.06.013
3. Altmeyer M, Messner S, Hassa PO, Fey M, Hottiger MO (2009) Molecular mechanism of poly(ADP-ribosyl)ation by PARP1 and identification of lysine residues as ADP-ribose acceptor sites. Nucleic Acids Res 37(11):3723–3738. doi:10.1093/nar/gkp229
4. Vandekerckhove J, Schering B, Barmann M, Aktories K (1987) *Clostridium perfringens* iota toxin ADP-ribosylates skeletal muscle actin in Arg-177. FEBS Lett 225(1–2):48–52
5. Zhang Y, Wang J, Ding M, Yu Y (2013) Site-specific characterization of the Asp- and Glu-ADP-ribosylated proteome. Nat Methods

10(10):981–984. doi:10.1038/nmeth.2603. http://www.nature.com/nmeth/journal/v10/n10/abs/nmeth.2603.html#supplementary-information

6. Vyas S, Matic I, Uchima L, Rood J, Zaja R, Hay RT, Ahel I, Chang P (2014) Family-wide analysis of poly(ADP-ribose) polymerase activity. Nat Commun 5:4426. doi:10.1038/ncomms5426
7. McDonald LJ, Moss J (1994) Enzymatic and nonenzymatic ADP-ribosylation of cysteine. Mol Cell Biochem 138(1–2):221–226
8. Daniels CM, Ong SE, Leung AK (2014) Phosphoproteomic approach to characterize protein mono- and poly(ADP-ribosyl)ation sites from cells. J Proteome Res 13(8):3510–3522. doi:10.1021/pr401032q
9. Min W, Cortes U, Herceg Z, Tong WM, Wang ZQ (2010) Deletion of the nuclear isoform of poly(ADP-ribose) glycohydrolase (PARG) reveals its function in DNA repair, genomic stability and tumorigenesis. Carcinogenesis 31(12):2058–2065. doi:10.1093/carcin/bgq205
10. Hanai S, Kanai M, Ohashi S, Okamoto K, Yamada M, Takahashi H, Miwa M (2004) Loss of poly(ADP-ribose) glycohydrolase causes progressive neurodegeneration in *Drosophila melanogaster*. Proc Natl Acad Sci U S A 101(1):82–86.doi:10.1073/pnas.2237114100
11. Yu SW, Andrabi SA, Wang H, Kim NS, Poirier GG, Dawson TM, Dawson VL (2006) Apoptosis-inducing factor mediates poly(ADP-ribose) (PAR) polymer-induced cell death. Proc Natl Acad Sci U S A 103(48):18314–18319. doi:10.1073/pnas.0606528103
12. Olsen JV, Mann M (2013) Status of large-scale analysis of post-translational modifications by mass spectrometry. Mol Cell Proteomics 12(12):3444–3452. doi:10.1074/mcp.O113.034181
13. Gibson BA, Zhang Y, Jiang H, Hussey KM, Shrimp JH, Lin H, Schwede F, Yu Y, Kraus WL (2016) Chemical genetic discovery of PARP targets reveals a role for PARP-1 in transcription elongation. Science 353(6294):45–50. doi:10.1126/science.aaf7865
14. Martello R, Leutert M, Jungmichel S, Bilan V, Larsen SC, Young C, Hottiger MO, Nielsen ML (2016) Proteome-wide identification of the endogenous ADP-ribosylome of mammalian cells and tissue. Nat Commun 7:12917. doi:10.1038/ncomms12917
15. Dani N, Stilla A, Marchegiani A, Tamburro A, Till S, Ladurner AG, Corda D, Di Girolamo M (2009) Combining affinity purification by ADP-ribose-binding macro domains with mass spectrometry to define the mammalian ADP-ribosyl proteome. Proc Natl Acad Sci U S A 106(11):4243–4248. doi:10.1073/pnas.0900066106. 0900066106 [pii]
16. Bonicalzi ME, Haince JF, Droit A, Poirier GG (2005) Regulation of poly(ADP-ribose) metabolism by poly(ADP-ribose) glycohydrolase: where and when? Cell Mol Life Sci 62(7–8):739–750. doi:10.1007/s00018-004-4505-1
17. Jungmichel S, Rosenthal F, Altmeyer M, Lukas J, Hottiger MO, Nielsen ML (2013) Proteome-wide identification of poly(ADP-ribosyl)ation targets in different genotoxic stress responses. Mol Cell 52(2):272–285. doi:10.1016/j.molcel.2013.08.026
18. Karras GI, Kustatscher G, Buhecha HR, Allen MD, Pugieux C, Sait F, Bycroft M, Ladurner AG (2005) The macro domain is an ADP-ribose binding module. EMBO J 24(11):1911–1920. doi:10.1038/sj.emboj.7600664
19. Rappsilber J, Mann M, Ishihama Y (2007) Protocol for micro-purification, enrichment, pre-fractionation and storage of peptides for proteomics using StageTips. Nat Protoc 2(8):1896–1906. doi:10.1038/nprot.2007.261
20. Kelstrup CD, Young C, Lavallee R, Nielsen ML, Olsen JV (2012) Optimized fast and sensitive acquisition methods for shotgun proteomics on a quadrupole orbitrap mass spectrometer. J Proteome Res 11(6):3487–3497. doi:10.1021/pr3000249
21. Poulsen JW, Madsen CT, Young C, Poulsen FM, Nielsen ML (2013) Using guanidine-hydrochloride for fast and efficient protein digestion and single-step affinity-purification mass spectrometry. J Proteome Res 12(2):1020–1030. doi:10.1021/pr300883y

Molecular Cell
Previews

Identification of PARP-Specific ADP-Ribosylation Targets Reveals a Regulatory Function for ADP-Ribosylation in Transcription Elongation

Mario Leutert,[1,2] Deena M. Leslie Pedrioli,[1] and Michael O. Hottiger[1,*]
[1]Department of Molecular Mechanisms of Disease, University of Zurich, 8057 Zurich, Switzerland
[2]Molecular Life Science PhD Program of the Life Science Zurich Graduate School, 8057 Zurich, Switzerland
*Correspondence: michael.hottiger@dmmd.uzh.ch
http://dx.doi.org/10.1016/j.molcel.2016.07.006

In a recent issue of *Science*, Gibson et al. (2016) describe an in vitro chemical genetic approach that maps the specific ADP-ribosylation sites targeted by the ADP-ribosyltransferases PARP-1, PARP-2, and PARP-3 and demonstrate that PARP-1 regulates RNA polymerase II promoter-proximal pausing.

The human genome encodes 17 intracellular ADP-ribosyltransferases, called PARPs (also known as ARTDs), that regulate different biological processes via post-translational modification of proteins with a single (MARylation) or multiple (PARylation) ADP-ribose units from NAD^+ (Hottiger, 2015). The identification of PARP-specific targets has been hampered by technical challenges for many years. Gibson et al. now report the development and application of an elegant in vitro chemical genetic methodology that allowed the identification of protein targets specific for PARP-1, PARP-2, or PARP-3 (Gibson et al., 2016). All three are DNA-dependent nuclear proteins that PARylate (PARP-1/2) or MARylate (PARP-3) their targets. The method is based on the combined use of a newly developed NAD^+ analog, 8-Bu(3-yne)T-NAD^+, and analog-sensitive PARP-1, PARP-2, and PARP-3 mutant isoforms (asPARPs). Analog sensitivity was achieved by modifying the PARP active site to accommodate the bulky 8-Bu(3-yne)T-NAD^+. Importantly, the modification of proteins using this NAD^+ analog allowed downstream azide-alkyne cycloaddition ("click" chemistry), which enabled PARP target labeling and purification. In contrast to previous attempts (Carter-O'Connell et al., 2014; Jiang et al., 2010), screening of an NAD^+ analog library with systematically mutated PARP-1 isoforms identified functional combinations that promote PARylation.

Using this approach, HeLa cell nuclear extracts were co-incubated with purified, salmon sperm DNA-activated asPARP-1, PARP-2, or PARP-3 and 8-Bu(3-yne)T-NAD^+. The asPARP-modified protein targets were purified by "click" chemistry-based azide-agarose crosslinking, trypsin digested, and identified by liquid chromatography-tandem mass spectrometry (LC-MS/MS) (Figure 1A). Asp and Glu ADP-ribosylated peptides were eluted with hydroxylamine (NH_2OH) and the ADP-ribosyl modification sites identified by LC-MS/MS (Zhang et al., 2013). The same workflow was also applied to nuclei isolated from *Parp1*$^{-/-}$ mouse embryonic fibroblasts (MEFs) overexpressing asPARP-1. A total of 467 in vitro ADP-ribosylated proteins were identified.

Using the same chemical strategy, the authors developed a "Click-ChIP-seq" method and mapped the asPARP-1-mediated genomic ADP-ribosylation sites in MEF nuclei (Figure 1B). Sites of asPARP-1-mediated chromatin ADP-ribosylation co-localized with actively transcribed (H3K4me3-enriched) gene promoters and actively transcribing Pol II (from GRO-seq data). ADP-ribosylation was found to contribute to negative elongation factor (NELF) complex function, and components of NELF were identified as ADP-ribosylation targets of asPARP-1 and asPARP-3. ADP-ribosylation of NELF-E was also shown for authentic PARP-1 and found to be dependent on CDK9/P-TEFb-mediated NELF-E phosphorylation, which results in release of Pol II promoter pausing. asPARP-1-mediated chromatin ADP-ribosylation positively correlated with PARP-1 and NELF-B binding at actively transcribed promoters with high CDK9 occupancy. GRO-seq analysis in PARP-1 knockdown or PARP inhibitor-treated MCF-7 cells confirmed the functional relevance of these observations. In both cases, paused Pol II accumulated at promoter regions, and corresponding gene body transcriptional elongation decreased. Similar findings were obtained by CDK9 inhibition or NELF knockdown, suggesting that PARP-1-dependent NELF-E ADP-ribosylation reinforces P-TEFb-mediated Pol II pause release and productive transcriptional elongation.

A caveat of this methodology is that 8-Bu(3-yne)T-NAD^+, like NAD^+, is not cell permeable, and can only be used in in vitro or isolated nuclei-based ADP-ribosylation reactions. ADP-ribosylation is a reversible, highly dynamic, and low abundant PTM. Thus, it will be interesting to see whether 8-Bu(3-yne)T-NAD^+-derived modifications are as reversible as authentic ADP-ribosyl modifications (Yu et al., 2006). Furthermore, exogenous addition of asPARPs and the NAD^+ analog may cause off-target modifications due to concentrations being non-physiological. Although in vivo ADP-ribosylation by PARP-1 was confirmed for NELF, additional asPARP-1, asPARP-2, and asPARP-3 ADP-ribosylation targets need to be tested to see whether the method is able to faithfully predict in vivo PARP targets.

Due to technical limitations of the method used to map ADP-ribosylation acceptor sites, only Asp and Glu sites were identified (Zhang et al., 2013). Thus, potential modifications of other amino acids, e.g., Lys or Arg (Altmeyer

CellPress

Molecular Cell
Previews

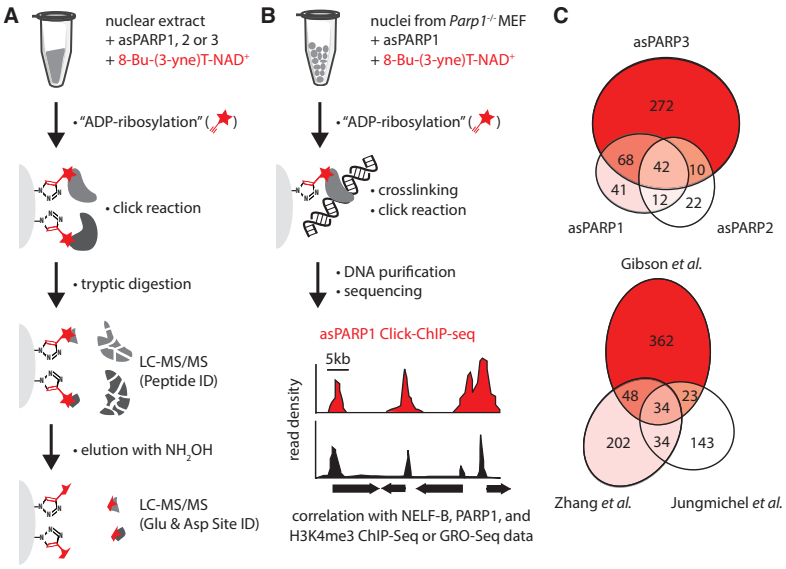

Figure 1. A Chemical Genetic Approach for Mapping PARP-Specific ADP-Riboslyated Protein Targets across the Proteome and Genome
(A) Proteomic workflow.
(B) Click-ChIP-seq workflow.
(C) Overlap between asPARP-1, asPARP-2, and asPARP-3 protein targets, and overlap between protein targets identified by Gibson et al. (2016), Jungmichel et al. (2013), and (Zhang et al., 2013).

et al., 2009), could not be identified. Surprisingly, Gibson et al. (2016) identified considerable overlaps between the targets modified by PARP-1, PARP-2, and PARP-3 (Figure 1C). This is intriguing, given that these PARPs have different biological functions. Furthermore, asPARP-3 generated the largest number of unique ADP-ribosylated targets, which is an interesting finding for a nuclear, MARylating enzyme that is not as well characterized as PARP-1 or PARP-2. The authors observed also partial overlap between their targets and those identified in previous studies. Some variation is expected due to different sample preparation and enrichment techniques, and the untargeted mass spectrometry measurements. The study is difficult to compare to previous ones (reviewed in Daniels et al., 2015), as it is unclear how exogenous addition of PARPs compares to studies using stimulated cells. While the initial discovery experiments used artificially activated asPARPs, subsequent experiments with purified nuclei were considered to have identified targets under unstimulated conditions. This raises the question as to how asPARP activity is regulated under these conditions and whether these nuclei truly represent unstimulated conditions. Previous ADP-ribosylation proteomic screens found that PARP activity is tightly regulated in vivo, and that successful target identification requires genotoxic stress (Jungmichel et al., 2013) and/or PARG knockdown (Zhang et al., 2013). Finally, it would be interesting to see whether the number of ADP-ribosylated targets increases when the asPARP-8-Bu(3-yne)T-NAD$^+$ technique is used in conjunction with MS workflows that identify all ADP-ribosyl acceptor amino acids.

PARP-1 knockdown or inhibition caused an accumulation of paused Pol II at gene promoters. Remarkably, Pol II pausing was observed genome-wide, even at genes that had not been previously reported to be regulated by ADP-ribosylation. This suggests that ADP-ribosylation regulates transcription in a highly complex manner. The genomic ADP-ribosylation profiles identified by Click-ChIP-seq were rather large (>5 kb) chromatin domains. This lack of resolution makes it difficult to define exact sites of ADP-ribosylation and assess their relation to PARP-1 binding. Intriguingly, the analysis also identified loci with significant PARP-1 binding but little or no ADP-ribosylation. A recently published in vivo ADP-ribosylated chromatin affinity purification (ADPr-ChAP) methodology found associations between oxidative stress, PARP1-mediated chromatin ADP-ribosylation, histone density, and heterochromatic histone marks (Bartolomei et al., 2016). These findings are not contradictory to the ones reported here, but rather suggest that ADP-ribosylation patterns are dependent upon cell type and stimulation.

In the paper by Gibson et al. (2016), PARP-1-mediated ADP-ribosylation of NELF-E was dependent on P-TEFb activity, which points to a potential functional link between ADP-ribosylation and phosphorylation. Increased Pol II pausing was observed when cells were complemented with an ADP-ribosylation-deficient NELF-E mutant. However, ADP-ribosylation-dependent release of Pol II pausing was only observed for less than half of the NELF-E-regulated genes. Further experiments are therefore required to fully substantiate a link. Finally, NELF-E was also identified as a PARP-3 target but not investigated further. Thus, additional studies are required to determine whether PARP-3 also regulates gene expression.

To provide novel therapeutic options and translate these, and emerging new insights, into patient benefits, it will be important to: (1) identify and validate protein targets for all PARP family members in vivo using the relevant cell culture and animal models, (2) define the molecular pathways regulated by the different PARPs, and (3) determine how and to what extent PARPs contribute to disease development. This knowledge will expedite the development of isozyme-specific PARP inhibitors that provide therapeutic benefits for diseases where one PARP primarily causes the pathophysiological condition.

REFERENCES

Altmeyer, M., Messner, S., Hassa, P.O., Fey, M., and Hottiger, M.O. (2009). Nucleic Acids Res. *37*, 3723–3738.

Molecular Cell

Previews

Bartolomei, G., Leutert, M., Manzo, M., Baubec, T., and Hottiger, M.O. (2016). Mol. Cell 61, 474–485 .

Carter-O'Connell, I., Jin, H., Morgan, R.K., David, L.L., and Cohen, M.S. (2014). J. Am. Chem. Soc. 136, 5201–5204 .

Daniels, C.M., Ong, S.E., and Leung, A.K. (2015). Mol. Cell 58, 911–924 .

Gibson, B.A., Zhang, Y., Jiang, H., Hussey, K.M., Shrimp, J.H., Lin, H., Schwede, F., Yu, Y., and Kraus, W.L. (2016). Science 353, 45–50 .

Hottiger, M.O. (2015). Annu. Rev. Biochem. 84, 227–263 .

Jiang, H., Kim, J.H., Frizzell, K.M., Kraus, W.L., and Lin, H. (2010). J. Am. Chem. Soc. 132, 9363–9372 .

Jungmichel, S., Rosenthal, F., Altmeyer, M., Lukas, J., Hottiger, M.O., and Nielsen, M.L. (2013). Mol. Cell 52, 272–285 .

Yu, S.W., Andrabi, S.A., Wang, H., Kim, N.S., Poirier, G.G., Dawson, T.M., and Dawson, V.L. (2006). Proc. Natl. Acad. Sci. USA 103, 18314–18319 .

Zhang, Y., Wang, J., Ding, M., and Yu, Y. (2013). Nat. Methods 10, 981–984 .

Comprehensive *in vivo* ADP-ribosylome analysis identifies tyrosine ADP-ribosylation of HPF1 and reveals that this modification modulates ARTD1 activity

Deena M. Leslie Pedrioli[1,*], Mario Leutert[1,2,*], Vera Bilan[1], Kathrin Nowak[1,2], Kapila Gunasekera[1], Elena Ferrari[1], Ralph Imhof[1], Lars Malmström[3], Michael O. Hottiger[1]

[1]Department of Molecular Mechanisms of Disease, University of Zurich, CH-8057 Zurich, Switzerland, [2]Molecular Life Science PhD Program of the Life Science Zurich Graduate School, CH-8057 Zurich, Switzerland, [3]S3IT, University of Zurich, CH-8057 Zurich.

[*] These authors contributed equally to this work.

Short title: Tyrosine ADP-ribosylation of HPF1 regulates ARTD1 activity
Keywords: ADP-ribosylation, Tyrosine ADP-ribosylation (Y-ADPr), HPF1, ARTD1, PARP1, Genotoxic stress

Corresponding author:

Prof. Michael O. Hottiger, PhD, DVM

Department of Molecular Mechanisms of Disease

University of Zurich

Winterthurerstrasse 190

CH-8057 Zurich

Switzerland

E-mail: michael.hottiger@dmmd.uzh.ch

2

ABSTRACT

Despite recent biochemical and mass spectrometry (MS)-based breakthroughs, comprehensive ADP-ribosylome identification and accurate ADP-ribose-site localization remain challenging. Here we report the establishment of an unbiased, multistep ADP-ribosylome data analysis workflow, where bioinformatic analyses were combined with manual spectra validation, that identified tyrosine as a novel *in vivo* ADP-ribose-acceptor. Using shRNA-based knockdown studies, we provide proteome-wide evidence demonstrating that genotoxic stress strongly and specifically induces ARTD1-dependent serine and tyrosine ADP-ribosylation *in vivo*. Site-directed mutagenesis and *in vitro* ADP-ribosylation assays confirmed that tyrosine functions as an ADP-ribose-acceptor amino acid in RPS3A and HPF1. ARTD1-mediated tyrosine modification was dependent on HPF1. Moreover, these studies revealed that ADP-ribosylation of HPF1 on Y238 is required for its activity as ADP-ribosylation cofactor. Together, our findings validate the functional importance of tyrosine as novel ADP-ribose-acceptor amino acid and demonstrate the broad and far-reaching influences low abundant ADP-ribosylation, like HPF1-Y238, can have on the cellular ADP-ribosylome.

3

INTRODUCTION

Protein ADP-ribosylation is a physiologically and pathologically important post-translational modification (PTM) that regulates cellular activities by chemically modifying proteins with a single (MARylation) or multiple (PARylation) ADP-ribose (ADPr) units from NAD^{+}[1,2]. The human genome encodes 17 intracellular ADP-ribosyltransferases (ARTDs or PARPs) that are distributed in different cellular compartments[1,3]. While ARTDs are structurally homologous, and resemble the diphtheria toxin, the molecular mechanisms by which they modify target proteins are not fully defined. It is not yet clear if each ARTD has enzymatic activity towards all or a specific subset of the known ADPr-acceptor amino acids or if they are all capable of modifying the same amino acid(s) within a given target protein.

For many years, technical challenges have limited the number of identified ARTD-specific target proteins. But, the introduction of mass spectrometry (MS)-based ADP-ribosylation optimized methodologies[4-7] and the development of MARylated-peptide enrichment and/or ADPr labeling techniques prior to MS analysis drastically improved the detection and identification of ADP-ribosylated proteins[8-12]. Our group and others have shown that genotoxic stress conditions strongly and specifically induce the ADP-ribosylation of hundreds of proteins. These studies identified ARTD1 and histones to be the main acceptors of ADPr under these conditions[10,11,13,14]. ARTD1 and ARTD2 are considered the two main ARTDs that "write" nuclear PARylation[1,3]. A recent permeabilized cell-based chemical proteomics study using NAD^{+} analogues demonstrated as well that ARTD1 and ARTD2 ADP-ribosylate several hundred proteins and revealed a significant target protein[12]. Although these groundbreaking studies have significantly advanced our understanding of cellular ADP-ribosylation, unfortunately it still remains unclear what the *bona fide* ADP-ribosylation targets of these ARTDs are *in vivo*.

Proteomics studies have also identified several ADPr-acceptor amino acids in mammalian cells, namely lysine (K), arginine (R), aspartic acid (D), glutamic acid (E), cysteine (C) and serine (S)[1,5,6,9,11,15,16]. Unfortunately, accurate ADPr acceptor site(s) localization remains challenging partially due to the fact that MS-search engines require the user to predefine all possible ADPr-acceptor amino acids. This can introduce bias, which was recently highlighted by the unexpected identification of S as the prominent genotoxic stress induced ADPr-acceptor[7,15]. Using ARTD1 as the writer of *in vitro* ADP-ribosylation modifications, a few of the described ADPr-acceptor amino acid have been biochemically validated by site directed mutagenesis or Edman sequencing[1,3,5,11]. Following the identification of S-ADP-ribosylation on histones and ARTD1[15], Bonfiglio *et al.* found that Histone PARylation Factor 1 (HPF1, previously C4orf27) functions as a cofactor for ARTD1 and ARTD2 that directs ADP-ribosylation specifically towards S-ADPr acceptor sites[5]. HPF1, was first identified as a regulator of ADP-ribosylation signaling in the DNA damage response via ARTD1-dependent recruitment to DNA lesions, which subsequently leads to ARTD1-dependent ADP-ribosylation of histones[17].

4

Here, we took advantage of the high-quality MS datasets that our group recently generated using an ADPr-optimized HCD-PP-EThcD/HCD MS workflow[7] and re-analyzed these data using several different variable ADPr search parameters. By expanding the ADPr-acceptor amino acid specificity search parameters, we identified Y-ADPr-acceptor sites. Using powerful, label-free quantitative proteomics methods we demonstrate that ARTD1 functions as the proteome-wide writer of H_2O_2-induced S-ADPr and Y-ADPr protein modifications. Biochemical assays, coupled with site-directed mutagenesis, confirm that ARTD1 ADP-ribosylates the MS-identified Y-ADPr acceptor sites of RPS3A (Y155) and HPF1 (Y238). Finally, in depth investigation of functional consequences of HPF1 ADP-ribosylation reveal that Y238 ADP-ribosylation drives all HPF1 ADP-ribosylation activities and that loss of this PTM obstructs the enzymatic activities of ARTD1.

RESULTS

Opening Mascot-based MS search parameters for ADPr variable modifications identifies tyrosine as a novel potential ADPr-acceptor site.

To investigate whether new ADPr-acceptor amino acids could be identified within our high-quality ADPr-enriched MS datasets, a revised Mascot searches were used[7]. The data used here were acquired from biological replicate H_2O_2-treated HeLa cell samples (n=4) using an ADPr-optimized HCD-PP-EThcD/HCD MS workflow (**Figure 1a**). For these new searches, we opened the variable ADPr PTM search parameters to include all 20 amino acids as potential ADPr-acceptor sites (**Table S1**). Potential ADP-ribosylated peptides were considered for further analysis and validation when Mascot scores >20 and expectation values <0.05 were obtained. The individual searches returned ~700 ADPr-site localizations per search (**Table S2**). Interestingly, these open search parameters returned ~500 ADPr modifications that localized to "new" potential ADPr-acceptor amino acids. The semi-repetitive search parameters used here returned several ADPr-site localizations for the same spectra. As a result, the spectra annotations were validated manually to determine which of the assigned ADPr-sites was most likely correct for each of the spectra. Prior to manual review, an additional ion score filter was applied (**Figure 1b**) and ADPr-site localizations for spectra with ion scores >0.5 (448 unique spectra/117 unique peptides) were validated. This identified 288 high quality spectra (181 EThcD and 107 HCD spectra) in which the ADPr-site was confidently localized within the ADPr-peptide. In agreement with previous studies [7,11,15,18], these spectra support the attachment of ADPr to known ADPr-acceptors (S, D, E, R, and K) and further supported previous findings that S is the prominent ADPr-acceptor amino acid *in vivo* (**Figures 1c** and **S1a**). In addition, several previously unidentified ADPr-acceptor amino acids were found including alanine (A), leucine (L), asparagine (N), glutamine (Q), valine (V) and tyrosine (Y) (**Figures 1c** and **S1a,** and **Table S3**).

Several of the side chains of these new potential ADPr-acceptors are biochemically inert. Moreover, all but Y were only identified in HCD spectra (**Figure S1a**) and, while high-resolution HCD fragmentation methods successfully and confidently identify ADP-ribosylated peptides, the inherent fragility of the ADPr modification under these conditions severely limits confident ADPr site localization[5,7,11,15]. We, therefore, reasoned that some of these new ADPr-acceptors were false positives. To tease this out, we used the 288 high-quality spectra (**Table S3**) to build a spectra library for ADPr-site localization training. The ADPr-site Localization Spectra Database (ADPr-LSD) (**Supplementary Information**) was then used to iteratively refine the search parameters to define the full ADP-ribosylome (peptide/protein), confidently and accurately assign the ADPr-site within each modified peptide and identify all biologically relevant ADPr-acceptor amino acids. Two search parameter refinement steps were carried out using Mascot where the ADPr-acceptor amino acid groups were varied (SDERKY or SRY). The refined peptide identification and ADPr-site localization results were compared (computationally and manually) with each other and the original assignments (**Figures 1c** and

S1a). Throughout this process, we found that ADPr-site localization scores increased as the search parameters were refined to only include amino acids that could be confirmed by manual spectra annotation (**Table S3**). Moreover, the step-wise bioinformatic and manual validation workflow presented here led to the identification of Y as an ADPr-acceptor amino acid. The improved spectra fragment ion assignments also confirmed all of the other potential "new" ADPr-acceptors (A, L, N, Q and V) as false positives (**Table S3** and **ADPr-LSD**).

To assess the performance of our improved ADPr-search parameters on the full data set, rather than just the ADPr-LSD spectra, we extended our analyses and compared our SDERKY and SRY results. In line with results published by Bilan *et al.*[7], each of our searches identified ~180 unique ADPr-peptides with perfect peptide identification overlaps (**Figure 1d, Tables 1** and **S4)**. Comparison of the ADPr-site localizations returned by the SDERKY and SRY searches revealed >60% ADPr-site localization agreement for EThcD fragmentation-based spectra (**Figure 1d**) and ~35% agreement for HCD spectra (**Figure S1b**). Half of the ADPr-peptides were identified by both HCD and EThcD fragmentation methods. For these peptides, the ADPr-site localizations were in agreement ~50% of the time (**Figure 1e**). Finally, and most intriguingly, these comparative analyses identified 7 proteins that carry potential Y-ADPr modifications (**Table 2**). Thus, validating Y as a novel, albeit low abundant, *in vivo* ADPr-acceptor amino acid.

ARTD1 is the main writer of genotoxic stress induced ADP-ribosylome

To dissect the contributions of ARTD1 and ARTD2 on the observed ADP-ribosylome, we inhibited their expression in HeLa cells via stable expression of shARTD1, shARTD2 or shControl siRNAs (**Figure S2a**). The engineered cell lines were treated in biological triplicate with H_2O_2 or left untreated and the resulting ADP-ribosylomes defined using HCD-based MS as previously described[11]. The resulting datasets were analysed for variable SDERKY or SRY ADP-ribosylation using Mascot. In general, while the untreated ADP-ribosylomes of each cell-line were quite similar, specific and significant decreases in the total number of ADP-ribosylated spectra and proteins identified were observed in H_2O_2-treated shARTD1 cells (**Figures 2a** and **S2b, Table S5**). In fact, shARTD1 ADP-ribosylation levels were most similar to untreated shControl or shARTD2 cells (**Figure S2b**). These findings confirmed that ARTD1 is the main driver of nuclear PARylation[19] Moreover, our data suggest that ARTD2 does not functionally complement ARTD1 *in vivo* and demonstrate that ARTD1 is the main enzyme that catalyzes of genotoxic stress induced nuclear de novo ADP-ribosylation. Finally, our findings also indicate that ARTD1 and ARTD2 only marginally contribute to the steady-state (untreated) ADP-ribosylome and that ARTD2 does not, in fact, significantly contribute to H_2O_2-induced ADP-ribosylation in HeLa cells (**Figures 2a** and **S2b**). To address a potential crosstalk between ARTD1 and ARTD2, we quantified the identified ADPr-sites using MS1-based label-free quantification (LFQ). While quantified relative ADPr-peptide abundances were consistent among biological replicates (Spearman rank's correlation coefficients 0.71-

0.83), poor correlation between the shARTD1 and the shControl or shARTD2 samples were observed (**Figure S2c-d**). Taken together, these findings suggest that ARTD1 is the main writer of HeLa cell cellular ADP-ribosylation following H_2O_2 treatment.

Proteome-wide S- and Y-ADP-ribosylation is mediated by ARTD1

To determine proteome-wide ARTD1 ADPr-acceptor amino acid specificity, comparative analysis of our optimized ADPr search parameters (SDERKY vs SRY) revealed a slight (~15%) increase in the number of unique peptides identified in the SRY search, while comparable numbers of ADPr spectra matches were identified (**Figure S3a-b**). Overall the increased search space (SDERKY) did not lead to a significant decrease in R-ADP-ribosylation, but reduced S-ADP-ribosylation assignments in favor of K-ADP-ribosylation, D-ADP-ribosylation and E-ADP-ribosylation (**Figure S3c-d**). These searches demonstrated that R is the primary steady-state ADPr-acceptor amino acid. Following H_2O_2 treatment, the major modification site identified was S and, to a much lesser extent, Y. Interestingly, our data indicates that both of these modifications required ARTD1 (**Figure S3c-d**). Quantification of the site-specific ADP-ribosylation changes in response to ARTD1 or ARTD2 knockdown, via volcano blot analyses and annotation of EThcD localized ADPr sites, further confirmed that S-ADP-ribosylation and Y-ADP-ribosylation were dependent on ARTD1, and specifically and strongly induced upon H_2O_2 treatment, while R-ADP-ribosylation remained uninfluenced by genotoxic stress (**Figure 2b**).

Pathway analysis identifies links between the ADP-ribosylome, cellular functions and the phospho-proteome

GO analysis of the ADPr-ribosylated proteins identified revealed that S-ADP-ribosylated and Y-ADP-ribosylated proteins are typically nuclear proteins that interact with RNA and/or DNA and play a role in chromatin organization (**Figure 2c** and Table S5). In contrast, R-ADP-ribosylated proteins localized to endomembranes and function in protein folding and/or endoplasmic reticulum (ER) stress-associated processes, similar to our previous studies[19]. Studies have demonstrated that ~90% of the phosphorylation-sites observed in mammalian cells localize to S[20]. Given that our studies identified S and Y as the main H_2O_2-induced ADPr-acceptor, we investigated the potential link between protein ADP-ribosylation and phosphorylation modifications. Comparison of our datasets with those recently published by Sharma *et al.*[20] found that 18% of our S-ADPr-sites could also serve as phosphorylation sites in Hela cells (**Figure 2d** and **Table S6**), which tentatively suggests that cross-talk between phosphorylation and O-linked ADP-ribosylation may control key cellular stress response pathways.

RPS3A-Y155 is ADP-ribosylated by ARTD1 in presence of HPF-1.

Our extensive bioinformatics analyses identified 7 proteins that are potentially ADP-ribosylated on Y residues *in vivo* (**Table 2**). Moreover, the LFQ-based data presented above indicated that these novel Y-ADP-ribosylations are written by ARTD1. The low abundance of these modifications, relative to S-ADP-ribosylation, and the uncertainty surrounding ADP-ribosylation sites localized using HCD spectra[5] prompted us to independently validate Y as an ADPr acceptor amino acid using *in vitro* ADP-ribosylation assays. For these studies, we proceeded with RPS3A, as several high quality EThcD spectra supporting Y155-ADPr modification were identified at each phase of our bioinformatic analyses (**Figure 3a** and **ADPr-LSD** (KTSYAQHQQVR)). Full-length recombinant wild-type RPS3A (RPS3A-WT) and Y155F mutant (RPS3A-Y155F) proteins were constructed for these studies. Strong and relatively indistinguishable amounts of [^{32}P]-ADPr were incorporated into full-length RPS3A-WT and RPS3-Y155F when the modification reactions were carried out with ARTD1 alone (**Figure 3b**). Recent studies have demonstrated that the *in vitro* enzymatic activity of ARTD1 can be promiscuous and that addition of HPF1 to these reactions changes the modified ADPr-acceptor specificity on histones and ARTD1 from E, D, R and K residues to S residues[5,17].

We reasoned that Y-ADP-ribosylation should be biochemically similar to O-linked S-ADP-ribosylation, thus addition of HPF1 could provide the ARTD1 enzymatic specificity required to confirm Y-ADP-ribosylation. Based on the incorporation of [^{32}P]-ADPr, we found that HPF1 augmented ARTD1 *auto*-modification and damped *trans*-modification of RPS3A (**Figure 3b**). Importantly, HPF1-mediated modulation of ARTD1 *trans*-ADP-ribosylation activity significantly reduced RPS3A-Y155F mutant protein ADP-ribosylation (~40%) relative to RPS3A-WT (**Figure 3b**). Together, these data demonstrate that RPS3A is ADP-ribosylated by ARTD1 at Y155, confirm that Y can act as an ADPr-acceptor amino acid and show that HPF1 provides Y-ADP-ribosylation specificity.

ADP-ribosylation of Y238 of HPF1 is important for its ADP-ribosylation cofactor functions

The addition of HPF1 to the *in vitro* ADP-ribosylation assays presented in Figure 3 revealed that ARTD1 also ADP-ribosylates HPF1. This finding was, in fact, supported by the MS data presented above (**Table S4**), in which a single ADPr-peptide from HPF1 (TFHGAGLVVPVDKNDVGYRELPETDADLKR) was identified which resulted in the identification of one ADPr-site – Y238 (**Figure S4**). The identification of Y238, which together with the adjacent R239 is highly conserved in all C4orf27 orthologues, led us to wonder if not just the amino acid itself, but ADP-ribosylation of Y238 controls HPF1 ADP-ribosylation cofactor functions; particularly given the large, aromatic and pH dependent charged state of Y amino acid side chain and the bulkiness an ADPr modification would add to HPF1.

To explore this, we first set out to determine if Y238 of HPF1 is ADP-ribosylated. We generated HIS-tagged recombinant wild-type HPF1 and mutant proteins in which Y238 was

mutated to a phenylalanine (Y238F) to maintain the aromatic structure of the amino acid at this position. The adjacent R239 was additionally mutated either alone to alanine (R239A) or together with Y238 (Y238F/R239A). *In vitro* ADP-ribosylation assays with these HPF1 isoforms and ARTD1 demonstrated strong incorporation of ^{32}P-ADPr into HPF1-WT (**Figure 4a**). In contrast, very weak modification of HFP1-Y238F was observed and quantification analysis revealed a ~75% decrease in the modification HPF1-Y238F relative to WT (**Figure 4a**), suggesting that Y238 is indeed an ADPr-acceptor. We found that HPF1-R239A was modified to almost wild-type levels (>80%) and, unexpectedly, observed ADP-ribosylation of the double mutant (HPF1-Y238F/R239A) under these conditions. While HPF1-Y238F/R239A modification was stronger than that observed for HPF1-Y238F, it was weaker than that observed for HFP1-WT or HPF1-R239A (**Figure 4a**). This suggests that, under these conditions, ADP-ribosylation of HPF1-Y238F/R239A could reflect promiscuous ARTD1 enzymatic activity. Moreover, the dramatic boost in ARTD1 auto-ADP-ribosylation observed in presence of HPF1-WT (350% +/-7%), was completely lost when the modification assays were carried out in the presence of any of the HPF1 mutants (**Figure 4a**). Quantification analysis ARTD1 ADP-ribosylation revealed that, relative to ARTD1 *auto*-modification in the absence of HPF1, HPF1-Y238F, HPF1-R239A and HPF1-Y238F/R239A inhibited ARTD1 *auto*-modification by ~20% (**Figure 4a**). This suggests that both of Y238-ADP-ribosylation and R239 are required for HPF1 to enhance ARTD1 *auto*-modification.

Unfortunately, it remains unclear whether the lack of modification of HPF-Y238F mutant resulted from ADPr-site mutagenesis (i.e. lack of ADP-ribosylation) or general loss-of ARTD1 binding. Moreover, modification of HPF1-Y238F/R239A suggested that nonspecific interactions with ARTD1, different from wild-type HPF1-ARTD1 interactions, facilitated promiscuous ADP-ribosylation of this HPF1 mutant. Defining the interactions between ARTD1 and our isoforms of HPF1 are of particular importance as previous *in vivo* immunoprecipitation-based with HPF1 mutants (HFP1-Y238A, HPF1-R239A and HPF1-Y238A/R239A) demonstrated that all of these mutations abolished ARTD1-HFP1 protein-protein interactions under unstressed conditions[17]. To explore this and determine if ADP-ribosylation alters ARTD1-HFP1 interactions, HPF1 proteins were pre-incubated with recombinant ARTD1 under non-modifying conditions or in the presence of NAD^+/Activating DNA to induce ADP-ribosylation. Purification of ARTD1-HPF1 protein complexes using α-ARTD1 protein A sepharose beads demonstrated that the interaction between ARTD1 and HPF1-WT was not dependent on ADP-ribosylation, but was augmented following ADP-ribosylation (**Figure S5a**). Interestingly, we discovered that while unmodified ARTD1 (i.e. in absence of NAD^+) was unable to interact with HFP1-Y238F or HFP1-Y238F/R239A, it did interact weakly with HPF1-R239A (**Figure S5b-d**). These findings suggest that Y238 provides a beneficial interface for ARTD1-HPF1 interactions. Furthermore, we found that ADP-ribosylation not only enhanced the interaction between ARTD1 and HPF1-R239A but also facilitated weak interactions between ARTD1 and HPF1-Y239F and HFP1-Y238F/R239A

(**Figure S5b-d**). Taken together, these findings indicate that Y238 provides a beneficial interface for ARTD1-HPF1 interactions, that ADP-ribosylation of ARTD1 and/or HPF1 stabilizes the protein-protein complex. It is possible that ADP-ribosylation of Y238 itself (in presence of the R239A mutation) provides the critical structural framework required to stabilize ARTD1-HFP1 interactions. Finally, we also confirm that R239 also contributes, although to a lesser extent, to ARTD1-HPF1 complex formation.

ADP-ribosylation of HPF1 at Y238 is required for its function as a trans-ADP-ribosylation cofactor.

Given that both ADP-ribosylation of Y238 and the presence of R239 are required for HPF1 to enhance the *auto*-modification enzymatic activity of ARTD1 (**Figure 4a**), we wondered whether ADP-ribosylation of HPF1 would also affect its *trans*-ADP-ribosylation cofactor functions. To this end, recombinant RPS3A-WT or RPS3A-Y155F proteins were ADP-ribosylated *in vitro* in the presence of ARTD1 alone or with ARTD1 and HPF1-WT, HPF1-Y238F, HPF1-R239A or HPF1-Y238F/R239A. In agreement with **Figure 3**, the HFP1-WT dampened the *trans*-ADP-ribosylation activities of ARTD1, which provides ADPr-ribosylation specificity (**Figure 4b**). Intriguingly, a dramatic and specific decrease in ARTD1 *trans*-ADP-ribosylation activity of was observed in the presence of HPF1-Y238F. Quantification of [^{32}P]-ADPr incorporation into RPS3A-WT and RPS3A-Y155F, relative to RPS3A-WT modified by ARTD1 alone, revealed a >75% decrease in ARTD1 *trans*-ADP-ribosylation activity (**Figure S6**). In stark contrast to this, the modification levels of both RPS3A proteins observed with HFP1-R239A or HFP1-Y238F/R239A were comparable to those achieved with ARTD1 alone (**Figure 5** and **S6**). Together, these findings suggest that ADP-ribosylation of HPF1 at Y238 is critical for the *trans*-ADP-ribosylation cofactor functions and, together with R239, provides amino acid ADPr-acceptor site specificity.

DISCUSSION

Here we report the establishment of a MS data analysis workflow for identifying the ADP-ribosylome that was developed using an alternative, multistep approach that combined bioinformatic analyses with manual validation of the spectra annotations to confidently localize the ADPr-sites within the identified ADP-ribosylated peptides. In addition to identifying spectra that strongly support the *in vivo* ADP-ribosylation of S and R, this approach led to the first identification of Y-ADP-ribosylation. Using shRNA-based knockdown studies, we have demonstrated that genotoxic stress strongly and very specifically induces proteome-wide S- and Y-ADP-ribosylation *in vivo* and that these PTMs are ARTD1 dependent. Site-directed mutagenesis and *in vitro* ADP-ribosylation methods biochemically confirmed Y-ADPr protein modifications for RPS3A and HPF1. Like O-linked S-ADP-ribosylation, we found that the HPF1 cofactor activity was also required for Y-ADPr modification specificity. Finally, and most intriguingly, *in vitro* biochemical validation methodologies provide strong evidence that ADP-ribosylation of HFP1-Y238 is required for HPF1's ARTD1-associated *trans*-ADP-ribosylation cofactor function.

As indicated above, analyzing ADP-ribosylome MS data is challenging and bias can be introduced when attempting to accurately localize ADP-acceptor sites. Indeed, earlier reports from our group identified K-ADPr-sites within a KS modification motif[7,11]. Interestingly, re-evaluation of the data to include S as an ADPr-acceptor amino acid led to the reassignment of most of the K-ADPr assignments to S-ADPr[5,7]. These findings suggested that new ADPr-acceptor amino acid potentially awaited discovery. We approached this by developing an alternative analysis workflow where all possible amino acids were queried as ADPr-acceptors and all peptides with strong theoretical spectra library annotations were validated manually for correct ADPr-site localization. Subsequent re-analysis of the same data for ADP-ribosylation on only those amino acids confirmed by manual spectra validation (S, D, E, R, K and Y) improved our ADPr search outcomes and assigned ADPr-sites with greater confidence. Importantly, this approach also revealed that Y functions as an ADPr-acceptor amino acid *in vivo.*

We have made great strides towards overcoming the bioinformatic challenges associated with analyzing ADP-ribosylome MS datasets, but improvements are still required. Confident ADPr-site localizations were only made for ~50% of the HCD and ~75% of the EThcD identified ADPr-peptides. We, therefore, needed to evaluate these spectra where the ADPr-site was not assigned to determine if new site determining ions can be identified that could facilitate ADPr-site localization. It will also be important to explore other MS search engines and data analysis pipelines identify more ADPr-peptides and assign ADPr-sites with greater confidence[21-23]. Moreover, our ability to confidently assign only S-ADPr, R-ADPr and Y-ADPr modifications *in vivo* raises concerns as to why E-ADPr and D-ADPr were not detected; especially given that other studies provide strong evidence that these modifications are written *in vivo* and *in vitro* [9,10,12]. It could simply be that AF1521-based ADPr-enrichment

and/or the peptide fragmentation (EThcD versus CID[24,25]) methods used here limit D-ADPr and E-ADPr modification identifications. T-ADP-ribosylation modifications were not identified, suggesting that T may not be ADP-ribosylated or that T-ADPr modifications are not detectable using our methodologies. Additional studies are required to clarify these potential biases.

It has remained unclear until now which ARTDs specifically write the *in vivo* ADP-ribosylome that has thus far been identified. Here, we demonstrate that H_2O_2-stress specifically induces S-ADPr and Y-ADPr protein ADP-ribosylation *in vivo* and that ARTD1, not ARTD2, catalyzes of these modifications. These findings are in agreement with earlier *in vitro* reports using microarrays[26,27] or purified histones[5]. We also demonstrate that R is the main steady-state ADP-ribosylation acceptor in HeLa cells. The ART responsible for this modification is not yet known but the cytoplasmic localization of proteins suggests that a cytoplasmic ART(s) writes these modifications. Previous studies observed PAR formation in ARTD1 knockout cells and suggested that ARTD2 may be responsible for these modifications[28]. Here, we found that ARTD1 and ARTD2 do not modify the same ADP-ribosylation target proteins in H_2O_2-treated HeLa cells. Indicating that ARTD2 does not compensate for ARTD1 in HeLa cells and is likely regulated by a different stress stimuli than ARTD1. Nevertheless, ARTD1$^{-/-}$/ARTD2$^{-/-}$ mice are not viable[29]; thus, it is possible that ARTD1 and ARTD2 functionally compensate for each indirectly by modifying different target proteins that function in the same cellular processes.

In vitro ADP-ribosylation assays revealed that ARTD1 can ADP-ribosylate RPS3A, and site-directed mutagenesis studies confirmed Y155 of RPS3A as an ADPr-site. ADP-ribosylation of RPS3A was not completely lost on RPS3A-Y155F mutant proteins, but our MS data analyses indicated the RPS3A may also be ADP-ribosylated on S154 (EThcD/HCD) and K152 (HCD). Thus, the residual ADP-ribosylation observed here likely reflects the *in vitro* modification of these and/or other additional RPS3A ADPr-sites. Importantly, we also established demonstrated HPF1 provides ARTD1 with the *trans*-ADP-ribosylation specificity required to specifically and accurately write Y-ADPr (and possibly S-ADPr) modifications on RPS3A. This elaborates on the S-specific ADP-ribosylation functions identified for HPF1[5] and indicates that HPF1 functions to tune the enzymatic activity of ARTD1 towards O-linked S- and Y-ADP-ribosylation.

Our HPF1 site-directed mutagenesis studies not only confirmed that Y238 is the ADPr-site in HPF1, but also teased out the functional contributions Y238 and R239 make to HPF1 ADP-ribosylation cofactor activities. Previous studies demonstrated that Y238 and R239 single and double HPF1 mutants failed to purify ARTD1 from unstressed cellular extracts, which suggested that both amino acids were required for ARTD1-HPF1 complex formation[17]. Using less complex binding conditions and more structurally relevant HPF1 mutant proteins, we demonstrate that unmodified ARTD1 mainly interacts strongly with HPF1-WT and weakly with the ADP-ribosylation proficient HFP1-R239A mutant. Interactions were not observed between unmodified ARTD1 and HPF1-Y238F (i.e. ADP-ribosylation deficient) or HPF1-

Y238F/R239A. Interestingly, we also demonstrate that ADP-ribosylation intensifies HPF1-WT and HPF1-R239A interactions and that ARTD1 *auto*-modification supports weak protein-protein interactions between HPF1-Y238F and HPF1-Y238F/R239A and ARTD1. Subsequent *in vitro* ADP-ribosylation assays revealed two important molecular mechanisms associated with HPF1 ADP-ribosylation cofactor functions. We found that Y238 ADP-ribosylation and R239 (which is not modified) were required for HPF1 to augment ARTD1 *auto*-modification. In addition, we discovered that Y238 ADP-ribosylation provides an important interface that controls the *trans*-ADP-ribosylation enzymatic activities of ARTD1 that together with R239, which appears to provide an additional interaction point, “clicks” the CAT domain of ARTD1 into the *trans*-ADP-ribosylation conformation required to specifically write O-linked ADPr modifications on hundreds of target proteins.

For researchers embarking on similar ADP-ribosylomics studies, we think that this study has clarified some of the bioinformatics challenges associated with ADP-ribosylomics and hope they take advantage of the insights gained. We recommend that ADPr-MS datasets be searches in duplicate with variable ADPr modifications on S, D, E, R, K and Y and on just S, R and Y. Comparative analyses of these results will identify ADPr-sites that are common to both searches and those that differ. While ADPr-site localizations that differ between these searches require manual validation of the spectra annotations, common assignments can confidently be considered “correct”. Finally, the ADPr-site Localization Spectra Database (ADPr-LSD) that we provide here is the first, and most comprehensive, HCD and EThcD ADPr spectra resource that has been made public to the research community. Not only does it provide spectral references for ADPr-sites identified within, but it can also be used by researchers as a training resource to improve high-quality ADPr-spectra identifications and ADPr-site localizations.

ACKNOWLEDGMENTS

We would like to thank Tobias Suter (University of Zurich) for the helpful discussions and for providing editorial assistance. We would also like to thank Patrick Pedrioli (ETH Zürich) for his valuable advice and helpful discussions. ML is supported by the Forschungskredit from the University of Zurich. ADP-ribosylation research in the laboratory of MOH is funded by the Canton of Zurich and the Swiss National Science Foundation Grants (SNF 310030_157019).

AUTHOR CONTRIBUTIONS

D.M.L.P., M.L., V.B., K.N., K.G., L.M. and M.O.H conceived the project, performed data analysis. D.M.L.P., E.F. and K.N. expressed and purified recombinant proteins, and/or performed biochemical assays. M.L. performed sample preparation and mass spectrometry analysis. L.M. provided bioinformatics support and compiled the ADPr-LSD. R.I. generated HPF1 mutant clones. D.M.L.P., M.L., and M.O.H. prepared the manuscript. M.O.H directed and supervised all aspects of the study. All authors critically reviewed the manuscript.

COMPETING FINANCIAL INTERESTS

The authors declare no competing financial interests.

References:

1. Hottiger, M.O. Nuclear ADP-Ribosylation and Its Role in Chromatin Plasticity, Cell Differentiation, and Epigenetics. *Annu Rev Biochem* **84**, 227-63 (2015).
2. Barkauskaite, E., Jankevicius, G. & Ahel, I. Structures and Mechanisms of Enzymes Employed in the Synthesis and Degradation of PARP-Dependent Protein ADP-Ribosylation. *Mol Cell* **58**, 935-46 (2015).
3. Luo, X. & Kraus, W.L. On PAR with PARP: cellular stress signaling through poly(ADP-ribose) and PARP-1. *Genes Dev* **26**, 417-432 (2012).
4. Chapman, J.D., Gagne, J.P., Poirier, G.G. & Goodlett, D.R. Mapping PARP-1 auto-ADP-ribosylation sites by liquid chromatography-tandem mass spectrometry. *J Proteome Res* (2013).
5. Bonfiglio, J.J. et al. Serine ADP-Ribosylation Depends on HPF1. *Mol Cell* **65**, 932-940 e6 (2017).
6. Rosenthal, F. & Hottiger, M.O. Identification of ADP-ribosylated peptides and ADP-ribose acceptor sites. *Front Biosci (Landmark Ed)* **19**, 1041-56 (2014).
7. Bilan, V., Leutert, M., Nanni, P., Panse, C. & Hottiger, M.O. Combining HCD and EThcD fragmentation in a product dependent-manner confidently assigns proteome-wide ADP-ribose acceptor sites. *Anal Chem* **89**, 1523-1530 (2017).
8. Jungmichel, S. et al. Proteome-wide identification of poly(ADP-Ribosyl)ation targets in different genotoxic stress responses. *Mol Cell* **52**, 272-85 (2013).
9. Daniels, C.M., Ong, S.E. & Leung, A.K. Phosphoproteomic Approach to Characterize Protein Mono- and Poly(ADP-ribosyl)ation Sites from Cells. *J Proteome Res* **13**, 3510-22 (2014).
10. Zhang, Y., Wang, J., Ding, M. & Yu, Y. Site-specific characterization of the Asp- and Glu-ADP-ribosylated proteome. *Nat Methods* (2013).
11. Martello, R. et al. Proteome-wide identification of the endogenous ADP-ribosylome of mammalian cells and tissue. *Nat Commun* **7**, 12917 (2016).
12. Gibson, B.A. et al. Chemical genetic discovery of PARP targets reveals a role for PARP-1 in transcription elongation. *Science* **353**, 45-50 (2016).
13. Andersson, A. et al. PKCalpha and HMGB1 antagonistically control hydrogen peroxide-induced poly-ADP-ribose formation. *Nucleic Acids Res* **44**, 7630-45 (2016).
14. Rank, L. et al. Analyzing structure-function relationships of artificial and cancer-associated PARP1 variants by reconstituting TALEN-generated HeLa PARP1 knock-out cells. *Nucleic Acids Res* **44**, 10386-10405 (2016).
15. Leidecker, O. et al. Serine is a new target residue for endogenous ADP-ribosylation on histones. *Nat Chem Biol* **12**, 998-1000 (2016).
16. Sharifi, R. et al. Deficiency of terminal ADP-ribose protein glycohydrolase TARG1/C6orf130 in neurodegenerative disease. *EMBO J* **32**, 1225-1237 (2013).
17. Gibbs-Seymour, I., Fontana, P., Rack, J.G. & Ahel, I. HPF1/C4orf27 Is a PARP-1-Interacting Protein that Regulates PARP-1 ADP-Ribosylation Activity. *Mol Cell* **62**, 432-42 (2016).
18. Rosenthal, F., Nanni, P., Barkow-Oesterreicher, S. & Hottiger, M.O. Optimization of LTQ-Orbitrap Mass Spectrometer Parameters for the Identification of ADP-Ribosylation Sites. *J Proteome Res* **14**, 4072-9 (2015).
19. Bilan, V. et al. New quantitative mass spectrometry approaches reveal different ADP-ribosylation phases dependent on the levels of oxidative stress. *Molecular and Cellular Proteomics* (2017).
20. Sharma, K. et al. Ultradeep human phosphoproteome reveals a distinct regulatory nature of Tyr and Ser/Thr-based signaling. *Cell Rep* **8**, 1583-94 (2014).
21. Codrea, M.C. & Nahnsen, S. Platforms and Pipelines for Proteomics Data Analysis and Management. *Adv Exp Med Biol* **919**, 203-215 (2016).
22. Kong, A.T., Leprevost, F.V., Avtonomov, D.M., Mellacheruvu, D. & Nesvizhskii, A.I. MSFragger: ultrafast and comprehensive peptide identification in mass spectrometry-based proteomics. *Nat Methods* **14**, 513-520 (2017).
23. Eng, J.K., Jahan, T.A. & Hoopmann, M.R. Comet: an open-source MS/MS sequence database search tool. *Proteomics* **13**, 22-4 (2013).

24. Rood, J.E., Leung, A.K. & Chang, P. Methods for purification of proteins associated with cellular poly(ADP-ribose) and PARP-specific poly(ADP-ribose). *Methods Mol Biol* **780**, 153-64 (2011).
25. Haag, F. & Buck, F. Identification and analysis of ADP-ribosylated proteins. *Curr Top Microbiol Immunol* **384**, 33-50 (2015).
26. Feijs, K.L. et al. ARTD10 substrate identification on protein microarrays: regulation of GSK3beta by mono-ADP-ribosylation. *Cell Commun Signal* **11**, 5 (2013).
27. Troiani, S. et al. Identification of candidate substrates for poly(ADP-ribose) polymerase-2 (PARP2) in the absence of DNA damage using high-density protein microarrays. *FEBS J* **278**, 3676-3687 (2011).
28. Althaus, F.R. et al. Poly ADP-ribosylation: a DNA break signal mechanism. *Mol Cell Biochem* **193**, 5-11 (1999).
29. Boehler, C. et al. Phenotypic characterization of Parp-1 and Parp-2 deficient mice and cells. *Methods Mol Biol* **780**, 313-336 (2011).
30. Ariumi, Y., Turelli, P., Masutani, M. & Trono, D. DNA damage sensors ATM, ATR, DNA-PKcs, and PARP-1 are dispensable for human immunodeficiency virus type 1 integration. *J Virol* **79**, 2973-8 (2005).
31. Hengel, S.M. & Goodlett, D.R. A Review of Tandem Mass Spectrometry Characterization of Adenosine Diphosphate-Ribosylated Peptides. *Int J Mass Spectrom* **312**, 114-121 (2012).
32. Tyanova, S. et al. The Perseus computational platform for comprehensive analysis of (prote)omics data. *Nat Methods* **13**, 731-40 (2016).
33. Thomas, P.D. et al. PANTHER: a library of protein families and subfamilies indexed by function. *Genome Res* **13**, 2129-41 (2003).
34. Messner, S. et al. PARP1 ADP-ribosylates lysine residues of the core histone tails. *Nucleic Acids Res* **38**, 6350-62 (2010).
35. Riffle, M. et al. Visualization and dissemination of multidimensional proteomics data comparing protein abundance during Caenorhabditis elegans development. *J Am Soc Mass Spectrom* **26**, 1827-36 (2015).

Figure Legends

Figure 1: *Refining MS search parameters for variable ADP-ribose peptide modifications identifies tyrosine as a novel ADPr-amino acid acceptor*. **a.** Schematic of the sample preparation and HCD-PP-EThcD/HCD MS acquisition method workflow employed by Bilan *et al.*[7] to generate the high quality EThcD and HCD datasets used here. **b.** Schematic of the bioinformatics workflow employed here. In the initial phase of these analyses, variable ADPr PTM search parameters were opened to include all 20 amino acids as potential ADPr-acceptor sites. Ion scores were then calculated to help identified the best quality ADPr-site localizations within modified peptides and peptides for manual validation of ADPr-site localization. Based on these manual validations, the search parameters were refined to include S, D, E, R, K and Y (SDERKY) or S, R and Y (SRY) as ADPr-acceptor amino acids and the workflow re-applied. **c.** The ADPr-site localization results from the initial (20aa) searches and refined searches were compared. The flow chart depicts how ADPr-acceptor amino acid identifications changed for the 181 EThcD ADPr-localization training spectra as the variable ADPr search parameters were refined. Importantly, these analyses identified novel tyrosine (Y) ADPr modifications at each phase of our analyses. **d.** Comparison of total number of unique ADP-ribosylated peptides and unique ADPr-sites identified (Mascot localization probability >60%) in the SDERKY and SRY searches. **e.** Comparison of the ADPr-site localizations (Mascot localization probability >60%) for ADP-ribosylated peptides that were identified by both EThcD and HCD fragmentation methods.

Figure 2: *ARTD1 mediates proteome-wide S and Y ADP-ribosylation.* **a.** Venn diagrams indicate the overlap of ADP-ribosylated proteins identified in untreated and H_2O_2 treated HeLa cells following ARTD1 or ARTD2 knockdown. **b.** Volcano plots comparing ADP-ribosylated peptides identified in the different cell lines and conditions (t-test with Permutation-based FDR < 0.05 and fold change of 2, indicated by the black line). ADP-ribosylation sites confirmed by EThcD spectra are color coded for S-ADPr (blue), Y-ADPr (green) and R-ADPr (red) modifications. Serine (DDX21), tyrosine (RPS3A) and arginine (PDIA3) modifications that were identified using our ADPr-localization training spectra library are annotated. The black hyperbolic line represents a permutation-based False Discovery Rate (FDR) of 5% and a minimal fold change of 2. **c.** Gene ontology cellular localisation annotation of ADP-ribosylated proteins following H_2O_2 treatment, SRY ADP-ribosylated proteins were considered with a Mascot localisation score >90% .**d.** Comparison of the S,Y-ADP-riboslyome identified here with the HeLa phosphoproteome identified by Sharma *et al.*[20].

Figure 3: *Biochemical validation of RPS3-Y155 ADPr modification.* **a.** High-resolution EThcD fragmentation spectrum of an RPS3A peptide modified with ADP-ribose on Y155. **b.** Recombinant RPS3A-WT or RPS3A-Y155F were *in vitro* ADP-ribosylated with [^{32}P]-NAD$^+$,

activated DNA and recombinant ARTD1 in the presence or absence of recombinant HPF1. Samples were resolved by SDS-PAGE and analyzed by autoradiography. top: Coomassie Blue-stained poly-acrylamide gel; middle: raw-scan of autoradiograph; bottom: autoradiograph with levels adjusted to enhance exposure. Relative percentages of the *in vitro* ADP-ribosylation (radioactive signal) of ARTD1 (relative to radioactive signal with [^{32}P]-NAD$^+$ and activated DNA alone), RPS3A-WT and RPS3A-Y155F (relative to radioactive signal for RPS3A-WT for each condition) are indicated (n = 3). Values in brackets represent the standard deviation of the mean.

Figure 4: *ARTD1/HPF1 protein-protein interactions and the serine and tyrosine ADP-ribosylation co-factor functions of HPF1 are dependent on HPF1 ADP-ribosylation on tyrosine 238.* **a.** Recombinant wild-type HPF1 (HPF1-WT) and HPF1 mutant (HPF1-Y238F, HPF1-R238A or HPF1-Y238F/R239A) proteins were *in vitro* ADP-ribosylated with [^{32}P]-NAD$^+$, activated DNA and recombinant ARTD1 (n = 3). **b.** Recombinant RPS3A-WT and or RPS3A-Y155F were *in vitro* ADP-ribosylated with [^{32}P]-NAD$^+$, activated DNA and recombinant ARTD1 (Trevigen, Gaithersburg, MD, USA) *in vitro* ADP-ribosylation assays were performed with [^{32}P]-NAD$^+$, DNA and recombinant ARTD1 without HPF1 or with recombinant HPF1-WT and HPF1-Y238F, HPF1-R239A, or HPF1-Y238F/R239A proteins (n = 2). For *in vitro* ADP-ribosylation assays, the samples were resolved by SDS-PAGE and analyzed by autoradiography (top: Coomassie Blue-stained poly-acrylamide gel; middle: raw-scan of autoradiograph; bottom: autoradiograph with levels adjusted to enhance exposure). Relative percentages of *in vitro* ADP-ribosylation (radioactive signal) of ARTD1 (relative to radioactive signal with [^{32}P]-NAD$^+$ and activated DNA alone) RPS3A-WT and RPS3A-Y155F (relative to radioactive signal for RPS3A-WT for each condition) and the HFP1 protein isoforms (relative to radioactive signal for HPF1-WT) are indicated. Values in brackets represent the standard deviation of the mean. **c.** Summary of the ARTD1 binding capacities of wild-type and mutant HFP1 proteins and the ADP-ribosylation cofactor activities of each of the isoforms of HFP1.

TABLE 1. Summary of ADPr-peptides and ADPr-sites identified using different variable ADPr localization parameters

Unique ADPr-Peptides		
	SDERKY	SRY
HCD-PP-EThcD	188	182
Unique EThcD	33	40
Unique HCD	74	67
overlap	81	75
Unique ADPr-Peptides with loc. probability >60%		
	SDERKY	SRY
HCD-PP-EThcD	145	129
EThcD	36	31
HCD	54	45
overlap	55	53
Unique ADPr-sites with loc. probability >60%		
	SDERKY	SRY
HCD-PP-EThcD	187	140
EThcD	70	45
HCD	85	64
overlap	32	32

TABLE 2. Y-ADPr modified Proteins

Gene Name	Peptide Sequence_ADPr-site	Y-ADPr Site on Protein	Spectra Type
RPS3A	KTSYAQHQQVR_Y4	Y155	EThcD
HPF1	TFHGAGLVVPVDKNDVGYRELPETDADLKR_Y18	Y239	EThcD/HCD
HNRNPA1	NQGGYGGSSSSSSYGSGR_Y5	Y252	HCD
HNRNPA2B1	NMGGPYGGGNYGPGGSGGSGGYGGR_Y6	Y319	HCD
HDGF	STANKYQVFFFGTHETAFLGPK_Y6	Y38	HCD
YY1	KSYLSGGAGAAGGGGADPGNKKWEQK_Y3	Y185	HCD
P4HB	LAKVDATEESDLAQQYGVRGYPTIK_Y16	Y94	HCD

ONLINE METHODS

Generation of stable shARTD1 and shARTD2 cell lines

Virus generation and HeLa cell transduction was carried out as previously described [30]. Briefly, short hairpin RNAs (shRNAs) targeting the mRNA coding sequences ARTD1 (CCGAGAAATCTCTTACCTCAA) or ARTD2 (TCTGAATCCAGATGGTTATA), or a scramble shRNA (CCTAAGGTTAAGTCGCCCTCGCTCGAGCGAGGGCGACTTAACCTTAGG) were cloned into pRDI292. These vectors were then used to generate replication incompetent retroviruses in HEK-293 cells. HeLa cells (Kyoto) were infected with the resulting retroviruses for 8 hours, cultured for 48 hours without selection and placed under selective growth conditions (2μg/mL puromycin) to select for transduced cells. ARTD1 and ARTD2 knockdown was confirmed on the mRNA and protein levels via qPCR and Western blot analyses, respectively.

Cell culture conditions and ADPr Peptide enrichment

shControl, shARTD1 and shARTD2 HeLa cells (Kyoto) were cultured in Dulbecco's modified Eagle's medium [DMEM, supplemented with 10% fetal calf serum (FCS) and 1% penicillin/streptavidin] at 37°C with 5% CO_2. Cells were either untreated or treated in triplicated with 1mM H_2O_2 in PBS containing and 1mM $MgCl_2$. Cells were lysed and processed for MS analysis as previously described [7,11].

Liquid Chromatography and Mass Spectrometry Analysis

The ADP-ribosylomes of shControl, shARTD1 and shARTD2 HeLa cells were identified using an Orbitrap Q Exactive HF mass spectrometer (Thermo Fisher Scientific) coupled to a nano EasyLC 1000 (Thermo Fisher Scientific). The peptides were loaded into the MS using a reverse-phase C18 (ReproSil-Pur 120 C18-AQ, 1.9 µm, Dr. Maisch GmbH) packed self-made column (75 µm × 150 mm) that was connected to an empty Picotip emitter (New Objective, Woburn, MA). Peptides were injected into the MS at a flow rate of 300nL/min and were separated using a 90 minute gradient of 2% to 25% buffer B. Solvent compositions of buffer A and buffer B were 0.1% formic acid and 0.1% formic acid/99.9% acetonitrile, respectively.

For mass spectrometer (MS) analysis, the MS was set to acquire full-scan MS spectra (300–1700 *m*/*z*) at a resolution of 60,000 after accumulation to an automated gain control (AGC) target value of 3×10^6. Charge state screening was enabled, and unassigned charge states and single charged precursors were excluded. Ions were isolated using a quadrupole mass filter with a 2 *m*/*z* isolation window. The maximum injection time was set to of 240 ms and HCD fragmentation performed at 28% normalized collision energy (NCE). Finally, selected ions were dynamically excluded for 20 seconds.

MS Data analysis

For the bioinformatic analyses aimed at identifiying novel ADPr-acceptor amino acids, raw files from Af1521-enriched H_2O_2-treated HeLa samples measured by the HCD-PP-EThcD/HCD method [7] were used. These files can be accessed via ProteomeXChange (PXD004676). MS and MS/MS spectra were converted to Mascot generic format (MGF) using Proteome Discoverer, v2.1 (Thermo Fisher Scientific, Bremen, Germany). Separate MGF files were created from the raw file for each type of fragmentation and the files processed further as previously described [7].

The resulting MGF files were searched against UniProtKB human database (taxonomy 9606, version 20140422) using Mascot 2.5.1.3 (Matrix Science) as previously described [7] (Supplementary Table 1). For HCD fragmentation, ADP-ribosylation was defined as previously described by Rosenthal et al [18]. For EThcD fragmentation, the modification was defined similarly, but marker ions at m/z 428.0372, 348.0709, 250.0940, 136.0623 were ignored for scoring. For initial analysis, the files were searched with fixed carbamidomethylation (C), except for the search with C as a potential ADPr-acceptor where C carbamidomethylation was set as variable, and variable oxidation (M). ADP-ribosylation was set as a variable modification and 14 separate searches for each MGF file were performed to cover all 20 amino acid acceptors: individual searches allowed ADPr modifications to be localized on the 5 experimentally validated ADPr-acceptor amino acids (S, D, E, R and K) and on one additional amino acid. Upon completion, all search results were integrated and the spectra filtered based on the presence of at least two of the known ADPr marker ions[31].

Peptides were considered correctly identified when a Mascot score >20 and an expectation value <0.05 was obtained. Prior to manual spectra validation, we applied an ion score filter to reduce the spectra for manual validation to properly fragmented peptides. The ion score was based on observed peptide fragment ions in the b, y, c and z ion series normalized to the maximum number of observable theoretical ions. We manually curated ADPr peptide spectra with an ion score > 0.5.

Using this filter, we identified 448 unique spectra in which the ADPr-localization was validated manually. Following manual validation, the files were searched again using Mascot with fixed carbamidomethylation (C), variable oxidation (M) and variable ADP-ribosylation on S, D, E, R, K and Y (SDERKY) or S, R and Y (SRY). All ADPr-site localizations mentioned in the text had Mascot localization scores >60%, unless otherwise stated.

Label-free Quantification MS Analysis of shControl, shARTD1 and shARTD2 ADP-ribosylomes

Progenesis QI software (v. 3.0.6039.34628, Nonlinear Dynamics, Purham, NC) was used for MS1 precursor-based label-free quantification of the shControl, shARTD1 and shARTD2 ADP-ribosylomes. For these analyses, the raw data were imported into Progenesis and aligned based on MS1 peak retention time. Sample loading variations were normalized

based on total signal intensity and the results obtained exported as MGFs. These MGFs were then searched for variable ADPr modifications (SDERKY and SRY) using Mascot as described above. The Mascot search results were then imported into Scaffold software (v.4.7.2) and filtered for protein and peptide False Discovery Rates (FDRs) ≤0.01. When multiple charge-state precursors were sequenced for the same peptide, total peptide amounts were calculated by summing individual charge-state values. To most confidently localized ADPr-sites within the identified ADPr-peptides, the HCD ADPr-peptides were compared to the EThcD ADPr-peptides identified in the Bilan *et al.* dataset presented above. All identified ADPr-peptides were included in this analysis, but only ADPr-peptides for which we had corresponding high quality EThcD fragmentation spectra were assigned a modification site. Volcano plot analysis of the quantified ADPr-peptides and their non-modified counterparts was performed using two-sample testing in Perseus, with permutation-based FDRs of 5% and minimal fold change of 2 [32]. Gene ontology analysis was performed using the PANTHER data base [33].

Cloning and protein purification

Human HPF1 (pET21a), human RPS3A-WT (pGEX6P-3) and human RPS3A-Y155F (pGEX-6P3) bacterial expression vectors were constructed by Genscript (Piscataway, NJ, USA). HPF1 mutants were generated via PCR-based site-directed mutagenesis using the following oligonucleotides: HPF1-Y238F sense 5'-GATGTTGGGTTCCGAGAGCTCCCTG-3'; HPF1-Y238F antisense 5'-CAGGGAGCTCTCGGAACCCAACATC-3'; HFP1-R239A sense 5'-GATGTTGGGTACGCAGAGCTCCCTG-3'; HPF1-R239A antisense 5'-CAGGGAGCTCTGCGTACCCAACATC-3'; HPF1-Y238F/R239A sense 5'-GATGTTGGGTTCGCAGAGCTCCCTG-3'; HPF1-Y238F/R239A antisense 5'-CAGGGAGCTCTGCGAACCCAACATC-3'. Sequencing of plasmids was performed at Microsynth. Plasmids were transformed into BL21 *E. coli*, and protein expression induced by adding 1 mM IPTG at OD_{600} 0.4-0.6 for 3 h at 30 °C. Batch purification of GST-tagged or His-tagged proteins were carried out using glutathione sepharose 4B beads (GE Healthcare) or ProBond™ Nickel-Chelating Resin (ThermoFisher Scientific) according to the manufacturer's manual. Expression and purification of all recombinant proteins was analyzed by sodium dodecyl sulfate-polyacrylamide gel electrophoresis (SDS-PAGE) followed by Coomassie staining.

***In vitro* ADP-ribosylation assay with recombinant proteins**

In vitro ADP-ribosylation assays were performed based on previously described methods [5,17]. Briefly, recombinant RPS3A (50pmol) and HPF1 (50pmol) proteins were mixed as indicated with ARTD1 (2.5pmol; Trevigen, Gaithersburg, MD, USA) in 1x PARP1 buffer (Trevigen). Activated DNA (Trevigen) and [^{32}P]NAD^+ (6.25μM, 0.3μCi/μl; Perkin Elmer) were then added to the reactions at final concentrations of 40ng/μL and 100nM, respectively.

Reactions were incubated at 25ºC for 20 min. Reactions were stopped via addition of SDS-PAGE sample buffer to 1x final concentration and heat denaturation at 95ºC for 10min. The reaction volume for all *in vitro* ADP-ribosylation assays was 25*µ*L. Samples were resolved by SDS-PAGE and analyzed by autoradiography.

ARTD1/HPF1 *in vitro* binding assays

Rabbit α-human-PARP1 polyclonal rabbit antibodies (in-house), obtained from rabbits immunized with human ARTD1 expressed and purified as previously described[34] were immobilized on protein A Sepharose 4 Fast Flow resin (GE Healthcare Life Sciences, Glattbrugg, Switzerland) following the manufacturer's instructions. The resulting α-hPARP1-pA beads were stored at 4ºC in *in vitro* binding buffer (IVB; 20mM Sodium Phosphate pH8.0, 50mM NaCl, 2mM β-Mercaptoethanol, 0.1% NP-40) with 0.01% sodium azide.

For the *in vitro* binding experiments, 10*µ*g (200pmol) of each HIS-tagged HPF1-WT, HPF1-Y238F, HPF1-R239A and HPF1-Y238F/R239A fusion protein was incubated either alone or with 1.15*µ*g (10pmol) ARTD1 (Trevigen) in 1x PARP1 buffer (Trevigen) in the presence or absence of 5*µ*M NAD^+ and 200nM of double-stranded 40 bp DNA oligonucleotides (40mer; 5'-TGCGACAACGATGAGATTGCCACTACTTGAACCAGTGCGG-3') for 20 min at 25°C. Each reaction was diluted with 1mL ice-cold IVB buffer and incubated with α-hPARP1-pA beads overnight at 4ºC. The beads were collected by centrifugation and the unbound proteins removed. The beads were then washed three times with IVB buffer for 10 min at 4ºC with end-over-end rotation and the bound proteins were eluted with 1x SDS-PAGE sample buffer. All samples were heat denatured at 75ºC for 20min and resolved in 10% SDS-PAGE gels. HPF1 protein isoforms were visualized by Coomassie Blue staining and ARTD1 was detected via western blot analysis with an α-ARTD1 antibody.

Western Blot Analysis

For Western blot analyses, protein samples were resolved using standard SDS-PAGE methods and transferred to nitrocellulose membranes (Merck Millipore). Membranes were then blocked for 3hrs at room temperature with blocking buffer (25 mM Tris-HCl pH 7.5, 150 mM NaCl, 0.1% Tween 20 and 3% bovine serum albumin) and probed overnight with primary antibodies, diluted in blocking buffer, at 4ºC. Membranes were then washed with TBS-T (25 mM Tris-HCl pH 7.5, 150 mM NaCl, 0.1% Tween-20) and incubated at room temperature for with IR-Dye-conjugated secondary antibodies (1:15'000, LI-COR). Blots were visualized using the Odyssey infrared imaging system (LI-COR). Dilutions used for the primary antibodies were: 1:1000 α-ARTD1 (H-250 sc-7150, Santa Cruz); 1:1000 α-ARTD2 (Active motif); 1:1000 α-PAR 10H (in house).

Manual inspection of MS spectra

Candidate spectra were visualized using lorikeet, a JavaScript-based viewer[35]. Using a custom python script, one HTML-document was created per candidate peptide, and each peptide page display all collected spectra (regardless of the source file) in a vertically stacked fashion to allow for fast comparison.

Figure 1

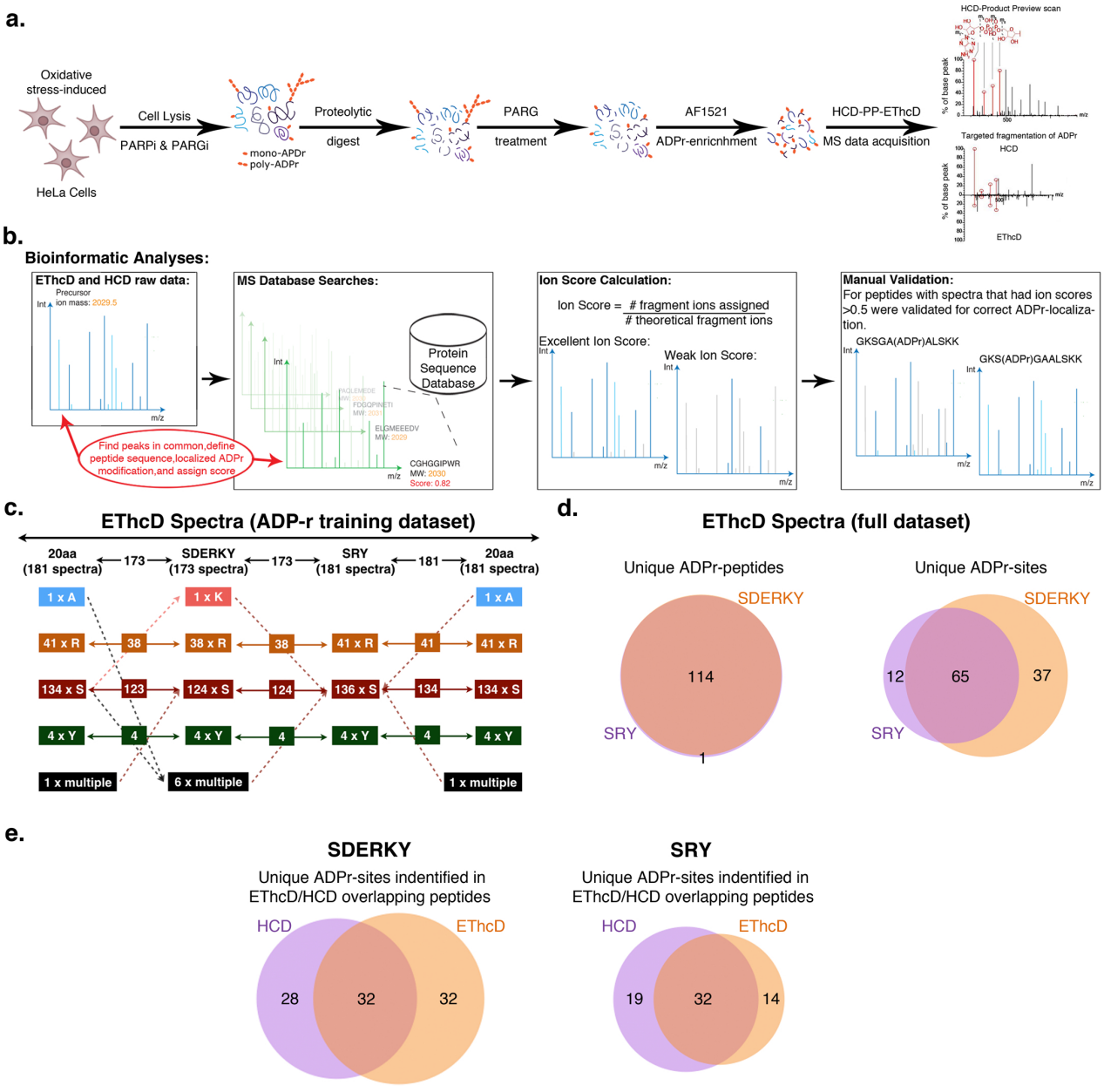
a.
Oxidative stress-induced
HeLa Cells
Cell Lysis
PARPi & PARGi
mono-APDr
poly-APDr
Proteolytic digest
PARG treatment
AF1521
ADPr-enrichment
HCD-PP-EThcD
MS data acquisition
HCD-Product Preview scan
Targeted fragmentation of ADPr
HCD
EThcD
b.
Bioinformatic Analyses:
EThcD and HCD raw data:
MS Database Searches:
Protein Sequence Database
Find peaks in common,define peptide sequence,localized ADPr modification,and assign score
Ion Score Calculation:
Ion Score = # fragment ions assigned / # theoretical fragment ions
Excellent Ion Score:
Weak Ion Score:
Manual Validation:
For peptides with spectra that had ion scores >0.5 were validated for correct ADPr-localization.
GKSGA(ADPr)ALSKK
GKS(ADPr)GAALSKK
c.
EThcD Spectra (ADP-r training dataset)
20aa (181 spectra)
173
SDERKY (173 spectra)
173
SRY (181 spectra)
181
20aa (181 spectra)
1 x A
1 x K
41 x R
38 x R
134 x S
124 x S
136 x S
4 x Y
1 x multiple
6 x multiple
d.
EThcD Spectra (full dataset)
Unique ADPr-peptides
SDERKY
SRY
114
1
Unique ADPr-sites
12
65
37
e.
SDERKY
Unique ADPr-sites indentified in EThcD/HCD overlapping peptides
HCD
EThcD
28
32
32
SRY
Unique ADPr-sites indentified in EThcD/HCD overlapping peptides
19
32
14

Figure 2

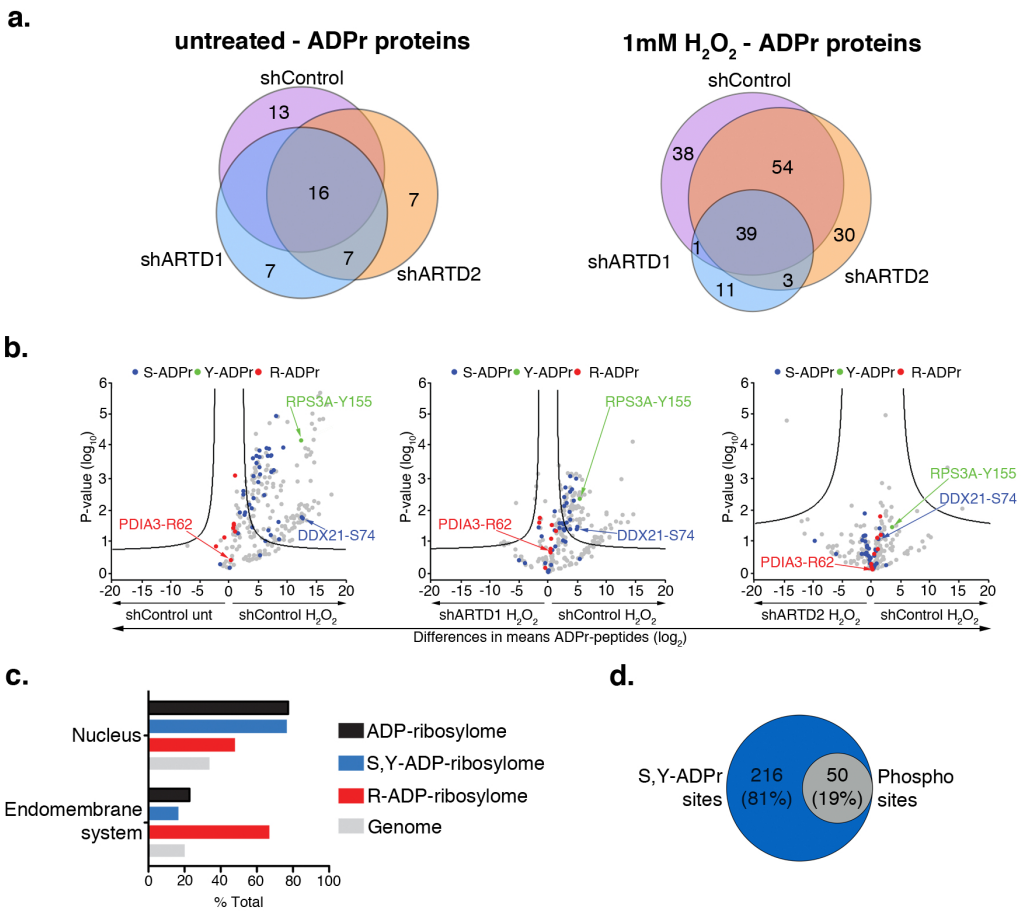
a.
untreated - ADPr proteins
shControl
13
16
7
shARTD1
7
7
shARTD2
1mM H2O2 - ADPr proteins
shControl
38
54
39
30
shARTD1
1
11
3
shARTD2
b.
S-ADPr Y-ADPr R-ADPr
RPS3A-Y155
DDX21-S74
PDIA3-R62
P-value (log10)
shControl unt
shControl H2O2
shARTD1 H2O2
shARTD2 H2O2
Differences in means ADPr-peptides (log2)
c.
Nucleus
Endomembrane system
ADP-ribosylome
S,Y-ADP-ribosylome
R-ADP-ribosylome
Genome
% Total
d.
S,Y-ADPr sites
216 (81%)
50 (19%)
Phospho sites

Figure 3

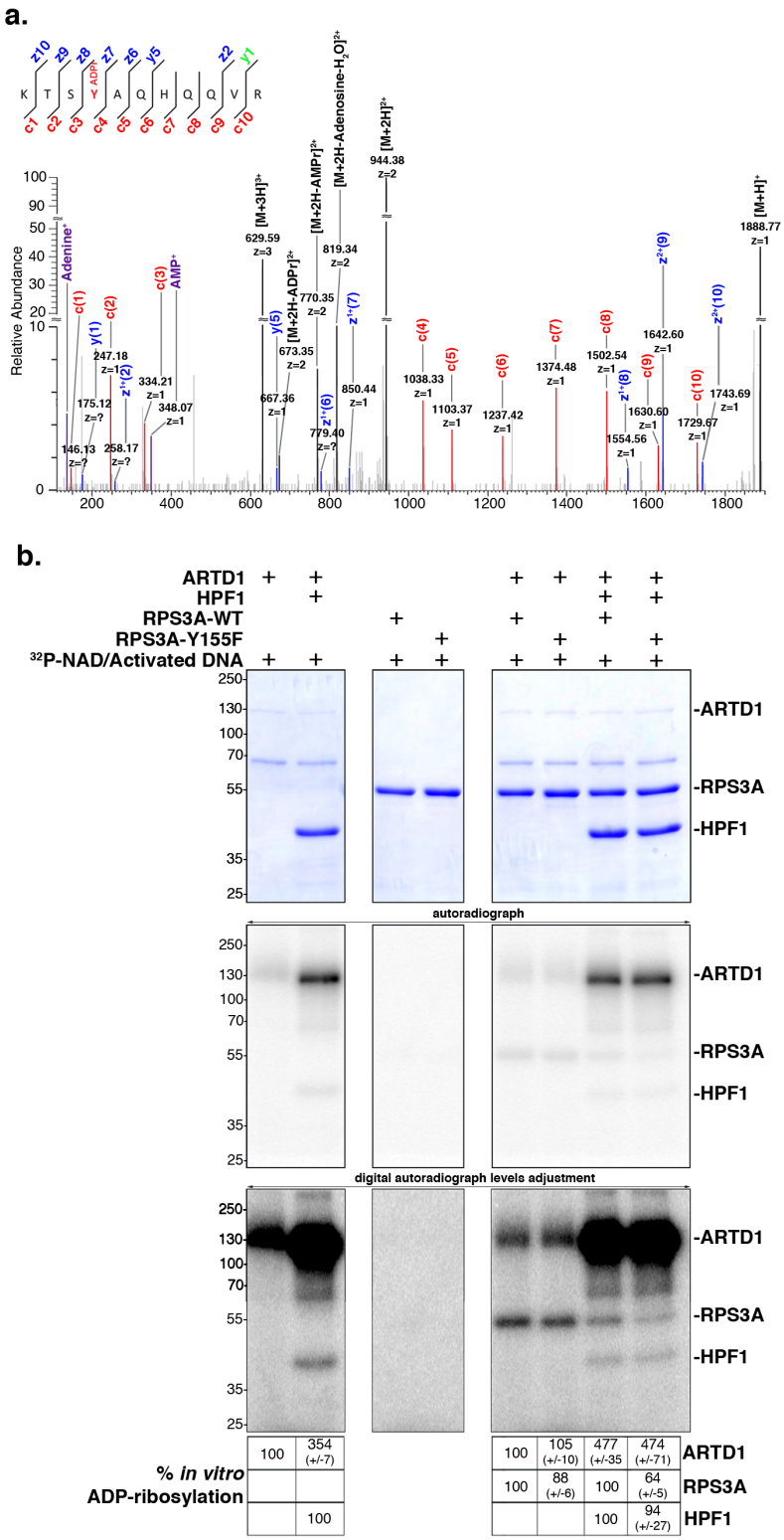
a.
K T S Y ADPr A Q H Q Q V R
Relative Abundance
Adenine+
AMP+
[M+3H]3+
[M+2H-AMPr]2+
[M+2H-Adenosine-H2O]2+
[M+2H]2+
[M+2H-ADPr]2+
944.38 z=2
629.59 z=3
819.34 z=2
770.35 z=2
673.35 z=2
667.36 z=1
779.40 z=?
850.44 z=1
1888.77 z=1
1642.60 z=1
1743.69 z=1
1729.67 z=1
1630.60 z=1
1554.56 z=1
1502.54 z=1
1374.48 z=1
1237.42 z=1
1103.37 z=1
1038.33 z=1
334.21 z=1
348.07 z=1
247.18 z=1
175.12 z=?
146.13 z=?
258.17 z=?
b.
ARTD1
HPF1
RPS3A-WT
RPS3A-Y155F
32P-NAD/Activated DNA
-ARTD1
-RPS3A
-HPF1
autoradiograph
digital autoradiograph levels adjustment
% in vitro ADP-ribosylation
100 354 (+/-7)
100
100 105 (+/-10) 477 (+/-35) 474 (+/-71) ARTD1
100 88 (+/-6) 100 64 (+/-5) RPS3A
100 94 (+/-27) HPF1

Figure 4

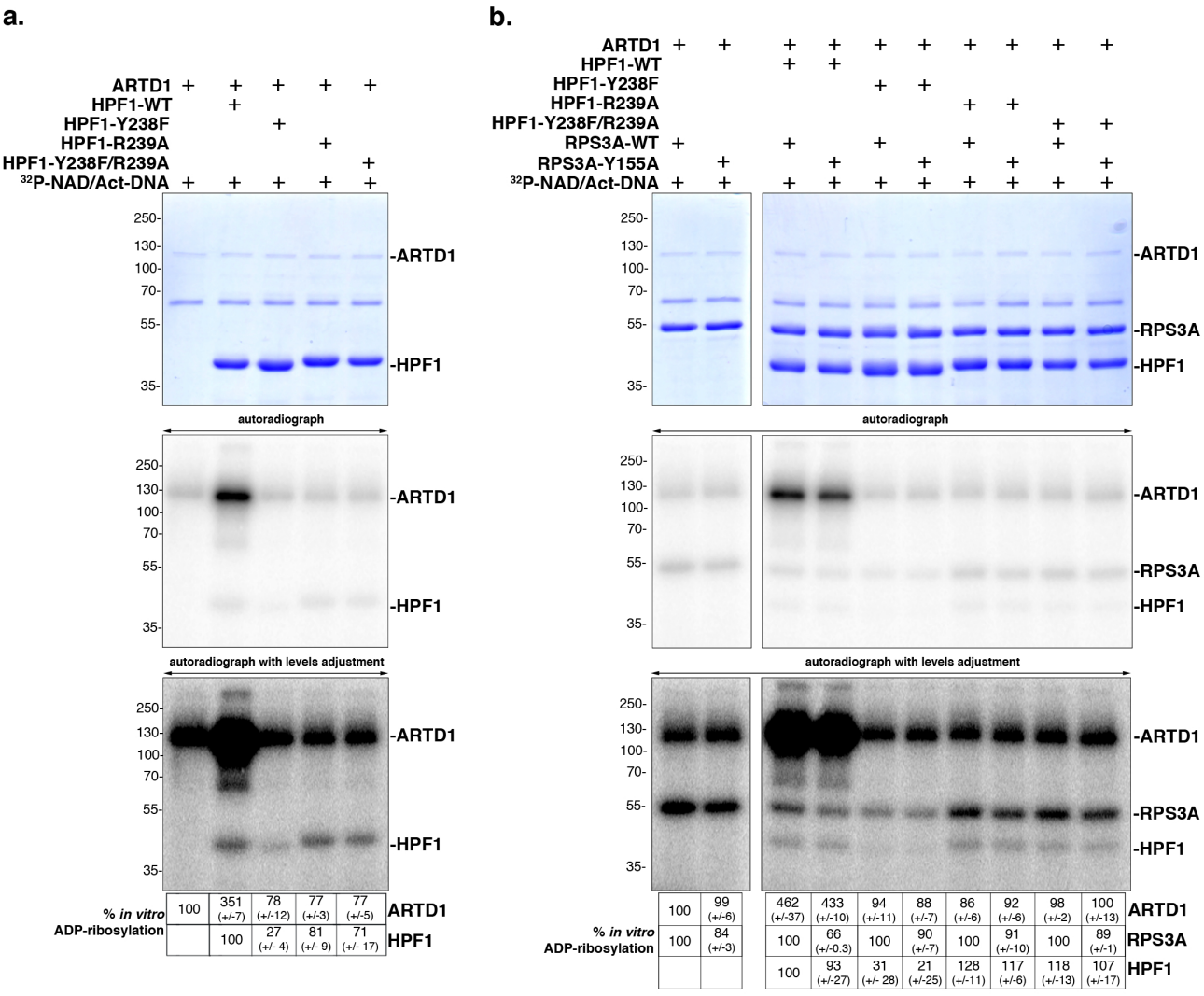

c.

	ADP-ribosylation	ADRTD1-HPF1 complex formation		HPF1 Cofactor Function		
		- NAD+	+ NAD+	*auto*-ADP-ribosylation	*trans*-ADP-ribosylation	
					Absolute modfication	ADPr-site specificity
HPF1-WT	+++	++	+++	+++	+++	+++
HPF1-Y238F	-	-	+	-	-	-
HPF1-R239A	++	+	++	-	+	-
HPF1-Y238F/R239A	+	-	+	-	+	-

SUPPLEMETARY INFORMATION

a.

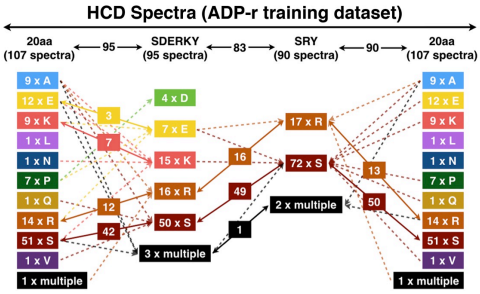

b.

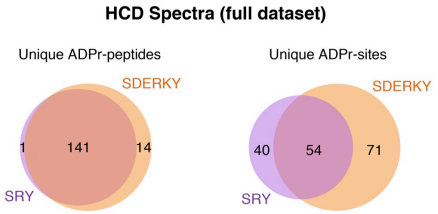

Figure S1: *HCD spectra ADPr-site localizations change considerably as the Mascot searches were refined.* **a.** ADPr-site localization results from the initial (20aa) searches and refined searches were compared. The flow chart depicts how ADPr-acceptor amino acid localizations changed for the 107 HCD ADPr-localization training spectra as the variable ADPr search parameters were refined. **b.** Comparison of total number of unique ADP-ribosylated peptides and unique ADPr-sites identified (Mascot localization probability >60%) from HCD spectra in the SDERKY and SRY searches.

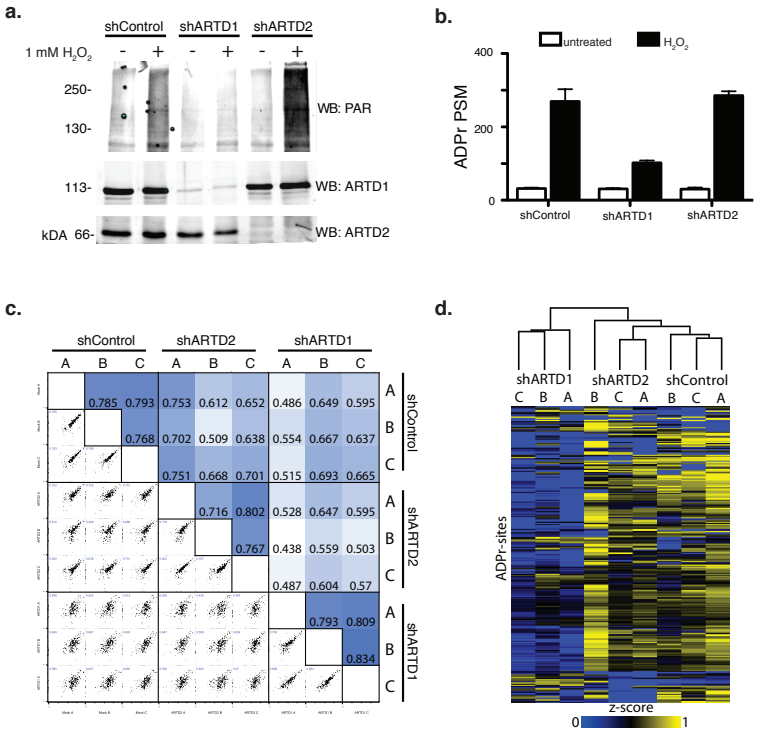

Figure S2: *Analysis of shControl, shARTD1 and ARTD2 knockdown HeLa cells*. **a.** α-ARTD1, α-ARTD2 and α-PAR western blot analysis of untreated and H_2O_2 treated shControl, shARTD1 and shARTD2 HeLa cell lysates confirms specific knockdown of ARTD1 or ARTD2 and specific inhibition of H_2O_2-induced PAR following loss-of ARTD1. **b**. Number of ADPr-PSMs identified in untreated and H_2O_2 treated HeLa cells following ARTD1 or ARTD2 knockdown. **c**. Heat map of spearman's rank correlation coefficient and multi-scatter plots showing reproducibility between cell line ADP-ribosylome identifications. **d**. Heat map of unsupervised clustering of the z-score of ADPr site abundance in the different cell lines.

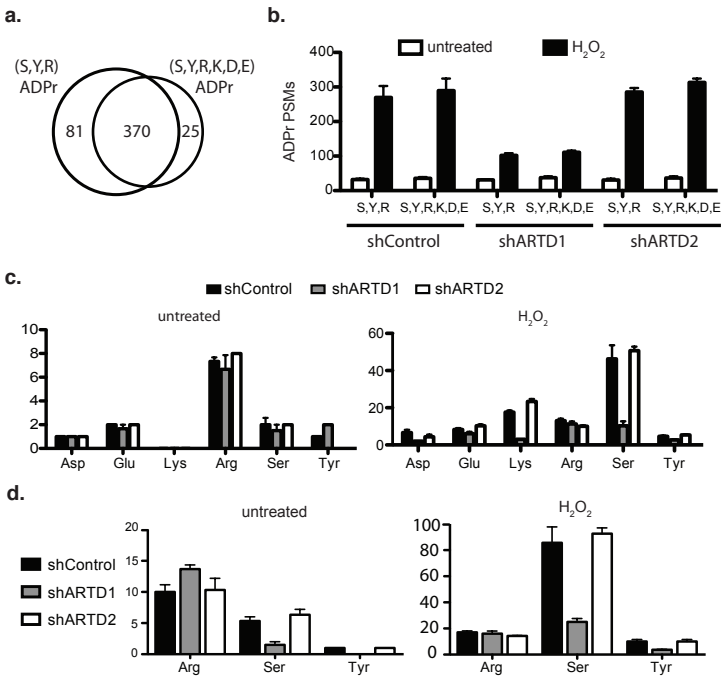

Figure S3: *Comparison of SRY and SDERKY ADPr searches following ARTD1 and ARTD2 knockdown reveals that ARTD1 is the writer of cellular Ser-ADPr and Try-ADPr modifications.* **a.** Venn diagram depicts the overlap of total number of unique ADPr-peptides identified by Mascot-based searches that considered S, R and Y or S, D, E, R, K, and Y as variable ADPr-acceptor amino acids following H_2O_2 treatment. Note that ADPr-site localization within the peptide was ignored for this analysis. **b.** Total number of ADPr-modified peptide spectrum matches (PSMs) identified in untreated or H_2O_2-treated shControl, shARTD1 and shARTD2 cells by SRY and SDERKY variable ADPr Mascot searches. **c-d.** Total number of ADPr-sites localized (Mascot localization score > 60%) in the SDERKY (c) and SRY (d) searches.

4

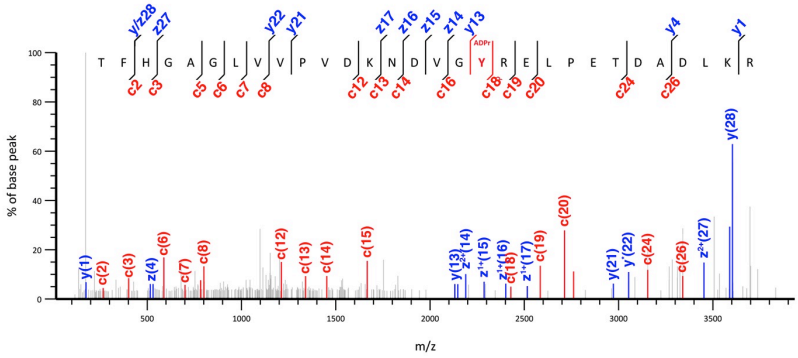

Figure S4: *Spectral evidence supporting HPF1-Y238 ADP-ribosylation.* High-resolution EThcD fragmentation spectrum of an HPF1 peptide modified with ADP-ribose on Y238.

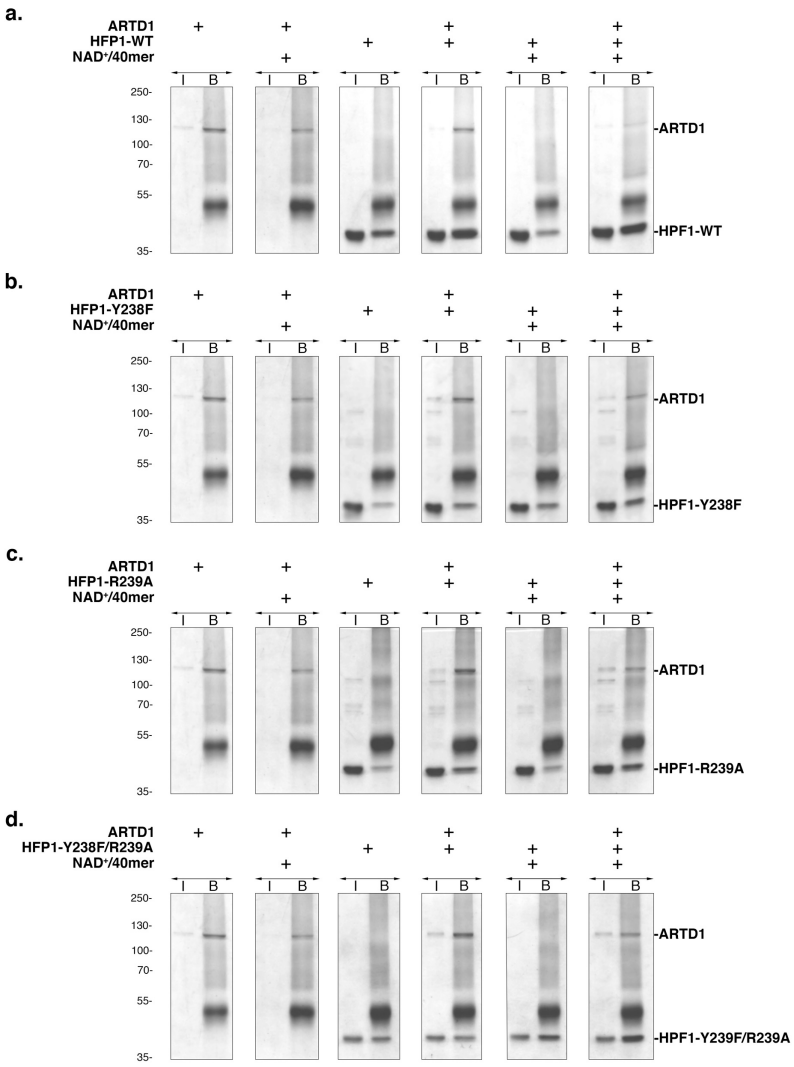

Figure S5: *ARTD1/HPF1 protein-protein interactions are dependent on ADP-ribosylation.* ARTD1/HPF1 *in vitro* binding assays were carried out with unmodified or ADP-ribosylated recombinant ARTD1 and HPF1-WT (**a.**), HPF1-Y238F (**b.**), HPF1-R238A (**c.**) or HPF1-Y238F/R239A (**d.**) using α-ARTD1-pA-speharose resin. Samples were resolved by SDS-PAGE and stained with Coomassie Blue. I = input (5%); B = bead-bound (25%)

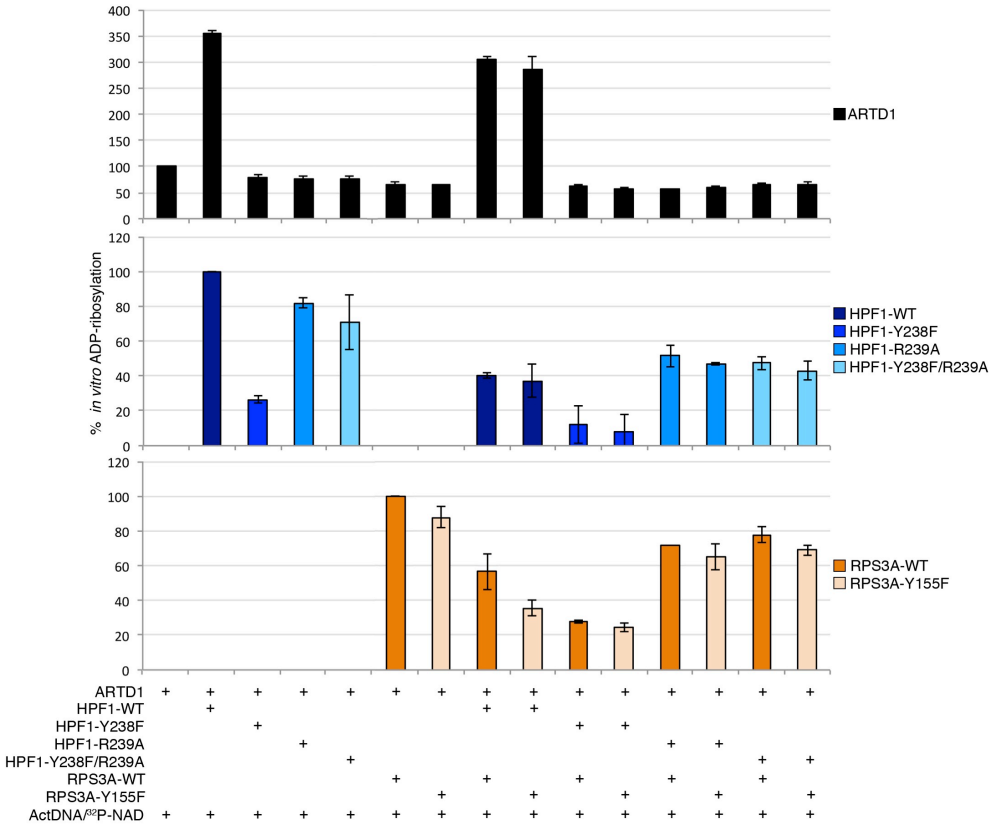

Figure S6 *Relative quantification of* in vitro *ADP-ribosylation of ARTD1, HPF1 and RPS3A.* The absolute amounts of *in vitro* ADP-ribosylation (radioactive signal) observed in Figure 4 for ARTD1, RPS3A protein isoforms and HFP1 protein isoforms were quantified. Relative quantification of ARTD1 modification was achieved by quantifying the modifications observed (radioactive signal) in the presence of *trans*-ADPr target proteins (HPF1 and/or RPS3A) relative to that observed with ^{32}P-NAD^{+} and activated DNA alone (considered baseline modification; Figure 4a). Relative quantification of RPS3A-WT and RPS3A-Y155F modifications was achieved by quantifying the modifications observed in the presence of HPF1 recombinant protein isoforms relative to that observed for RPS3A-WT with ARTD1, ^{32}P-NAD^{+}, and activated DNA alone (Figure 4b). Relative quantification of HFP1 protein isoform modifications was achieved by quantifying the modifications observed with variants of HPF1 and RPS3A relative to that observed for HFP1-WT with ARTD1, ^{32}P-NAD^{+}, and activated DNA (n=2). Error bars depict standard deviations of the mean.

Supplementary Table 1: *Description of Mascot variable-ADPr search parameter settings.*

	HCD MS/MS Ion Search	EThcD MS/MS Ion Search
Fixed modifications	Carbamidomethyl (C)	Carbamidomethyl (C)
Variable modifications	ADP-Ribosyl-HCD (SDERK_A), Oxidation (M) ADP-Ribosyl-HCD (SDERK_C), Oxidation (M) ADP-Ribosyl-HCD (SDERK_F), Oxidation (M) ADP-Ribosyl-HCD (SDERK_G), Oxidation (M) ADP-Ribosyl-HCD (SDERK_H), Oxidation (M) ADP-Ribosyl-HCD (SDERK_L), Oxidation (M) ADP-Ribosyl-HCD (SDERK_M), Oxidation (M) ADP-Ribosyl-HCD (SDERK_N), Oxidation (M) ADP-Ribosyl-HCD (SDERK_P), Oxidation (M) ADP-Ribosyl-HCD (SDERK_Q), Oxidation (M) ADP-Ribosyl-HCD (SDERK_T), Oxidation (M) ADP-Ribosyl-HCD (SDERK_V), Oxidation (M) ADP-Ribosyl-HCD (SDERK_W), Oxidation (M) ADP-Ribosyl-HCD (SDERK_Y), Oxidation (M) ADP-Ribosyl-HCD (SDERKY), Oxidation (M) ADP-Ribosyl-HCD (SRY), Oxidation (M)	ADP-Ribosyl-EThcD (SDERK_A), Oxidation (M) ADP-Ribosyl-EThcD (SDERK_C), Oxidation (M) ADP-Ribosyl-EThcD (SDERK_F), Oxidation (M) ADP-Ribosyl-EThcD (SDERK_G), Oxidation (M) ADP-Ribosyl-EThcD (SDERK_H), Oxidation (M) ADP-Ribosyl-EThcD (SDERK_L), Oxidation (M) ADP-Ribosyl-EThcD (SDERK_M), Oxidation (M) ADP-Ribosyl-EThcD (SDERK_N), Oxidation (M) ADP-Ribosyl-EThcD (SDERK_P), Oxidation (M) ADP-Ribosyl-EThcD (SDERK_Q), Oxidation (M) ADP-Ribosyl-EThcD (SDERK_T), Oxidation (M) ADP-Ribosyl-EThcD (SDERK_V), Oxidation (M) ADP-Ribosyl-EThcD (SDERK_W), Oxidation (M) ADP-Ribosyl-EThcD (SDERK_Y), Oxidation (M) ADP-Ribosyl-EThcD (SDERKY), Oxidation (M) ADP-Ribosyl-EThcD (SRY), Oxidation (M)
Mass values	Monoisotopic	Monoisotopic
Peptide mass tolerance:	± 10 ppm (# 13C = 1)	± 10 ppm (# 13C = 1)
Fragment mass tolerance:	± 0.05 Da	± 0.05 Da
Instrument type setting	LTQ-ORBI HCD (Deconv)	FUSION EThcD (Deconv)
	ADP-ribosyl-HCD	**ADP-ribosyl-EThcD**
Delta	C(15) H(21) N(5) O(13) P(2): 541.06111	C(15)H(21)N(5)O(13)P(2) 541.06111
Specificity	S,D,E,R,K,Y,A,C,F,G,H,L,M,N,P,Q,T,V,W (as indicated): anywhere	S,D,E,R,K,Y,A,C,F,G,H,L,M,N,P,Q,T,V,W (as indicated): anywhere
Marker Ions ignored for scoring	C(5) H(6) N(5): 136.0623 C(10) H(12) N(5) O(3): 250.0940 C(10) H(15) N(5) O(7) P: 348.0709 C(10) H(16) N(5) O(10) P(2): 428.0372	C(5) H(6) N(5): 136.0623 C(10) H(12) N(5) O(3): 250.0940 C(10) H(15) N(5) O(7) P: 348.0709 C(10) H(16) N(5) O(10) P(2): 428.0372
Neutral loss scoring	C(10) H(14) N(5) O(7) P: 347.063085 C(10) H(11) N(5) O(3): 249.086189	-
Satellite neutral losses	C(5) H(5) N(5): 135.054495 C(5) H(7) N(5) O: 153.065060 C(5) H(9) N(5) O(2): 171.075625 C(10) H(13) N(5) O(4): 267.096754 C(10) H(16) N(5) O(8) P: 365.073650 C(10) H(15) N(5) O(10) P(2): 427.029416 C(10) H(17) N(5) O(11) P(2): 445.039981 C(10) H(19) N(5) O(12) P(2): 463.050545 C(15) H(21) N(5) O(13) P(2): 541.061110	-

Supplementary Table 2: *Summary of number of ADPr-site localizations returned by each of the Mascot searches performed.*

	Assigned ADPr Acceptor Amino Acids																	
Potential ADPr Acceptors	M	A	D	E	F	G	H	K	L	N	P	Q	R	S	T	V	Y	Total ADPr Assignments
Mascot_SRDEK_A		99	8	33				89					118	408				755
Mascot_SRDEK_C			18	34				76					108	454				690
Mascot_SRDEK_F			17	36	22			87					123	477				762
Mascot_SRDEK_G			20	31		153		81					98	374				757
Mascot_SRDEK_H			14	35			6	101					126	536				818
Mascot_SRDEK_L			13	38				75	29				88	426				669
Mascot_SRDEK_M	23		12	36				78					104	453				706
Mascot_SRDEK_N			15	27				96		24			123	508				793
Mascot_SRDEK_P			12	32				99			47		116	462				768
Mascot_SRDEK_Q			17	33				86				41	111	505				793
Mascot_SRDEK_T			18	32				97					126	518	21			812
Mascot_SRDEK_V			11	37				83					101	502		37		771
Mascot_SRDEK_W			17	33				92					114	511				767
Mascot_SRDEK_Y			17	32				90					103	498			30	770
Mascot_SRY													247	838			64	1149
Mascot_SDERKY			44	85				192					229	645			57	1252

Supplementary Table 3: *Peptide information and ADPr-site localization summaries for ADPr-site localization training library spectra.*

SupTable3.xlsx

Supplementary Table 4: *Full protein, peptide and ADPr-site localization information for SDERKY and SRY search results.*

SupTable4.xlsx

Supplementary Table 5: *List of ADPr-peptides identified in untreated and H_2O_2-treated shControl, shARTD1 and shARTD2 cell-lines.*

SupTable 5.xlsx

Supplementary Table 6: *Serine ADP-ribosylated proteins that share Phospho Acceptor sites.*

SupTable 6.xlsx

ADPr-site Localization Spectra Database (ADPr-LSD)

The spectra provided here can be visualized by opening the spectra.html file in a web browser.

ADPr-LSD.zip

Proteomic analyses identify ARH3 as a serine mono-ADP-ribosylhydrolase

Jeannette Abplanalp[1,2], Mario Leutert[1,2], Emilie Frugier[3], Kathrin Nowak[1,2], Roxane Feurer[1], Jiro Kato[4], Hans A. V. Kistemaker[5], Dmitri V. Filippov[5], Joel Moss[4], Amedeo Caflisch[3], Michael O. Hottiger[1,*]

[1] Department of Molecular Mechanisms of Disease, University of Zurich, Winterthurerstrasse 190, 8057 Zurich, Switzerland

[2] Molecular Life Science PhD Program of the Life Science Zurich Graduate School, Winterthurerstrasse 190, 8057 Zurich, Switzerland

[3] Department of Biochemistry, University of Zurich, Winterthurerstrasse 190, 8057 Zurich, Switzerland

[4] Laboratory of Translational Research, National Heart, Lung, and Blood Institute, NIH, Bethesda, MD 20892-1590, USA

[5] Leiden Institute of Chemistry, Department of Bio-organic Synthesis, Leiden University, Einsteinweg 55, 2333 CC Leiden, The Netherlands

[*] corresponding author: michael.hottiger@dmmd.uzh.ch

Abstract

ADP-ribosylation is a posttranslational modification that exists in monomeric and polymeric forms. Whereas the writers (e.g. ARTD1/PARP1) and erasers (e.g. PARG, ARH3) of poly-ADP-ribosylation (PARylation) are relatively well described, the enzymes involved in mono-ADP-ribosylation (MARylation) have been less well investigated. While erasers for the MARylation of glutamate/aspartate and arginine have been identified, the respective enzymes with specificity for serine are still missing. Here, we report that *in vitro*, ARH3 specifically binds and demodifies proteins and peptides that are MARylated. Molecular modeling and site-directed mutagenesis of ARH3 revealed that numerous residues are critical for both the mono- and the poly-ADP-ribosylhydrolase activity of ARH3. Notably, a mass spectrometry approach showed that ARH3-deficient MEFs are characterized by a specific increase in serine-ADP-ribosylation *in vivo* under untreated conditions as well as following hydrogen-peroxide stress. Together, our results establish ARH3 as a serine mono-ADP-ribosylhydrolase and as an important regulator of the basal and stress induced ADP-ribosylome.

Keywords: Mono-ADP-ribosyl(-acceptor) hydrolases, serine, post-translation modification, PARG, ARH3, PARP, proteomics

Ecto-ADP-ribosyltransferase ARTC2.1 functionally modulates FcγR1 and FcγR2B on murine microglia

Björn Rissiek[1*], Stephan Menzel[2], Mario Leutert[3], Maike Cordes[1], Sarah Behr[1], Larissa Jank[1], Peter Ludewig[1], Mathias Gelderblom[1], Anne Rissiek[2], Sahil Adriouch[2,4], Friedrich Haag[2], Michael O. Hottiger[3], Friedrich Koch-Nolte[2†], Tim Magnus[1†]

[1]Department of Neurology and [2]Institute of Immunology at
University Medical Centre, Hamburg-Eppendorf, Germany;
[3]Department of Molecular Mechanisms of Disease, University of Zurich, Switzerland
[4]Normandie Univ, UNIROUEN, INSERM, U1234, Rouen, France; Institute for Research and Innovation in Biomedicine (IRIB), Rouen, France.

Equally contributing †senior authors
*To whom correspondence should be addressed:

Abstract

Mammalian ecto-ADP-ribosyltransferases (ecto-ARTs or also ARTCs) catalyze the ADP-ribosylation of cell surface proteins using extracellular nicotinamide adenine dinucleotide (NAD^+) as substrate. By this post-translational protein modification, ecto-ARTs modulate the function of various target proteins. A functional role of ARTC2 has been demonstrated for peripheral immune cells such as T cells and macrophages. Yet, little is known about the role of ecto-ARTs in the central nervous system and on microglia. Here, we identified ARTC2.1 as the major ecto-ART expressed on murine microglia. ARTC2.1 expression was strongly upregulated on microglia upon co-stimulation with LPS and an ERK1/2 inhibitor or upon IFNβ stimulation. We identified several target proteins modified by ARTC2.1 on microglia with a recently developed mass spectrometry approach, including two receptors for immunoglobulin G (IgG), FcγR1 and FcγR2B. Both proteins were verified as targets of ARTC2.1 *in vitro* using a radiolabeling assay with ^{32}P-NAD^+ as substrate. Moreover, ADP-ribosylation of both targets strongly inhibited their capacity to bind IgG. In concordance, ARTC2.1 induction in WT microglia and subsequent cell surface ADP-ribosylation, significantly reduced the phagocytosis of IgG-coated latex beads, which was unimpaired in NAD^+/DTT treated microglia from ARTC2.1ko mice. Hence, induction of ARTC2.1 expression under inflammatory conditions, and subsequent ADP-ribosylation of cell surface target proteins could represent a hitherto unnoticed mechanism to regulate the immune response of murine microglia.

Proteomic characterization of the heart and skeletal muscle reveals widespread Arginine ADP-ribosylation by the ectopic ADP-ribosyltransferase ARTC1

Mario Leutert[1,2], Stephan Menzel[3], Rickmer Braren[3#], Björn Rissiek[3#], Peter Gehrig[4], Anna Zolkiewska[5], Friedrich Koch-Nolte[3*] and Michael O. Hottiger[1*]

[1]Department of Molecular Mechanisms of Disease, University of Zurich, Winterthurerstrasse 190, CH-8057 Zurich, Switzerland,
[2]Molecular Life Science PhD Program of the Life Science Zurich Graduate School, Winterthurerstrasse 190, CH-8057 Zurich, Switzerland,
[3] Institute of Immunology, University Medical Center Hamburg-Eppendorf, Martinistrasse 52, D-20246 Hamburg, Germany.
[4] Functional Genomics Center Zurich, University of Zurich, Winterthurerstrasse 190, CH-8057 Zurich, Switzerland,
[5] Department of Biochemistry and Molecular Biophysics, Kansas State University, 141 Chalmers Hall, Manhattan, KS, 66506, USA. zolkiea@ksu.edu.

[#] current addresses:
RB: Department of Radiology, Klinikum rechts der Isar der Technischen Universität München, Munich, Germany. rbraren@tum.de
BR: Department of Neurology, University Medical Center Hamburg-Eppendorf Hamburg, Germany. b.rissiek@uke.de

Corresponding authors:
michael.hottiger@dmmd.uzh.ch
nolte@uke.de

* FK-N and MOH share senior authorship

ABSTRACT/Summary

ADP-ribosylation has thus far been studied on the proteomic level mainly in cell lines and in combination with genotoxic stress. The clostridium-like ADP-ribosyltransferases (i.e. ARTC) are GPI-anchored or secreted proteins that are expressed in a highly tissue specific manner. Transcriptomic data revealed that ARTC1 is expressed in skeletal muscle and heart tissue. Although ARTC1 is highly active *in vitro*, identification of ARTC1 targets *in vivo* and subsequent characterization of ARTC1-regulated cellular processes on the proteome level has been challenging and only a few ADP-ribosylated targets are known. Using a new MS-based workflow, we provide the thus far most extensive identification of endogenous ADP-ribosylomes with hundreds of ARTC1-ADP-ribosylated proteins in C2C12 myotubes and in skeletal muscle and heart tissues from wild type and newly generated ARTC1 knockout mice. These proteins are ADP-ribosylated on arginine residues and mainly located on the cell surface or in the extracellular space. They are associated with signal transduction, transmembrane transport and muscle function. Validation of hemopexin (HPX) as a newly identified ARTC1-target protein confirmed the functional importance and prevalence of ARTC1-mediated extracellular arginine ADP-ribosylation on the organism level. Together we provide the first comprehensive systems-level analysis of endogenous ADP-ribosylation in two different muscle tissues revealing a widespread function of ARTC1 and its targets.

Key words: ADP-ribosylation, proteomics, mass spectrometry, ARTC1, Arg, muscle, heart, hemopexin

INTRODUCTION

Protein ADP-ribosylation is an ancient post-translational modification (PTM) found in a wide range of species[1-3]. Protein ADP-ribosylation has been shown to regulate several cellular processes by altering the function of the modified protein and/or providing a scaffold for the recruitment of other proteins. ADP-ribosylation is a complex PTM that can be divided into two subtypes: mono-ADP-ribosylation (MARylation), in which only a single ADP-ribose (ADPr) is transferred to an amino acid of a target protein, and poly-ADP-ribosylation (PARylation), which involves the addition of further ADP-ribose moieties to generate poly-ADP-ribose (PAR)[4]. These modifications are enzymatically mediated by ADP-ribosyltransferases (ARTs). In mammalians, ARTs are divided into the two families of ARTC (C2/C3 toxin-like, also ecto-ARTs) and ARTD (diphtheria toxin-like, formerly PARPs) enzymes[5]. While all known enzymes catalyzing PARylation belong to the ARTD family, and MARylation has traditionally been the domain of the ARTC transferases, it has recently been appreciated that some ARTDs and even some family members of the structurally unrelated sirtuin family can also mediate MARylation[6].

Four human (ARTC1, 3, 4, 5, formerly also hART1-5) and six mouse (ARTC1, 2.1, 2.2, 3, 4, 5, formerly also mART1-5) ARTC genes have been identified. For both species, ARTC1 is expressed mainly in skeletal and heart muscles, non-lactated mammary gland, brown adipocytes, epithelial cells or activated granulocytes[7-9]. The human and mouse ARTC family members, ARTC1-ARTC4, are expressed as GPI-anchored ecto-enzymes[5,7,8,10]. ARTC1, comparable to 2 and 5 contain the characteristic cholera toxin R-S-E catalytic motif in their active center. R and S are important for NAD^+ binding and E has a catalytic function[11]. Arginine-specific mono-ADP-ribosylation activity has been confirmed for human and mouse ARTC1, the two mouse isoforms of ARTC2 and for human and mouse ARTC5[8].

An important question when examining the biological function of ARTCs is the endogenous source of extracellular NAD^+ under normal and pathophysiological conditions, since NAD^+ is not cell membrane permeable. The concentration of extracellular NAD^+ in serum has been reported to range from 0.1 to 0.3 μM, while intracellular NAD^+ concentrations are much higher (400–500 μM)[12]. Moreover, plasma NAD^+ concentrations are approximately five-fold lower than that required *in vitro* to observe ARTC2.2-mediated ADP-ribosylation events[13,14]. Several studies have, however, demonstrated that NAD^+ can be released from intracellular sources during lytic processes like tissue damage and necrosis[14-16]. Furthermore, it is thought that NAD^+ and other nucleotides are released by controlled mechanisms during hypoxia and inflammation[17,18]. In line with this, acute inflammation was reported to be associated with the liberation of significant amounts of NAD^+ (1–10 μM range) into the extracellular milieu[17]. Moreover, extracellular NAD^+ has a longer half-life compared to ATP (15 min vs. only a few seconds in plasma)[15,19,20]. Hence, upon its release into the extracellular space at sites of inflammation or following cell injury, extracellular NAD^+ can either be used by ARTCs to covalently modify specific ADP-

ribosylation target proteins or be degraded into smaller metabolites. Hence, the net biological effect of extracellular NAD^+ depends on the amount of NAD^+ released into the extracellular space, the quality and quantity of specific receptors/enzymes expressed by surrounding cells, and on the activities of the catabolising-enzymes[14,21]. Such a balance between local production of a signalling molecule that is normally absent from the extracellular space and its rapid degradation/consumption is characteristic of the class of molecules that mediates ‘‘danger signals’’ and that can alert immune cells[22].

Functional consequences of eukaryotic arginine ADP-ribosylation have mainly been studied for ARTC2.2 targets. One of the ARTC2.2 targets on T cells is the P2X7 ion channel. MARylation of R125 of P2X7 leads to its activation, which induces the influx of Ca^{2+} and Na^+ as well as the efflux of K^{+}[23]. Downstream effects of P2X7 activation include inflammasome activation, processing and cytokine release (IL-1β, IL-18, IL-1 receptor antagonist and IL-36α), release and activation of proteases (mainly ADAM10 and 17) resulting in the shedding of cell-surface molecules, including ARTC2.2 itself [24,25]. Prolonged activation of P2X7 stimulates T cell death, also called NAD^+-induced cell death (NICD)[17]. ARTC1 was found in bronchoalveolar lavage fluid from smokers. Here, it modifies the defensin human neutrophil peptide 1 (HNP1) on Arg14 and Arg24, which specifically reduces its antimicrobial and cytotoxic activities[26,27]. ARTC1 ADP-ribosylation was also found to have a role in endoplasmic reticulum stress responses[28]. In addition, ARTC1 ADP-ribosylates members of the integrin family of adhesion molecules on skeletal muscle cells and leukocytes[29]. ADP-ribosylation of integrin α7 (ITGA7) by ARTC1 modulates the binding of integrin α7β1 to laminin[30]. It is proposed that an arginine residue located in the central region of ITGA7 is involved in the interaction with a negative region of ITGB1 and, at low NAD^+ concentrations (10 μM), this arginine is ADP-ribosylated to repel ITGB1 and induce the formation of a high affinity conformer. In contrast, increasing NAD^+ concentrations (100 μM) lead to ADP-ribosylation of additional site(s) located in the headpiece of ITGA7, where the ligand-binding site is located, that sterically hinder and directly inhibit ligand binding[31]. However, it is not clear if ARTC1 has other functions and targets on myotubes. Furthermore, it is also not known if ARTC1 mediated ADP-ribosylation has any role under steady-state conditions.

Despite these recent discoveries, the substrates of the different ARTCs as well as their implications in cellular processes are still not very well understood. This is in large due to the fact that mass spectrometry (MS) based methods were only developed for and applied to the identification of ADP-ribosylated proteins and their ADP-ribose acceptor site in cultured cells. Very recently we developed an approach that allowed the analysis of ADP-ribosylated proteins in the liver, a tissue that has already been described to regulate cellular processes in an ADP-ribosylation-dependent manner[32]. This characterization identified 901 modified peptides with unique ADP-ribosylation acceptor sites[32-35]. The majority (86%) of the identified ADP-ribosylation acceptor sites in the mouse liver were Arg residues and associated with plasma membrane or cytoplasmic proteins. Interestingly, ARTC2.2 was found among the modified

targets. Moreover, we have shown that the GPI-anchored ARTC2.2 is restricted to a small subset of target proteins by virtue of its association with lipid rafts, but promiscuously modifies many different targets upon detergent solubilization of the plasma membrane[11,36]. It remained so far unclear whether ARTC1 has a comparable target spectrum, or whether it would only modify a few specific target proteins, as it has been observed for the bacterial ART toxins.

Here, we analyzed the ARTC1-specific ADP-ribosylome in C2C12 myotubes as well as skeletal and heart muscle of wildtype and ARTC1-deficient mice, which were generated to facilitate systems-level analyses. These studies revealed that ARTC1 is essential for the modification of numerous membrane proteins under basal conditions, which provides strong evidence for the physiological importance of ARTC1. In particular, we confirm that ARTC1-dependent ADP-ribosylation of hemopexin (HPX) on Arg218 strongly reduces its capacity to bind heme, which is likely highly relevant for the function of this strongest known heme binding protein.

Together we provide the first comprehensive systems-level analysis of ARTC1-mediated ADP-ribosylation in two different muscle tissues. The identification of the site-specific profile of the ARTC1 dependent ADP-ribosylome provides evidence for a widespread contribution of ADP-ribosylation on the cell surface and the extracellular space and provides an extensive resource that allows to further discover the functional relevance of ADP-ribosylation in muscle physiology and pathophysiology.

RESULTS

ARTC1 mediates widespread extracellular ADP-ribosylation in C2C12 myotubes

To assess the extent of ARTC1-mediated ADP-ribosylation and to identify ADP-ribosylated proteins, we first verified the expression of ARTC1 in differentiating C2C12 by quantitative reverse transcription PCR (RT-qPCR) and could confirm previous reports[29] showing that ARTC1 is specifically expressed in mouse heart tissue and fully differentiated C2C12 myotubes (**Suppl. Figure 1A**). The other active membrane-bound extracellular ART expressed in mice is ARTC2[37]. We were, however, unable to detect ARTC2 in C2C12 by RT-qPCR (data not shown), which is in agreement with the reports that ARTC2 is predominantly expressed in immune cells[8,38]. Hence, ARTC1 is likely the only active ectopically expressed ADP-ribosyltransferase in differentiated C2C12 myotubes.

To investigate whether ARTC1 is enzymatically active in C2C12 myotubes and to assess its target space, we treated *in vitro* differentiated C2C12 myotubes with NAD^+ and subsequently mapped site specific ADP-ribosylation using our established ADP-ribosylome proteomic workflow[32,39]. While only a few peptides were identified under basal (i.e. untreated) conditions, we identified a strong increase in ADP-ribosylation sites following NAD^+ treatment (144 vs. 9 unique ADP-ribosylated peptides (**Figure 1A**); 84 vs. 8 ADP-ribosylated proteins (**Suppl. Figure 1B**) corresponding to 120 ± 47 vs 9 ± 1 ADP-ribosylated peptide spectra matches (**Suppl. Figure 1C**). Under these conditions, arginine was identified as the main ADPr-acceptor amino acid (**Figure 1B**). Gene ontology analyses revealed that the NAD^+-treatment dependent ADP-ribosylation targets are predominantly extracellular and plasma membrane proteins having a molecular function in extracellular matrix binding and receptor activity and participating in biological processes associated with cell adhesion, muscle contraction and regulation of signal transduction (**Figure 1C**).

To quantitatively assess the observed increase of ADP-ribosylation, we performed label-free MS1 based quantification of all identified ADP-ribosylated peptides using three biological replicates of untreated and NAD^+-treated C2C12 myotubes. A good Pearson correlation among untreated ($R>0.76$) and NAD^+-treated ($R>0.87$) replicates, respectively, demonstrated that the measured ADP-ribosylated peptide signal intensities could be used as a reliable measure for modification site abundance (**Suppl. Figure 1D**). Most detected ADP-ribosylated targets were strongly induced upon NAD^+ treatment and, importantly, are novel ARTC1 targets (**Figure 1D and Suppl. Table 1**). The heat map representation of the ADP-ribosylation site abundance reveals three minor clusters of sites that were already ADP-ribosylated under basal conditions (**Figure 1D**). From the indicated clusters, the ADP-ribosylated peptides of the top and lower cluster were more abundantly modified after NAD^+ treatment, and included four members of the integrin family (ITGA7, ITGA6, ITGAV and ITGB5) (**Figure 1D**), with ITGA7 representing the only previously reported ARTC1 target[29]. A small portion of the ADP-ribosylation sites identified remained

largely unchanged following NAD^+ treatment as visualized in the middle cluster. This cluster included histone H2B, which however is unlikely a target of ARTC1, since the two proteins are not in the same cellular compartment[32,40]. Interestingly, most of the proteins of this small middle cluster (approx. 80%) were annotated to be localized to the endomembrane system, and thus likely not affected by addition of exogenous NAD^+.

To understand if whole protein complexes are targeted by ADP-ribosylation we mapped and visualized high confidence interactions (minimum required interaction scores >0.7) between the ADP-ribosylated proteins identified above using the STRING database of physical and functional protein interactions[41]. The analysis identified several ADP-ribosylated protein complexes, but revealed no significant enrichment of fully ADP-ribosylated protein complexes. We could unravel an interaction network of 13 ADP-ribosylated proteins with a high enrichment in extracellular matrix (ECM)-receptor interactions, suggesting that ADP-ribosylation of this ECM interaction complex might specifically modulate the function of protein complexes involved in cell adhesion and ECM-receptor signaling (**Figure 1E**). The other interacting protein groups that were identified function in cell-cell adhesion, calcium ion trans membrane transport and vesicular transport (**Figure 1E**). In summary, these data show that ARTC1 is expressed in differentiated muscle cells and demonstrated that these cells exhibit NAD^+-inducible ADP-ribosylation responses that mainly affect plasma membrane and/or extracellular proteins.

ARTC1 knockout animals are viable and develop normally, but show reduced skeletal muscle ADP-ribosylation

To ascertain whether ARTC1 is the predominant *in vivo* writer of the ADP-ribosylome in muscle cells, we generated ARTC1-deficient ($Artc1^{-/-}$) mice. This was achieved via insertion of loxP sites into the *Artc1* gene (**Suppl. Figure 2A-D**), transgene-positive offspring were mated with a deleter strain, which resulted in the generation of $Artc1^{-/-}$ knockout animals. *Artc1* gene deletion was confirmed by PCR and Western blotting of a glycoprotein-enriched muscle extract (**Suppl. Figure 2E, Figure 2A**). $Artc1^{-/-}$ mice were fertile and did not show any overt phenotype. The overall body constitution as judged by body weight did not seem to be overtly impaired (**Figure 2B**). We did observe a slight reduction in circadian movement, which could be due to muscle weakness (**Figure 2C**). Consistently, $Artc1^{-/-}$ mice showed signs of muscle weakness in an accelerated Rotarod test (**Figure 2D**), suggesting that the lack of ARTC1 affects the skeletal or heart muscle function. Next, we wanted to confirm the importance of ARTC1 for muscle cell ADP-ribosylation. To this end, primary myoblasts from WT and $Artc1^{-/-}$ mice were differentiated *in vitro* and treated with radioactively labeled NAD^+. Autoradiograms showed complete absence of surface protein ADP-ribosylation in $Artc1^{-/-}$ myoblasts, while WT and heterozygous animals displayed an *Artc1* gene dose dependent ADP-ribosylation signal (**Figure 2E**). Furthermore, the dominant band at 120 kD, presumably corresponding to integrin alpha 7, is undetectable in the $Artc1^{-/-}$ samples (**Figure 2D**).

Together, these results confirm that ARTC1 is essential in differentiated muscle cells for ADP-ribosylation of cell surface proteins and hint at a functional *in vivo* relevance for ARTC1-mediated ADP-ribosylation in skeletal and heart muscle.

ARTC1 is essential for the skeletal muscle ADP-ribosylation *in vivo*

Having established the *Artc1*$^{-/-}$ mice, we aimed to define the *in vivo* ARTC1-dependent ADP-ribosylome of murine skeletal muscle. Total skeletal muscle protein extracts were prepared in a denaturing Guanidine-HCl lysis buffer from unstressed WT and *Artc1*$^{-/-}$ mice, the ADP-ribosylated fraction enriched and subsequently analyzed by MS as described earlier[32]. Importantly, these animals were perfused with the ARTC inhibitor novobiocin prior to muscle extraction to inhibit stress-induced ADP-ribosylation. MS analyses identified a very large basal ADP-ribosylome that consisted of 1295 unique ADP-ribosylated peptides (**Figure 3A, Suppl. Table 2**). Good correlations were observed between biological replicates (**Suppl. Figure 2F**). Moreover, a >20-fold reduction in the number of unique ADPr-peptides in *Artc1*$^{-/-}$ muscle tissues was observed, strongly indicating that ARTC1 is the main writer of skeletal muscle ADP-ribosylation under endogenous conditions (**Figure 3A**). The importance of ARTC1 for the muscle ADP-ribosylome was further validated by ADPr-acceptor site specificity analyses. As expected for ARTC1 targets[42], the vast majority of the ADPr-acceptor sites identified in wild-type tissues were Arg residues, which were almost completely absent in the corresponding *Artc1*$^{-/-}$ samples (**Figure 3B**). In fact, the remaining ADP-ribosylated proteins observed in *Artc1*$^{-/-}$ muscles were modified on Ser, Lys, Glu or Asp residues. Over 70% of the ADP-ribosylated proteins in wild-type muscle tissues carried only a single modification (**Figure 3C**), which suggests that ARTC1-dependent ADP-ribosylation is a tightly controlled and very specific process. These findings were further substantiated by gene ontology analyses, which demonstrated that the identified ADP-ribosylated proteins almost exclusively localized to the extracellular/membrane and/or mitochondrial compartments and function in transmembrane transport, calcium signaling and/or ATP metabolic processes (**Figure 3D**). ADP-ribosylated proteins from *Artc1*$^{-/-}$ muscle only showed a significant enrichment in mitochondrial proteins having a role in ATP-metabolic processes.

Together these experiments provide evidence that ARTC1 modifies a defined set of proteins already under unstressed conditions and that the observed skeletal muscle ADP-ribosylome is rather stable. When comparing the ADP-ribosylomes of WT skeletal muscle and C2C12 myotubes, we found that around 15% of the ADP-ribosylated proteins identified in NAD^+-treated C2C12 myotubes were also modified in the skeletal muscle (**Suppl. Figure 2G**).

The ARTC1-dependent heart and skeletal muscle ADP-ribosylomes differ

To investigate whether ARTC1 activity or the obtained skeletal muscle ADP-ribosylome is specific to this tissue or shares similarities with heart tissue, proteome analyses were performed on mouse hearts from WT and *Artc1*$^{-/-}$ mice. Compared to the skeletal muscle, less ADP-ribosylation sites were identified in wild-type hearts under basal conditions, however Arg was still the most abundant ADP-ribosylation site and was strongly reduced in the corresponding *Artc1*$^{-/-}$ tissues (**Figure 4A, Suppl. Figure 3A, Suppl. Table 3**). Around 85% of the observed ADP-ribosylation sites were dependent on ARTC1 (**Figure 4A**). The performed MS analyses were reproducible with 70% and 60% of the ADP-ribosylated proteins identified in at least two biological replicates for the WT and the *Artc1*$^{-/-}$ tissue samples respectively (**Suppl. Figure 3B**). The variation in the measurement of non-ARTC1 mediated targets was significantly bigger than of ARTC1 targets. Closer analyses of the ADP-ribosylation sites revealed preferential modification of Arg residues in wild-type heart tissues only, while Ser, Lys, Glu or Asp residues were the only sites identified in *Artc1*$^{-/-}$ hearts (**Figure 4B**). Similar to what was observed in skeletal muscle (**Figure 3C**), approximately 70% of the modified proteins that were identified in mouse hearts were ADP-ribosylated at only one site (**Figure 4C**).

To characterize the mouse heart ADP-ribosylome in more detail, the ADP-ribosylome data were subjected to gene-ontology analysis, which produced a pattern of term enrichment similar to what was observed for skeletal muscle. WT heart samples were enriched for proteins that localize to the plasma membrane and/or extracellular space, function in receptor binding and/or transporter activity and are involved in the regulation of muscle contraction and apoptotic processes. In contrast, these terms were absent from the ADP-ribosylomes identified in the *Artc1*$^{-/-}$ samples, which only showed enrichment for mitochondrial proteins and proteins involved in the TCA cycle and ATP synthesis (**Figure 4D)**. This suggests that ARTC1 most probably manifests its functionality by ADP-ribosylation of a broad array of membrane associated protein targets. To analyze whether specific protein complexes would be ADP-ribosylated and whether the modified proteins functionally co-regulate certain cellular processes, STRING analyses based protein-protein interactions were carried out for ADP-ribosylated proteins identified either exclusively in WT (**Figure 4E)** or *Artc1*$^{-/-}$ animals (i.e. ARTC1-independent targets, **Suppl. Figure 3C**). Nine high confident ADP-ribosylated protein interaction networks were identified exclusively in the WT heart muscle samples (**Figure 4E)**. These interaction networks mostly contained extracellular and plasma membrane proteins that are involved in stress responses. Similar to the C2C12 cells, we found an interaction network of ADP-ribosylated proteins that mediates ECM-receptor interactions, but also identified heart specific functional interaction networks. Interestingly we identified an ADP-ribosylated protein network that plays a role in oxidative phosphorylation and is situated in the mitochondria, however these proteins were not modified at Arg and therefore unlikely ARTC1 targets. In fact, this network fits better to the pattern observed in the *Artc1*$^{-/-}$ animals. There we identified three ARTC1 independent ADP-

ribosylated protein networks for mostly mitochondrial and some cytosolic proteins that function in oxidative phosphorylation, TCA cycle and fatty acid degradation (**Suppl. Figure 3C)**.

Despite the fact that we started our analysis with the same amount of tissue (i.e. heart and skeletal muscle tissue) and we observed quite a large overlap (60%) of ADP-ribosylated proteins identified in the heart compared to the skeletal muscle tissues (compare **Figure 3A to Figure 4A** and **Suppl. Figure 3D**), 4 times more ADP-ribosylated proteins were identified in skeletal compared to heart muscle tissues. To test our sample-handling regime that was focused on eliminating ADP-ribosylation reactions due to sample preparation, we tested lysis of the tissue under different conditions (**Suppl. Figure 3E**). The lysis was performed either with a modified RIPA buffer[43] or a denaturing 6M guanidine-HCl buffer[44] in combination with Novobiocin perfusion, as already performed previously with the skeletal muscle samples. In addition, animals were pretreated with Novobiocin (*intra venous* (*i.v.*), 30 min, before sacrifice). MS-analysis of these three samples revealed that guanidine-HCl lysis buffer prevented lysis-induced ADP-ribosylation since pretreatment with Novobiocin (*i.v.*) did not reduce the observed amount of modification. On the other hand, modified RIPA buffer alone was not able to prevent lysis-induced ADP-ribosylation, which resulted in an increased number of ADP-ribosylation identifications, consistent with our previous findings for ARTC2.2[36] (**Supp. Figure 3E**).

The reduced ADP-ribosylation in the heart could also be due to different plasma membrane compositions (i.e. affecting ARTC1 complex formation) in heart and muscle, which might affect ARTC1 activity and affinity to NAD^+ or due to overall less NAD^+ in the heart tissue. To test whether the lower amount of ADP-ribosylation is due to lack of substrate in healthy unstressed mouse hearts, animals were pretreated with NAD^+ (i.v.) 30 min before sacrifice, the hearts were harvested and ADP-ribosylome MS analysis performed. Injection of NAD^+ did not increase the overall number of identified unique ADP-ribosylated peptides significantly, neither in WT nor in *Artc1*$^{-/-}$ background (**Suppl. Figure 4A**). Moreover, NAD^+ pretreatment did neither alter the ADPr acceptor site profile nor the number of unique ADPr acceptor sites significantly (**Suppl. Figure 4B**). To strengthen this aspect, we aimed at detecting potential quantitative changes after NAD^+-treatment by applying a label free MS1 quantification approach. Replicate comparison of ADP-ribosylated peptide intensities revealed a very strong Pearson correlation among the triplicates of untreated and NAD^+ treated WT tissue (>0.92) and a lower but acceptable correlation among the *Artc1*$^{-/-}$ replicates (>0.73), respectively (**Suppl. Figure 4C**). Also untreated versus NAD^+ treated WT and *Artc1*$^{-/-}$ samples correlated well (>0.8 and >0.73) (**Suppl. Figure 4C**). Principal component analyses of ADP-ribosylated peptide abundance revealed that the ADP-ribosylomes of untreated and NAD^+ pre-treated WT hearts differed and segregated in two groups, whereas the *Artc1*$^{-/-}$ heart samples were much more variable and the treatment did not seem to induce distinct changes in ADP-ribosylated peptide abundances (**Figure 4F)**. Quantitative MS analysis of three independent samples confirmed that NAD^+ treatment of WT mice induces only little *de novo* ADP-

ribosylation but leads to quantitative changes of discrete ADP-ribosylation sites, most of them already present in untreated hearts (**Figure 4G, Suppl. Figure 4D**). Interestingly, this analysis showed that 12 ADP-ribosylation sites were significantly more abundant after the NAD^+-treatment, including integrin alpha 7 and hemopexin (HPX), as well as five ADP-ribosylation sites which were less abundant after the treatment, including on ARTC1 itself (**Figure 4G)**. The NAD^+ treatment only changed the degree of the ADP-ribosylation at specific sites of these proteins, however total protein level remained constant for the ones we could detect (**Suppl. Figure 5)**. Integrin alpha 7, which has been shown before *in vitro* to be a target of ARTC1 shows the most significantly induced ADP-ribosylation (on Arg896 and Arg608) after NAD^+ treatment, which is in line with our results from NAD^+ treated C2C12 cells. Also, integrin alpha 7 interacting extracellular matrix proteins LAMB2 showed a significant increase of ADP-ribosylation at two sites (Arg103 and Arg1458). Moreover, a significantly increased proportion of ADP-ribosylation on the two soluble extracellular proteins Hemopexin (HPX) and Fibronectin1 (FN1) could be detected upon NAD^+ treatment (**Figure 4G)**. In contrast, ARTC1 itself, ARTC3, GPC1, NECTIN2, CSPG4 and EFNB3, all of them plasma membrane proteins, were less abundantly modified after NAD^+-treatment. The reduction in modification on these proteins could be due to shedding by metalloproteases which would sequester them from the membrane-bound ARTC1 [25,45-48].

Arginine ADP-ribosylation marker ions and motifs.

Studies of *in vitro* modified peptides have suggested that ADP-ribosylated Arg residues can give rise to an Arg-specific ADP-ribose marker ion (ADPr-carbodiimide, **Figure 5A**) during MS2 fragmentation[49]. ADP-ribose marker ions can be extracted from MS2 spectra without applying peptide search engines and/or matching the spectra to a specific peptide sequence, and have proven beneficial in the identification of ADP-ribosylated peptides[50]. Observation of ADPr-carbodiimide ions in our samples would allow an alternative estimation and validation of Arg-ADP-ribosylation levels. To this end, we screened MS2 spectra from the measured heart samples using the PTM marker finder software to extract ADPr maker ions[51]. Indeed, when we looked at spectra containing at least 4 ADPr maker ions we could identify 361 spectra containing an ADPr-carbodiimide ion (10% of spectra) in the WT samples and only 3 in *Artc1*$^{-/-}$ samples (0.9% of spectra) (**Figure 5B**). As expected ADPr-carbodiimide ions showed a lower intensity than the other marker ions, however in many cases they were readily identified and could be used to estimate the Arg-specific ADP-ribosylation levels (**Figure 5C, Supplementary Figure 4E**).

Next we attempted to identify an Arg-ADP-ribosylation consensus motif as previously identified for nuclear Ser-ADP-ribosylation [33,52]. Analysis of 21 amino acid windows with the identified Arg-ADP-ribosylation sites in the middle for the different samples revealed five significantly enriched motifs ($p<0.0005$, binomial test), comprising 78%, 30% and 63% of all identified Arg-ADP-ribosylation sites in C2C12, skeletal and heart muscle, respectively (**Figure 5C**). The most prominent motif identified

consisted of an R(-ADPR)G motif (in all sample types), followed by an RR(-ADPR) motif (in skeletal and heart muscle).

ADP-ribosylation of hemopexin at Arg218 reduces its capacity to bind heme

To validate our findings, we investigated the functional relevance of HPX ADP-ribosylation on Arg218 in heart and skeletal muscle tissue. HPX plays a crucial role during inflammatory conditions[53] and is the strongest known heme binder[53]. To confirm that HPX is a direct ARTC1 target, recombinant HPX was incubated with ARTC1 and radiolabeled NAD^+. We found that recombinant ARTC1 modified HPX *in vitro* and that no glycation or passive attachment of NAD^+ to HPX occurs (**Figure 6A**). ARTC1 dependent HPX modification was sensitive to ARTC inhibitor Novobiocin and slightly decreased in the presence of heme (**Figure 6B**). MS analysis of the *in vitro* reaction confirmed the ADP-ribosylation of Arg218 *in vitro* and additionally identified ADP-ribosylation on R83. Manual annotation of HCD and EThcD fragmentation spectra for *in vivo* and *in vitro* modified HPX peptides confirmed ADP-ribosylation on Arg218 and revealed Arg-ADP-ribosylation specific marker ions and neutral losses (**Figure 6C**). Arg218 faces the heme binding pocket of HPX and might therefore interfere with heme binding upon ADP-ribosylation (**Figure 6D**). To test this possibility, a heme binding assay measuring the HPX-heme protein complex formation absorbance at 413 nm was established. ADP-ribosylated HPX was strongly impaired in its heme binding capacity as compared to unmodified HPX (**Figure 6E and F**), indeed suggesting that the ADP-ribosylation of HPX might regulate its heme binding capacity and might therefore be a physiologically relevant function.

DISCUSSION:

In this study, we investigated the targets of ARTC1 in C2C12 myotubes, as well as in skeletal and heart muscle tissues at the systems-level. These proteome-profiling studies, which compared tissues from WT and newly generated *Artc1*$^{-/-}$ mice, uncovered a very large previously unidentified ARTC1-dependent ADP-ribosylome composed of several membrane and secreted proteins that were most often modified on a single Arg. Ser, Lys, Glu and Asp modifications were also identified, but these ADP-ribosylation events were not dependent on ARTC1. We showed that Arg-specific ADP-ribosylation could be additionally confirmed using a diagnostic ADPr-carbodiimide ion specific for the modified Arg, thereby expanding the toolbox of ADP-ribose marker ions to the screening of complex samples. Comparison of the identified peptides revealed sequence motifs with enriched Gly and Arg adjacent to the modified Arg within ARTC1 target proteins.

Based on the proteins identified under steady-state conditions *in vivo,* ARTC1 seems to be constitutively active and to play a role under steady-state conditions. The very strong drop in the number of detectable ADP-ribosylation sites in *Artc1*$^{-/-}$ compared to WT mice strongly suggests that ARTC1 is the main contributor to the skeletal and heart ADP-ribosylome under untreated conditions (**Figure 2** – **Figure 3**). The only additional active and cell bound ARTC family member in mouse, ARTC2.2 is not expressed in C2C12 or the tested tissues. Interestingly, the large number of identified ADP-ribosylated proteins showed that the applied Af1521 enrichment method is suitable for Arg-ADP-ribosylated proteins.

NAD^+ can be released upon necrosis or mechanical stress in tissue, which could activate ARTCs during organ collecting[12]. Considering that ARTCs have higher affinity for NAD^+ compared to intracellular ARTDs, ARTCs are more prone to activation following NAD^+ release during tissue collecting[12]. However, the ADP-ribosylomes we profiled were quite stable and constrained to the extracellular compartment, the plasma membrane and the mitochondria with modification of many low abundant proteins. The finding of some cytoplasmic and mitochondrial Arg-ADP-ribosylated proteins indicates that the applied extraction procedure might still lead to ADP-ribosylation of intracellular proteins due to tissue damage induced upon excising the tissues, as previously reported for ARTC2.2 [36]. It will be interesting to test if ARTC1 mediated ADP-ribosylation also has a function in endogenously occurring tissue damage. Besides cell necrosis or physical tissue damage, another reason for intracellular Arg-ADP-ribosylation could be the modification of proteins during their maturation (ER and Golgi) as both ARTC1 and its target proteins are processed in and traffic through these compartments. Furthermore, mitochondrial proteins might be non-enzymatically ADP-ribosylated due to the high NAD^+ concentration in the mitochondria [12].

The remarkable stability of the observed ARTC1-mediated ADP-ribosylomes contrasts to the observed ADP-ribosylomes catalyzed by ARTD1 upon oxidative stress, which can be detected only during a few minutes [32]. Reversibility of cell surface ADP-ribosylation was previously studied on integrin

alpha 7 revealing that surface ADP-ribosylation is not readily reversed by ADP-ribosylhydrolases [54]. These findings suggested that the responsible erasers operate outside the postulated ADP-ribosylation cycle. ARH1, the only known arginine specific ADP-ribosylhydrolase, is solely expressed within the cell, but not secreted. It is thus tempting to speculate that the extracellular ADP-ribosylation could only be removed from the cell membrane proteins by internalization and protein degradation or shedding, potentially rendering the removal of Arg-ADP-ribosylation a slow process. Alternatively, ADP-ribose can also be processed by extracellular phosphodiesterases, thereby converting it to phospho-ribosylated proteins. However, with the applied enrichment method we can unfortunately not anticipate the level of phospho-ribosylated proteins [54].

Comparison of ADP-ribosylated proteins in the three sample types revealed a 40% overlap between the C2C12 sample and the *in vivo* samples and a 44% overlap between the two *in vivo* muscle samples. Although the proteome of C2C12 is different from skeletal muscle (44% of the proteins show a different expression profile[55]), this does not explain the small overlap of the ADP-ribosylomes but rather suggests that ARTC1's activation, specificity and expression levels are different *in cell culture* compared to *in vivo*. These differences could stem from variations in the extracellular matrix and local fluids that control ARTC1 activity. In analogy to ARTC2, it is possible that the targets of ARTC1 are also restricted to raft associated target proteins[36]. Alternatively, differential concentrations of available NAD^+ could lead to a different ADP-ribosylome.

Computational analysis of all modified peptide sequences revealed motifs for many Arg-ADP-ribosylation sites and showed that often another Arg or a Gly residue is positioned adjacent to a modified Arg (**Figure 5C**). The Arg/Arg motif might provide a beneficial environment for the catalytic ART process or might serve as a positively charged protein-protein interaction patch whose functionality could be annihilated by ADP-ribosylation of one of the arginines. A double Arg motif was already observed for individual proteins in *in vitro* ARTC2.2 assays[23]. Interestingly, the Ser modified by ARTD was also found to be adjacent to a positively charged Lys or Arg residue[33], suggesting that a positively charged amino acid beside the ADPr acceptor site might be important for the biochemical reaction independent whether the modification is catalyzed by ARTC or ARTD family members. The Gly/Arg and Arg/Gly motifs might render the Arg more accessible to ARTC1. Interestingly, an Arg/Gly/Asp motif in proteins constitutes a major recognition system for cell adhesion and half of all integrins recognize and bind protein ligands containing this motif [56]. Together with the previous findings and the analysis provided in this study this strongly suggests that ARTC1 is involved in modulating cell adhesion.

The identification of the relatively intense Arg-specific ADPr-carbodiimide marker ion for Arg-ADP-ribosylated peptides in complex samples opens the possibility to include the marker ion in product dependent MS methods[33,40,49,57]. This will be beneficial while studying ARTC targets in complex

backgrounds by specifically targeting Arg-ADP-ribosylated peptides for fragmentation and thereby acquiring high quality spectra.

In *ARTC1*$^{-/-}$ samples, also a residual ARTC1-independent ADP-ribosylome could be detected which was not affected by NAD^+ pretreatment. Our data reveal that these proteins were mainly modified at Ser, Lys, Glu or Asp. However, these sites were by far less abundant than the identified ARTC1 targets. Compared to the arginine-modified sites, it was much more difficult to obtain good localization for these alternative modification sites, probably due to their labile ADPr-peptide bond upon MS2 fragmentation [52]. These proteins with ARTC1–independent ADP-ribosylation were involved in metabolic processes, oxidative-reduction processes and mainly localized to the mitochondria, suggesting that these processes may be influenced by the modification. As mentioned above, the high NAD^+ concentration found in mitochondria (approx. 0.5mM) might also favor non-enzymatic ADP-ribosylation for these proteins [12]. NAD^+ *i.v.* injection (i.e. a DAMP signal) did not markedly alter the total amount of ADP-ribosylated sites of the analyzed heart tissues, however changed their quantitative composition. It is likely that NAD^+ treatment induces a metalloprotease (e.g, ADAM17) [25], which would lead to shedding of plasma membrane proteins. Indeed, GPC1 as well as NECTIN4, the close relative of NECTIN2, are known to be shed by ADAM17 [45,46]. CSPG4 and EFNB3 can be cleaved by ADAM10, the close relative of ADAM17 [46-48] The soluble form of these proteins might be less efficiently targeted by membrane bound ARTC1. ARTC2.2, the close relative of ARTC1 and 3, has been shown to be released by ADAM17 [25]. Interestingly, the region close to the GPI-anchor where ARTC2.2 is cleaved is conserved in GPI-anchored ARTC1 as well as in ARTC3, indicating that they might also be shed[25]. Release of ARTC1 itself might lead to a shift in its activity towards soluble proteins such as HPX and FN1 as shown previously for ARTC2.2 [25]. So far it is not clear which targets are modified by soluble ARTC2.2.

Moreover, we characterized and functionally validated the ADP-ribosylation of hemopexin (HPX) at Arg218 using purified recombinant proteins and observed that *in vitro* modification of HPX strongly interfered with its capacity to bind heme (**Figure 6**). HPX is a soluble protein that it is usually found in heart and skeletal muscle tissue[55,58]. After acute hemolysis (e.g. after post-ischemic reperfusion or sepsis) excess heme is bound by HPX[59]. HPX-heme complexes are taken up by macrophages or hepatocytes and heme is degraded[60]. HPX is also important for heme export from cells, by accepting heme from export proteins, indicating that HPX also has a function directly at the plasma membrane, placing it in the potential vicinity of ARTC1[61]. The inhibitory role of ARTC1 mediated ADP-ribosylation on the HPX-heme complex might thus play a role in heme homeostasis by shifting the binding of heme to other proteins and reduce heme degradation under non-stressed conditions. Interestingly, a recent report provides evidence that post-translational oxidative modification of HPX's Tyr199, which is in close structural proximity to R218, also impairs heme binding[62].

The identified ARTC1 target proteins seem to be involved in various pathways controlling muscle function, which might explain the observed reduced endurance of the muscle activity in *Artc1*$^{-/-}$ mice. Whether this observation is only due to skeletal, heart or both muscle tissues needs to be further addressed. Moreover, we could identify different protein interaction clusters of which several proteins were modified by ARTC1. ARTC1 is GPI-anchored and seems to be concentrated in lipid rafts at the cell surface. This topology could regulate ARTC1's specificity to other membrane proteins associated with lipid rafts[16]. The STRING analyses surprisingly identified a modified protein network in the mitochondria in WT tissue, which was not detected in *Artc1*$^{-/-}$ tissue. We found that these mitochondrial ADP-ribosylation sites are lower abundant than the extracellular ARTC1 targets making them more prone to biological as well as sample and measurement variations.

Together, using a new MS-based workflow, we identified and compared the ADP-ribosylomes of the murine skeletal muscle and heart tissue and we showed that they are largely ARTC1-dependent. Furthermore, our system level analyses show that, *in vivo,* ARTC1 has an immense target space, which is remarkably stable. Ultimately, we also provided evidence for a functional role of ARTC1-mediated ADP-ribosylation in muscle by showing that heme-binding of HPX is sensitive to ADP-ribosylation and that *Artc1*$^{-/-}$ mice exhibit reduced endurance. We provide a rich resource for ARTC mediated ADP-ribosylation research, which was so far limited to a few targets and cumbersome biochemical identification of sites by site directed mutations and *in vitro* experiments. The ADPr-acceptor site localization database that we provide here is the first, and most comprehensive HCD and EThcD ADPr spectra resource of primary tissue that has been made public to the research community and can also be used by researchers as a resource to further investigate the functional implication of ADP-ribosylation in muscle tissues.

ACKNOWLEDGMENTS

We would like to thank Tobias Suter, Deena Leslie Pedrioli and Kathrin Nowak (University of Zurich) for the helpful discussions and for providing editorial assistance. We also thank Paolo Nanni, Christian Panse and Jonas Grossmann from the Functional Genomics Center of the University of Zurich for helpful discussions and advise. We thank Marion Nissen and Fabienne Seyfried, Hamburg, for excellent technical assistance. B.R. thanks Drs. Nigel Killeen and Dan Litmann for their support with ES cell transfections and blastocyst injections and their generous hospitality during his stay as a visiting scientist in their lab at the University of California at San Francisco. This work was supported by grants No310/6 and SFB877/A5 from the DFG to F.K.N. M.L. is supported by the Forschungskredit of the University of Zurich. ADP-ribosylation research in the laboratory of MOH is funded by the Kanton of Zurich and the Swiss National Science Foundation (grant 310030_157019).

AUTHOR CONTRIBUTIONS

M.L., S.M., F.K.N. and M.O.H conceived the project and performed data analysis. M.L. performed sample preparation and together with P.G. mass spectrometry analysis. R.B., B.R. and A.Z. generated and analyzed *Artc1*$^{-/-}$ mice. M.L., and M.O.H. prepared the manuscript. M.O.H and F.K.N directed and supervised all aspects of the study. All authors critically reviewed the manuscript.

COMPETING FINANCIAL INTERESTS

The authors declare no competing financial interests.

References

1. Corda, D. & Di Girolamo, M. Functional aspects of protein mono-ADP-ribosylation. *EMBO J* **22**, 1953-8 (2003).
2. Ueda, K. & Hayaishi, O. ADP-ribosylation. *Annu Rev Biochem* **54**, 73-100 (1985).
3. Koch, T. & Ruger, W. The ADP-ribosyltransferases (gpAlt) of bacteriophages T2, T4, and T6: sequencing of the genes and comparison of their products. *Virology* **203**, 294-8 (1994).
4. Hottiger, M.O. Nuclear ADP-Ribosylation and Its Role in Chromatin Plasticity, Cell Differentiation, and Epigenetics. *Annu Rev Biochem* **84**, 227-63 (2015).
5. Hottiger, M.O., Hassa, P.O., Luscher, B., Schuler, H. & Koch-Nolte, F. Toward a unified nomenclature for mammalian ADP-ribosyltransferases. *Trends Biochem Sci* **35**, 208-19 (2010).
6. Feijs, K.L., Verheugd, P. & Luscher, B. Expanding functions of intracellular resident mono-ADP-ribosylation in cell physiology. *FEBS J* **280**, 3519-3529 (2013).
7. Koch-Nolte, F. et al. ADP-ribosylation of membrane proteins: unveiling the secrets of a crucial regulatory mechanism in mammalian cells. *Ann Med* **38**, 188-99 (2006).
8. Glowacki, G. et al. The family of toxin-related ecto-ADP-ribosyltransferases in humans and the mouse. *Protein Sci* **11**, 1657-70 (2002).
9. Braren, R., Glowacki, G., Nissen, M., Haag, F. & Koch-Nolte, F. Molecular characterization and expression of the gene for mouse NAD+:arginine ecto-mono(ADP-ribosyl)transferase, Art1. *Biochem J* **336 (Pt 3)**, 561-8 (1998).
10. Glowacki, G. et al. Structure, chromosomal localization, and expression of the gene for mouse ecto-mono(ADP-ribosyl)transferase ART5. *Gene* **275**, 267-77 (2001).
11. Laing, S., Unger, M., Koch-Nolte, F. & Haag, F. ADP-ribosylation of arginine. *Amino acids* **41**, 257-69 (2011).
12. Koch-Nolte, F., Fischer, S., Haag, F. & Ziegler, M. Compartmentation of NAD+-dependent signalling. *FEBS Lett* **585**, 1651-6 (2011).
13. Davies, C.A. et al. Simultaneous analysis of nitrite, nitrate and the nicotinamide nucleotides by capillary electrophoresis: application to biochemical studies and human extracellular fluids. *Electrophoresis* **20**, 2111-7 (1999).
14. Haag, F. et al. Extracellular NAD and ATP: Partners in immune cell modulation. *Purinergic Signal* **3**, 71-81 (2007).
15. Scheuplein, F. et al. NAD+ and ATP released from injured cells induce P2X7-dependent shedding of CD62L and externalization of phosphatidylserine by murine T cells. *J Immunol* **182**, 2898-908 (2009).
16. Seman, M., Adriouch, S., Haag, F. & Koch-Nolte, F. Ecto-ADP-ribosyltransferases (ARTs): emerging actors in cell communication and signaling. *Curr Med Chem* **11**, 857-72 (2004).
17. Adriouch, S. et al. NAD+ released during inflammation participates in T cell homeostasis by inducing ART2-mediated death of naive T cells in vivo. *J Immunol* **179**, 186-94 (2007).
18. Bruzzone, S., Guida, L., Zocchi, E., Franco, L. & De Flora, A. Connexin 43 hemi channels mediate Ca2+-regulated transmembrane NAD+ fluxes in intact cells. *FASEB J* **15**, 10-12 (2001).

19. Burnstock, G. Pathophysiology and therapeutic potential of purinergic signaling. *Pharmacol Rev* **58**, 58-86 (2006).
20. Burnstock, G. & Kennedy, C. P2X receptors in health and disease. *Adv Pharmacol* **61**, 333-72 (2011).
21. Koch-Nolte, F. & Ziegler, M. Physiology of ADP-ribosylation. *FEBS J* **280**, 3483 (2013).
22. Matzinger, P. The danger model: a renewed sense of self. *Science* **296**, 301-5 (2002).
23. Adriouch, S. et al. ADP-ribosylation at R125 gates the P2X7 ion channel by presenting a covalent ligand to its nucleotide binding site. *FASEB J* **22**, 861-9 (2008).
24. Bartlett, R., Stokes, L. & Sluyter, R. The P2X7 receptor channel: recent developments and the use of P2X7 antagonists in models of disease. *Pharmacol Rev* **66**, 638-75 (2014).
25. Menzel, S. et al. Nucleotide-Induced Membrane-Proximal Proteolysis Controls the Substrate Specificity of T Cell Ecto-ADP-Ribosyltransferase ARTC2.2. *J Immunol* **195**, 2057-66 (2015).
26. Paone, G. et al. ADP ribosylation of human neutrophil peptide-1 regulates its biological properties. *Proc Natl Acad Sci U S A* **99**, 8231-5 (2002).
27. Stevens, L.A., Levine, R.L., Gochuico, B.R. & Moss, J. ADP-ribosylation of human defensin HNP-1 results in the replacement of the modified arginine with the noncoded amino acid ornithine. *Proc Natl Acad Sci U S A* **106**, 19796-800 (2009).
28. Fabrizio, G. et al. ARTC1-mediated ADP-ribosylation of GRP78/BiP: a new player in endoplasmic-reticulum stress responses. *Cell Mol Life Sci* **72**, 1209-25 (2015).
29. Zolkiewska, A. & Moss, J. Integrin alpha 7 as substrate for a glycosylphosphatidylinositol-anchored ADP-ribosyltransferase on the surface of skeletal muscle cells. *J Biol Chem* **268**, 25273-6 (1993).
30. Okazaki, I.J. & Moss, J. Characterization of glycosylphosphatidylinositiol-anchored, secreted, and intracellular vertebrate mono-ADP-ribosyltransferases. *Annu Rev Nutr* **19**, 485-509 (1999).
31. Zhao, Z., Gruszczynska-Biegala, J. & Zolkiewska, A. ADP-ribosylation of integrin alpha7 modulates the binding of integrin alpha7beta1 to laminin. *Biochem J* **385**, 309-17 (2005).
32. Martello, R. et al. Proteome-wide identification of the endogenous ADP-ribosylome of mammalian cells and tissue. *Nat Commun* **7**, 12917 (2016).
33. Bilan, V., Leutert, M., Nanni, P., Panse, C. & Hottiger, M.O. Combining HCD and EThcD fragmentation in a product dependent-manner confidently assigns proteome-wide ADP-ribose acceptor sites. *Anal Chem* **89**, 1523-1530 (2017).
34. Daniels, C.M., Ong, S.E. & Leung, A.K. Phosphoproteomic Approach to Characterize Protein Mono- and Poly(ADP-ribosyl)ation Sites from Cells. *J Proteome Res* **13**, 3510-22 (2014).
35. Gibson, B.A. et al. Chemical genetic discovery of PARP targets reveals a role for PARP-1 in transcription elongation. *Science* **353**, 45-50 (2016).
36. Bannas, P. et al. Activity and specificity of toxin-related mouse T cell ecto-ADP-ribosyltransferase ART2.2 depends on its association with lipid rafts. *Blood* **105**, 3663-70 (2005).
37. Koch-Nolte, F., Kernstock, S., Mueller-Dieckmann, C., Weiss, M. & Haag, F. Mammalian ADP-ribosyltransferases and ADP-ribosylhydrolases. *Front Biosci* **13**, 6716-29 (2008).

38. Koch-Nolte, F. et al. A new monoclonal antibody detects a developmentally regulated mouse ecto-ADP-ribosyltransferase on T cells: subset distribution, inbred strain variation, and modulation upon T cell activation. *J Immunol* **163**, 6014-22 (1999).
39. Bilan, V. et al. New quantitative mass spectrometry approaches reveal different ADP-ribosylation phases dependent on the levels of oxidative stress. *Molecular and Cellular Proteomics* (2017).
40. Leidecker, O. et al. Serine is a new target residue for endogenous ADP-ribosylation on histones. *Nat Chem Biol* **12**, 998-1000 (2016).
41. Szklarczyk, D. et al. STRING v10: protein-protein interaction networks, integrated over the tree of life. *Nucleic Acids Res* **43**, D447-52 (2015).
42. *Endogenous ADP-Ribosylation*, VIII, 213 (Springer International Publishing, 2015).
43. Larsen, S.C. et al. Proteome-Wide Identification of In Vivo ADP-Ribose Acceptor Sites by Liquid Chromatography-Tandem Mass Spectrometry. *Methods Mol Biol* **1608**, 149-162 (2017).
44. Poulsen, J.W., Madsen, C.T., Young, C., Poulsen, F.M. & Nielsen, M.L. Using guanidine-hydrochloride for fast and efficient protein digestion and single-step affinity-purification mass spectrometry. *J Proteome Res* **12**, 1020-30 (2013).
45. Kawahara, R. et al. Mass spectrometry-based proteomics revealed Glypican-1 as a novel ADAM17 substrate. *J Proteomics* **151**, 53-65 (2017).
46. Buchanan, P.C. et al. Ectodomain shedding of the cell adhesion molecule Nectin-4 in ovarian cancer is mediated by ADAM10 and ADAM17. *J Biol Chem* **292**, 6339-6351 (2017).
47. Sakry, D. et al. Oligodendrocyte precursor cells modulate the neuronal network by activity-dependent ectodomain cleavage of glial NG2. *PLoS Biol* **12**, e1001993 (2014).
48. Janes, P.W. et al. Cytoplasmic relaxation of active Eph controls ephrin shedding by ADAM10. *PLoS Biol* **7**, e1000215 (2009).
49. Osago, H. et al. Precursor ion scanning and sequencing of arginine-ADP-ribosylated peptide by mass spectrometry. *Anal Biochem* **393**, 248-54 (2009).
50. Bilan, V., Leutert, M., Nanni, P., Panse, C. & Hottiger, M.O. Combining Higher-Energy Collision Dissociation and Electron-Transfer/Higher-Energy Collision Dissociation Fragmentation in a Product-Dependent Manner Confidently Assigns Proteomewide ADP-Ribose Acceptor Sites. *Analytical chemistry* **89**, 1523-1530 (2017).
51. Nanni, P. et al. PTM MarkerFinder, a software tool to detect and validate spectra from peptides carrying post-translational modifications. *Proteomics* **13**, 2251-5 (2013).
52. Bonfiglio, J.J. et al. Serine ADP-Ribosylation Depends on HPF1. *Mol Cell* **65**, 932-940 e6 (2017).
53. Tolosano, E. & Altruda, F. Hemopexin: structure, function, and regulation. *DNA Cell Biol* **21**, 297-306 (2002).
54. Zolkiewska, A. & Moss, J. Processing of ADP-ribosylated integrin alpha 7 in skeletal muscle myotubes. *J Biol Chem* **270**, 9227-33 (1995).
55. Deshmukh, A.S. et al. Deep proteomics of mouse skeletal muscle enables quantitation of protein isoforms, metabolic pathways, and transcription factors. *Mol Cell Proteomics* **14**, 841-53 (2015).
56. Ruoslahti, E. RGD and other recognition sequences for integrins. *Annu Rev Cell Dev Biol* **12**, 697-715 (1996).

57. Rosenthal, F. & Hottiger, M.O. Identification of ADP-ribosylated peptides and ADP-ribose acceptor sites. *Front Biosci (Landmark Ed)* **19**, 1041-56 (2014).
58. Lau, E. et al. A large dataset of protein dynamics in the mammalian heart proteome. *Sci Data* **3**, 160015 (2016).
59. Fasano, M. et al. The extraordinary ligand binding properties of human serum albumin. *IUBMB Life* **57**, 787-96 (2005).
60. Hvidberg, V. et al. Identification of the receptor scavenging hemopexin-heme complexes. *Blood* **106**, 2572-9 (2005).
61. Yang, Z. et al. Kinetics and specificity of feline leukemia virus subgroup C receptor (FLVCR) export function and its dependence on hemopexin. *J Biol Chem* **285**, 28874-82 (2010).
62. Hahl, P. et al. Identification of oxidative modifications of hemopexin and their predicted physiological relevance. *J Biol Chem* **292**, 13658-13671 (2017).
63. Koch-Nolte, F. et al. Use of genetic immunization to raise antibodies recognizing toxin-related cell surface ADP-ribosyltransferases in native conformation. *Cell Immunol* **236**, 66-71 (2005).
64. Wisniewski, J.R., Zougman, A., Nagaraj, N. & Mann, M. Universal sample preparation method for proteome analysis. *Nat Methods* **6**, 359-62 (2009).
65. Eden, E., Navon, R., Steinfeld, I., Lipson, D. & Yakhini, Z. GOrilla: a tool for discovery and visualization of enriched GO terms in ranked gene lists. *BMC Bioinformatics* **10**, 48 (2009).
66. Chou, M.F. & Schwartz, D. Biological sequence motif discovery using motif-x. *Curr Protoc Bioinformatics* **Chapter 13**, Unit 13 15-24 (2011).
67. Paoli, M. et al. Crystal structure of hemopexin reveals a novel high-affinity heme site formed between two beta-propeller domains. *Nat Struct Biol* **6**, 926-31 (1999).
68. Vizcaino, J.A. et al. 2016 update of the PRIDE database and its related tools. *Nucleic Acids Res* **44**, D447-56 (2016).

Material and Methods

All chemicals were purchased from Sigma unless otherwise stated.

Generation and characterization of *Artc1*$^{-/-}$ mice

Mice were obtained from the Animal Resources Units of the University of California at San Francisco and the University Hospital, Hamburg. A targeting vector for the *Art1* locus was constructed in which loxP sites were introduced up- and downstream of the *Art1*-encoding exons 3 and 4 and a pgk-neomycin resistance cassette. The targeting construct was linearized with NotI and transfected into RF8 ES cells. Neomycin resistant clones were screened by Southern Blot analyses using informative 5' and 3' flanking probes. Two of 600 tested clones showed additional bands indicating homologous recombination at the target locus. Following injection of these ES cells into B6 blastocysts, chimeric male and female mice were obtained. Germline transmission of the targeted locus was obtained for both clones upon mating of chimeric and B6 mice. PCR analyses using primers flanking the distal loxP site confirmed the presence and Mendelian inheritance of this site. *Art1* floxed mice were mated with mice expressing the cre recombinase under control of the ß-actin promoter (deleter mice). PCR analyses using primers from the neomycin gene and the 3' flanking region of the ART1 gene yielded a diagnostic band in progeny but not parental mice, indicating deletion of exons 3 and 4 in the targeted *Art1* allele. *Artc1*$^{-/-}$ mice were backcrossed onto the C57Bl/6 background for 12 generations. Sex and age matched adult WT and *Artc1*$^{-/-}$ mice were monitored for voluntary activity using the Mouse E-Motion universal mobile datalogger system (INFRA-E-MOTION GmbH, Hamburg, Germany). Mice were placed in individual cages and movements were recorded in three consecutive 12 h light/12 h dark cycles. Endurance of muscle activity was assessed using the rotarod performance system (TSE systems, Bad Homburg, Germany). For this, mice were adapted to the rotarod at low speed (4 rpm) in trials 1 and 2. Trials 3-5 were then performed at an accelerated speed (8 rpm) with a pause of 45 min between each trial. Trial 6 was performed the next day at the accelerated speed. The maximum duration of mice on the rotarod was 5 min.

Cell Culture and Treatments

The mouse skeletal muscle cell line C2C12 was maintained below 60% confluence in Dulbecco's modified Eagle's medium (DMEM) supplemented with 20% fetal calf serum and 1x penicillin/streptomycin (Invitrogen). For differentiation into myotubes, growth medium was exchanged for DMEM supplemented with 0.5% fetal calf serum and 1x penicillin/streptomycin (Invitrogen). For the NAD^+ treatment cells were washed twice with serum free DMEM and subsequently treatment was performed for 30min in serum free DMEM containing 50 μM NAD^+.

Primary myoblasts were isolated from hindlimbs and forelimbs of neonatal mice (2-5 days old). The muscle tissue was incubated in Dulbecco's phosphate-buffered saline (DPBS) with 1% collagenase II

(Invitrogen), 2.4U/ml dispase II (Roche) and 2.5 mM $CaCl_2$ for 45 minutes at 37°C, and then passed through 100µm-nylon mesh filter (BD Biosciences). The filtrate was centrifuged, the cell pellet was suspended in Ham's F-10 medium (Cambrex) containing 20% FBS and 1% penicillin/streptomycin, pre-plated for 30 minutes on collagen I-coated plates, and then plated on tissue culture-treated plastic plates. To stimulate differentiation of myoblasts to myotubes, 90-100% confluent myoblasts were incubated for 3 days in medium containing 2% horse serum.

Mouse treatment and organ harvesting for proteomic experiment.

WT and *ARTC1*$^{-/-}$ C57BL/6 mice were maintained on a 12-h light-dark cycle with regular unrestricted diet. WT (male, 15weeks) and *ARTC1*$^{-/-}$ (male, 9 weeks) mice were injected with 10 mg NAD^+ or stayed untreated and sacrificed after 30 min. Mice (n=3 per group) were anesthetized with isofluran and perfused with PBS containing 1 mM Novobiocin. Heart and skeletal muscle from legs were collected and immediately snap-frozen in liquid nitrogen. All samples were stored at -80°C. In order to optimize the analysis and to rule out ADP-ribosylation artifacts induced by stress and lysis, we evaluated different sample preparation methods and decided for a strongly denaturing Gnd-HCl lysis protocol and *in vivo* perfusion with the ARTC inhibitor Novobiocin. An additional Novobiocin treatment 30 min before euthanasia of the animals did not lead to further reduction in the ARTC1-dependent ADP-ribosylome and was thus judged to be unnecessary (**Suppl. Figure 3E**).

Gene expression

RNA extraction was performed with the NucleoSpin RNA II kit (Macherey-Nagel). Mouse tissue samples were lysed using a tissue lyser II (Qiagen) with the provided lysis buffer. C2C12 myotubes cells were washed with PBS, before lysis with the same buffer. After RNA extraction RNA was quantified with a NanoDrop (Thermo Fisher Scientific) and reverse transcribed according to the supplier's protocol (High Capacity cDNA Reverse Transcription Kit, Applied Biosystems). Quantitative real-time polymerase chain reactions (qPCR) were performed with KAPA SYBR fast (Kapa Biosystems) and a Rotor-Gene Q 2plex HRM System (Qiagen).

Immunoblotting

Three-month old wild-type and *Artc1*$^{-/-}$ mice were euthanized by CO_2 inhalation in accordance with a protocol approved by the Kansas State University Institutional Animal Care and Use Committee. Hind limb muscles were excised, ground, and homogenized in 50 mM Tris-Cl, pH 7.4, 150 mM NaCl, 50 mM octylglucoside, 1 mM AEBSF, 5 mg/ml aprotinin, 5 mg/ml leupeptin, 5 mg/ml pepstatin A (5 ml homogenization buffer/1 g tissue). The homogenate was centrifuged at 13,000g for 20 min, the supernatant was filtered through a 0.45 mm filter, and incubated with 0.2 ml of Concanavalin A agarose

beads at 4°C for 2 h with gentle shaking. The beads were washed with 5 ml of homogenization buffer and eluted with SDS-PAGE loading buffer, the eluate was resolved by SDS-PAGE and transferred to a nitrocellulose membrane. The membrane was blocked with 3% (w/v) dry milk and 0.3% (v/v) Tween-20 in DPBS, then incubated with goat anti-ART1 antibody (Santa Cruz, S-15; 1:200 dilution in blocking buffer), followed by incubation with horseradish peroxidase-labeled secondary antibody and detection using the WestPico chemiluminescence kit (Pierce).

ADP-ribosylation reaction on cells

Differentiated primary myoblasts (myotubes) were washed with DPBS and incubated for 30 min in DPBS (with Ca^{2+} and Mg^{2+}) containing 5 mM [adenylate-^{32}P] NAD^+ and 1 mM ADP-ribose. Cellular proteins were extracted with extraction buffer (50mM Tris-HCl, pH 7.4, 150 mM NaCl, 1 mM ADP-ribose, 1% Triton X-100, 1% sodium deoxycholate, 0.1% SDS, 1 mM 4-(2-aminoethyl)-benzene-sulfonylfluoride hydrochloride (AEBSF), 5 mg/ml aprotinin, 5 mg/ml leupeptin, 5 mg/ml pepstatin A, 10 mM 1,10-phenanthroline; 0.5 ml extraction buffer/well in a 6-well plate). Cell extracts were centrifuged at 21,000g for 15 min, and supernatants were analyzed by autoradiography after SDS-PAGE under reducing conditions.

ADP-ribosylation reaction with recombinant proteins

Recombinant mouse ARTC1 was purified from DC27.10 lymphoma cells stably transfected with FLAG-tagged ARTC1[63]. DC27.10_ARTC1 cells were incubated with Phospholipase C (Sigma) for 1 h at 37°C. Cell supernatants were clarified by centrifugation (20 min, 2000 3 g) and ARTC1 was purified by affinity chromatography on agarose immobilized anti-FLAG mAb M2 (Sigma). The column was washed with PBS, 1% Triton X-100 and ARTC1 was eluted with 100 mM glycine, 10 mM Tris (pH 2.7). The eluate was neutralized with one-tenth volume of 1 M Tris (pH 9.0) and the buffer was exchanged to PBS by gel filtration (PD-10 columns; Pharmacia). ARTC1 was concentrated using centrifugal filters (Millipore; molecular weight cutoff 10 kDa). Recombinant mouse hemopexin was purchased from Sino Biological. To monitor trans ADP-ribosylation of HPX by radiography we incubated 50nM ARTC1 with 2.5 μM HPX using 0.5 μCi [^{32}P]-NAD^+ (Perkin Elmer) in PBS and incubated at 37 °C for 30min or 60min. For some reactions 10μM Novobiocin or 10μM heme was added. Reactions were stopped by adding SDS-loading buffer, with subsequent boiling at 95 °C for 5 min. Samples were run on an SDS-PAGE gel, stained with Coomassie blue, photographed, destained, and exposed on phosphorscreens overnight. Images were taken with a Typhoon FLA 9400 phosphorimager (GE Healthcare).

For the Heme-HPX binding assay as well as for subsequent MS analysis 10 μM HPX was incubated with 100 μM NAD^+ with or without 250 nM ARTC1 in PBS, overnight at 37 °C. The next day, indicated amounts of heme were added to the reaction, incubated at 37 °C and absorbance was measured

with a NanoDrop (Thermo Fisher Scientific) and the OD at 413 nM was quantified for the different reactions. All reactions were done and measured as independent triplicates.

ADPr-peptide enrichment

C2C12 cells were washed twice with PBS and subsequently lysed and scraped by adding 95°C Gnd-HCL-lysis buffer (6 M guanidine-hydrochloride, 5 mM tris(2-carboxyethyl)phosphine (TCEP), 10mM chloroacetamide (CAA), in 100 mM Tris pH 8). Frozen murine heart and skeletal muscle samples were added to 95 °C Gnd-HCL-lysis buffer and ground in a tissue lyser II (Qiagen), for 3min at 30hz. Samples were subsequently incubated at 95 °C for 10min and sonicated for 1min at an amplitude of 30%. Lysate was cleared by centrifugation at 4000g, ten times diluted with 25 mM Tris pH 8, and digested with sequencing grade trypsin (Promega). The peptide mixture was treated with PARG enzyme to reduce potentially PARylated peptide to MARylated peptides, and the peptides were enriched using an Af1521 macrodomain affinity enrichment and prepared for MS analysis as described previously[32]. The in vitro modified HPX protein was processed using filter aided sample preparation (FASP) protocol using Microcon-30-kDa-cutoff filter units (Milipore) and sequencing grade trypsin (Promega)[64].

Liquid chromatography and mass spectrometry analysis

Identification of ADP-ribosylated peptides from C2C12, skeletal muscle, heart and recombinant HPX was performed on an Orbitrap Fusion Tribrid mass spectrometer (Thermo Fisher Scientific), coupled to a nano EasyLC 1000 liquid chromatograph (Thermo Fisher Scientific). We applied an ADP-ribose product-dependent method called HCD-PP-EThcD[33] Briefly, the method includes high-energy data-dependent HCD, followed by high-quality HCD and EThcD MS/MS when two or more ADP-ribose fragment peaks (136.0623, 250.0940, 348.07091, and 428.0372) were observed in the HCD scan. A detailed description of the MS parameters can be found in[33]. Solvent compositions in channels A and B were 0.1% formic acid in H2O and 0.1% formic acid in acetonitrile, respectively. Peptides were loaded onto an Acclaim PepMap 100 (Thermo Scientific) trap column, 75 µm x 2 cm, packed with C18 material, 3 µm, 100 Å, and separated on an analytical EASY-Spray column (Thermo Scientific, 75 µm × 500 mm) packed with reverse-phase C18 material (PepMap RSLC, 2 µm, 100 Å). Peptides were eluted over 110 min at a flow rate of 300 nL/min. An elution gradient protocol from 2% to 25% B, followed by two steps, 35% B for 5 min and 95% B for 5 min, was used.

Heart samples were additionally analyzed using an Orbitrap Q Exactive HF mass spectrometer (Thermo Fisher Scientific) coupled to a nano EasyLC 1000 (Thermo Fisher Scientific). The peptides were loaded onto a reverse-phase C18 (ReproSil-Pur 120 C18-AQ, 1.9 µm, Dr. Maisch GmbH) packed self-made column (75 µm × 150 mm) that was connected to an empty Picotip emitter (New Objective, Woburn, MA). Peptides were injected into the MS at a flow rate of 300 nL/min and were separated using a

90 minute gradient of 2% to 25% buffer B. The MS was set to acquire full-scan MS spectra (300–1700 *m*/*z*) at a resolution of 60,000 after accumulation to an automated gain control (AGC) target value of 3×10^6. Charge state screening was enabled, and unassigned charge states and single charged precursors were excluded. Ions were isolated using a quadrupole mass filter with a 2 *m*/*z* isolation window. The maximum injection time was set to 240 ms and HCD fragmentation performed at 28% normalized collision energy. Finally, selected ions were dynamically excluded for 20 seconds.

Raw mass spectrometry data analysis and label free quantification

MS and MS/MS spectra were converted to Mascot generic format (MGF) by use of Proteome Discoverer, v2.1 (Thermo Fisher Scientific, Bremen, Germany). When multiple fragmentation techniques (HCD and EThcD) were utilized, separate MGF files were created from the raw file for each type of fragmentation. MGF files were further processed[33]. The MGFs were searched against the UniProtKB mouse database (taxonomy 10090, version 20160902), which included 24'905 Swiss-Prot, 34'616 TrEMBL entries, 59'783 reverse sequences, and 262 common contaminants.

Mascot 2.5.1.3 (Matrix Science) was used for peptide sequence identification with previously described search settings and some modification for the EThcD searches[33]. Enzyme specificity was set to trypsin, allowing up to 4 missed cleavages. The ADP-ribose variable modification was set to a mass shift of 541.0611, with scoring of the neutral losses equal to 347.0631 and 249.0862. The marker ions at m/z 428.0372, 348.0709, 250.0940, 136.0623 were ignored for scoring. Ser, Arg, Lys, Asp and Glu residues were set as variable ADP-ribose acceptor sites. Carbamidomethylation was set as a fixed modification on C and oxidation as a variable modification on M. Peptides are considered correctly identified when a Mascot score >20 and an expectation value <0.05 are obtained. For the ADP-ribosylation site analyses, peptides identified with EThcD fragmentation, having a mascot localization score > 90% were used if not stated otherwise.

To perform label-free quantification based on the MS1 precursor peak area of the identified peptides and proteins, Progenesis QI software (v. 3.0.6039.34628, Nonlinear Dynamics, Purham, NC) was applied. Raw data was imported into Progenesis and aligned based on the MS1 peak retention time. All samples were normalized based on the total signal intensity. The obtained results were exported as MGF and searched with Mascot as indicated above. The Mascot search results were imported into Scaffold software (v.4.7.2) and filtered for protein and peptide FDR values of 1% and 0.5% respectively. When multiple precursors were observed for the same peptide, the values were summed up to obtain the total level of the peptide.

Bioinformatic analyses

Statistical analysis, volcano plot analysis, principal component analysis and hierarchical clustering were performed using the Perseus software suite (Max Planck Institute of Biochemistry, Department of Proteomics and Signal Transduction, Munich). Normalized LFQ intensities were imported and missing values were imputed.

For GO enrichment analyses the GOrilla online tool[65] was applied, using a C2C12 myotube, a mouse skeletal muscle or a mouse heart proteome as background [55,58]. A p-value threshold of 10^{-3} was set and higher-ranking terms were chosen from GO Biological Processes, GO Molecular Functions, GO Cellular Compartments or Kyoto Encyclopedia of Genes and Genomes (KEGG) for display.

Protein-protein interactions in between ADP-ribosylated protein were analyzed using the interaction data from the STRING database (v. 10.5) using high confidence interaction scores (≥0.7) and hiding disconnected ADP-ribosylated nodes from the network. Significantly enriched, interesting GO Biological Processes and KEGG pathway terms were annotated according to the STRING database and GO Cellular Compartments were annotated using the PANTHER database.

The heart samples measured on the Q Exactive HF MS, using a non-product dependent HCD fragmentation method, were used to extract MS2 ADP-ribose marker ion patterns from the Mascot ouput.dat files. For this we used the PTM marker finder tool and following marker ions were included 136.0618, 250.0935, 348.0704, 428.0367 and 584.0901 [51]. Only spectra were considered where at least four marker ions were identified with an intensity of at least 5% of the highest peak and a mascot score of >20.

For the ADP-ribosylation site motif analysis we used the web-based motif-x program[66]. We included all Arg-ADPr sites identified with a localization score >90% for the analysis. A p-value threshold <0.0005 was chosen for the binomial probability and a 21 amino acid window with the ADP-ribosylation site in the center was analyzed against the whole mouse proteome as a background. All identified motifs were reported as a 13 amino acid windows. Their fraction to all analyzed sites is indicated as well as the motif score. The motif score is the sum of the negative log probabilities used to fix each position of the reported motif. The higher the score the more statistically significant and specific the motif.

The protein structure of HPX [67] was visualized an annotated using PyMOL v1.7.4. All Venn diagrams were generated using biovenn (http://www.biovenn.nl).

Data availability

The mass spectrometry proteomics data for the C2C12 cells, the mouse skeletal and heart muscle tissues, including the RAW files, peak list files (MGFs), and result files (mzIdent) have been deposited to the ProteomeXchange Consortium via the PRIDE[68] partner repository with the dataset identifier PXD008041 and 10.6019/PXD008041. The additional data that support the findings of this study are available from the corresponding author on request.

Figure legends:

Figure 1 – Profiling of ADP-ribosylation in mouse myotubes

A) Increase in unique ADP-ribosylated peptides after NAD^+ treatment of C2C12 myotubes. Venn diagram of identified unique ADP-ribosylated peptides in C2C12 myotubes left untreated or treated with 50 μM NAD^+.

B) R-ADP-ribosylation is specifically induced upon NAD^+ treatment of C2C12 myotubes. Identified unique ADP-ribose acceptor sites in C2C12 myotubes left untreated or treated with 50 μM NAD^+ (n=3; bar graph represents mean and SD).

C) Term-enrichment analysis displaying significantly enriched (P<0.001) gene ontology terms of the identified ADP-ribosylated proteins (n=85) according to their cellular localization, molecular function and the biological processes. Term enrichment is calculated relative to a deep C2C12 myotube proteome (n=8476) [55]. Numbers in parentheses indicate participation size and category size, respectively.

D) Unsupervised hierarchical clustering analysis of normalized intensity values determined by MS1 based label free quantification of detected ADP-ribosylation sites. A black cell corresponds to not present or a relatively low abundant ADP-ribosylation site, blue indicates a site of intermediate abundance and green a highly abundant site. Protein names for three indicated clusters, where ADPr peptides are observed already under untreated conditions are indicated. Names in bold correspond to proteins with a function in biological adhesion.

E) STRING database analysis of high confidence protein interactions (interaction score >0.7) between identified ADP-ribosylated proteins in C2C12 cells. Only ADP-ribosylated proteins with at least one interaction with another ADP-ribosylated protein are shown. Subcellular localization and biological process are annotated.

Figure 2 – Characterization of the *Artc1*$^{-/-}$ mouse

A) Western blotting of glycoprotein-enriched muscle extracts using anti-ART1 antibody confirmed the absence of the 39-kDa ART1 protein in *Art1c*$^{-/-}$ mice. Two different mice of WT and *Artc1*$^{-/-}$ genotype were analyzed.

B) Adult male *Artc1*$^{-/-}$ mice (n= 8) have similar average weights as their WT litter mates (n=9; bar graph represents mean and SD).

C) Monitoring of voluntary activity using the Mouse E-Motion system. Mice were placed in individual cages and movements were recorded in three consecutive 12 h light/12 h dark cycles. Data points represent the activity of individual mice over 72 h, expressed as the movement index +/- SEM (student's t-test).

D) Endurance of muscle activity was assessed using the rotarod performance system. Mice were adapted to the rotarod at low speed (4 rpm) in trials 1 and 2. Trials 3-5 were then performed at an accelerated speed (8 rpm) with a pause of 45 min between each trial. Trial 6 was performed the next day at the accelerated speed. The maximum duration of mice on the rotarod was 5 min. The latency to fall for each group is expressed as mean +/- SEM (student's t test $p < 0.05$ = *; $p < 0.01$ = **).

E) Primary myoblasts isolated from 6 littermate pups (genotypes shown at the top, mice numbers at the bottom), differentiated (D) *in vitro* into myotubes or undifferentiated (U), were incubated with [32P]-NAD^+ and analyzed by SDS-PAGE and autoradiography (left panel) or Coomassie blue-staining (right panel). Position of ADP-ribosylated integrin α7 is indicated by arrow, molecular weight markers (kDa) are on the right.

Figure 3 – Analysis of skeletal muscle

A) The ADP-ribosylome of skeletal muscle is strongly dependent on ARTC1. Venn diagram of unique identified ADP-ribosylated peptides in skeletal muscle tissue from WT and *Artc1*$^{-/-}$ mice (3 animals per group).

B) R-ADP-ribosylation in skeletal muscle tissue is strongly ARTC1-dependent. Identified ADP-ribose acceptor sites in WT and *Artc1*$^{-/-}$ skeletal muscle tissue (n=3; bar graph represents mean and SD).

C) Histogram analysis shows that the majority (78%) of ADP-ribosylated skeletal muscle proteins carry only one ADPr modification.

D) Term-enrichment analysis displaying significantly enriched (P<0.001) gene ontology terms of the identified ADP-ribosylated proteins in WT (n=573) and *Artc1*$^{-/-}$ (n=33) tissue according to their cellular localization and the biological processes. Term-enrichment is calculated relative to a deep mouse skeletal muscle proteome (n=5647) [55]. Numbers in parentheses indicate participation size and category size, respectively.

Figure 4 – Profiling of the mouse heart ADP-ribosylome

A) The ADP-ribosylome of the heart tissue is strongly dependent on ARTC1. Venn diagram of unique identified ADP-ribosylated peptides in heart muscle tissue from WT and *Artc1*$^{-/-}$ mice (3 animals per group).

B) R-ADP-ribosylation in skeletal muscle tissue is strongly ARTC1-dependent. Identified ADP-ribose acceptor sites in WT and *Artc1*$^{-/-}$ skeletal muscle tissue (n=3; bar graph represents mean and SD).

C) Histogram analysis shows that the majority (71%) of ADP-ribosylated skeletal muscle proteins carry only one ADPr modification.

D) Term-enrichment analysis displaying significantly enriched (P<0.001) gene ontology terms of the identified ADP-ribosylated proteins in WT (n=131) and *Artc1*$^{-/-}$ (n=26) tissues according to their cellular localization, molecular function and the biological processes. Term enrichment is calculated relative to a deep mouse heart proteome (n=3157) [58]. Numbers in parentheses indicate participation size and category size, respectively.

E) STRING database analysis of high confidence interaction (interaction score >0.7) between identified ADP-ribosylated proteins in heart tissue, dependent on ARTC1 expression. Only ADP-ribosylated proteins with at least one interaction with another ADP-ribosylated protein are shown. Subcellular localization and biological process are annotated.

F) Principal component analysis of ADP-ribosylated peptide abundance separates WT and *Artc1*$^{-/-}$ hearts as well as untreated and NAD^+ treated WT samples (3 animals per group). Analysis done with Perseus.

G) Volcano plot analysis of WT heart untreated versus NAD^+ treated. Significantly different sites are shown in black (FDR<0.5) and ADP-ribosylation sites annotated.

Figure 5 – Arginine ADP-ribosylation marker ions and motifs.

A) MS2 fragmentation pattern of an ADP-ribosylated arginine, indicating ADP-ribose marker ions that should theoretically be generated when using HCD fragmentation, including partial fragmentation of the Arg side chain giving rise to an R-ADPr specific ADPr-carbodiimide marker ion (marked in red).

B) Count of peptide spectra containing ADP-ribose marker ions in measurements of WT and *Artc1*$^{-/-}$ heart samples (3 animals per group). Only spectra containing at least four ADP-ribose marker ions, with an intensity of at least 5% of the highest peak and a mascot score of >20 were considered. Log10 based intensities of specific ADP-ribose marker ions are plotted in a box plot. The Arg specific ADP-ribose marker ion is marked in red and its contribution to the total number of ADP-ribosylated spectra is indicated.

C) R/G and R/R motifs identified at Arg-ADP-ribosylation sites with a localization probability >90% in C2C12 cells, WT muscle and heart tissue compared against the whole mouse proteome as background (binomial test, p< 0.0005) using x-motif [66]. Percentage of all Arg-ADP-ribosylation sites containing the motif and motif score are shown on top of the respective sequence motif.

Figure 6– ARTC1 mediated ADP-ribosylation of HPX interferes with heme binding

A) Autoradiography of mouse hemopexin (HPX) *in vitro* ADP-ribosylation by recombinant mouse ARTC1 or NAD^+ alone. Heme (10µM) was added to some reactions.

B) Autoradiography of mouse hemopexin (HPX) *in vitro* ADP-ribosylation by recombinant mouse ARTC1. Heme (10µM) or Novobiocin (10µM) were added to some reactions.

C) Manual annotation of high resolution HCD (top) and EThcD (bottom) MS2 fragmentation spectrum of a HPX peptide confirms ADP-ribosylation on R218. Spectra were retrieved from measured WT heart tissue and *in vitro* modified HPX, respectively. Y and z ion series are shown in green, b and c ion series in blue, ADP-ribose specific marker ions and neutral losses are indicated in red.

D) Crystal structure of HPX bound to heme (red)[67] with indicated ADP-ribosylation sites. The ADPr sites on Arg218 detected in WT heart and skeletal muscle might interfere with HPX ability to sequester heme due to its very close proximity to the heme-binding site. ADP-ribosylated Arg218 and Arg83 are highlighted.

E) Absorbance measurement of non-modified HPX (HPX incubated with NAD^+) or ADP-ribosylated HPX (HPX incubated with NAD^+ and ARTC1) incubated in the presence of different concentrations of heme. Average absorbance measurement from 300-600 nm for the different reactions in triplicates are shown, the HPX-heme complex absorbs light at 413nm.

F) ARTC1 mediated ADP-ribosylation of HPX inhibits heme binding *in vitro*. Binding was assessed as in E) and OD413 is shown as a bar plot for triplicate measurement of the indicated reactions. (n=3; bar graph represents mean and SD, t-test ** $p<0.01$).

Supplementary Figure 1 - ADP-ribosylation in myotubes

A) RT-qPCR analysis of ARTC1 expression in C2C12 myoblast, C2C12 myotubes and in the mouse heart. The expression of ARTC1 is expressed relative to the house-keeping gene RPS12.

B) Venn diagram of all identified ADP-ribosylated proteins in untreated and NAD^+ treated C2C12 myotubes.

C) Count of identified ADP-ribosylated peptide spectra matches (PSMs) for untreated and NAD^+ treated C2C12 myotubes (n=3;bar graph represents mean and SD).

D) Multi-scatter plot and Pearson correlation coefficients of measured ADP-ribosylated peptide signal intensities from triplicate ADP-ribosylome measurements.

Supplementary Figure 2 – Generation of the *Artc1*$^{-/-}$ mouse

A) Schematic diagram of the conditional *Artc1* targeting construct (tc) in which the neomycin resistance cassette was inserted into the second intron of the ART1 gene. The 3' arm of homology was assembled by PCR, thereby incorporating lox P sites (arrowheads) up- and downstream of the main ART1-encoding exons 3 and 4. The neo cassette and 3' loxp site contained diagnostic NcoI and EcoRI sites, respectively. The targeting construct was linearized with NotI and transfected into RF8 ES cells.

B) Neomycin resistant clones were screened by Southern Blot analyses using informative 5' and 3' flanking probes. Two of 600 tested clones showed additional EcoR1 and Nco1 bands indicating homologous recombination at the target locus.
C) PCR analysis for floxed allel. Following injection of these ES cells into B6 blastocysts, chimeric male and female mice were obtained. Germline transmission of the targeted locus was obtained in both cases upon mating of chimeric and B6 mice. PCR analyses using primers flanking the distal loxP site confirmed the presence and Mendelian inheritance of this site (lanes a: 260 bp band = floxed ART1 vs. 250 bp band = wt ART1). The floxed ART1 site is co-inherited with the linked neo cassette (lanes b).
D) PCR analysis for deleted allel. ART1 floxed mice were mated with mice expressing the cre recombinase under control of an unbiquitous promoter (deleter mice). PCR analyses using primers from the neomycin gene and the 3' flanking region of the ART1 gene yielded a diagnostic 1.5 kb band in progeny but not parental mice, indicating deletion of exons 3 and 4 in the targeted ART1 allele (lanes c).
E) Mice genotyping. PCR reaction with primer set "a" (Art1.3 and Art1.4) yields a diagnostic band of 250 bp for the wild-type and no band for the targeted allele. PCR reaction with primer set "b" (NF1 and Art1.4) yields a diagnostic band of 1.5 kb for the targeted allele and no band for the wild-type allele. Positions of the molecular weights (bp) are shown on the right.
F) Venn diagram comparing unique ADP-ribosylated peptides in triplicates of WT skeletal muscle tissue.
G) Venn diagram comparing unique ADP-ribosylated proteins in skeletal muscle and C2C12 myotubes.

Supplementary Figure 3 – ADP-ribosylation in the mouse heart

A) Count of identified ADP-ribosylated PSMs for untreated and NAD^+ treated WT and *Artc1*$^{-/-}$ hearts (n=3; bar graph represents mean and SD) .
B) Venn diagram comparing unique ADP-ribosylated proteins identified in triplicates of WT and *Artc1*$^{-/-}$ heart tissue, respectively.
C) STRING database analysis of high confidence protein interactions between identified ADP-ribosylated proteins in *Artc1*$^{-/-}$ heart tissue. Only ADP-ribosylated proteins with at least one interaction with another ADP-ribosylated protein are shown. Subcellular localization and biological process are annotated.
D) Venn diagram of all identified ADP-ribosylated proteins in C2C12, skeletal and heart muscle tissue.
E) Count of identified ADP-ribosylated PSMs for different sample preparation protocols for the analysis of endogenous ADP-ribosylated proteins from heart extracts.

Supplementary Figure 4 – ADP-ribosylation in the mouse heart after NAD^+ treatment

A) Count of identified ADP-ribosylated PSMs for untreated and NAD^+ treated WT and *Artc1*$^{-/-}$ hearts (n=3 per condition; mean and SD).

B) Identified ADP-ribose acceptor sites in untreated and NAD^+ treated WT and *Artc1*$^{-/-}$ hearts (n=3 per condition; mean and SD).

C) Multi-scatter plot and Pearson correlation coefficients of measured peptide signal intensities in untreated and NAD^+ treated WT and *Artc1*$^{-/-}$ hearts (n=3 per condition). A Pearson correlation close to 1 signifies high reproducibility in the measured abundance of ADP-ribosylated peptide species.

D) Unsupervised hierarchical clustering analysis of normalized intensity values determined by MS1 based label free quantification of ADPr-peptides detected across all heart samples.

E) LC-MS2 overview of a representative sample for WT and *Artc1*$^{-/-}$ heart samples, respectively. Peptide charge states are color-coded and peptide spectra containing at least four ADP-ribose marker ions are indicated with a black square. ADP-ribosylated peptides show mainly 2^+ and 3^+ charges.

Supplementary Figure 5 – Total protein levels remain unchanged, whereas the ADP-ribosylation site abundance changes for selected proteins identified in untreated and NAD^+ treated hearts

Low-high bar graphs with indicate means of total protein or APD-ribosylated peptide abundances in hearts of untreated or NAD^+-treated WT animals are shown. Data was produced using MS1 label free quantification of non-enriched or Af1521 enriched samples, respectively (3 animals per group). Unpaired t-test was performed (*P<0.05, **P <0.01, ***P <0.001)

Supplementary Tables 1-3

Figure 1 - Profiling of ADP-ribosylation in mouse myotubes.

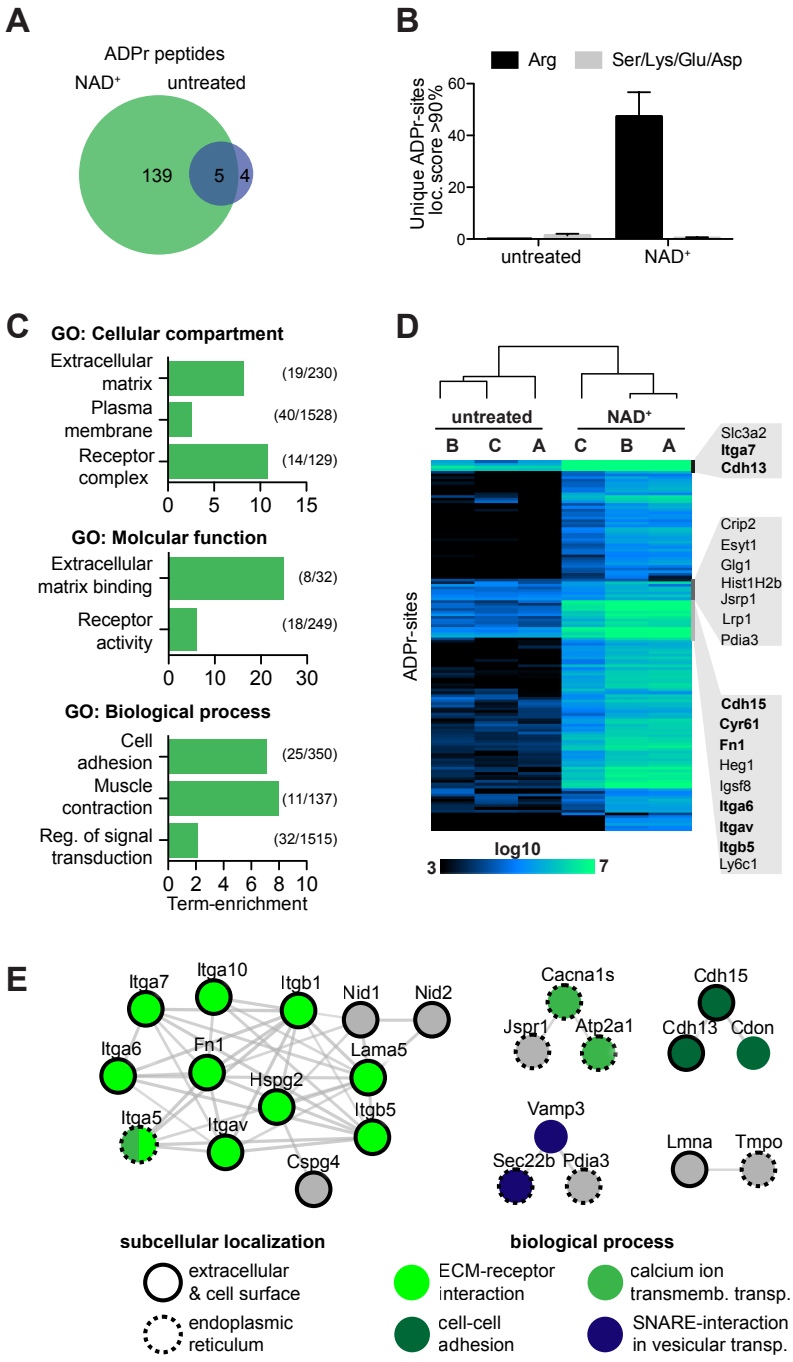

Figure 2 - Characterization of the *Artc1*$^{-/-}$ mouse.

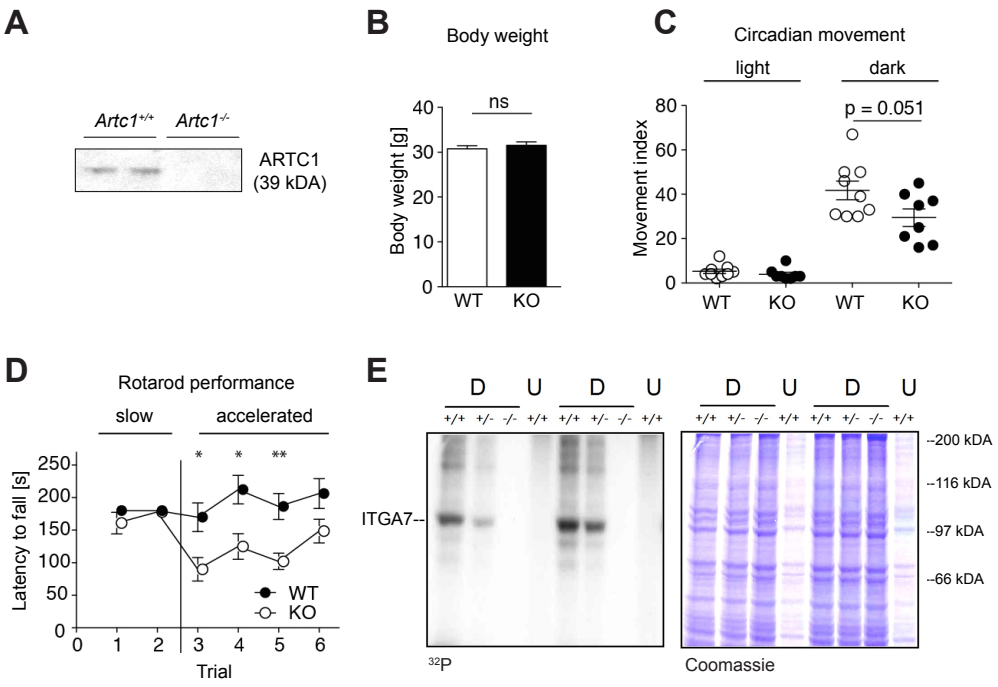

Figure 3 - Profiling of ADP-ribosylation in skeletal muscle

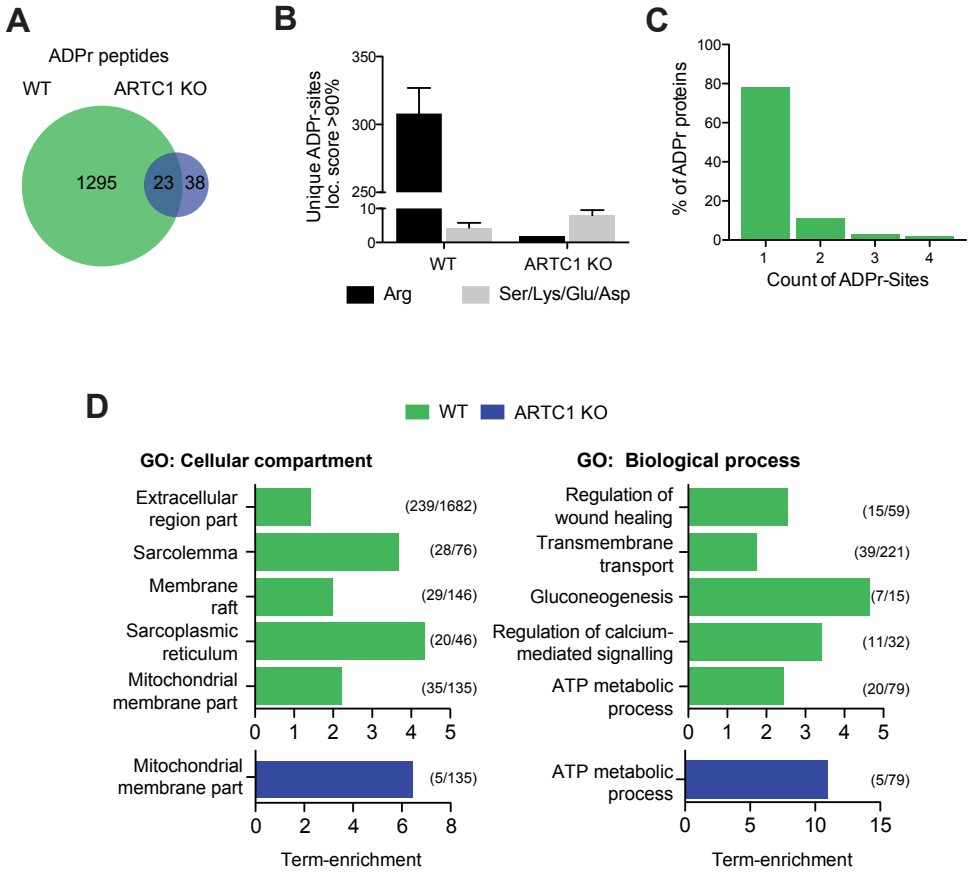

Figure 4 - Profiling of the mouse heart ADP-ribosylome

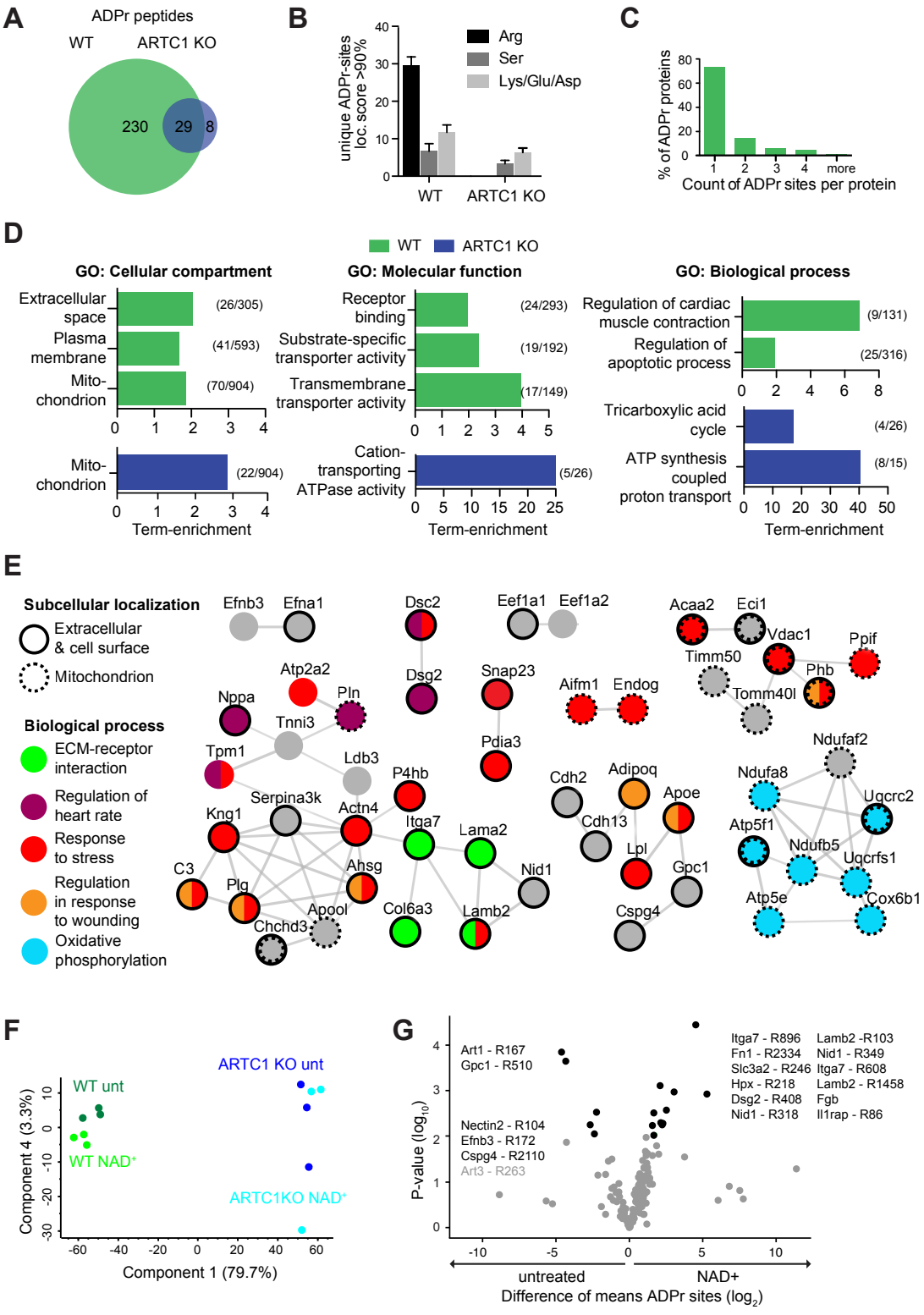

Figure 5 - Arginine ADP-ribosylation marker ions and motifs

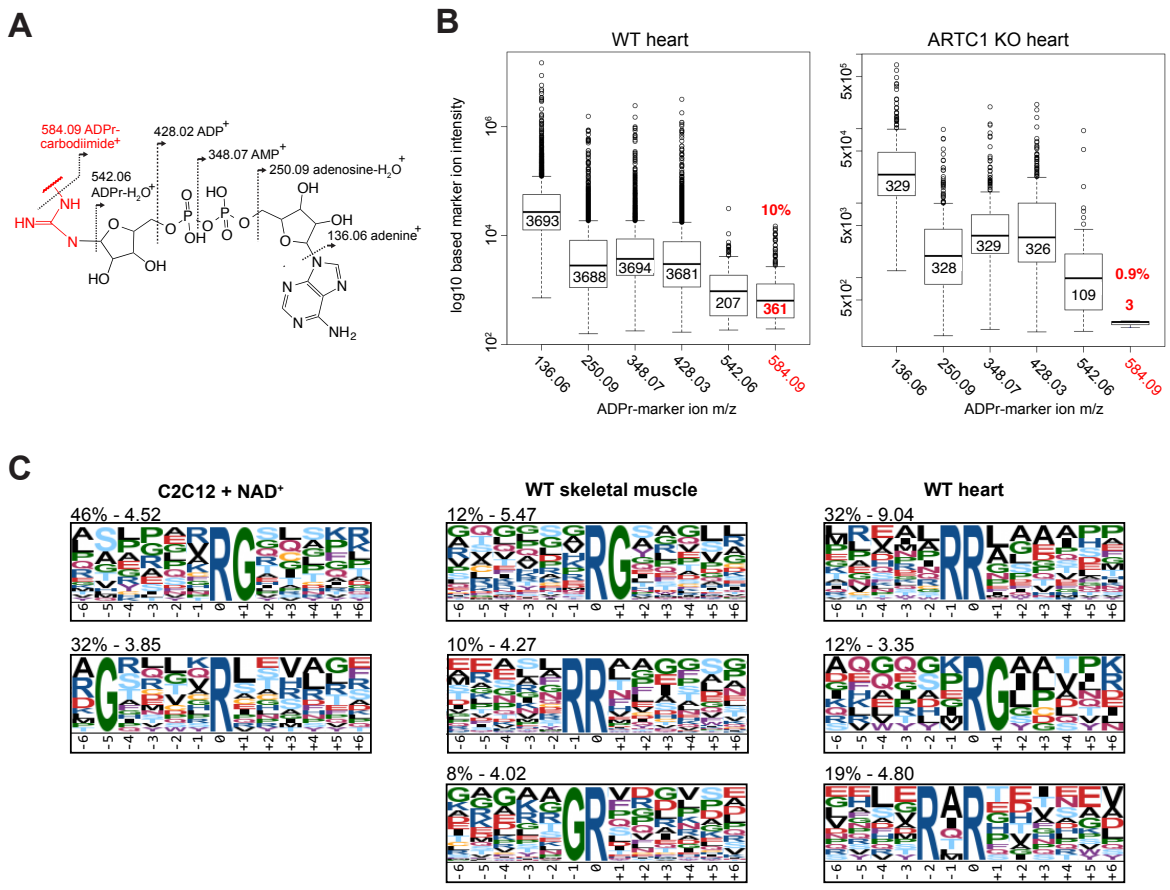

Figure 6 - ARTC1 mediated ADP-riboslyation of HPX inhibits heme binding.

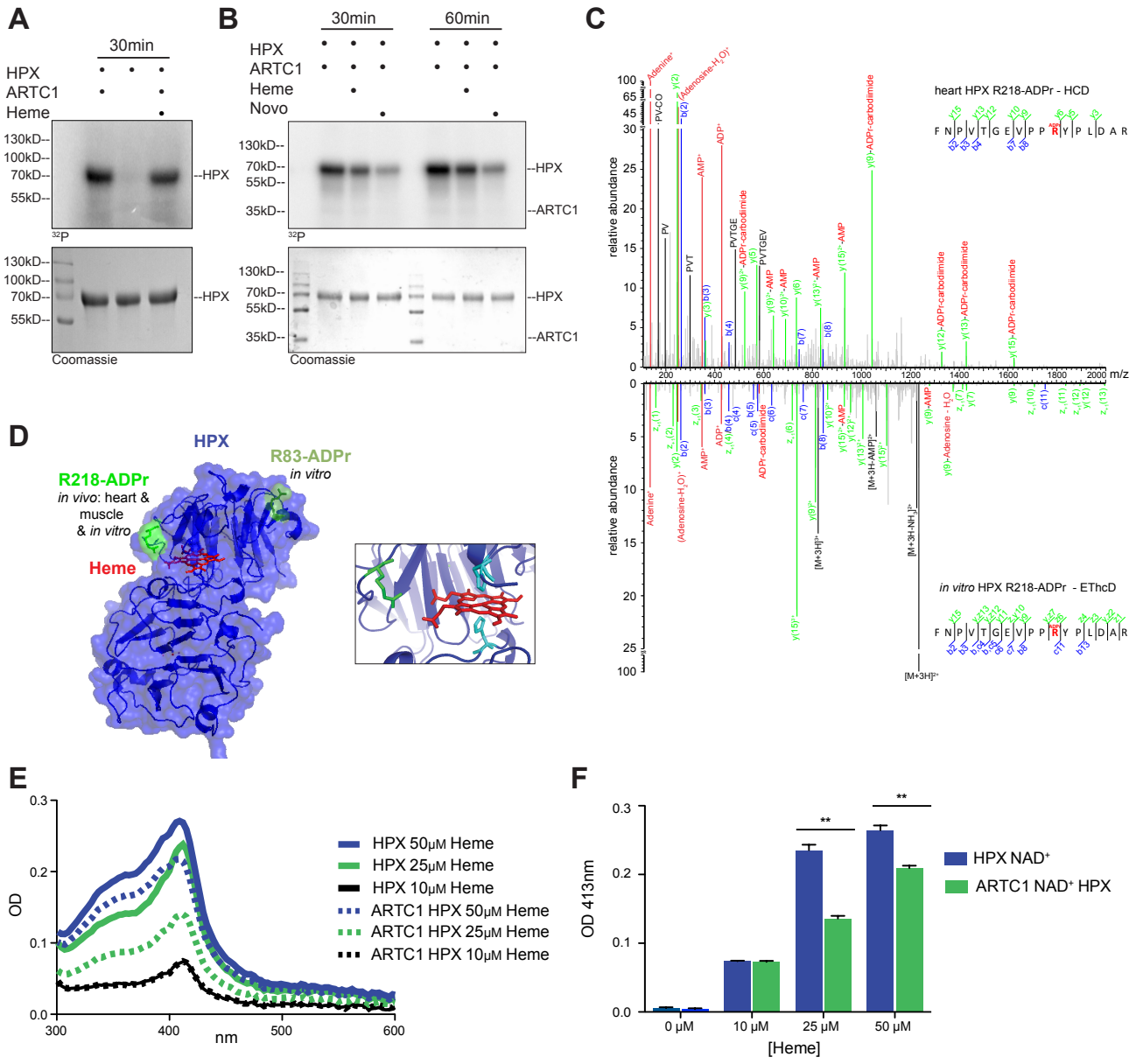

Supplementary Figure 1 - ADP-ribosylation in myotubes.

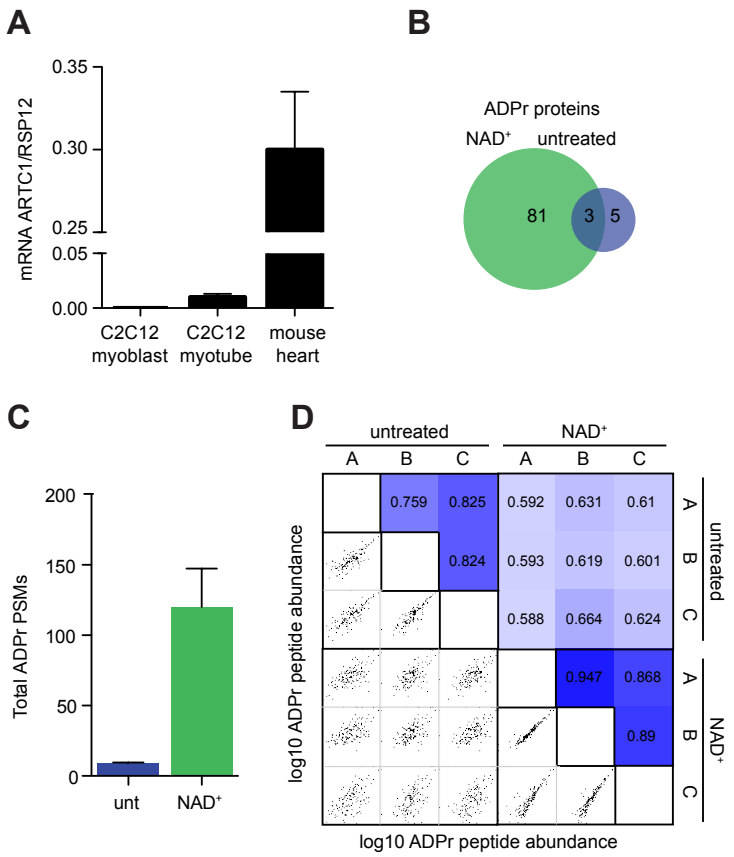

Supplementary Figure 2 - Generation of ARTC1-KO mice.

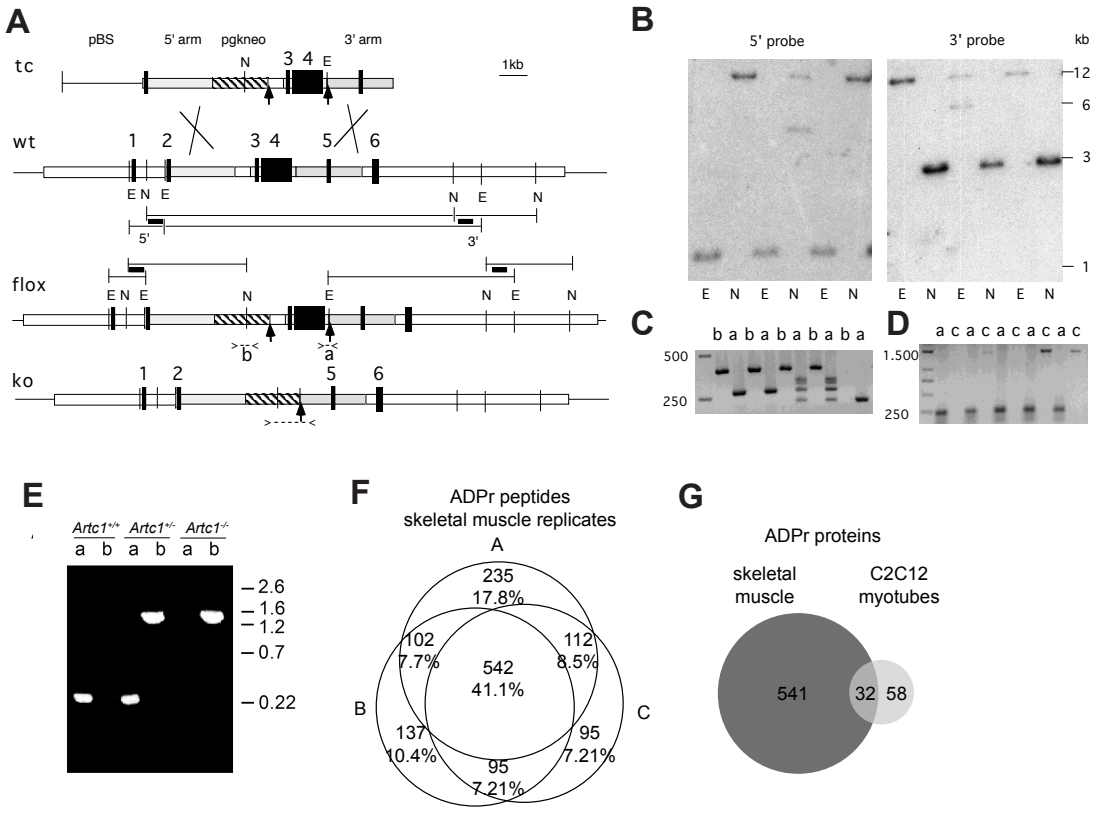

Supplementary Figure 3 - ADP-ribosylation in the mouse heart.

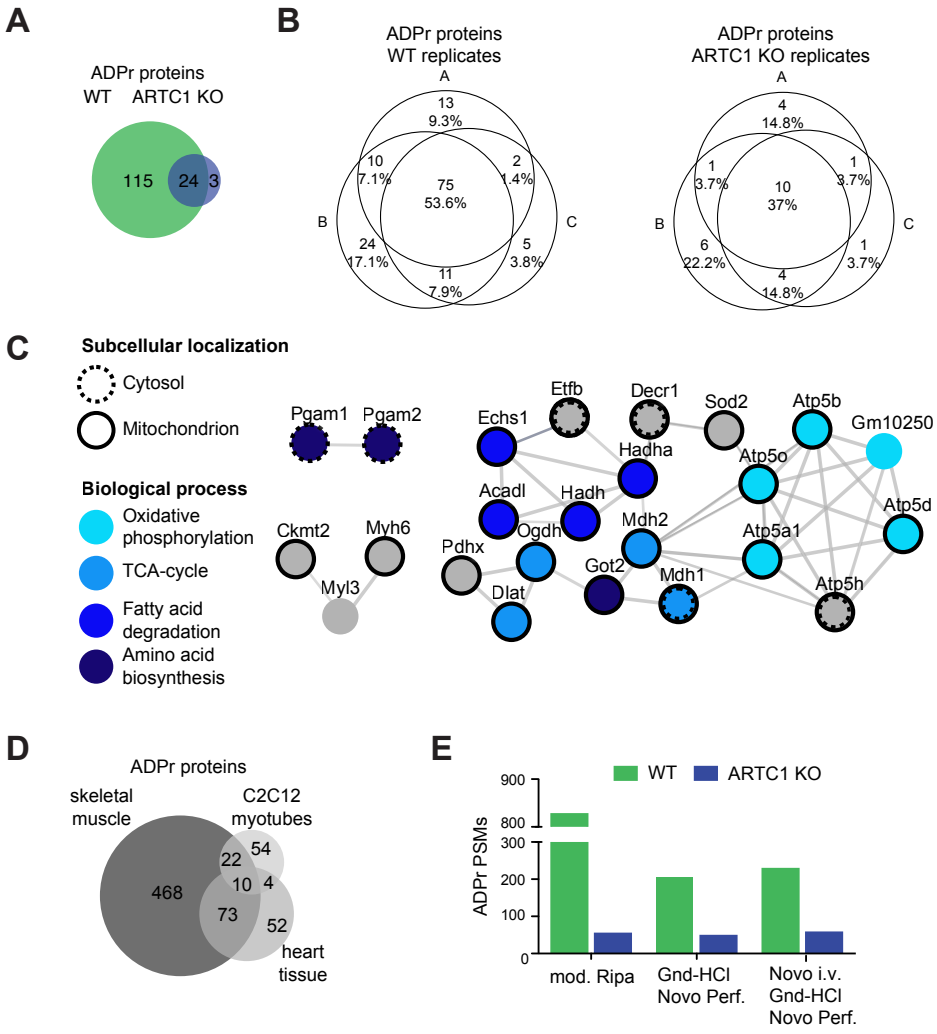

Supplementary Figure 4 - ADP-ribosylation in the mouse heart after NAD+ treatment.

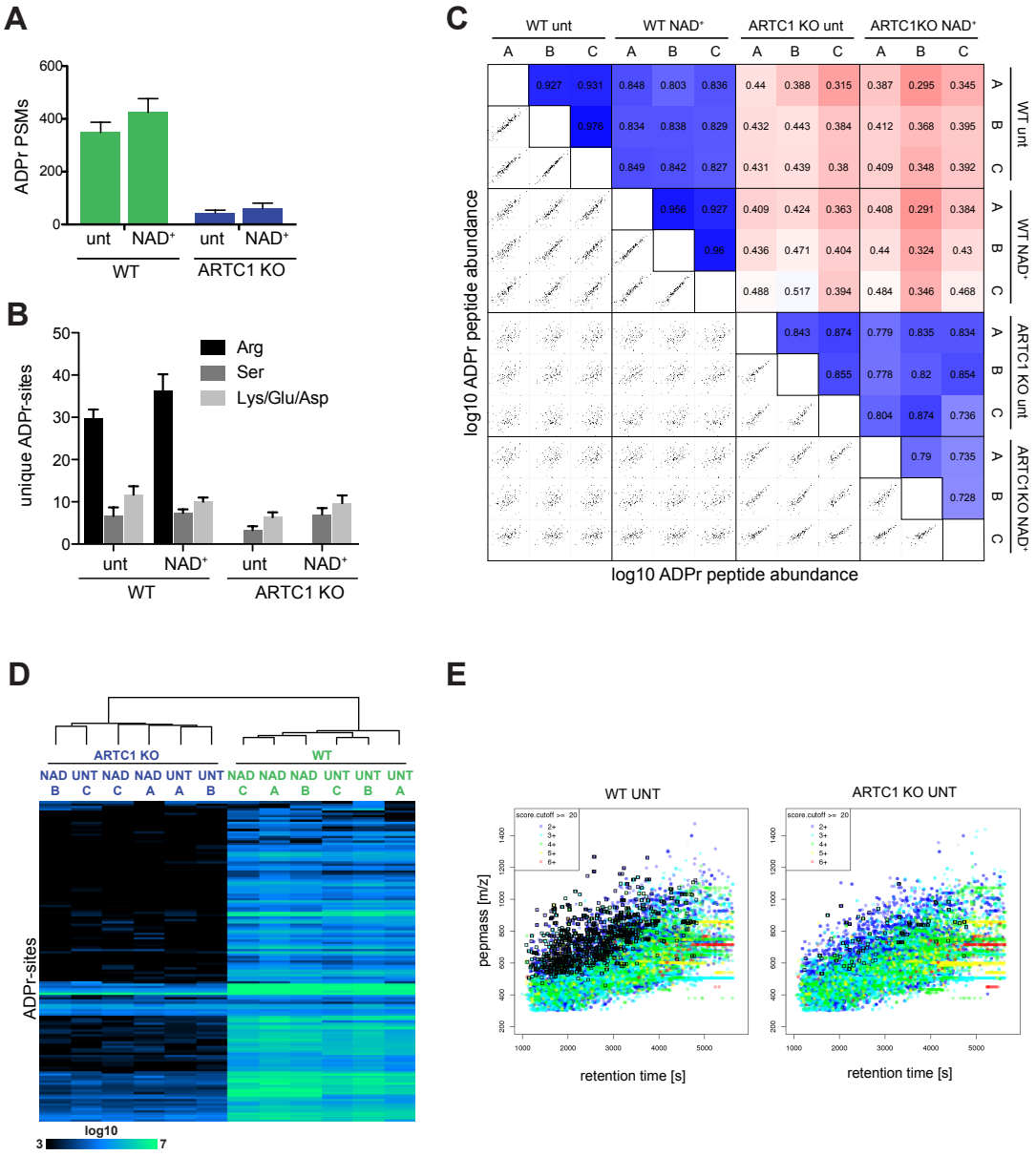

Supplementary Figure 5 – Total protein level and levels of ADP-ribosylated peptides for selected proteins identified in untreated and NAD+ treated hearts.

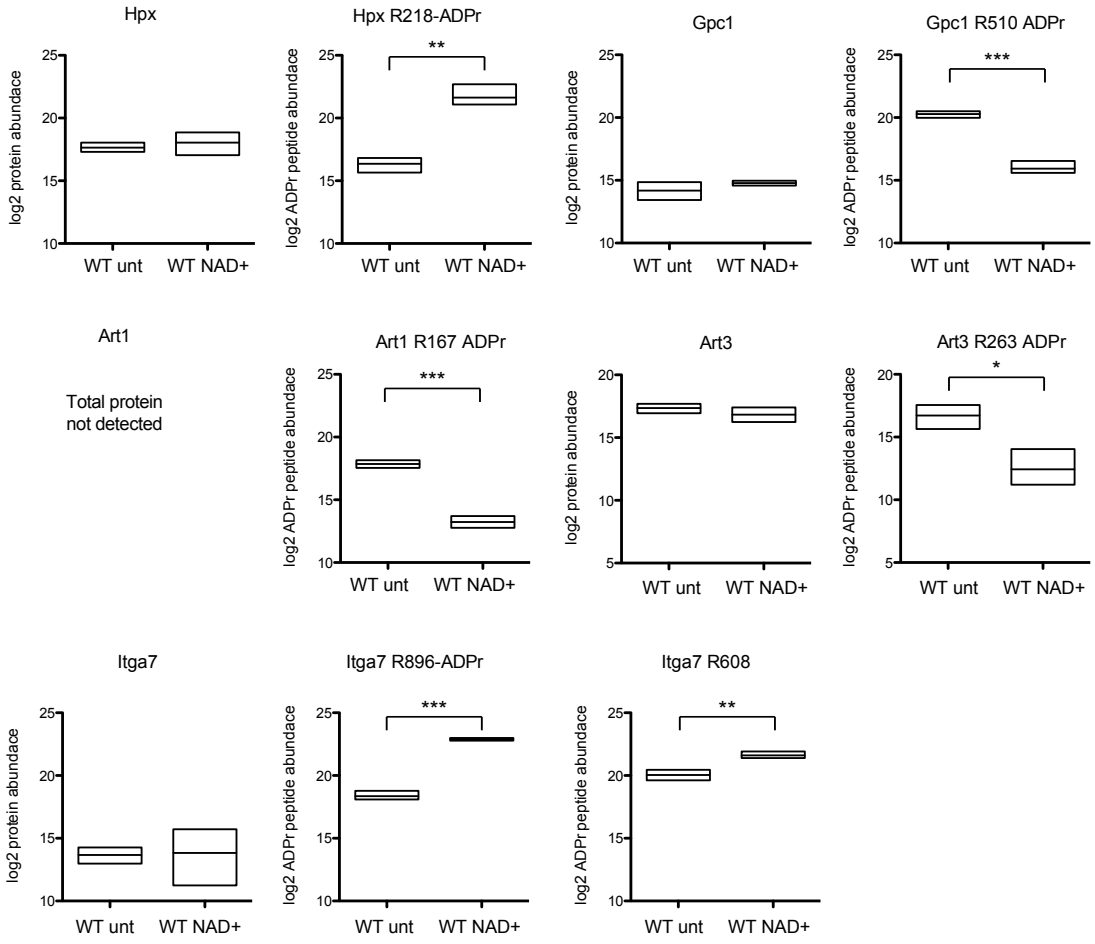

4 Unpublished Results

The established MS workflow was also applied to different other organs, cell type or samples to elucidate the potential of the technology, but also to get first insights of the different ADP-ribosylomes. The validation and functional analysis of the identified ADP-ribosylated proteins is currently under investigation or still has to be done.

4.1 ADP-ribosylation in NASH liver is sensitive to PARPi and NR treatment

One very interesting area of therapeutic NAD^+ intervention is non-alcoholic fatty liver disease (NAFLD). NAFLD includes pathophysiologies ranging from simple fatty liver (steatosis), to non-alcoholic steatohepatitis (NASH), cirrhosis, hepatocellular carcinoma and may finally cause death. NAFLD is considered the most common liver disease in the Western world and without approved pharmacological treatment [138]. It is known that the expression of several ARTDs is increased in the liver of mouse NAFLD or NASH models and it was shown that PARP inhibitor or NR treatment restored the hepatic NAD^+ content, opposing the decrease in SIRT1 activation, which has been identified as a disease driver [139, 140]. The positive outcome of both treatments (PARP inhibitor and NR) was linked to beneficial effects on the metabolic-, inflammatory-, and oxidative stress-related conditions [139]. In collaboration with Prof. Johan Auwerx (EPFL) we aimed to determine, whether the beneficial effect would correlate with changes of the ADP-ribosylome in the liver and whether ADP-ribosylation targets could be identified that might be functionally important in the context of disease progression.

Mice were fed with a chow diet or a methionine- and choline-deficient diet (MCD), as a model for NASH [139], complemented with either nothing, PARPi or NR, and liver samples prepared from three individual mice for every tested condition. In order to measure the ADP-ribosylome, tissues samples were lysed using an 8M Urea lysis buffer and the ADP-ribosylated peptide subsequently enriched using the Af1521 approach [57]. Around 25 proteins were found to be ADP-ribosylated in all tested samples. One protein cluster was ADP-ribosylated in all samples, whereas the chow diet and MCD diet additionally induced characteristic ADP-ribosylated protein

clusters (Figure 10A, B). Treatment with NR or PARPi strongly reduced the ADP-ribosylomes in both tested cases (Figure 10A, B).

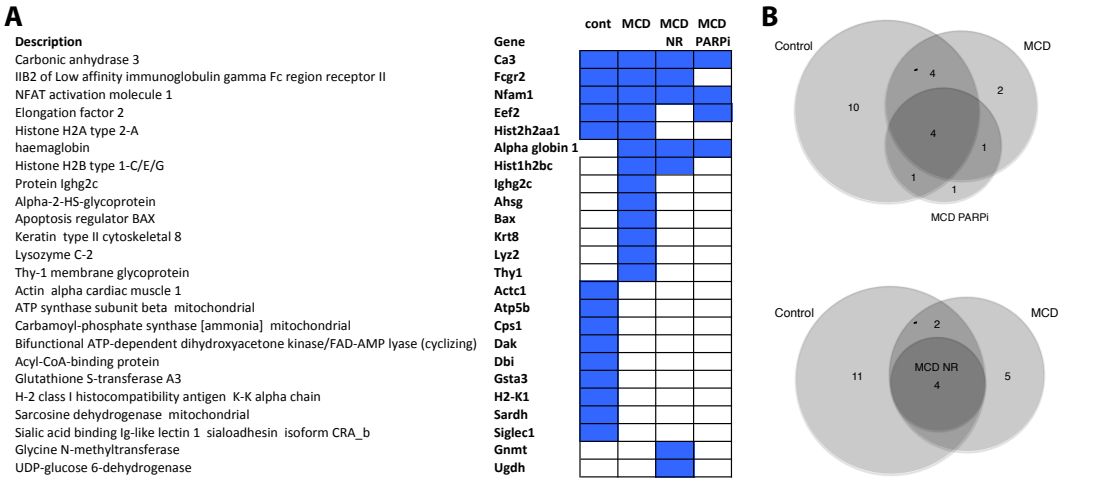

Figure 10 ADP-ribosylated proteins in NASH liver are sensitive to PARPi and NR treatment. A) ADP-ribosylated proteins detected in at least two out of three biological replicates. Columns correspond to biological samples, consisting of three individual mouse livers respectively; a blue cell indicates that the corresponding protein was found to be modified. B) ADP-ribosylated proteins detected in at least two out of three biological replicates shown as a Venn diagram.

ARTD1 was not found to be ADP-ribosylated, indicating that it is not strongly induced upon the tested conditions and another ART might be responsible for the observed ADP-ribosylation sites. In the NASH model, one of the most biological interesting ADP-ribosylated proteins was apoptosis regulator BAX that was specifically modified on R37, but was not modified anymore after NR or PARPi treatment, indicating that it is most probably ADP-ribosylated by an ARTD family member activated by the MCD diet. This is moreover interesting, since it was already reported that BAX and ARTD1 act in the same molecular pathway through calpain [141], resulting in the translocation of BAX form the cytosol to the mitochondria, subsequently facilitating the release of AIF, which translocates to the nucleus to induce necrosis [141]. Moreover, BAX can also localize to the nucleus to exhibit yet unknown nuclear functions, placing it to the same cellular compartment of ARTD1, 2 or 3 [142]. It is unclear which ARTD is ADP-ribosylating BAX and what the functional consequence of this modification is. To address which ART is responsible for the ADP-ribosylation of BAX, *in vitro* modification assays with different recombinant ARTDs could be performed. In addition, BAX ADP-

ribosylation could be monitored by targeted proteomics under basal conditions and different disease models in WT as well as ARTD1/2 KO mice.

It is surprising that after NR treatment, less ADP-ribosylation sites were observed, since NR is known to increase intracellular NAD^+ levels. An explanation for the low number of ADP-ribosylation sites could also be that NAD^+ consumption by ARTD enzymes does not necessarily correlate with the amount of PARylation or numbers of ADP-ribosylation sites, since these are also very much dependent on the activity of ADP-ribosylhydrolases [143]. It would be interesting to measure in NASH liver beside protein ADP-ribosylation the expression levels of different ADP-ribosylhydrolases as well as the turnover of ADPr metabolites to further characterize the molecular effects of ARTD inhibition or restoration of NAD^+ in the context of NASH.

4.2 Widespread ARTC2.2 dependent ADP-ribosylation in the spleen

Mouse ARTC2.2 is mainly expressed in the spleen, on immune cells and in lymph nodes [25]. Although not many ADP-ribosylation targets have been identified for ARTC2.2, it is expected that it modifies a broad range of proteins, since addition of labeled NAD^+ to cells expressing ARTC2.2 led to the detection of many ADP-ribosylated proteins [99]. In collaboration with Prof. Friedrich Koch-Nolte we thus aimed to profile the ADP-ribosylome of the spleen from WT, ARTC1 KO and ARTC2.2 KO animals. Spleens from untreated mice were isolated, samples prepared and ADP-ribosylated peptides enriched using the AF1521 approach [57]. 151 ADP-ribosylated proteins were identified in the WT spleen, mostly modified on R. While 183 ADP-ribosylated proteins were found in the ARTC1 KO, only 5 modified proteins were identified in the ARTC2.2 KO spleen (Figure 11A), suggesting that ARTC2.2 is indeed responsible for the ADP-ribosylation of the majority of identified proteins. The observation that more ADP-ribosylated proteins are observed in ARTC1 KO samples can potentially be explained by higher extracellular NAD^+ levels in these animals, however this is so far only speculation. PANTHER gene ontology analysis of the modified proteins in WT spleen revealed that the modified proteins

are mainly localized on the cell surface and in the extracellular space, involved in stress responses, immune system processes and signal transduction (Figure 11B, C).

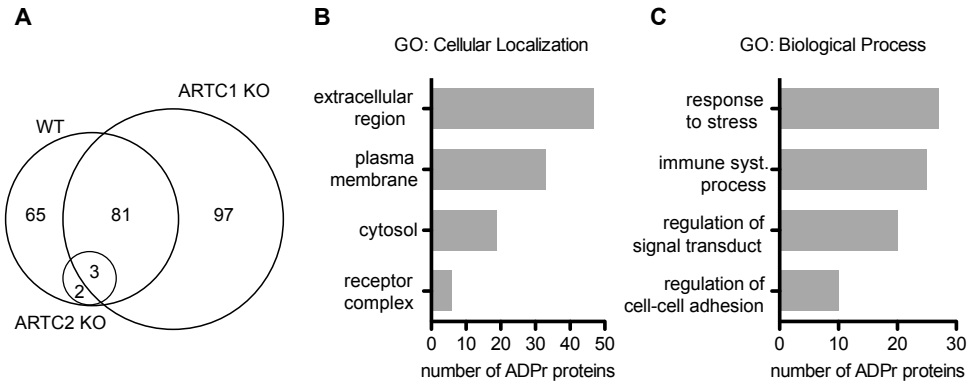

Figure 11 Arginine ADP-ribosylation in spleen is dependent on ARTC2.2. A) Venn diagram of identified ADP-ribosylated protein observed in untreated spleen samples from WT, ARTC1 KO and ARTC2 KO mice. B) PANTHER gene ontology analysis of proteins detected in the WT spleen of their cellular localization and C) biological processes.

4.3 Identification of the ARTC2.2 specific ADP-ribosylation of T Cells

Although ARTC2.2 is known to be specifically expressed on mouse T cells and a few ARTC2.2 ADP-ribosylation targets were previously identified, such as IL-2ra and P2X7, and followed up by functional studies [97, 99, 144], the T cell surface ADP-ribosylome was so far not systematically analyzed. In collaboration with Dr. Björn Rissiek (Medical Center Hamburg-Eppendorf), we mapped the ADP-ribosylation of T cells isolated from mice under untreated conditions or after *ex vivo* treatment with NAD^+. $CD3^+$ T cells were FACS sorted from spleen or liver of 7 C57BL/6 mice. 50µM exogenous NAD^+ was added to one aliquot of the isolated splenic T cells and incubated for 15min. All cells were subsequently treated with ARTC2.2-blocking Nanobody (i.e. s+16a) for 15min and lysed with denaturing RIPA buffer. 100 µg protein from each sample were processed using the PARG-FASP-Af1521 approach described in the method section and analyzed on a Fusion MS [145]. While only 3 ADP-ribosylated proteins were observed in the liver T cells, 18 were found to be modified in the splenic T cells under untreated conditions and 57 after NAD^+ treatment, corresponding to 3, 24 or 75 unique ADP-ribosylated peptides respectively (Figure 12A).

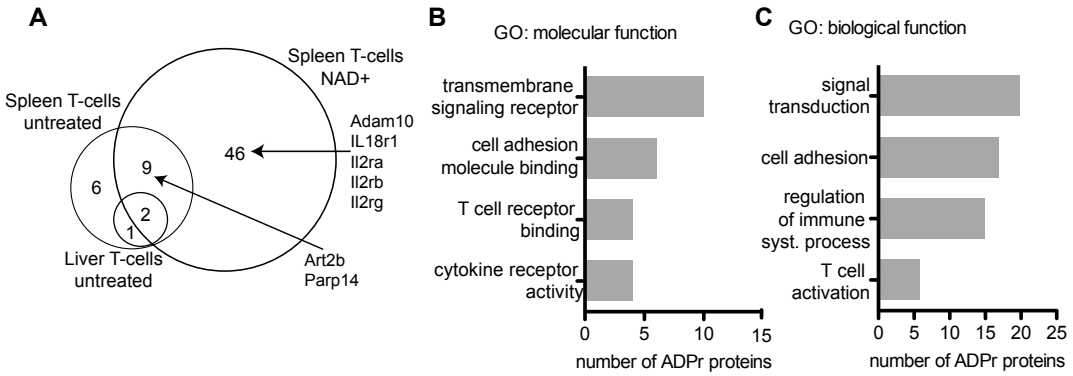

Figure 12 Identified ADP-ribosylomes in mouse T cells. A) Venn diagram of ADP-ribosylated proteins found in T cells sorted from liver tissue, left untreated or sorted from splenic tissue left untreated or treated with NAD^+ *ex vivo*. Particularly interesting identified proteins are marked B) PANTHER gene ontology annotation of ADP-ribosylated proteins found in splenic liver cells treated with NAD^+ for molecular function and C) biological function.

Gene ontology analysis for molecular and biological function was performed for the identified ADP-ribosylated proteins in splenic T cells treated with NAD^+ and revealed that these proteins are mainly associated with trans membrane receptors involved in signal transduction, cell adhesion molecules and overall proteins associated with T cell activation and immune system processes (Figure 12B,C). When applying an ADP-ribosylation site localization score of >80%, only R sites were found to be ADP-ribosylated, except for one S site. Based on the current knowledge of ARTC2.2 functions and considering that an extracellular rise in NAD^+ concentration is possible upon stress conditions, these results strongly suggest a broad role of ARTC2.2 ADP-ribosylation regulating T cell responses [35, 97, 144]. While ARTC2.2 itself was ADP-ribosylated in untreated splenic T cells on one site (R206), NAD^+ treatment induced an additional ADP-ribosylation site (R173). It is not yet clear if ARTC2.2 auto-modification has a regulatory effect on ARTC2.2 activity. To further investigate this aspect, the identified sites should be mutated and ARTC2.2 activity tested *in vitro* or by genetically complementing ARTC2.2 KO cells with a modification deficient ARTC2.2 mutant *in vivo*.

Remarkably, the heteromeric IL-2 receptor subunits, IL2ra, IL2rb and Il2rγ, were all found to be ADP-ribosylated after addition of NAD^+. The receptor complex forms if either two of these proteins or all three assemble. The different combinatorial assemblies of the receptor modulate its affinity for binding to IL-2,

with the receptor containing all three proteins showing the highest affinity [146]. Upon IL-2 signaling regulatory T cells start proliferating [146]. Although it was reported that IL2ra is ADP-ribosylated by ARTC2.2 and that this tunes IL2 signaling, ADP-ribosylation might impact IL-2 signaling more than previously anticipated, since also IL2rb and Il2rγ were found to be ADP-ribosylated [144]. Also the IL-18 receptor was ADP-ribosylated. IL-18 receptor signaling induces the release of interferon-γ (IFNγ), which plays a role in promoting cell-mediated immunity [147]. Investigating the functional relevance of IL-18 receptor ADP-ribosylation on IFNγ associated processes would be very interesting and could be tested using WT versus ARTC2.2 T cells, treated with IL-18 and quantifying IFNγ levels by qPCR or ELISA.

Interestingly, the only high confident ADP-ribosylation site not localized on R was S842 of ARTD8 in splenic T cells untreated as well as treated with NAD^+. It is very likely that this site is an ARTD8 auto-modification site, however it is not yet clear what its function might be. Interestingly ARTD8 was previously associated with immunological processes trough ADP-ribosylation of STAT1 and subsequent induction of pro-inflammatory gene expression in macrophages [148]. It remains to be tested if ARTD8 has a similar role in T cells and if the identified modification site plays a role in ARTD8 activity and STAT1 modification.

4.4 Determining ADP-ribosylation in thrombocytes

Thrombocytes, also called platelets, are blood cells and responsible for clumping and clotting of the blood during vessel injuries [149]. Their activation and aggregation is involved in arterial thrombosis and in the pathophysiology of ischemic stroke [85, 150]. PARPi showed beneficial outcomes in animal models of ischemic stroke potentially due to the effect of PARPi on thrombocyte activation [85, 151, 152]. Since thrombocytes do not have a nucleus it is unlikely that they contain ARTD1-3, although older studies reported ADP-ribosylation in thrombocytes [153]. An alternative proposed mechanism why PARPi would still be beneficial, is that PARPi, as NAD^+ analogues, might bind to ADP-receptors on the surface of thrombocytes, therefore influencing their function in an ADP-ribosylation independent manner [152]. To clarify if ADP-ribosylation can be detected in

thrombocytes and if these ADP-ribosylation sites might contribute to the observed PARPi effect, we measured the ADP-ribosylome using our proteomic method. Untreated thrombocytes of pooled buffy coats or treated thrombocytes with either 4 U/ml thrombin at 37 °C for 10min, which leads to thrombocyte activation, or with 1mM H_2O_2 to activate several ARTDs were prepared and their proteome isolated, trypsin digested, enriched by Af1521 as well as analyzed on a Q Exactive MS [57]. We identified 19 ADP-ribosylated proteins with only a minor increase upon H_2O_2 or thrombin treatment (Figure 13).

Displaying:Total Unique Peptide Count Identified Proteins (39)	untreated	H_2O_2 1mM	thrombin 4 U/ml
Cluster of Actin, alpha cardiac muscle 1	4	8	4
Myosin-9	1	2	1
Talin-1	2	2	1
Thrombospondin-1	1	1	1
Cluster of Isoform 2 of Tropomyosin alpha-3 chain	1	1	1
Cluster of Tubulin alpha-4A chain	1	1	0
Integrin-linked protein kinase	1	0	1
Cluster of 14-3-3 protein zeta/delta	1	1	0
Platelet basic protein	1	1	1
ATP synthase subunit beta, mitochondrial	1	1	0
Cytochrome b-c1 complex subunit 1, mitochondrial	1	0	0
Cluster of Hemoglobin subunit beta	0	1	1
Cluster of Isoform 2 of Fermitin family homolog 3	0	1	2
Serum albumin	0	1	0
Profilin-1	0	1	0
Fibrinogen beta chain	0	1	0
Isoform Gamma-A of Fibrinogen gamma chain	0	1	0
PDZ and LIM domain protein 1	0	0	1
Protein disulfide-isomerase A3	0	0	1
Peptidyl-prolyl cis-trans isomerase A	0	0	1
Peptidyl-prolyl cis-trans isomerase F, mitochondrial	0	2	2
Isoform 3 of UDP-glucose 6-dehydrogenase	0	1	1

Figure 13 ADP-ribosylation was detected in thrombocytes. Identified ADP-ribosylated proteins are shown on the left and the table shows the corresponding number of identified unique ADP-ribosylated peptides for the different treatments.

Most of the identified ADP-ribosylated proteins did not correlate with classical ARTD1 or 2 targets identified previously. Several modified proteins were cytoskeletal and structural proteins, including Actin. Actin ADP-ribosylation by bacterial toxin was reported to degrade the cytoskeleton [16], however the ADP-ribosylation sites identified in this study on Actin were localized to a different part of the protein, and could therefore have a different effect. A few extracellular cell surface proteins were identified to be ADP-ribosylated as well, which could point at the presence of an endogenous or co purified ARTC. ARTC mediated ADP-ribosylation could be confirmed by including the ARTC inhibitor Novobiocin or

treating the cells with NAD^+ to stimulate ARTC ADP-ribosylation. To investigate whether the modified sites are indeed sensitive to PARPi treatment, the experiment should be repeated with PARPi pre-treatment.

4.5 Identifying ADP-ribosylation targets of bacterial toxins

Many different prokaryotic toxins ADP-ribosylate specific host proteins in order to promote bacterial pathogenesis. Unlike ARTDs, they are thought to ADP-ribosylate very specifically only one single amino acids of the target protein (see introduction chapter 3.1) [16]. *Photorhabdus luminescens* belongs to the family of *Enterobacteriaceae* and produces ADP-ribosylating toxins, which have been shown to be deadly for insect [120]. Several human pathogens produce structurally related toxins [120]. Dr. Alexander E. Lang and Prof. Klaus Aktories (University of Freiburg) have identified two presumably ADP-ribosylating bacterial toxins belonging to the TccC4 protein class from two *Photorhabdus luminescens* strains (i.e. "W014" and "TT01"). W014 and TT01 have different amino acid sequences and it is currently not clear, if they are acting in a similar manner. Dr. Alexander E. Lang had expressed and purified the recombinant His-tagged enzymatic domains of both toxins. Incubation of HeLa cell lysate with the toxins in presence of ^{32}P-NAD^+ let to ADP-ribosylation of two unknown distinctive proteins. In a collaborative approach we aimed at determining the eukaryotic targets of these toxins *in vivo.* We infected HeLa cells with either one of the toxins in presence of the protective antigen (PA) from *Bacillus anthracis*, to allow internalization of the toxins [120]. Optimal intoxication conditions (i.e. dose and time) were determined by microscopy readout using the shape change of the cells (Figure 14A). Infected and control cells were lysed, proteins were digested, enriched with Af1521 and modified peptides analyzed by MS measurement [145]. To identify potential toxin mediated ADP-ribosylation sites MS searches were performed in an error tolerant mode or by taking every theoretically modifiable amino acid into account (described in [62])(Figure 14B, C).

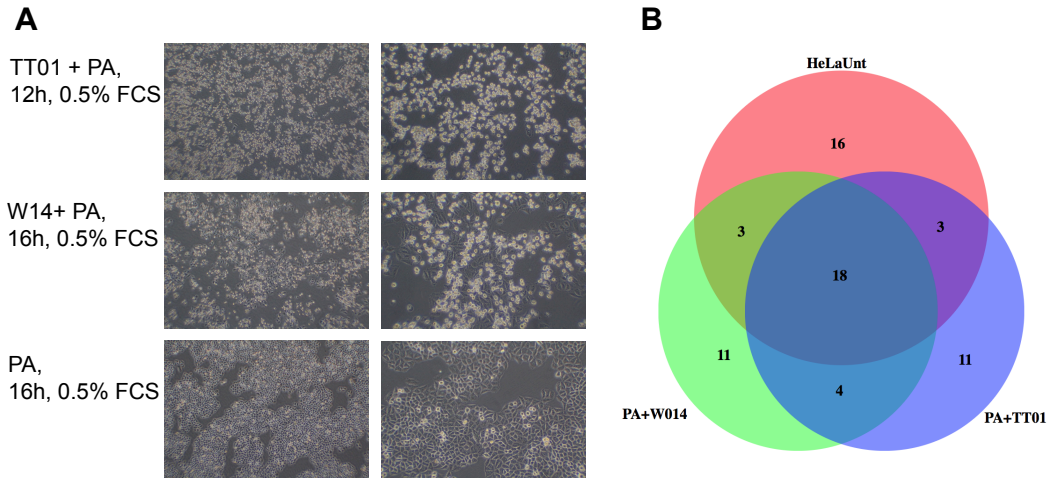

C

W014		TT01		W014 – TT01
HIST2H2BF	HIST1H3A	PRDX4	HSPA5	HNRNPA1
HIST1H2BM	DDX21	LEPRE1	HSP90B1	CNPY2
HIST1H1E	CIRBP	PON2	CBX5	HNRNPA0
RPS3A	MAGT1	DNAJB11	WFS1	ATRAID
HNRNPA2B1	MRE11A	LMAN1	KDELC2	
H3F3B		LRPAP1	LMAN1	

Figure 14 ADP-ribosylation in HeLa cells after infection with TccC4 related toxins W014 and TT01 from two different *Photorhabdus luminescens* strains. A) Light microscopic pictures of infected and control HeLa cells show the effect of the toxins on cell shape. B) Overlap of identified ADP-ribosylated proteins. C) ADP-ribosylated proteins specifically observed after infection with the individual toxins. Proteins labeled in red were subjected to *in vitro* ADP-ribosylation by the respective toxin.

Although several targets were selected (ie. MAGT1, PON2, LRPAP1, KDELC2, LMAN1) and validated using *in vitro* ADP-ribosylation assays of purified recombinant protein or overexpression cell lysate with TccC4 toxins, none of the selected targets could be confirmed to be a *bona fid*e toxin target. We do currently not know if any of the identified ADP-ribosylated proteins are the real targets of toxin ADP-ribosylation or whether they are ADP-ribosylated by an endogenous ART, as a consequence of toxin internalization. This could be elucidated by repeating the experiments with enzymatically inactive mutants of the toxins. The other identified proteins remain to be confirmed as toxin targets. Should none of the identified proteins be confirmed, alternative proteomic approaches should be considered. Limitations of the current MS assay include the sensitivity of the global ADP-

ribosylome approach and a certain constrain regarding the tryptic digestion. One possibility that would overcome this obstacle would be different proteases (such as Glu-C or Lyc-C) in combination with the current workflow or the application of ADP-ribosylated protein affinity purification, as described in [50].

4.6 Targeted proteomic measurement of ADP-ribosylation sites on immunopurified proteins.

To detect protein ADP-ribosylation in complex samples, such as cell lysates, it is necessary to apply ADP-ribosylation specific enrichment methods (see introduction chapter 9). However, the Af1521 macrodomain based as well as phosphoproteomic or boronic acid based enrichment methodologies, require large amounts of input material and might have biases towards specific modification sites [109]. To reproducibly detect *in vivo* ADP-ribosylation sites independently of an ADPr specific enrichment method, we established a protein immunopurification (IP) protocol in combination with targeted proteomic measurements. For this we overexpressed FLAG-tagged proteins, which were previously identified to be ADP-ribosylated using the Af1521 enrichment. In particular, we choose proteins, which were modified by ARTD1 (result chapter 2.1). The proteins were overexpressed in control HeLa cells or in HeLa cells with stable knockdown of either ARTD1 or ARTD2. Cell lines were subsequently treated with H_2O_2 and protein overexpression was verified by Western Blot analysis (Figure 15A). We also probed the cell lysates with an anti PAR antibody (10H, in house), but failed to detect PARylation of the overexpressed proteins, which could be due to the limited sensitivity of currently available antibodies [118] (Figure 15A).

The overexpressed proteins were enriched using anti-FLAG beads, eluted from the beads using FLAG peptide solution, PARG treated and digested on a filter (see *PARG-FASP-Af1521* in material and methods). Parallel reaction monitoring (PRM) targeted MS measurements were performed to monitor known ADP-ribosylated peptides and unmodified peptides of the overexpressed protein.

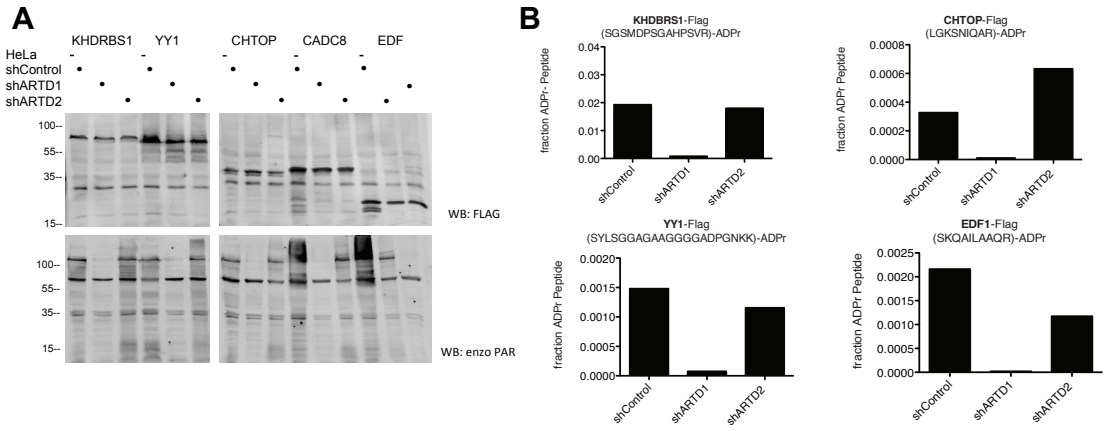

Figure 15 The targeted proteomic approach allows the measurement of ADP-ribosylated peptides of overexpressed and immunoprecipitated proteins. A) Western blot analysis confirmed overexpression of the proteins (upper panel). PARylation of overexpressed constructs cannot be detected with a common anti PAR antibody. B) In the PRM measurements modified as well as unmodified peptides were targeted and quantified. Fractions of ADP-ribosylated peptides were calculated by dividing the measured levels of ADP-ribosylated peptides by the total protein levels (as measured by PRM).

The PRM measurements of ADP-ribosylated peptides were based on a method previously established in our lab on Af1521 enriched ADP-ribosylated peptides [154]. For four out of five overexpressed proteins we were able to target and measure the previously identified ADP-ribosylated peptides in the PRM measurement. ADP-ribosylation of all four peptides was dependent on ARTD1 (Figure 15B). Unfortunately, we were not able to resolve the exact modification site on to the identified peptide due to extensive fragmentation of the ADP-ribose moiety with HCD, which let to the detection of only few peptide fragment ions still carrying parts of the ADP-ribose. To overcome this fragmentation issue it would be worth testing the PRM approach using EThcD or ETD instead of HCD fragmentation, which could be a very powerful method in accurately determining ADP-ribose site localization.

4.7 SIRT6 is auto-ADP-ribosylated on Y12

SIRT6 is a broadly expressed, nuclear protein with functions in genomic stability, inflammation, and glucose/lipid metabolism [155]. It was published that SIRT6 mono-ADP-ribosylates itself as well as ARTD1 [31, 156]. However, the ADP-ribose acceptor site(s) and amino acid type has not been identified. We thus purified recombinant SIRT6 form bacteria and performed an *in vitro* ADP-ribosylation assay.

Samples were processed with a tryptic FASP digestion, an Af1521 enrichment and finally analyzed on a Qexactive HF MS. Under the tested conditions, we identified Y12 of SIRT6 as ADP-ribosylated acceptor site with a high probability and supported by two good ADP-ribosylated peptide spectra (Figure 16), suggesting that SIRT6 is modifying another acceptor sites than the intracellular and extracellular ARTs.

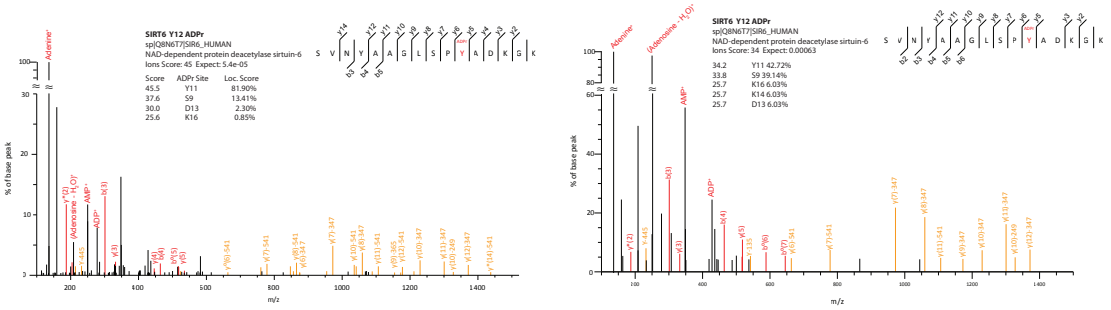

Figure 16 SIRT6 is auto-ADP-ribosylated at Y12. Two HCD ADP-ribosylated - peptide spectra of automodified recombinant SIRT6 protein recorded with a Qexactive HF MS.

Site directed mutagenesis and *in vitro* modification with ^{32}P-NAD^{+} will reveal whether Y12 is the only auto modification site and whether auto-modification of Y12 is necessary for SIRT6 function. It remains to be tested if SIRT6 is modified on Y12 *in vivo* at the same amino acid residue.

4.8 ADPRibase-Mn treatment of ADP-ribosylated peptides

Rat Mn^{2+}-dependent ADP-ribose/CDP-alcohol pyrophosphatase (ADPRibase-Mn) belongs to a metallophosphoesterase superfamily, which efficiently hydrolyzes free ADP-ribose and PAR comparable to NUDIX hydrolases [157]. Our group reported earlier that incubation of *in vitro* ADP-ribosylated ARTD1, ARTD10 or histone H3 tail with recombinant ADPRibase-Mn decreased PARylation or MARylation, respectively (Florian Rosenthal, PhD Thesis, unpublished results). MS-analysis revealed that the ADP-ribose is cleaved at the pyrophosphate bond, which results in a defined phospho-ribose moiety attached to the protein (Florian Rosenthal, PhD Thesis, unpublished results). Conversion of ADP-ribosylated peptides into phosphor-ribosylated peptides by NUDIX hydrolases or snake venom dieseterases can be useful for MS analysis, due to the reduced size and charge of the phosphor-ribose compared to the ADP-ribose [109, 122]. We thus aimed to analyze whether

replacing PARG with ADPRibase-Mn in our Af1521 proteomic workflow would be beneficial for the identification of ADP-ribosylation sites (Figure 17A). We used lysates of hydrogen-peroxide stressed HeLa cells to generate a large number of ADP-ribosylated proteins. Proteins were digested with trypsin, but unlike in the original protocol [57] PARG treatment was omitted at this step and PARylated as well as MARylated peptides directly enriched using the Af1521 macrodomain. These peptides were subsequently subjected to demodification by either recombinant PARG or ADPRibase-Mn. Measurements were done in triplicates to label-free quantify and to monitor the relative abundance of modified peptides (Figure 17A).

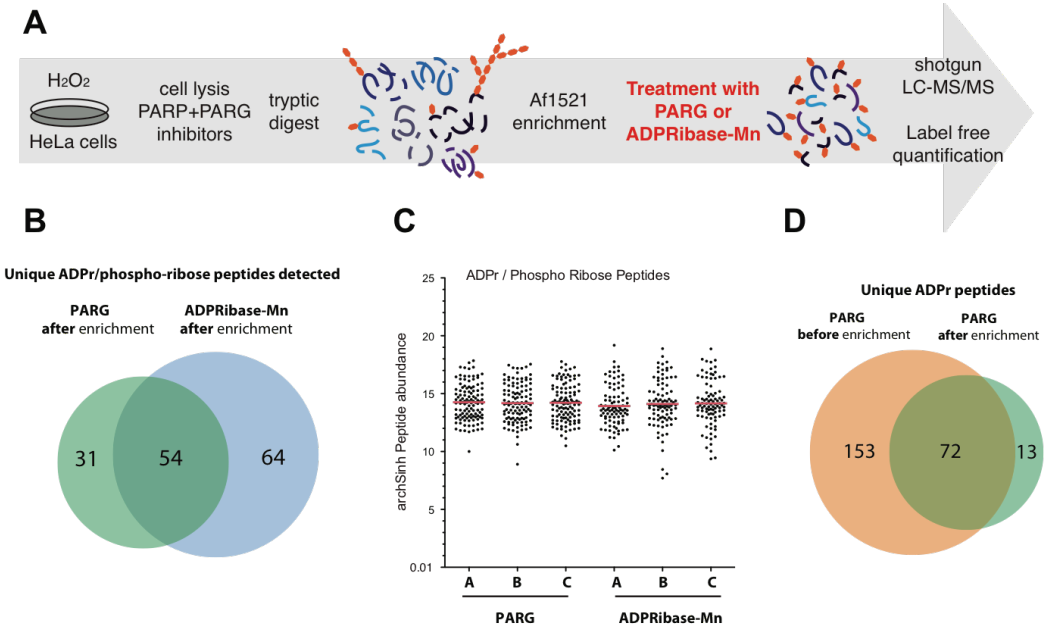

Figure 17 ADPRibase-Mn treatment can be used instead of PARG treatment in the Af1521 approach. A) Adjusted enrichment strategy for ADP-ribosylation sites (orange). Hydrolase treatment is performed after Af1521 enrichment (indicated in red). B) Venn diagram of modified peptides after PARG or ADPRibse-Mn treatment. C) Relative abundance or ADP-ribosylated and phposhoribosylated peptides in the different samples. D) Overlap of identified ADP-ribosyalted peptides if the PARG treatment is done before or after the Af1521 enrichment.

ADPRibase-Mn led to a 46% increase in identified unique modified (ADPr and phospho-ribose) peptides compared to the same sample treated with PARG (Figure 17b). After the ADPRibase-Mn treatment, only 70% of ADP-ribosylation sites were converted into phospho-ribose sites, the remaining 30% were still ADP-ribosylated, indicating that the ADPRibase-Mn treatment was not very efficient. The abundance of ADP-ribosylated peptides after PARG treatment compared to the phospho-

ribosylated and ADP-ribosylated peptides after ADPRibase-Mn treatment was comparable, however with a slightly increased variability in the modified peptide abundance after the ADPRibase-Mn treatment, which can be explained by the simultaneous appearance of a phospho-ribosylated and an ADP-ribosylated version of the peptide in some cases (Figure 17 C). The performed ADPRibase-Mn treatment was not fully efficient and requires additional optimization or the substitution by NUDIX hydrolases, which cleave the pyrophosphate bond even more efficiently [123]. Together, the conversion of PARylation and MARylation sites into phophoribosylation sites was beneficial to increase the coverage of ADP-ribosylated peptides and the number of identified proteins.

In order to test if the reduction of PAR after enrichment is beneficial in contrast to the original protocol where PAR is reduced before the enrichment we compared the two methods in terms of their ability to identify unique ADP-ribosylated peptides (Figure 17d). When starting with a similar input peptide amount, we observed that performing the PARG treatment after the enrichment led to a significant loss of 64% of unique ADP-ribosylated peptide compared to the ones identified with the PARG pretreatment. This could be explained by a loss of material due to the additional steps after the enrichment (see methods section). Thus, the original enrichment protocol seemed overall to be the most efficient version and outperformed the benefits gained by the ADP-ribose to phospho-ribose conversion, due to the additional steps. The conversion of ADP-ribose to phospho-ribose seems only useful for enrichment approaches that directly recognize the phospho-ribose, such as the conventional phospho enrichment or potentially antibodies raised against phospho-ribose sites. Furthermore, it could be useful for approaches such as protein immunopurification (described in result chapter 4.6) or for *in vit*ro analyses. Shifting the hydrolase treatment after the enrichment can be beneficial in very specific cases, for example in order to characterize the specificity of ADP-ribosylhydrolases as exemplified by the MAR degrading function of the ADP-ribosylhydrolases 3 (ARH3) (result chapter 2.2).

4.9 Methods to unpublished results

Filter aided sample preparation (FASP) in combination with PARG treatment and Af1521 enrichment (PARG-FASP-Af1521).

FASP was done in accordance to the original protocol [158]. Depending on the size of the protein of interest a Microcon-30-kDa-cutoff or a Microcon-10-kDa-cutoff centrifugal filter unit (Millipore) was used. Filter units were always centrifuged at 14,000g at 20 °C for 20 min or longer if needed for all indicated washes and buffer exchange steps. We processed samples with amounts ranging from 5-250 µg proteins. Samples were diluted and reduced in Urea Buffer (8 M Urea, 0.1M Tris-HCl pH 8) containing 1 mM DTT and transferred to a size exclusion centrifugal filter and washed with 200 µl urea buffer. Samples were subsequently alcylated using urea buffer containing 20 mM chloroacetamide and washed twice with 100 µl urea buffer and three times with 100 µl 50 mM ammonium bicarbonate. If it was necessary to reduce PARylation of the corresponding protein to MARylation, proteins were resolved on the filter with PARG buffer (50 mM Tris-HCL pH 8, 10mM $MgCl_2$, 250 uM DTT, 50 mM NaCl) and treated with PARG as described in [159]. The filter was subsequently washed again with 100 µl 50 mM ammonium bicarbonate and the "on filter digestion" performed in 50 mM ammonium bicarbonate using the recommended ratio of a sequencing grade modified protease (mainly trypsin, but in certain cases also chymotrypsin, Glu-C or Arg-C all from Promega) overnight at room temperature. Peptides were eluted from the filter units by centrifugation and the filters washed once more with 50 µl 50 mM ammonium bicarbonate. Samples were subsequently purified over a C18 stage tip and prepared for MS analysis as describe in [159]. In some indicated cases, the Af1521 peptide enrichment was performed after the FASP digest. For this the eluted peptides were resolved in 500 µl PARG buffer (50 mM Tris-HCL pH 8, 10mM $MgCl_2$, 250 uM DTT, 50 mM NaCl) and enriched as well as analyzed by MS as described in [159].

RESULTS

PRM measurement of ADP-ribosylation sites on FLAG purified protein

FLAG-tagged proteins were overexpressed in HeLa cell using GenJet™ In Vitro DNA Transfection Reagent (SignaGen). Two days after transfection cells were treated with 1mM H_2O_2 for 10min and subsequently lysed in the presence of PJ34 and tannic acid. Purification and FLAG peptide elution was performed using FLAG Immunoprecipitation Kit (Sigma) according to the provided protocol. Proteins were eluted using a FLAG peptide elution, were PARG treated and digested on filter and prepared for MS analysis.

The PRM assay was developed using the data from the previous shotgun experiments (result chapter 2.1). The MS was operated and data was analyzed as described in [154].

Thrombocyte treatment and extract preparation

Thrombocyte-rich plasma of 5-pooled buffy coats (39% plasma out of 5x 450ml blood donation) was incubated with 1 mM acetylsalicylic acid. After addition of EDTA, the thrombocytes were collected by centrifugation at 800×g for 15 min. The pellet was resuspended in a Ca^{2+} free Tyrode's buffer (140 mM NaCl, 3 mM KCl, 12 mM $NaHCO_3$, 0.4 mM NaH_2PO_4, 2 mM $MgCl_2$, 5.6 mM glucose; pH 6.2) in the presence of 1 µM prostaglandin E1 and again centrifuged at 600 × g at 37°C for 10 min. The pellet was then resuspended using a Tyrode's buffer (140 mM NaCl, 3 mM KCl, 12 mM $NaHCO_3$, 0.4 mM NaH_2PO_4, 1 mM $MgCl_2$, 2 mM $CaCl_2$, 5.6 mM glucose; pH 7.4) to a final concentration of 5×10^8/mL (standard thrombocyte suspension), and divided into 3 aliquots. The aliquots were incubated for 10 min at 37°C either without treatment or stimulated by either 4 U/ml Thrombin or 1 mM H_2O_2 for 10 min. After these treatments, cells were immediately lysed and processed as described in [159]. Enriched ADP-ribosylated peptides were analyzed on a Q Exactive MS.

DISCUSSION AND PERSPECTIVES

1 Summary of the results

The first aim of this thesis was to establish methodologies to study ADP-ribosylation at the proteomic level. In collaboration with the Nielsen laboratory (University of Copenhagen) we established an approach to enrich ADP-ribosylated peptides, which allows us now to map ADP-ribosylation sites in cultured cells and primary tissues [57, 159]. Next, we systematically optimized the MS measurement and established a method, which is highly efficient in identifying and accurately localizing ADP-ribosylation sites by using a dual peptide fragmentation approach [145]. Moreover, we revised our bioinformatics pipeline and performed systematic manual validation of annotated MS spectra in order to check for unexpected ADP-ribose acceptor amino acids (results chapter 2.1). These technological improvements led to several important findings. We identified more than 900 ADP-ribosylation sites in HeLa cells and mouse liver tissue. ADP-ribosylation in HeLa cells under genotoxic stress conditions revealed mainly modification of nuclear proteins, which were involved in transcription, chromosome organization as well as DNA and RNA metabolism.

In the second aim we addressed the specificity and contribution of ARTD1 and ARTD2 to the H_2O_2-induced ADP-ribosylome in HeLa cells. We identified ARTD1 as the main mediator of nuclear ADP-ribosylation during this condition, while ARTD2 seemed to play only a marginal role. ARTD1-mediated ADP-ribosylation was selectively modifying S and Y acceptor sites, but not R sites.

In the third aim, we identified the ADP-ribosylomes of heart and skeletal muscle tissue, which revealed a widespread role of ARTC1-mediated R-specific-ADP-ribosylation of extracellular and plasma membrane proteins, as well as an ARTC1-independent ADP-ribosylome in mitochondria. We found that the heme-binder HPX is a target of ARTC1 and confirmed with a biochemical assay that ARTC1 modifies HPX also *in vitro* and that this modification inhibits its heme binding function.

2 Towards identifying the complete ADP-ribosylome and limitations of current proteomic approaches to do so

For a complete characterization of a single ADP-ribosylation site, the following points need to be addressed [109]: 1) determination of the exact ADP-ribosylated amino acid acceptor site; 2) identification of the enzymes responsible for transfer and hydrolysis of the specific ADP-ribosylation site; 3) assessment of the ADP-ribosylation state (MAR, PAR, branched) and 4) definition of the site occupancy/stoichiometry that is, the fraction of a given modification site occupied by ADP-ribosylation. During my PhD I have undertaken efforts to approach several of these points at the level of the ADP-ribosylome.

To identify the exact ADP-ribose amino acid acceptor sites (point 1), the Af1521 enrichment approach was developed. The approach is very well suited for this and currently the method of choice that allows the broadest coverage of ADP-ribosylation sites in untreated, non-genetically modified samples [57, 145]. In combination with ETD based peptide fragmentations, this method allows the highly accurate identification of *bona fide* ADP-ribosylation sites. However, it is not yet clear whether the established approach is unbiased regarding certain amino acid ADP-ribose acceptor site, as already discussed by another group [122]. In theory Af1521 should bind free ADP-ribose and thus binds to the terminal ADP-ribose unit of a PAR chain or to a MARylated site [47]. However, we could so far not exclude that the ADP-ribose acceptor amino acid or the surrounding peptide sequence influence the binding affinity and efficiency of Af1521 to modified peptides. This could be systematically investigated by characterizing the binding affinity of several synthetically ADP-ribosylated peptides with defined sequences and ADP-ribose acceptor sites.

Another bias in identifying ADP-ribose acceptor sites could be introduced during MS analysis. Specific ADP-ribosylation sites might not be detected, wrongly assigned or underestimated, since different amino acid ADP-ribose linkages have distinct stabilities, of which some are labile and might fully fragment not allowing any acceptor site assignment [132].

Furthermore, the number of charges on peptide ions is a very important parameter for MS analysis and defines whether a specific peptide is at all detectable. Peptides are usually measured in a positive ion mode and the charge state of a peptide is mainly controlled by its length, number of basic amino acids and chemical modifications [160]. ADP-ribosylation contains two negative charges and has therefore a significant influence on the charge state of the peptide, potentially leading to ionization or detection problems for certain peptides. Potential approaches to tackle these problems could be to increase the charges on the peptides, for example by partially digesting proteins or digesting with another protease and thus increasing the length of the peptide [125], or by reducing the negative charges of ADP-ribose (by converting ADP-ribose to phospho-ribose or a hydroxamic acid derivative). Yet, other possibilities would include analyzing the peptides in a negative ion MS mode, to include single charged species or to use gentler fragmentation and ionization methods.

In order to move towards a more complete coverage of the ADP-ribosylome (e.g. also to detect very low abundant, but functionally important sites), it will be important to increase the coverage of the ADP-ribosylation sites. Approaches that might help to do so include proteome fractionation prior to the enrichment (e.g. high pH fractionation [108]), tandem enrichments (e.g. enrichment on protein as well as on peptide level, or a combination of different enrichments [161]) or introduction of ADP-ribose binding reagents with higher affinity (e.g. antibodies or engineered proteins). Furthermore, altering the protease or digestion protocol might allow the identification of previously undetected ADP-ribosylation sites.

We have started addressing the relationship between ADP-ribosylation site and ADP-ribosyltransferase/hydrolase (point 2), by using siRNA or knockout approaches in cellular systems and animal models. These “subtractive ADP-ribosylome approaches” have been useful in identifying the ADP-ribosylome targeted by ARTD1, ARTD2, ARTC1, ARTC2.2 and ARH3 (Results chapter 2.2, 2.1, 4.2). However, this approach is only applicable for a subset of biological samples and provides only indirect proof of the enzyme-substrate relationship. A genetic chemical proteomic approach has been established that identifies direct ARTD1, 2

and 3 targets by target labeling, but which is limited to cell lysates or extracted nuclei [59]. A very promising new direction could be the combination of labeled, cell permeable NAD^+ precursors analogs [127] with modified analog sensitive endogenous ARTDs (e.g. by CRISPR/Cas9 genome editing) [59].

The structure of MARylation versus PARylation (point 3) has been largely neglected in current proteomic approaches, although MARylation and PARylation are two distinct PTMs, with different biological functions (see introduction). Furthermore, PARylation is very heterogeneous in terms of its length and degree of branching, which could serve as a distinct mode of signaling. None of the current established proteomic techniques can discriminate between *bona fide* MAR and PAR sites. This could be addressed by exchanging the Af1521 macrodomain with MAR or PAR specific binding modules or alternatively, by using selective MAR or PAR hydrolases to erase one modification type or label the demodified ADP-ribosylated acceptor site (e.g by providing heavy water for the hydrolysis).

The estimation of stoichiometry (point 4) is an inherent challenge for all PTM analyses. For protein ADP-ribosylation first attempts were done using the Af1521 enrichment approach for H_2O_2 treated HeLa cells in a SILAC setting, combined with data characterizing general protein regulation during H_2O_2 treatment [57]. This analysis provided stoichiometric information for 55 ADP-ribosylation sites. Half of the ADP-ribosylation sites had less than 11% stoichiometry. Interestingly R residue had the highest ADP-ribosylation site occupancy. Alternatively, targeted proteomic approaches (i.e. PRM as demonstrated in [154] and results chapter 4.6) are also well suited to define occupancy information for specific modified sites. It will be interesting to monitor stoichiometric changes of defined ADP-ribosylation sites during specific treatments, since this might help identifying the functional and physiological relevant sites. Modification sites that are important for a response to specific stimuli are expected to be tightly regulated and to exhibit a defined stoichiometric change, while the irrelevant sites should remain unchanged. By combining PRM measurements with previous immunopurification of single proteins or proteome fractionation it should be possible to measure total protein level as well as the abundance of a certain modification site.

3 Towards an atlas of tissue specific ADP-ribosylation.

The human protein atlas consists of a tissue-based and a subcellular map of the human proteome as well as a pathology atlas and is a core resource in the field of human biology and disease, cited by thousands of research paper [162-164]. Other efforts in this direction include the cell surface protein atlas, the cancer proteome atlas and the mouse brain protein atlas [165-167]. Various similar approaches were undertaken to systematically map and categorize PTMs and several bioinformatics efforts exist in summarizing and integrating this information in databases such as PhosphoSitePlus, IPTMnet or SwissPalm [168-170]. These resources are readily integrated into UniProt and thus easy accessible and broadly used by researchers. Proteomic attempts to study ADP-ribosylation at the resolution of a single ADP-ribose acceptor site with high accuracy is now coming of age and a wealth of literature already exists where ADP-ribosylation sites have been identified biochemically or by Edman sequencing [134]. It is clear that some kind of database or central repository is needed to summarize, annotate and curate measured ADP-ribosylation sites in a protein centric way, in order to make the existing data easy accessible for the broader scientific community. *Leung et al* have undertaken a first approach to summarize the findings from the last 40 years in a protein ADP-ribosylation database, called ADPriboDB [171]. Each entry into the database was annotated manually by at least two independent curators and the database contains 12'428 entries, comprising 2'389 proteins form 459 papers by September 2017. If the ADP-riboslation field is embarking now on creating a true cellular or tissue specific ADP-ribosylation atlas, the following highly critical points need to be considered: 1) origin of sample, 2) sample preparation and 3) method for ADP-ribosylation site identification. Information about the sample origin (point 1) includes whether the sample was derived from an *in vitro* or *in vivo* system. For *in vitro* modified samples, the reaction conditions need to be reviewed and for *in vivo* systems the genetic background is key. Caution should be taken with *in vitro* samples. It is known that *in vitro* PTM reactions might result in the catalysis of non-physiological modification sites [172]. Some of the main reasons are non-

physiological protein concentration, missing (co)factors, altered PTM pattern of the recombinant protein or differential folding of the proteins as well as the overall absent of the cellular context [172]. In the case of ARTD1, it was reported that its activity and selectivity is strongly dependent on the presence of HPF1 [61]. Moreover, depending on the used NAD^+ concentration, different modification sites have been observed [94]. It is therefore important to accurately describe under which conditions *in vitro* reactions were performed (i.e. buffer composition, NAD^+ concentration and origin of proteins) and the ADP-ribosylation field should make additional efforts to systematically test different reaction conditions and to agree on standard procedures. For investigations *in cells* or *in vivo* the genetic background is crucial. One type of proteomic method requires the knock down of PARG in order to "stabilize" or "amplify" the ADP-ribosylation signal [58], however the excessive accumulation of PAR chains that are not rapidly degraded under these conditions, might induce additional perturbation of the physiological settings [173]. For *in vivo* experiments it is important to first quantify the ADP-ribosyltransferases and hydrolases in a respective biological sample and to second compare the ADP-ribosylome of tissues or cells lacking a specific ADP-ribosyltransferase or hydrolase against an unperturbed counterpart.

In terms of sample preparation (point 2), cell and tissue harvesting as well as cell lysis are critical. It was shown that shearing of DNA or release of NAD^+ can lead to unphysiological ADP-ribosylation, if buffers are not supplemented with PARPi and ARTC inhibitor or ideally by harvesting the lysates with a denaturing lysis buffer [50]. For tissue harvesting the release of NAD^+ and unphysiological ADP-ribosylation is the biggest challenge, which can however be overcome by immediate snap freezing the tissue, or by the injection of ARTC inhibitor or ARTC inactivating antibody before extracting the tissues [174]. Furthermore, non-inhibited activity of PARG and ARH3 can lead to an underestimation of ADP-ribosylation sites. It is thus important that the field is sensitized to these aspects and only procedures, which take all measures to preserve the endogenous ADP-ribosylome, should be accepted for publication.

Considering which method to apply for the identification of the ADP-ribosylation site (point 3) is very important in order to appreciate the confidence of the identified modification site. As discussed above, enrichment techniques and the applied MS methods significantly influence which sites are detectable and determine the accuracy of the localization. To make this aspect more visible, we have created an interactive ADP-ribosylation spectra database, where good quality sample spectra of ADP-ribosylated peptides fragmented with HCD or EThcD are deposited and described (Results Chapter 2.1). This allows now colleagues performing MS analyses or who analyze data created by MS to judge the quality/accuracy of the ADP-ribosylation site localization and adjust their measurements accordingly.

4 Nuclear serine ADP-ribosylation

Nuclear ADP-ribosylation has come a long way since the first detection of PAR synthesis in isolated nulcei in 1963 [175]. While for a long time the main focus for PARylation was on the DNA damage response, it is now clear that nuclear PARylation has many different molecular functions ranging from DNA repair to regulation of chromatin structure, gene expression and RNA processing, as well as various biological processes such as responses to genotoxic stress, development, aging, inflammation, metabolism or cancer [176].

The first large scale ADP-ribosylation-site proteomic study by *Zhang et al* claimed to have found hundreds of ADP-ribosylation sites on E and D in HCT116 cells in response to genotoxic stress which were mostly sensitive to PARPi treatment [58]. In the initial Af1521 peptide enrichment proteomic study performed by us, we could not confirm the broad E and D ADP-ribosylation observed by *Zhang et al*, however we found K to be the main ADP-ribose acceptor site [57, 145]. Reanalysis of the same data by others and us, as well as the introduction of better suited EThcD peptide fragmentation by us, revealed that a large number of the previously annotated lysine ADP-ribose acceptor sites were rather serine ADP-ribose acceptor sites [62, 145] (Results Chapter 2.1). We have now evidence, that most of the nuclear ADP-ribosylation measured by our methods consist of S-specific

and to a much less extent Y-specific ADP-ribosylation, although we cannot rule out that also K, D and E are modified. The predominant nuclear S-specific ADP-ribosylation was also identified and confirmed by other groups with alternative methods [62, 125].

Zhang et al have observed a "broad" distribution of E and D ADP-ribosylation sites along different proteins (e.g 38 distinct ADP-ribosylation sites in ARTD1), with 53% of the identified ADP-ribosylated proteins containing more than one site [58]. In contrast to this analysis, we found only 30% of proteins having more than one ADP-ribosylation site and often in relative close proximity (e.g. 11 K or S sites on ARTD1, all within its auto modification domain). From SILAC and targeted proteomic measurements we know that the ADP-ribosylation sites on ARTD1 detected by us belong to the highest abundant ADP-ribosylation sites in these sample types [57, 154]. In fact we were even able to detect two of the S-ADP-ribosylation sites on ARTD1 without any enrichment in whole cell lysates from H_2O_2 treated HeLa cells, strongly indicating that these are highly abundant ADPr-sites [57, 154]. It is unlikely that the discrepancy in ADP-ribosylation site distribution of our datasets compared to the ones from *Zhang et al*. are due to different used cell lines (HeLa versus HCT116). However, one possibility to explain this discrepancy might be that E and D ADP-ribosylation sites have a much lower stoichiometry than S sites. The boronic acid enrichment applied by *Zhang et al* presumably has a higher affinity for ADP-ribosylation sites than the Af1521 enrichment, is however biased in detecting only E and D sites, hence it is not possible to directly compare this E and D ADP-ribosylation sites to the S ADP-ribosylation sites. To address this discrepancy the boronic acid approach needs to be repeated in a way that side stoichiometry can be calculated and compared to the ones obtained for the S ADP-ribosylation sites identified by us or adjusted in a way that the method would allow the detection of other ADP-ribosylation sites. Furthermore, expanding the toolbox of ADP-ribose binders for enrichment will answer if the Af1521 enrichment is biased against enriching E and D ADP-ribosylation sites.

We and others have identified that nuclear S-ADP-ribosylation sites are favorably adjacent to a K or R amino acid residue. The reason or requirement for

this amino acid motif is so far unclear. One could speculate that these positively charged amino acids interact with the negatively charged phospho groups of the ADP-ribose or create a favorable environment for the catalysis of S-specific ADP-ribosylation. It is currently not clear if this simple motif contributes to the selectivity of ARTDs against certain sites, which is more likely mediated by protein-protein interactions and tertiary structural properties. The relevance of the identified motif on S-ADP-ribosylation by ARTD1 could be further investigated by *in vitro* ADP-ribosylation assays where the motif in substrate proteins is altered, abolished or newly introduced.

One of the most striking findings in the field in the recent years was the identification of histone parylation factor 1 (HPF1) and its influence on ARTD1's activity and specificity. Association of HPF1 with ARTD1 not only seems to shift its activity from auto-modification to PARylation of histones, but it also alters the specificity of ARTD1 towards S-ADP-ribosylation sites [61, 62]. In principle, the concept of protein factors to activate or modulate ADP-ribosylation is not new, since so-called ADP-ribosylation factors (ARF) in eukaryotic cells were found to stimulate ADP-ribosylation catalyzed by *E. Coli* enterotoxins and cholera toxins, however the finding that this is also the case for an endogenous ARTD was unexpected [177]. The obvious remaining question now is, whether other ADP-ribosylation factors exist to modulate different ARTD1 activities and specificities or even activities of ARTDs in general. A mechanism that shows some similarities to HPF1/ARTD1 complex formation was recently also identified for ARTD9. ARTD9 was thought to be a catalytically inactive enzyme, however in complex with ubiquitin ligase Dtx3L, it ADP-ribosylates the carboxyl terminus of ubiquitin [22]. When comparing the S-ADP-ribosylation mediated by the ARTD1/HPF1 complex to the ubiquitination system, it is attractive to hypothesize that the few ARTDs that exist in eukaryotic cells have a similar role as the E1 ubiquitin-activating enzymes and the E2 ubiquitin-conjugating enzymes, whereas ADP-ribosylation factors (such as HPF1) would act in a way comparable to the large group of E3-ligases (more than 600 in humans), providing a degree of specificity to the PTM and defining which targets are modified.

5 Extracellular arginine ADP-ribosylation and its medical relevance

In this PhD thesis we have shown that cell surface and extracellular R-specific ADP-ribosylation is mediated in a tissue specific manner either by ARTC1 or ARTC2.2. ARTC2.2 is not present in human, however ARTC1 is conserved and shows a similar tissue specific expression profile as in mouse, therefore it is likely that R-specific MARylation is also occurring in human tissues. We only started to estimate the extent of ARTC1 mediated R-specific MARylation, already under endogenous conditions, since almost nothing is known about its biological functions. This extracellular modification has the potential to be biologically and medically relevant since it targets several key nodes in signal transduction. For ARTC2.2 it has been shown that it sensitizes cells for extreme conditions, where an excess of danger signals (i.e. NAD^+) are present in the extracellular milieu, as observed in the vicinity of dying cells and during inflammation [35]. It is very well possible that ARTC1 is also activated by high local NAD^+ concentrations, which potentially occur during muscle overuse, stress or tissue damage as well as more severe conditions like ischemia-reperfusion. The function of ARTC1 mediated ADP-ribosylation for the muscle tissue remains unclear. This could be studied in specific mouse models of muscle tissue injury or myocardial ischemia-reperfusion injury in WT versus ARTC1 KO mice. In a first step, it would be interesting to test if lack of ARTC1 in these pathological models has a sensitizing or protective effect. Comparing the ARTC1 mediated ADP-ribosylome from untreated controls might identify modified targets, which have a known function during the stress response and which can be followed up in functional studies.

We have already collected data for hundreds of ARTC1 dependent ADP-ribosylation sites in the heart and skeletal muscle. Now it would be important to determine, which sites are functionally relevant in the context of physiological and pathophysiological responses. Modified signaling receptors are promising targets to follow up with functional studies in cultured cells or animal models [97, 144]. Transmembrane signal receptors are often positioned at key nodes of signaling pathways; therefore modulation of their ligand-binding properties or complex

assemblies have the potential to influence a broad spectrum of downstream effectors [178]. We identified R86 of the IL-1α/β co-receptor, i.e. interleukin 1 receptor accessory protein (IL1RAP), to be ADP-ribosylated in mouse heart and skeletal muscle tissue. It will be interesting to test if ADP-ribosylation of the IL-1 receptor complex is promoting or inhibiting IL-1α or β binding and thereby modulating its downstream signaling. Ligand binding or receptor complex formation of the IL-1 receptor can be tested by *in vitro* ADP-ribosylation of IL1RAP and subsequent affinity binding measurements with IL-1α for example by surface plasmon resonance [179]. Downstream signaling effects of IL1RAP ADP-ribosylation could be determined by monitoring induced gene expression changes (e.g. IL6 as a direct downstream target of IL-1α/β signaling), reporter gene assays or phosphorylation states of intracellular signaling components (e.g. IRAK) [180].

Due to their accessibility by antibodies *in vivo*, extracellular PTMs provide an interesting avenue for diagnostic tools and medical interventions. Extracellular ADP-ribosylation could be used as a marker for stressed cells or to visualize cells exposed to NAD^+ in proximity of dying cells. Blockade of ARTC2.2 activity in mice by an inactivating nanobody protected regulatory T cell and Natural Killer T cells from NAD^+ induced cell death (i.e. NICD) and showed benefits in mouse model of autoimmune diabetes [35, 174, 181]. This observation strongly suggests that blocking individual ARTC member by antibodies or specific inhibitors might be beneficial for the treatment of pathological conditions. Along this line, it would be interesting to treat mice with ARTC1 inactivating antibodies in mouse model (e.g LPS induced sepsis or ischemia-reperfusion) to evaluate possible beneficial effects. Antibodies against mono-ADP-ribosylated proteins or specific ARTC1-induced ADP-ribosylation sites could be tested by immunohistochemistry to visualize cells or tissue areas that are stressed ore were exposed to NAD^+

6 How to proceed to the next level – a short perspective

A series of proteome-wide analyses for ADP-ribosylated proteins across different cell lines and tissues have so far been published or are included in this thesis [57]. An open issue remains now, how these lists of modified proteins can be used in the

most efficient way to foster further validation and to elucidate the functional relevance of ADP-ribosylation. The most important part is to categorize and summarize all identified ADP-ribosylation sites in an easy accessible database as discussed above. However, researchers interested in the biological function and clinical relevance of ADP-ribosylation sites need to be able to prioritize ADP-ribosylated proteins and chose promising targets for follow up studies. An obvious criterion would be ADP-ribosylation site(s) that have been identified with independent methods, on a protein that has previously been associated with key biological processes and whose structural analysis suggest that the ADP-ribosylation site could interfere or enhance protein function. However, with the growing list and increasing numbers of modified proteins these choices can become very difficult and cumbersome. Alternatively and if enough data is available, PTM sites could also be systematically prioritized by sophisticated bioinformatics approaches that identify sites which likely have a regulatory role in protein function by considering their participation in cross-regulatory events, regulating domain activity or mediating protein-protein interactions [182]. This type of selection has shown before for phosphorylation that most probably only a small fraction of the identified modification sites are likely to have a significant biological role, underlining the importance of choosing targets to follow up by mechanistic studies [182]. Additionally, further proteomic experiments should aim at testing samples under pathological conditions or sensitive to clinical available inhibitors (i.e. ARTC or ARTD inhibitors) and could reveal which ADP-ribosylation sites are functionally important. Modification sites that are evolutionary conserved between different species or groups of sites that are temporally or spatially correlated might also point at their significance [109, 113].

It might be promising to collect all available data and to establish a spectral library, that can be used for targeted or data-independent proteomic measurements with the aim to quantify stress specific, functionally relevant and ARTD specific ADP-ribosylation sites. This could be extended to characterize protein levels of ADP-ribosyltransferases, ADP-ribosylhydrolases, NAD^+ producing or consuming enzymes and potential ADP-ribosylation factors. Ideally, this tool would allow generating a

snapshot of all components and their activities of the expanded “ADP-ribosylation machinery” in a certain condition. The MS assay could be used to screen a large cohort of medically relevant samples and might allow identifying samples or conditions during which the ADP-ribosylation machinery is altered or deregulated and might thus allow an assessment if it is worthwhile to study a particular ADP-ribosylation site in greater detail for the specific condition.

ABBREVIATIONS

ADP	Adenosine diphosphate
ADPr	ADP-ribose
ADPRibase-Mn	ADP-ribose/CDP-alcohol pyrophosphatase
ARF	ADP-ribosylation factor
ARH	ADP-ribosylhydrolase
ART	ADP-ribosyltransferase
ARTC	ADP-ribosyltransferase C2/C3 cholera toxin-like
ARTD	ADP-ribosyltransferase diphtheria toxin like
BRCA1/2	Breast Cancer gene 1/2
BRCT	BRCA1 C-terminal (BRCT) domains
CID	Collision-induced dissociation
DDA	Data dependent acquisition
DIA	Data independent acquisition
ETD	Electron transfer dissociation
EThcD	Electron-transfer/higher-energy collision dissociation
FASP	Filter aided sample preparation
FHA	Forkhead-associated
GDH	Glutamate dehydrogenase
GPI	Glycosylphophatidylinositol
HCD	Higher-energy collisional dissociation
HNP1	human neutrophil peptide 1
HPF1	Histone parylation factor 1
IFNγ	Interferone gamma
IL17	Interleukin 17
IMAC	Immobilized Metal Affinity Chromatography
IP	Immunopurification
ITGA	Integrin alpha 7
ITGB1	Integrin beta 1
kDA	Kilo Daltion
LC	Liquid chromatography column
m/z	Ion mass-to-charge ratio
MAR	Mono ADP-ribosylation
MCD	Methionine- and choline-deficient diet
MEF	Mouse embryonic fibroblast
MS	Mass spectrometry
NA	Nicotinamide
NAD^+	Nicotinamide adenine dinucleotide
NAFLD	Non-alcoholic fatty liver disease
NAM	Nicotinic acid
NASH	Non-alcoholic steatohepatitis
NR	Nicotinamide riboside

ABBREVIATIONS

OB-fold	oligonucleotiode/oligosaccharide-binding fold
PA	Protective antigen
PAR	Poly-ADP-ribosylation
PARG	poly-ADP-ribose glycohydrolase
PARP	Poly(ADP-ribose)polymerases
PARPi	PARP inhibitor
PBM	PAR-binding motif
PBZ	PAR-binding zinc finge PAR-binding motif
PRM	Parallel reaction monitoring
PTM	Post-translational modification
RRM	RNA recognition motif
SP	Signal peptide
TNFα	Tumor necrosis factor alpha

REFERENCES

1. Pruitt, K.D., T. Tatusova, and D.R. Maglott, *NCBI reference sequences (RefSeq): a curated non-redundant sequence database of genomes, transcripts and proteins.* Nucleic Acids Res, 2007. **35**(Database issue): p. D61-5.
2. Harper, J.W. and E.J. Bennett, *Proteome complexity and the forces that drive proteome imbalance.* Nature, 2016. **537**(7620): p. 328-38.
3. Smith, L.M., N.L. Kelleher, and P. Consortium for Top Down, *Proteoform: a single term describing protein complexity.* Nat Methods, 2013. **10**(3): p. 186-7.
4. Jensen, O.N., *Interpreting the protein language using proteomics.* Nat Rev Mol Cell Biol, 2006. **7**(6): p. 391-403.
5. Khoury, G.A., R.C. Baliban, and C.A. Floudas, *Proteome-wide post-translational modification statistics: frequency analysis and curation of the swiss-prot database.* Sci Rep, 2011. **1**.
6. Walsh, C.T., S. Garneau-Tsodikova, and G.J. Gatto, Jr., *Protein posttranslational modifications: the chemistry of proteome diversifications.* Angew Chem Int Ed Engl, 2005. **44**(45): p. 7342-72.
7. Manning, G., et al., *The protein kinase complement of the human genome.* Science, 2002. **298**(5600): p. 1912-34.
8. Chen, M.J., J.E. Dixon, and G. Manning, *Genomics and evolution of protein phosphatases.* Sci Signal, 2017. **10**(474).
9. Junger, M.A. and R. Aebersold, *Mass spectrometry-driven phosphoproteomics: patterning the systems biology mosaic.* Wiley Interdiscip Rev Dev Biol, 2014. **3**(1): p. 83-112.
10. Humphrey, S.J., D.E. James, and M. Mann, *Protein Phosphorylation: A Major Switch Mechanism for Metabolic Regulation.* Trends Endocrinol Metab, 2015. **26**(12): p. 676-87.
11. Xu, J., et al., *Comparison of FDA Approved Kinase Targets to Clinical Trial Ones: Insights from Their System Profiles and Drug-Target Interaction Networks.* Biomed Res Int, 2016. **2016**: p. 2509385.
12. Hottiger, M.O., *Nuclear ADP-Ribosylation and Its Role in Chromatin Plasticity, Cell Differentiation, and Epigenetics.* Annu Rev Biochem, 2015. **84**: p. 227-63.
13. Henkel, J.S., M.R. Baldwin, and J.T. Barbieri, *Toxins from bacteria.* EXS, 2010. **100**: p. 1-29.
14. Hottiger, M.O., et al., *Toward a unified nomenclature for mammalian ADP-ribosyltransferases.* Trends Biochem Sci, 2010. **35**(4): p. 208-19.
15. Hottiger, M.O., *SnapShot: ADP-Ribosylation Signaling.* Mol Cell, 2015. **58**(6): p. 1134-1134 e1.
16. Simon, N.C., K. Aktories, and J.T. Barbieri, *Novel bacterial ADP-ribosylating toxins: structure and function.* Nat Rev Microbiol, 2014. **12**(9): p. 599-611.
17. Aravind, L., et al., *The natural history of ADP-ribosyltransferases and the ADP-ribosylation system.* Curr Top Microbiol Immunol, 2015. **384**: p. 3-32.
18. Otto, H., et al., *In silico characterization of the family of PARP-like poly(ADP-ribosyl)transferases (pARTs).* BMC Genomics, 2005. **6**: p. 139.

19. Vyas, S., et al., *Family-wide analysis of poly(ADP-ribose) polymerase activity.* Nat Commun, 2014. **5**: p. 4426.
20. Kleine, H., et al., *Substrate-assisted catalysis by PARP10 limits its activity to mono-ADP-ribosylation.* Mol Cell, 2008. **32**(1): p. 57-69.
21. Marsischky, G.T., B.A. Wilson, and R.J. Collier, *Role of glutamic acid 988 of human poly-ADP-ribose polymerase in polymer formation. Evidence for active site similarities to the ADP-ribosylating toxins.* J Biol Chem, 1995. **270**(7): p. 3247-54.
22. Yang, C.S., et al., *Ubiquitin Modification by the E3 Ligase/ADP-Ribosyltransferase Dtx3L/Parp9.* Mol Cell, 2017. **66**(4): p. 503-516 e5.
23. Koch-Nolte, F., et al., *ADP-ribosylation of membrane proteins: unveiling the secrets of a crucial regulatory mechanism in mammalian cells.* Ann Med, 2006. **38**(3): p. 188-99.
24. Haag, F., et al., *Premature stop codons inactivate the RT6 genes of the human and chimpanzee species.* J Mol Biol, 1994. **243**(3): p. 537-46.
25. Seman, M., et al., *Ecto-ADP-ribosyltransferases (ARTs): emerging actors in cell communication and signaling.* Curr Med Chem, 2004. **11**(7): p. 857-72.
26. Houtkooper, R.H., E. Pirinen, and J. Auwerx, *Sirtuins as regulators of metabolism and healthspan.* Nat Rev Mol Cell Biol, 2012. **13**(4): p. 225-238.
27. Kasamatsu, A., et al., *Hydrolysis of O-acetyl-ADP-ribose isomers by ADP-ribosylhydrolase 3.* J Biol Chem, 2011. **286**(24): p. 21110-7.
28. Hirsch, B.M., E.S. Burgos, and V.L. Schramm, *Transition-state analysis of 2-O-acetyl-ADP-ribose hydrolysis by human macrodomain 1.* ACS Chem Biol, 2014. **9**(10): p. 2255-62.
29. Feijs, K.L., et al., *Macrodomain-containing proteins: regulating new intracellular functions of mono(ADP-ribosyl)ation.* Nat Rev Mol Cell Biol, 2013. **14**(7): p. 443-51.
30. Haigis, M.C., et al., *SIRT4 inhibits glutamate dehydrogenase and opposes the effects of calorie restriction in pancreatic beta cells.* Cell, 2006. **126**(5): p. 941-54.
31. Mao, Z., et al., *SIRT6 promotes DNA repair under stress by activating PARP1.* Science, 2011. **332**(6036): p. 1443-6.
32. Katsyuba, E. and J. Auwerx, *Modulating NAD+ metabolism, from bench to bedside.* EMBO J, 2017. **36**(18): p. 2670-2683.
33. Canto, C., K.J. Menzies, and J. Auwerx, *NAD(+) Metabolism and the Control of Energy Homeostasis: A Balancing Act between Mitochondria and the Nucleus.* Cell Metab, 2015. **22**(1): p. 31-53.
34. Bai, P. and C. Canto, *The role of PARP-1 and PARP-2 enzymes in metabolic regulation and disease.* Cell Metab, 2012. **16**(3): p. 290-5.
35. Adriouch, S., et al., *NAD+ released during inflammation participates in T cell homeostasis by inducing ART2-mediated death of naive T cells in vivo.* J Immunol, 2007. **179**(1): p. 186-94.
36. Bruzzone, S., et al., *Connexin 43 hemi channels mediate Ca2+-regulated transmembrane NAD+ fluxes in intact cells.* FASEB J, 2001. **15**(1): p. 10-12.
37. Hottiger, M.O., *SnapShot: ADP-Ribosylation Signaling.* Mol Cell, 2016. **62**(3): p. 472.

38. Oka, S., J. Kato, and J. Moss, *Identification and characterization of a mammalian 39-kDa poly(ADP-ribose) glycohydrolase.* J Biol Chem, 2006. **281**(2): p. 705-13.
39. Mueller-Dieckmann, C., et al., *The structure of human ADP-ribosylhydrolase 3 (ARH3) provides insights into the reversibility of protein ADP-ribosylation.* Proc Natl Acad Sci U S A, 2006. **103**(41): p. 15026-31.
40. Moss, J., M.K. Jacobson, and S.J. Stanley, *Reversibility of arginine-specific mono(ADP-ribosyl)ation: identification in erythrocytes of an ADP-ribose-L-arginine cleavage enzyme.* Proc Natl Acad Sci U S A, 1985. **82**(17): p. 5603-7.
41. Slade, D., et al., *The structure and catalytic mechanism of a poly(ADP-ribose) glycohydrolase.* Nature, 2011. **477**(7366): p. 616-20.
42. Rosenthal, F., et al., *Macrodomain-containing proteins are new mono-ADP-ribosylhydrolases.* Nat Struct Mol Biol, 2013. **20**(4): p. 502-7.
43. Jankevicius, G., et al., *A family of macrodomain proteins reverses cellular mono-ADP-ribosylation.* Nat Struct Mol Biol, 2013. **20**(4): p. 508-514.
44. Teloni, F. and M. Altmeyer, *Readers of poly(ADP-ribose): designed to be fit for purpose.* Nucleic Acids Res, 2016. **44**(3): p. 993-1006.
45. Altmeyer, M., et al., *Liquid demixing of intrinsically disordered proteins is seeded by poly(ADP-ribose).* Nat Commun, 2015. **6**: p. 8088.
46. DaRosa, P.A., et al., *Allosteric activation of the RNF146 ubiquitin ligase by a poly(ADP-ribosyl)ation signal.* Nature, 2015. **517**(7533): p. 223-6.
47. Karras, G.I., et al., *The macro domain is an ADP-ribose binding module.* EMBO J, 2005. **24**(11): p. 1911-20.
48. Eckei, L., et al., *The conserved macrodomains of the non-structural proteins of Chikungunya virus and other pathogenic positive strand RNA viruses function as mono-ADP-ribosylhydrolases.* Sci Rep, 2017. **7**: p. 41746.
49. McPherson, R.L., et al., *ADP-ribosylhydrolase activity of Chikungunya virus macrodomain is critical for virus replication and virulence.* Proc Natl Acad Sci U S A, 2017. **114**(7): p. 1666-1671.
50. Jungmichel, S., et al., *Proteome-wide identification of poly(ADP-Ribosyl)ation targets in different genotoxic stress responses.* Mol Cell, 2013. **52**(2): p. 272-85.
51. Burzio, L.O., P.T. Riquelme, and S.S. Koide, *ADP ribosylation of rat liver nucleosomal core histones.* J Biol Chem, 1979. **254**(8): p. 3029-37.
52. Adamietz, P. and H. Hilz, *Poly(adenosine diphosphate ribose) is covalently linked to nuclear proteins by two types of bonds.* Hoppe Seylers Z Physiol Chem, 1976. **357**(4): p. 527-34.
53. Ogata, N., et al., *ADP-ribosylation of histone H1. Identification of glutamic acid residues 2, 14, and the COOH-terminal lysine residue as modification sites.* J Biol Chem, 1980. **255**(16): p. 7616-20.
54. Ogata, N., K. Ueda, and O. Hayaishi, *ADP-ribosylation of histone H2B. Identification of glutamic acid residue 2 as the modification site.* J Biol Chem, 1980. **255**(16): p. 7610-5.
55. Altmeyer, M., et al., *Molecular mechanism of poly(ADP-ribosyl)ation by PARP1 and identification of lysine residues as ADP-ribose acceptor sites.* Nucleic Acids Res, 2009. **37**(11): p. 3723-38.

56. Messner, S., et al., *PARP1 ADP-ribosylates lysine residues of the core histone tails.* Nucleic Acids Res, 2010. **38**(19): p. 6350-62.
57. Martello, R., et al., *Proteome-wide identification of the endogenous ADP-ribosylome of mammalian cells and tissue.* Nat Commun, 2016. **7**: p. 12917.
58. Zhang, Y., et al., *Site-specific characterization of the Asp- and Glu-ADP-ribosylated proteome.* Nat Methods, 2013. **10**(10): p. 981-4.
59. Gibson, B.A., et al., *Chemical genetic discovery of PARP targets reveals a role for PARP-1 in transcription elongation.* Science, 2016. **353**(6294): p. 45-50.
60. Rank, L., et al., *Analyzing structure-function relationships of artificial and cancer-associated PARP1 variants by reconstituting TALEN-generated HeLa PARP1 knock-out cells.* Nucleic Acids Res, 2016. **44**(21): p. 10386-10405.
61. Gibbs-Seymour, I., et al., *HPF1/C4orf27 Is a PARP-1-Interacting Protein that Regulates PARP-1 ADP-Ribosylation Activity.* Mol Cell, 2016. **62**(3): p. 432-42.
62. Bonfiglio, J.J., et al., *Serine ADP-Ribosylation Depends on HPF1.* Mol Cell, 2017. **65**(5): p. 932-940 e6.
63. Langelier, M.F. and J.M. Pascal, *PARP-1 mechanism for coupling DNA damage detection to poly(ADP-ribose) synthesis.* Curr Opin Struct Biol, 2013. **23**(1): p. 134-43.
64. Bai, P., *Biology of Poly(ADP-Ribose) Polymerases: The Factotums of Cell Maintenance.* Mol Cell, 2015. **58**(6): p. 947-58.
65. Gupte, R., Z. Liu, and W.L. Kraus, *PARPs and ADP-ribosylation: recent advances linking molecular functions to biological outcomes.* Genes Dev, 2017. **31**(2): p. 101-126.
66. Reynolds, P., et al., *Disruption of PARP1 function inhibits base excision repair of a sub-set of DNA lesions.* Nucleic Acids Res, 2015. **43**(8): p. 4028-38.
67. Beck, C., et al., *Poly(ADP-ribose) polymerases in double-strand break repair: focus on PARP1, PARP2 and PARP3.* Exp Cell Res, 2014. **329**(1): p. 18-25.
68. Wang, Z.Q., et al., *PARP is important for genomic stability but dispensable in apoptosis.* Genes Dev, 1997. **11**(18): p. 2347-58.
69. de Murcia, J.M., et al., *Requirement of poly(ADP-ribose) polymerase in recovery from DNA damage in mice and in cells.* Proc Natl Acad Sci U S A, 1997. **94**(14): p. 7303-7.
70. Abplanalp, J. and M.O. Hottiger, *Cell fate regulation by chromatin ADP-ribosylation.* Semin Cell Dev Biol, 2017. **63**: p. 114-122.
71. Asher, G., et al., *Poly(ADP-ribose) polymerase 1 participates in the phase entrainment of circadian clocks to feeding.* Cell, 2010. **142**(6): p. 943-53.
72. Welsby, I., D. Hutin, and O. Leo, *Complex roles of members of the ADP-ribosyl transferase super family in immune defences: looking beyond PARP1.* Biochem Pharmacol, 2012. **84**(1): p. 11-20.
73. Altmeyer, M. and M.O. Hottiger, *Poly(ADP-ribose) polymerase 1 at the crossroad of metabolic stress and inflammation in aging.* Aging (Albany NY), 2009. **1**(5): p. 458-69.
74. Leger, K., et al., *ARTD2 activity is stimulated by RNA.* Nucleic Acids Res, 2014. **42**(8): p. 5072-82.

75. Krishnakumar, R. and W.L. Kraus, *The PARP side of the nucleus: molecular actions, physiological outcomes, and clinical targets.* Mol Cell, 2010. **39**(1): p. 8-24.
76. Schreiber, V., et al., *Poly(ADP-ribose) polymerase-2 (PARP-2) is required for efficient base excision DNA repair in association with PARP-1 and XRCC1.* J Biol Chem, 2002. **277**(25): p. 23028-36.
77. Menissier de Murcia, J., et al., *Functional interaction between PARP-1 and PARP-2 in chromosome stability and embryonic development in mouse.* EMBO J, 2003. **22**(9): p. 2255-63.
78. Bryant, H.E., et al., *PARP is activated at stalled forks to mediate Mre11-dependent replication restart and recombination.* EMBO J, 2009. **28**(17): p. 2601-15.
79. Haikarainen, T., S. Krauss, and L. Lehtio, *Tankyrases: structure, function and therapeutic implications in cancer.* Curr Pharm Des, 2014. **20**(41): p. 6472-88.
80. Thorsell, A.G., et al., *Structural Basis for Potency and Promiscuity in Poly(ADP-ribose) Polymerase (PARP) and Tankyrase Inhibitors.* J Med Chem, 2017. **60**(4): p. 1262-1271.
81. Lord, C.J. and A. Ashworth, *PARP inhibitors: Synthetic lethality in the clinic.* Science, 2017. **355**(6330): p. 1152-1158.
82. Farmer, H., et al., *Targeting the DNA repair defect in BRCA mutant cells as a therapeutic strategy.* Nature, 2005. **434**(7035): p. 917-21.
83. Bryant, H.E., et al., *Specific killing of BRCA2-deficient tumours with inhibitors of poly(ADP-ribose) polymerase.* Nature, 2005. **434**(7035): p. 913-7.
84. Lin, K.Y. and W.L. Kraus, *PARP Inhibitors for Cancer Therapy.* Cell, 2017. **169**(2): p. 183.
85. Curtin, N.J. and C. Szabo, *Therapeutic applications of PARP inhibitors: anticancer therapy and beyond.* Mol Aspects Med, 2013. **34**(6): p. 1217-56.
86. Mabley, J.G., et al., *Anti-inflammatory effects of a novel, potent inhibitor of poly (ADP-ribose) polymerase.* Inflamm Res, 2001. **50**(11): p. 561-9.
87. Kapoor, K., et al., *PARP inhibitor, olaparib ameliorates acute lung and kidney injury upon intratracheal administration of LPS in mice.* Mol Cell Biochem, 2015. **400**(1-2): p. 153-62.
88. Chang, R., et al., *LPS preconditioning ameliorates intestinal injury in a rat model of hemorrhagic shock.* Inflamm Res, 2014. **63**(8): p. 675-82.
89. Zingarelli, B., M. O'Connor, and P.W. Hake, *Inhibitors of poly (ADP-ribose) polymerase modulate signal transduction pathways in colitis.* Eur J Pharmacol, 2003. **469**(1-3): p. 183-194.
90. Yamazaki, K., et al., *Prevention of myocardial reperfusion injury by poly(ADP-ribose) synthetase inhibitor, 3-aminobenzamide, in cardioplegic solution: in vitro study of isolated rat heart model.* Eur J Cardiothorac Surg, 2004. **26**(2): p. 270-275.
91. Laing, S., et al., *ADP-ribosylation of arginine.* Amino Acids, 2011. **41**(2): p. 257-69.
92. Harburger, D.S. and D.A. Calderwood, *Integrin signalling at a glance.* J Cell Sci, 2009. **122**(Pt 2): p. 159-63.

93. Okazaki, I.J. and J. Moss, *Characterization of glycosylphosphatidylinositiol-anchored, secreted, and intracellular vertebrate mono-ADP-ribosyltransferases.* Annu Rev Nutr, 1999. **19**: p. 485-509.
94. Zhao, Z., J. Gruszczynska-Biegala, and A. Zolkiewska, *ADP-ribosylation of integrin alpha7 modulates the binding of integrin alpha7beta1 to laminin.* Biochem J, 2005. **385**(Pt 1): p. 309-17.
95. Paone, G., et al., *ADP ribosylation of human neutrophil peptide-1 regulates its biological properties.* Proc Natl Acad Sci U S A, 2002. **99**(12): p. 8231-5.
96. Stevens, L.A., et al., *ADP-ribosylation of human defensin HNP-1 results in the replacement of the modified arginine with the noncoded amino acid ornithine.* Proc Natl Acad Sci U S A, 2009. **106**(47): p. 19796-800.
97. Adriouch, S., et al., *ADP-ribosylation at R125 gates the P2X7 ion channel by presenting a covalent ligand to its nucleotide binding site.* FASEB J, 2008. **22**(3): p. 861-9.
98. Bartlett, R., L. Stokes, and R. Sluyter, *The P2X7 receptor channel: recent developments and the use of P2X7 antagonists in models of disease.* Pharmacol Rev, 2014. **66**(3): p. 638-75.
99. Menzel, S., et al., *Nucleotide-Induced Membrane-Proximal Proteolysis Controls the Substrate Specificity of T Cell Ecto-ADP-Ribosyltransferase ARTC2.2.* J Immunol, 2015. **195**(5): p. 2057-66.
100. Aebersold, R. and M. Mann, *Mass-spectrometric exploration of proteome structure and function.* Nature, 2016. **537**(7620): p. 347-55.
101. Mann, M., R.C. Hendrickson, and A. Pandey, *Analysis of proteins and proteomes by mass spectrometry.* Annu Rev Biochem, 2001. **70**: p. 437-73.
102. Altelaar, A.F., J. Munoz, and A.J. Heck, *Next-generation proteomics: towards an integrative view of proteome dynamics.* Nat Rev Genet, 2013. **14**(1): p. 35-48.
103. Lawrence, R.T., et al., *Plug-and-play analysis of the human phosphoproteome by targeted high-resolution mass spectrometry.* Nat Methods, 2016. **13**(5): p. 431-4.
104. Olsen, J.V., et al., *Higher-energy C-trap dissociation for peptide modification analysis.* Nat Methods, 2007. **4**(9): p. 709-12.
105. Syka, J.E., et al., *Peptide and protein sequence analysis by electron transfer dissociation mass spectrometry.* Proc Natl Acad Sci U S A, 2004. **101**(26): p. 9528-33.
106. Olsen, J.V. and M. Mann, *Status of large-scale analysis of post-translational modifications by mass spectrometry.* Mol Cell Proteomics, 2013. **12**(12): p. 3444-52.
107. Bian, Y., et al., *Ultra-deep tyrosine phosphoproteomics enabled by a phosphotyrosine superbinder.* Nat Chem Biol, 2016. **12**(11): p. 959-966.
108. Batth, T.S., C. Francavilla, and J.V. Olsen, *Off-line high-pH reversed-phase fractionation for in-depth phosphoproteomics.* J Proteome Res, 2014. **13**(12): p. 6176-86.
109. Daniels, C.M., S.E. Ong, and A.K. Leung, *The Promise of Proteomics for the Study of ADP-Ribosylation.* Mol Cell, 2015. **58**(6): p. 911-24.

110. Doll, S. and A.L. Burlingame, *Mass spectrometry-based detection and assignment of protein posttranslational modifications.* ACS Chem Biol, 2015. **10**(1): p. 63-71.
111. Sharma, K., et al., *Ultradeep human phosphoproteome reveals a distinct regulatory nature of Tyr and Ser/Thr-based signaling.* Cell Rep, 2014. **8**(5): p. 1583-94.
112. Humphrey, S.J., S.B. Azimifar, and M. Mann, *High-throughput phosphoproteomics reveals in vivo insulin signaling dynamics.* Nat Biotechnol, 2015. **33**(9): p. 990-5.
113. Studer, R.A., et al., *Evolution of protein phosphorylation across 18 fungal species.* Science, 2016. **354**(6309): p. 229-232.
114. Matalon, O., B. Dubreuil, and E.D. Levy, *Young phosphorylation is functionally silent.* Science, 2016. **354**(6309): p. 176-177.
115. Gagne, J.P., et al., *Proteome-wide identification of poly(ADP-ribose) binding proteins and poly(ADP-ribose)-associated protein complexes.* Nucleic Acids Res, 2008. **36**(22): p. 6959-76.
116. Gagne, J.P., et al., *Quantitative proteomics profiling of the poly(ADP-ribose)-related response to genotoxic stress.* Nucleic Acids Res, 2012. **40**(16): p. 7788-805.
117. Isabelle, M., et al., *Quantitative proteomics and dynamic imaging reveal that G3BP-mediated stress granule assembly is poly(ADP-ribose)-dependent following exposure to MNNG-induced DNA alkylation.* J Cell Sci, 2012. **125**(Pt 19): p. 4555-66.
118. Bartolomei, G., et al., *Analysis of Chromatin ADP-Ribosylation at the Genome-wide Level and at Specific Loci by ADPr-ChAP.* Mol Cell, 2016. **61**(3): p. 474-485.
119. Matic, I., I. Ahel, and R.T. Hay, *Reanalysis of phosphoproteomics data uncovers ADP-ribosylation sites.* Nat Methods, 2012. **9**(8): p. 771-2.
120. Lang, A.E., et al., *Photorhabdus luminescens toxins ADP-ribosylate actin and RhoA to force actin clustering.* Science, 2010. **327**(5969): p. 1139-42.
121. Chapman, J.D., et al., *Mapping PARP-1 auto-ADP-ribosylation sites by liquid chromatography-tandem mass spectrometry.* J Proteome Res, 2013. **12**(4): p. 1868-80.
122. Daniels, C.M., S.E. Ong, and A.K. Leung, *Phosphoproteomic approach to characterize protein mono- and poly(ADP-ribosyl)ation sites from cells.* J Proteome Res, 2014. **13**(8): p. 3510-22.
123. Daniels, C.M., et al., *Nudix hydrolases degrade protein-conjugated ADP-ribose.* Sci Rep, 2015. **5**: p. 18271.
124. Leutert, M., et al., *Identification of ADP-Ribose Acceptor Sites on In Vitro Modified Proteins by Liquid Chromatography-Tandem Mass Spectrometry.* Methods Mol Biol, 2017. **1608**: p. 137-148.
125. Leidecker, O., et al., *Serine is a new target residue for endogenous ADP-ribosylation on histones.* Nat Chem Biol, 2016. **12**(12): p. 998-1000.
126. Leutert, M., D.M. Pedrioli, and M.O. Hottiger, *Identification of PARP-Specific ADP-Ribosylation Targets Reveals a Regulatory Function for ADP-Ribosylation in Transcription Elongation.* Mol Cell, 2016. **63**(2): p. 181-3.

127. Westcott, N.P., et al., *Chemical proteomics reveals ADP-ribosylation of small GTPases during oxidative stress.* Nat Chem Biol, 2017. **13**(3): p. 302-308.
128. Gagne, J.P., et al., *Quantitative site-specific ADP-ribosylation profiling of DNA-dependent PARPs.* DNA Repair (Amst), 2015. **30**: p. 68-79.
129. Carter-O'Connell, I., et al., *Engineering the substrate specificity of ADP-ribosyltransferases for identifying direct protein targets.* J Am Chem Soc, 2014. **136**(14): p. 5201-4.
130. Jiang, H., et al., *Clickable NAD analogues for labeling substrate proteins of poly(ADP-ribose) polymerases.* J Am Chem Soc, 2010. **132**(27): p. 9363-72.
131. Carter-O'Connell, I., et al., *Identifying Family-Member-Specific Targets of Mono-ARTDs by Using a Chemical Genetics Approach.* Cell Rep, 2016. **14**(3): p. 621-31.
132. Bonfiglio, J.J., T. Colby, and I. Matic, *Mass spectrometry for serine ADP-ribosylation? Think o-glycosylation!* Nucleic Acids Res, 2017. **45**(11): p. 6259-6264.
133. Hengel, S.M., et al., *Tandem mass spectrometry investigation of ADP-ribosylated kemptide.* J Am Soc Mass Spectrom, 2009. **20**(3): p. 477-83.
134. Rosenthal, F. and M.O. Hottiger, *Identification of ADP-ribosylated peptides and ADP-ribose acceptor sites.* Front Biosci (Landmark Ed), 2014. **19**: p. 1041-56.
135. Wiesner, J., T. Premsler, and A. Sickmann, *Application of electron transfer dissociation (ETD) for the analysis of posttranslational modifications.* Proteomics, 2008. **8**(21): p. 4466-83.
136. Hengel, S.M. and D.R. Goodlett, *A Review of Tandem Mass Spectrometry Characterization of Adenosine Diphosphate-Ribosylated Peptides.* Int J Mass Spectrom, 2012. **312**: p. 114-121.
137. Rosenthal, F., et al., *Optimization of LTQ-Orbitrap Mass Spectrometer Parameters for the Identification of ADP-Ribosylation Sites.* J Proteome Res, 2015. **14**(9): p. 4072-9.
138. Chalasani, N., et al., *The diagnosis and management of non-alcoholic fatty liver disease: Practice guideline by the American Association for the Study of Liver Diseases, American College of Gastroenterology, and the American Gastroenterological Association.* Am J Gastroenterol, 2012. **107**(6): p. 811-26.
139. Mukhopadhyay, P., et al., *PARP inhibition protects against alcoholic and non-alcoholic steatohepatitis.* J Hepatol, 2017. **66**(3): p. 589-600.
140. Gariani, K., et al., *Eliciting the mitochondrial unfolded protein response by nicotinamide adenine dinucleotide repletion reverses fatty liver disease in mice.* Hepatology, 2016. **63**(4): p. 1190-204.
141. Moubarak, R.S., et al., *Sequential activation of poly(ADP-ribose) polymerase 1, calpains, and Bax is essential in apoptosis-inducing factor-mediated programmed necrosis.* Mol Cell Biol, 2007. **27**(13): p. 4844-62.
142. Hoetelmans, R., et al., *Bcl-2 and Bax proteins are present in interphase nuclei of mammalian cells.* Cell Death Differ, 2000. **7**(4): p. 384-92.
143. Diefenbach, J. and A. Burkle, *Introduction to poly(ADP-ribose) metabolism.* Cell Mol Life Sci, 2005. **62**(7-8): p. 721-30.
144. Teege, S., et al., *Tuning IL-2 signaling by ADP-ribosylation of CD25.* Sci Rep, 2015. **5**: p. 8959.

145. Bilan, V., et al., *Combining Higher-Energy Collision Dissociation and Electron-Transfer/Higher-Energy Collision Dissociation Fragmentation in a Product-Dependent Manner Confidently Assigns Proteomewide ADP-Ribose Acceptor Sites.* Anal Chem, 2017. **89**(3): p. 1523-1530.
146. Boyman, O. and J. Sprent, *The role of interleukin-2 during homeostasis and activation of the immune system.* Nat Rev Immunol, 2012. **12**(3): p. 180-90.
147. Dinarello, C.A., et al., *Interleukin-18 and IL-18 binding protein.* Front Immunol, 2013. **4**: p. 289.
148. Iwata, H., et al., *PARP9 and PARP14 cross-regulate macrophage activation via STAT1 ADP-ribosylation.* Nat Commun, 2016. **7**: p. 12849.
149. Semple, J.W., J.E. Italiano, Jr., and J. Freedman, *Platelets and the immune continuum.* Nat Rev Immunol, 2011. **11**(4): p. 264-74.
150. del Zoppo, G.J., *The role of platelets in ischemic stroke.* Neurology, 1998. **51**(3 Suppl 3): p. S9-14.
151. Lechaftois, M., et al., *Another "string to the bow" of PJ34, a potent poly(ADP-Ribose)polymerase inhibitor: an antiplatelet effect through P2Y12 antagonism?* PLoS One, 2014. **9**(10): p. e110776.
152. Alexy, T., et al., *Inhibition of ADP-evoked platelet aggregation by selected poly(ADP-ribose) polymerase inhibitors.* J Cardiovasc Pharmacol, 2004. **43**(3): p. 423-31.
153. Kahn, N.N., *Insulin-induced expression of prostacyclin receptors on platelets is mediated through ADP-ribosylation of Gi alpha protein.* Life Sci, 1998. **63**(22): p. 2031-8.
154. Bilan, V., et al., *New Quantitative Mass Spectrometry Approaches Reveal Different ADP-ribosylation Phases Dependent On the Levels of Oxidative Stress.* Mol Cell Proteomics, 2017. **16**(5): p. 949-958.
155. Kugel, S. and R. Mostoslavsky, *Chromatin and beyond: the multitasking roles for SIRT6.* Trends Biochem Sci, 2014. **39**(2): p. 72-81.
156. Liszt, G., et al., *Mouse Sir2 homolog SIRT6 is a nuclear ADP-ribosyltransferase.* J Biol Chem, 2005. **280**(22): p. 21313-20.
157. Canales, J., et al., *Mn2+-dependent ADP-ribose/CDP-alcohol pyrophosphatase: a novel metallophosphoesterase family preferentially expressed in rodent immune cells.* Biochem J, 2008. **413**(1): p. 103-13.
158. Wisniewski, J.R., et al., *Universal sample preparation method for proteome analysis.* Nat Methods, 2009. **6**(5): p. 359-62.
159. Larsen, S.C., et al., *Proteome-Wide Identification of In Vivo ADP-Ribose Acceptor Sites by Liquid Chromatography-Tandem Mass Spectrometry.* Methods Mol Biol, 2017. **1608**: p. 149-162.
160. Shi, J. and F.X. Wu, *Peptide charge state determination of tandem mass spectra from low-resolution collision induced dissociation.* Proteome Sci, 2011. **9 Suppl 1**: p. S3.
161. Hendriks, I.A., et al., *Site-specific mapping of the human SUMO proteome reveals co-modification with phosphorylation.* Nat Struct Mol Biol, 2017. **24**(3): p. 325-336.
162. Uhlen, M., et al., *A pathology atlas of the human cancer transcriptome.* Science, 2017. **357**(6352).

163. Uhlen, M., et al., *Proteomics. Tissue-based map of the human proteome.* Science, 2015. **347**(6220): p. 1260419.
164. Thul, P.J., et al., *A subcellular map of the human proteome.* Science, 2017. **356**(6340).
165. Bausch-Fluck, D., et al., *A mass spectrometric-derived cell surface protein atlas.* PLoS One, 2015. **10**(3): p. e0121314.
166. Li, J., et al., *TCPA: a resource for cancer functional proteomics data.* Nat Methods, 2013. **10**(11): p. 1046-7.
167. Sharma, K., et al., *Cell type- and brain region-resolved mouse brain proteome.* Nat Neurosci, 2015. **18**(12): p. 1819-31.
168. Blanc, M., et al., *SwissPalm: Protein Palmitoylation database.* F1000Res, 2015. **4**: p. 261.
169. Hornbeck, P.V., et al., *PhosphoSitePlus, 2014: mutations, PTMs and recalibrations.* Nucleic Acids Res, 2015. **43**(Database issue): p. D512-20.
170. Ross, K.E., et al., *iPTMnet: Integrative Bioinformatics for Studying PTM Networks.* Methods Mol Biol, 2017. **1558**: p. 333-353.
171. Vivelo, C.A., et al., *ADPriboDB: The database of ADP-ribosylated proteins.* Nucleic Acids Res, 2017. **45**(D1): p. D204-D209.
172. Manning, B.D. and L.C. Cantley, *Hitting the target: emerging technologies in the search for kinase substrates.* Sci STKE, 2002. **2002**(162): p. pe49.
173. Yu, S.W., et al., *Apoptosis-inducing factor mediates poly(ADP-ribose) (PAR) polymer-induced cell death.* Proc Natl Acad Sci U S A, 2006. **103**(48): p. 18314-9.
174. Menzel, S., et al., *The art of blocking ADP-ribosyltransferases (ARTs): nanobodies as experimental and therapeutic tools to block mammalian and toxin ARTs.* FEBS J, 2013. **280**(15): p. 3543-50.
175. Chambon, P., J.D. Weill, and P. Mandel, *Nicotinamide mononucleotide activation of new DNA-dependent polyadenylic acid synthesizing nuclear enzyme.* Biochem Biophys Res Commun, 1963. **11**: p. 39-43.
176. Kraus, W.L., *PARPs and ADP-Ribosylation: 50 Years ... and Counting.* Mol Cell, 2015. **58**(6): p. 902-10.
177. Moss, J. and M. Vaughan, *Activation of cholera toxin and Escherichia coli heat-labile enterotoxins by ADP-ribosylation factors, a family of 20 kDa guanine nucleotide-binding proteins.* Mol Microbiol, 1991. **5**(11): p. 2621-7.
178. Lemmon, M.A. and J. Schlessinger, *Cell signaling by receptor tyrosine kinases.* Cell, 2010. **141**(7): p. 1117-34.
179. Zeng, S., et al., *Nanomaterials enhanced surface plasmon resonance for biological and chemical sensing applications.* Chem Soc Rev, 2014. **43**(10): p. 3426-52.
180. Weber, A., P. Wasiliew, and M. Kracht, *Interleukin-1 (IL-1) pathway.* Sci Signal, 2010. **3**(105): p. cm1.
181. Hubert, S., et al., *Extracellular NAD+ shapes the Foxp3+ regulatory T cell compartment through the ART2-P2X7 pathway.* J Exp Med, 2010. **207**(12): p. 2561-8.
182. Beltrao, P., et al., *Systematic functional prioritization of protein posttranslational modifications.* Cell, 2012. **150**(2): p. 413-25.

ACKNOWLEDGMENTS

Firstly, I would like to express my sincere gratitude to my advisor Prof. Michael Hottiger for the great opportunity to do my PhD in his group, for continuous support, his motivation, his immense knowledge, his patience and for not losing faith in me even if I might have lost one or the other important sample (I partially blame it on the speedvac). Additionally I would like to thank my thesis committee Prof. Bernd Wollscheid, Prof. Alex Sartori and Prof. Alexander Bürkle for their insightful comments, their individual scientific advices and their technical recommendations. I would also like to thank Prof. Klaus Aktories, who kindly agreed to review this thesis. Additionally, I am grateful to Dr. Tobias Suter, Dr. Stephan Christen and Dr. Deena Leslie Pedrioli for their great help in writing and revising manuscripts.

I have greatly benefited from the support, guidance and knowledge of the FGCZ proteomics crew, particularly Dr. Paolo Nanni, Dr. Peter Gehrig, Dr. Christian Panse, Dr. Jonas Grossman and Dr. Natalie Selevsek. I apologize for loading all these poylmers onto your columns, suppressing the ions and crashing the servers!

Thanks to the Hottiger group, all new and old members, it was an honor to spend so much time with you and lighten up the miraculous ADP-ribosylation world. In search of a way to measure the ADP-ribosylome I was standing on the shoulder of giants, namely the ADP-ribosylation MS pioneers Dr. Florian Rosenthal and Dr. Vera Bilan, thank you. Thanks to Ann-Kathrin Hopp and Lavinia Bisceglie for teaching me about all living things, thanks to Friedrich Kunze for his generosity in buying always the next round of beers, thanks to Jeannette Abplanalp for keeping the fire burning and filling up all the buffers, thanks to Giody Bartolomei for learning me how to ChIP and ChAP, congrats to Kathrin Nowak for developing into the best ADP-ribosylome follower one could wish for. I am deeply grateful for the support of all my friends at the DMMD and outside the lab.

My deepest appreciation goes to my parents, my sister, my lovely girlfriend Meret, my grandparents and the whole family for their infinite and constant support, the greatest gift that was ever given to me!

CURRICULUM VITAE

Personal Information

Name:	LEUTERT
First name:	Mario Peter
Date of Birth:	13.12.1989
Place of Birth:	Schaffhausen SH
Address:	Stokarbergstrasse 105, CH-8200 Schaffhausen
Email:	marioleutert@gmail.com

Education

PhD Candidate in Molecular Life Sciences May 2014-present
University of Zurich (UZH)
Dept. of Molecular Mechanisms of Disease
PhD Program in Molecular Life Sciences, LSZGS

Thesis Title: "Proteome-wide Identification and Characterization of Protein ADP-ribosylation in Mammalian Cells and Mouse Tissues"
Supervisor: Prof. Michael O. Hottiger

Master of Science ETH in Biotechnology Sept. 2012-Feb.2014
Swiss Federal Institute of Technology (ETH)
Dept. of Biosystems Science and Engineering
Major in Synthetic Biology

Master Thesis, Harvard Medical School, Dept. of Systems Biology:
"Artificial CRISPR/Cas9 Based Transcriptional Activators and Synthetic Interferon Sensing Circuits"
Supervisors: Prof. Pamela Silver (Harvard), Prof. Renato Paro (ETH)

Research Project: "Combinatorial Library of Synthetic Inducible Promoters Responsive to Higher Alcohols"
Supervisor: Prof. Sven Panke

Bachelor of Science ETH in Biotechnology Sept. 2009-Apr. 2013
Swiss Federal Institute of Technology (ETH)
Dept. of Biology (chemical specialization) and
Dept. of Biosystems Science and Engineering

Swiss Matura Type N: Science and Mathematics Aug. 2004-Aug. 2008
Kantonsschule Schaffhausen

CURRICULUM VITAE

Scholarships

URPP Translational Cancer Research Project support, CHF 10'000.--	2015
Candoc Forschungskredit, 12 months, CHF 55'800.--	2015

Publications

Bilan V.*, **Leutert M.***, Nanni P.*, Panse C., and Hottiger M. O. (2016) Combining HCD and EThcD Fragmentation in a Product-Dependent Manner Confidently Assigns Proteomewide ADP-Ribose Acceptor Sites. *Analytical chemistry*, 10.1021/acs.analchem.6b03365

Martello R.*, **Leutert M.***, Jungmichel S.*, Bilan V., Larsen S.C., Young C., Hottiger M.O., and Nielsen M.L. (2016) Proteome-wide identification of the endogenous ADP-ribosylome of mammalian cells and tissue. *Nature Communications* 30,7:12917.

Leutert M.*, Bilan V.*, Gehrig P., and Hottiger M.O. (2016). Identification of ADP-ribose acceptor sites on in vitro modified Proteins by Liquid Chromatography – Tandem Mass Spectrometry. *Methods Mol Biol* 1608, 137-148.

Larsen S.C.*, **Leutert M.***, Bilan V., Martello R., Jungmichel S., Young, C., Hottiger M.O., and Nielsen M.L. (2016) Proteome-wide identification of endogenous ADP-ribose acceptor sites by Liquid Chromatography–Tandem Mass Spectrometry. *Methods Mol Biol* 1608, 149-162.

Bartolomei G., **Leutert M**., Manzo M., Baubec T., Hottiger M.O. (2016) Analysis of Chromatin ADP-Ribosylation at the Genome-wide Level and at Specific Loci by ADPr-ChAP. Molecular Cell, 10.1016/j.molcel

Leutert M., Pedrioli D.M., Hottiger M.O (2016). Identification of PARP-Specific ADP-Ribosylation Targets Reveals a Regulatory Function for ADP-Ribosylation in Transcription Elongation. *Molecular Cell*, 10.1016/j.molcel.2016.07.006.

*** equal contribution**